

**Zur Synthese, Reaktivität und Moleküldynamik von
Diacetylplatinkomplexen mit κ^2 - und κ^3 -koordinierten
tripodalen N-Liganden**

Dissertation

zur Erlangung des
Doktorgrades der Naturwissenschaften (Dr. rer. nat.)

der

Naturwissenschaftlichen Fakultät II
Chemie, Physik und Mathematik

der Martin-Luther-Universität
Halle-Wittenberg

vorgelegt

von Herrn Dipl.-Chem. Martin Bette
geb. am 03.06.1982 in Meißen

Gutachter:

1. Prof. Dr. D. Steinborn, Martin-Luther-Universität Halle-Wittenberg
2. Prof. Dr. R. Beckhaus, Carl von Ossietzky Universität Oldenburg

Halle (Saale), den 10.07.2013

Inhaltsverzeichnis

Abkürzungsverzeichnis

Nummerierung der Verbindungen

1. Einleitung und Problemstellung	4
2. Ergebnisse und Diskussion	8
2.1. Diacetylplatin-Komplexe mit κ^2 - und κ^3 -koordinierten Skorpionatliganden	8
2.1.1. Einführung	8
2.1.2. Synthese und Reaktivität	10
2.1.3. Spektroskopische Charakterisierung	12
2.1.4. Strukturelle Charakterisierung	14
2.2. Diacetylplatin-Komplexe mit κ^2 - und κ^3 -koordinierten Tris(pyrazolyl)methan-Liganden	15
2.2.1. Einführung	15
2.2.2. Synthese und Reaktivität	17
2.2.3. Strukturelle Charakterisierung	18
2.2.4. Zur Moleküldynamik in Diacetylplatin(II)-Komplexen	20
2.2.5. Spektroskopische Charakterisierung von Diacetylplatin(IV)-Komplexen	22
2.3. Diacetylplatin(II)-Komplexe mit κ^2 -koordinierten (2-py) ₃ COR-Liganden	23
2.3.1. Einführung	23
2.3.2. Synthese und Reaktivität	25
2.3.3. Strukturelle Charakterisierung	26
2.3.4. Spektroskopische Charakterisierung	27
2.3.5. Zu dynamischen Prozessen in Diacetylplatin(II)-Komplexen	29
2.4. Diskussion der Ergebnisse	31
3. Zusammenfassung	39
4. Literaturverzeichnis	43
Anhang: Publikationen zur Arbeit	
Publikation A	51
Publikation B	62
Publikation C	79
Publikation D	91

Abkürzungsverzeichnis

Me	Methyl
Et	Ethyl
Bn	Benzyl
Ph	Phenyl
<i>m</i> -Tol	<i>meta</i> -Tolyl
'Bu	<i>tert</i> -Butyl
'Pr	Isopropyl
pz	Pyrazol-1-yl
pz ^x	Pyrazol-1-yl mit nicht näher spezifiziertem Substitutionsmuster
py	Pyridyl
R	organischer Rest
THF	Tetrahydrofuran
Bpy	2,2'-Bipyridin

Nummerierung

Komplexe werden wie in den Publikationen **A–D** nummeriert, wobei der vorangestellte Buchstabe auf die entsprechende Publikation verweist.

[Pt(COMe) ₂ H{(pz) ₃ BH}]	(A4a)	[Pt(COMe) ₂ H{(3,5-Me ₂ pz) ₃ BH}]	(A4b)
[Pt(COMe) ₂ Cl{(pz) ₃ BH}]	(A5a)	[Pt(COMe) ₂ Cl{(3,5-Me ₂ pz) ₃ BH}]	(A5b)
K[Pt(COMe) ₂ {(pz) ₃ BH}]	(A6a)	K[Pt(COMe) ₂ {(3,5-Me ₂ pz) ₃ BH}]	(A6b)
K[Pt(COMe) ₂ {(pz) ₄ B}]	(A7)	K[{Pt(COMe) ₂ } ₂ {(pz) ₄ B}]	(A8)
[Pt(COMe) ₂ Me{(pz) ₃ BH}]	(A9a)	[Pt(COMe) ₂ Et{(pz) ₃ BH}]	(A9b)
[Pt(COMe) ₂ Bn{(pz) ₃ BH}]	(A9c)	[Pt(COMe) ₂ Me{(pz) ₄ B}]	(A10a)
[Pt(COMe) ₂ Et{(pz) ₄ B}]	(A10b)	[Pt(COMe) ₂ Bn{(pz) ₄ B}]	(A10c)
[Pt(COMe) ₂ H{(pz) ₃ CH}]Cl	(B3a)	[Pt(COMe) ₂ H{(3,5-Me ₂ pz) ₃ CH}]Cl	(B3b)
[Pt(COMe) ₂ {(pz) ₃ CH}]	(B4a)	[Pt(COMe) ₂ {(3,5-Me ₂ pz) ₃ CH}]	(B4b)
[Pt(COMe) ₂ H{(pz) ₃ CH}]OTf	(B5a)	[Pt(COMe) ₂ H{(3,5-Me ₂ pz) ₃ CH}]OTf	(B5b)
[Pt(COMe) ₂ D{(pz) ₃ CH}]OTf	(B5c)	[Pt(COMe) ₂ D{(3,5-Me ₂ pz) ₃ CH}]OTf	(B5d)
[Pt(COMe) ₂ Me{(pz) ₃ CH}]OTf	(B6a)	[Pt(COMe) ₂ Me{(3,5-Me ₂ pz) ₃ CH}]OTf	(B6b)
[Pt(COMe) ₂ Me{(pz) ₃ CH}]I	(B7a)	[Pt(COMe) ₂ Me{(3,5-Me ₂ pz) ₃ CH}]I	(B7b)
[Pt(COMe) ₂ {(2-py) ₃ COH}]	(C3a)	[Pt(COMe) ₂ {(2-py) ₂ PhCOH}]	(C4a)
[Pt(COMe) ₂ {(2-py) ₃ COEt}]	(C3c)	[Pt(COMe) ₂ {(2-py) ₂ PhCOMe}]	(C4b)
[Pt(COMe) ₂ {(2-py) ₃ COMe}]	(C3b)	[Pt(COMe) ₂ {(2-py) ₂ (<i>m</i> -Tol)COH}]	(C5a)
[Pt(COMe) ₂ {(2-py) ₃ COBn}]	(C3d)	[Pt(COMe) ₂ {(2-py) ₂ (<i>m</i> -Tol)COMe}]	(C5b)
[Pt(COMe) ₂ (C≡CSiMe ₃) ₂ {(3,5-Me ₂ pz) ₃ CH}]OTf			(C8a)
[Pt(COMe) ₂ (C≡CPh){(3,5-Me ₂ pz) ₃ CH}]OTf			(C8b)
[Pt(COMe) ₂ (C≡C'Bu){(3,5-Me ₂ pz) ₃ CH}]OTos			(C8c)
[Pt(COMe) ₂ (C≡C'Pr){(3,5-Me ₂ pz) ₃ CH}]OTos			(C8d)
Sn(2-py) ₄	(D1a)	Sn(6-Me-2-py) ₄	(D1b)

Die beiden häufig verwendeten Platin(II)-Precursorskomplexe sind mit Ziffern nummeriert:

[Pt ₂ {(COMe) ₂ H} ₂ (μ-Cl) ₂]	(1)	[Pt(COMe) ₂ (NH ₂ Bn) ₂]	(2)
---	-----	--	-----

1. Einleitung und Problemstellung

Organometallverbindungen der Platinmetalle spielen in der industriellen homogenen Katalyse eine herausragende Rolle. Hydrierungsreaktionen von Olefinen (Wilkinson) bzw. Hydroformylierungsreaktionen unter Verwendung von Rh-Katalysatoren [1] oder der vielfältige Einsatz von Pd-Katalysatoren bei der Oxidation von Ethylen (Wacker-Prozess) [2], in der Olefinmetathese [3] sowie bei C–C-Kupplungsreaktionen (Heck, Stille, Suzuki, Sonogashira) [4] seien hier als Beispiele genannt. Platin hingegen wird hauptsächlich in heterogen katalysierten Verfahren wie bei der Oxidation von NH₃ am Pt-Netz (Ostwald-Verfahren) oder für Hydrierungsreaktionen verwendet, während der Speier- und Karstedt-Katalysator [5] in Hydrosilylierungsreaktionen eines der wenigen Beispiele für die Anwendung von Organoplatinverbindungen in der homogenen Katalyse darstellt. Dieser Unterschied (Pt vs.Pd) ist auf eine vergleichsweise hohe thermodynamische Stabilität von Pt–C-Bindungen gepaart mit einer relativ hohen kinetischen Stabilität von vielen metallorganischen Platinkomplexen zurückzuführen. Das steht im Allgemeinen einer hohen katalytischen Aktivität verglichen mit analogen Palladiumkomplexen entgegen.

Aufgrund der vergleichsweise hohen Stabilität vieler Organoplatinverbindungen finden diese jedoch in der Grundlagenforschung eine breite Anwendung, beispielsweise zur Isolierung und Untersuchung relevanter katalytischer Zwischenstufen wie π -Olefin-, π -Alkin- oder Hydrido-komplexe sowie zum Studium von Elementarschritten, die in der metallorganischen Chemie und der homogenen Katalyse von Bedeutung sind. Das trifft insbesondere auf oxidative Additions- und reduktive Eliminierungsreaktionen zu, die bei der Aktivierung und Funktionalisierung von C–H-Bindungen von zentraler Bedeutung sind. Ein weiterer Vorteil von Platinumverbindungen ist die magnetische Aktivität des ¹⁹⁵Pt-Kerns (Häufigkeit: 33.8%; Kernspin: $\frac{1}{2}$), da mit $\delta(^{195}\text{Pt})$ und den entsprechenden Kopplungskonstanten eine nützliche Sonde zur Charakterisierung der Elektronenstruktur in Platinkomplexen zur Verfügung steht [6]. Das ermöglicht zum Beispiel detaillierte Aussagen zum *trans*-Einfluss von Liganden [7].

Auch Carbenkomplexe, darunter Hydroxycarbenkomplexe, spielen sowohl in der metallorganischen Chemie als auch der homogenen Katalyse eine wichtige Rolle. Hydroxycarbenkomplexe weisen jedoch im Allgemeinen eine vergleichsweise geringe Stabilität auf [8]. Das ist in Metalla- β -diketonen, die sich von der Enolform organischer 1,3-Diketone durch (formale) Substitution der zentralen Methingruppe durch ein Metallfragment L_xM ableiten, nicht der Fall, weil hier der Hydroxycarbenligand durch eine O–H…O-Wasserstoffbrücke zu einem *cis*-ständigen Acylliganden stabilisiert ist (Abbildung 1).

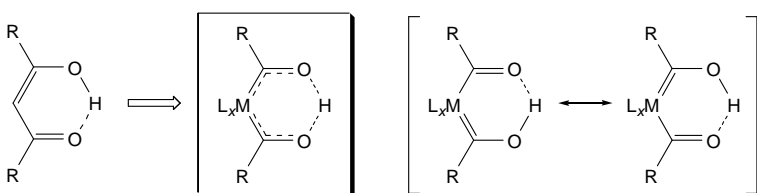


Abbildung 1. Formaler Weg vom organischen 1,3-Diketon zum Metalla-β-diketon.

Die ersten Metalla-β-diketone des Typs $[M\{(COR)(COR')H\}L_x]$ ($M = Mn, Re, Fe, \dots; L = CO, Cp, \dots$; Typ **I** in Abbildung 2) wurden von Lukehart und Mitarbeitern durch Umsetzung von Acyl(carbonyl)-Metallkomplexen mit Lithiumorganylen und anschließender Protonierung des gebildeten Diacylmethat-Komplexes erhalten [9, 10]. Diese Metalla-β-diketone sind kinetisch inert und elektronisch gesättigt (18 ve; ve = Valenzelektronen). Im Unterschied dazu handelt es sich bei den in unserer Arbeitsgruppe hergestellten Platina-β-diketonen (Typ **II** in Abbildung 2) um kinetisch vergleichsweise labile, elektronisch ungesättigte (16 ve) Verbindungen [11], was eine grundsätzlich andere Reaktivität zur Folge hat. Die in der Arbeitsgruppe von Garralda hergestellten Irida-β-diketone wie $[IrHCl\{(PPh_2(o-C_6H_4CO))_2H\}]$ (**III** in Abbildung 2) sind zwar auch 18-ve-Komplexe, unterscheiden sich aber bedingt durch den Hydrido- und Chloridoliganden in ihrer Reaktivität sowohl von den Lukehart'schen Metalla-β-diketonen (**I**) als auch von den Platina-β-diketonen (**II**) [12].

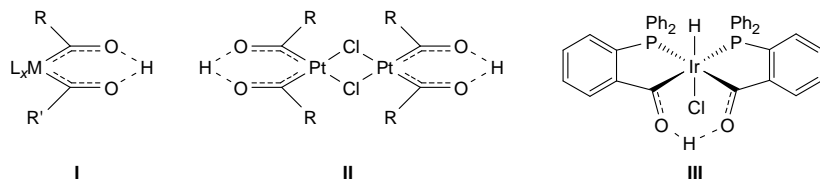
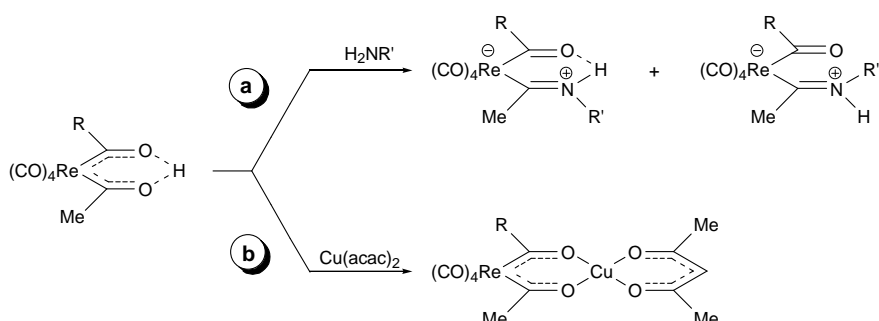


Abbildung 2. Lukehart'sche Metalla-β-diketone (**I**), Platina-β-diketone (**II**) und Irida-β-diketone (**III**).

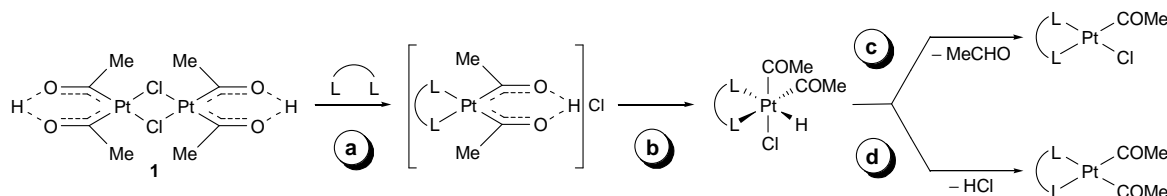
Die kinetisch inerte und elektronisch gesättigte Struktur der Lukehart'schen Metalla-β-diketone bedingt zwei typische Reaktionswege: a) Nucleophile greifen im Allgemeinen das Carbenkohlenstoffatom an. So erfolgt im Fall der Umsetzung mit Ammoniak und primären Aminen wie beispielsweise Anilin die Bildung von Metalla-β-ketoiminen (Schema 1, **a**)



Schema 1.

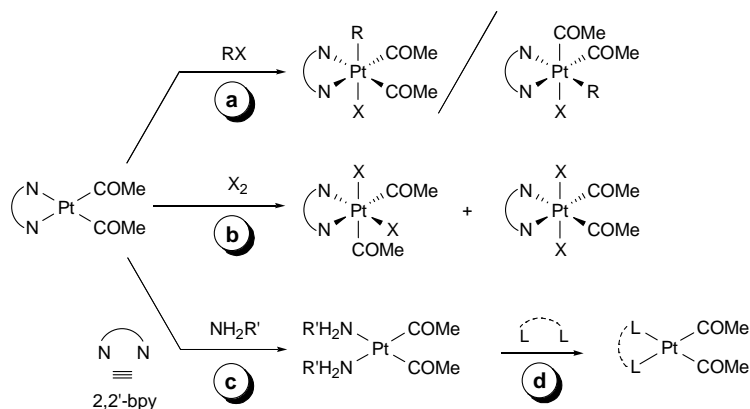
[10,13]. b) Eine Deprotonierung des Hydroxycarbens führt in Umkehrung der Bildung zu anionischen Diacylkomplexen oder zur Bildung von Metallkomplexen mit Metalla- β -diketonato-Liganden (Schema 1, **b**) [10].

Im Unterschied dazu sind bei den dinuklearen, kinetisch labileren und elektronisch ungesättigten Platina- β -diketonen das Zentralatom (Pt) selbst und die Pt–Cl–Pt-Brücken Zentren hoher Reaktivität. Das spiegelt sich in der Umsetzung mit bidentaten Liganden wider, die am Beispiel der „Stammverbindung“ (Typ **II** in Abbildung 2; R = Me, **1**) gemäß der Reaktionskaskade in Schema 2 abläuft: Einer Brückenspaltung (**a**) folgt eine H-Verschiebung (**b**), die als oxidative Addition angesehen werden kann und zu Hydrido(acetyl)platin(IV)-Komplexen führt [14]. Diese können einer reduktiven C–H-Eliminierung unter Abspaltung von Acetaldehyd (**c**) [14, 15] oder – insbesondere in Gegenwart von Basen – einer reduktiven HCl-Eliminierung unterliegen (**d**) [16, 17], wobei Acetyl(chlorido)- bzw. Diacetylplatin(II)-Komplexe gebildet werden. Coliganden des Typs P[^]P wie Bis(diphenyl)-phosphinoethan führen zu wenig stabilen Acetyl(hydrido)platin(IV)-Komplexen, während N[^]N-Donoren vom Bipyridin- bzw. Phenanthrolin-Typ thermisch außergewöhnlich stabile Acetyl(hydrido)platin(IV)-Komplexe ergeben. Im festen Zustand erfolgt eine Zersetzung unter reduktiver C–H-Eliminierung erst bei Temperaturen oberhalb von 170 °C.



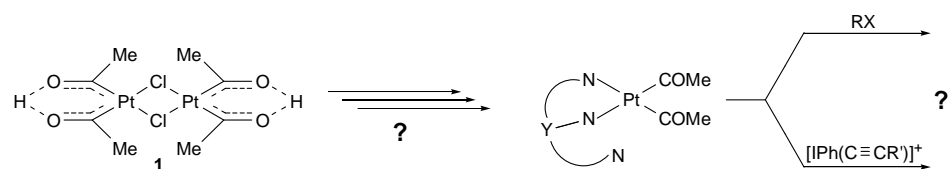
Schema 2.

Die Untersuchungen zur Reaktivität von Platina- β -diketonen haben somit neben Erkenntnissen zu den damit verknüpften metallorganischen Elementarschritten auch zu einem leichten Zugang zu Acetyl(chlorido)- und Diacetylplatin(II)-Komplexen geführt. Das hat wiederum Untersuchungen zur oxidativen Addition von Alkyhalogeniden, Halogenen oder Halogenwasserstoffen vor allem an Komplexen des Typs [Pt(COME)₂(N[^]N)] ermöglicht (Schema 3, **a/b**) [18]. Des Weiteren hat sich gezeigt, dass primäre Amine den 2,2'-Bipyridin-Liganden in [Pt(COME)₂(bpy)] leicht substituieren können, sofern sie in einem großen Überschuss vorliegen (Schema 3, **c**) [19]. Die erhaltenen Bis(amin)diacetylplatin(II)-Komplexe, insbesondere der Bis(benzylamin)-Komplex [Pt(COME)₂(NH₂Bn)₂] (**2**), stellen – bedingt durch den hohen *trans*-Einfluss bzw. -Effekt der Acetylgruppen – weitere nützliche Precursorkomplexe zur Synthese von Diacetylplatin(II)-Komplexen mit bidentaten *N*-Donor-[20] oder monodentaten *P*-Donorliganden [21] dar (Schema 3, **d**).

**Schema 3.**

Während also Umsetzungen des Platina- β -diketons **1** mit mono- und vor allem bidentaten *N*-Donorliganden und darauf aufbauend die Reaktivität von Diacetylplatin(II)-Komplexen des Typs $[\text{Pt}(\text{COMe})_2(\text{N}^{\wedge}\text{N})]$ in oxidativen Additionsreaktionen bereits sehr gut untersucht sind, stellt die Reaktion von **1** mit Bis(2-picolylo)amin, welche zur Bildung eines kationischen Diacetyl(hydrido)platin(IV)-Komplexes mit facial κ^3 -koordinierten Bis(2-picolylo)amin-Liganden führt, das einzige Beispiel für Reaktionen von **1** mit tridentaten *N*-Donorliganden dar [22].

Im Rahmen der vorliegenden Arbeit sollte die Reaktivität vom Platina- β -diketon **1** gegenüber facial κ^3N,N',N'' -koordinierenden Liganden mit dem Ziel untersucht werden, Diacetylplatin(II)-Komplexe zu erhalten (Schema 4). Die bevorzugte quadratisch-planare Koordination von Platin(II)-Komplexen ließ erwarten, dass in diesen Verbindungen die Liganden nur κ^2N,N' -gebunden sind. Das wiederum ermöglicht Studien zum Einfluss des dritten nicht koordinierten „Ligandenarms“ auf oxidative Additionsreaktionen. Dieser kann erheblich sein, weil eine Stabilisierung von koordinativ ungesättigten Zwischenstufen in Betracht zu ziehen ist. Insgesamt ist dabei die Bildung von neuartigen Acetylplatin(IV)-Komplexen mit facial koordinierenden tridentaten Liganden zu erwarten, möglicherweise auch solchen, die mit bidentaten Coliganden nur wenig stabil sind (Schema 4).

**Schema 4.**

2. Ergebnisse und Diskussion

2.1. Diacetylplatin-Komplexe mit κ^2 - und κ^3 -koordinierten Skorpionatliganden (siehe Publikation A im Anhang)

2.1.1. Einführung

Seit ihrer erstmaligen Darstellung im Jahre 1966 durch Trofimenko [23] haben Poly-(pyrazolyl)borate der allgemeinen Struktur $[RR'B(pz^x)_2]^-$ (pz^x = Pyrazol-1-yl mit nicht näher spezifiziertem Substitutionsmuster; R, R' = H, Alkyl, Aryl, pz^x , py...; Abbildung 3, **I**) eine breite Anwendung in der Haupt- und Übergangsmetallchemie gefunden [24]. Neben der Verwendung als bloßer „Zuschauerligand“ („spectator ligands“) in der Koordinationschemie werden besonders Tris(pyrazolyl)borate ($[RB(pz^x)_3]^-$) auch als Coliganden in katalytischen Reaktionen [24, 25] und zum Studium von Elementarschritten der Metallorganik eingesetzt [26]. Der Grund hierfür ist, dass eine Vielzahl von Verbindungen mit unterschiedlichen Substituenten an den Pyrazolylringen und/oder dem zentralen Boratom leicht zugänglich sind. Dies erlaubt eine gezielte Modifizierung der sterischen und/oder elektronischen Eigenschaften dieser anionischen Liganden. So können beispielsweise speziell unter Verwendung von Tris(pyrazolyl)borat-Liganden, bei denen die Pyrazolylringe an Position 3 substituiert sind, Metallzentren effektiv abgeschirmt werden und somit ungewöhnliche Bindungsverhältnisse untersucht oder reaktive Spezies stabilisiert werden. Substituenten an Position 4 und 5 hingegen dienen meistens zur Steuerung der Elektronendichte, als Kristallisantsanker oder zur Abschirmung der B–R-Gruppe [24].

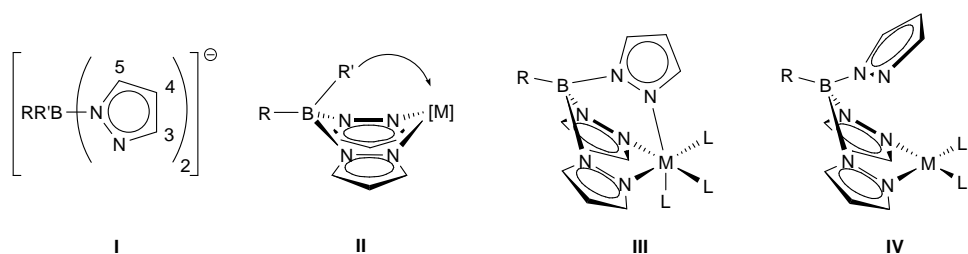
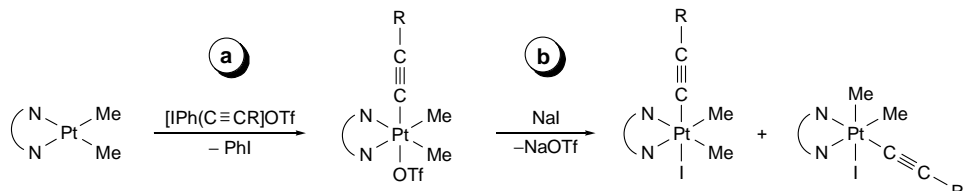


Abbildung 3. Nummerierungsschema von Skorpionatliganden (**I**) und typische Bootstruktur von Skorpionatkomplexen (**II**). Typische Koordinationsmodi von Tris(pyrazolyl)borat-Liganden in oktaedrischen (**III**) und quadratisch-planaren (**IV**) Metallkomplexen.

Trofimenko führte für diese Ligandenklasse den Oberbegriff „Skorpionate“ ein, wobei der Name auf die Struktur der Liganden bei Koordination an ein Metallzentrum zurückgeht. Aufgrund der sp^3 -Hybridisierung des Boratoms entsteht bei der Koordination von zwei Pyrazolyrringen an ein Metallzentrum ein sechsgliedriger Ring. Dieser weist eine Bootkonformation mit dem Metall- und dem Boratom an den Spitzen auf, was zu einem äquatorialen (R) und einem axialen (R') Substituenten am Boratom führt (Abbildung 3, **II**). Der

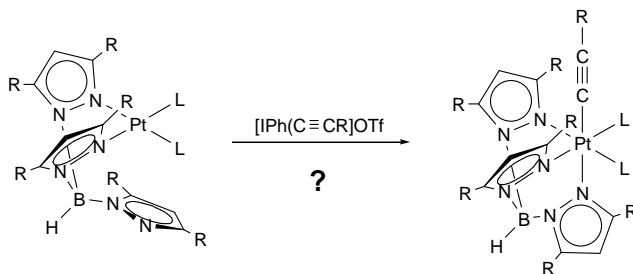
Substituent in axialer Position ist dabei zum Metallzentrum gerichtet. Wenn dieser über eine Donorgruppe ($R' = pz^x$, 2-py,...) verfügt, kann eine tridentate Koordination erreicht werden. Diese hat eine gewisse Ähnlichkeit mit einem Skorpion, der mit seinen beiden Zangen die Beute (das Metallzentrum) festhält und mit dem Stachel zusticht. Aus diesen geometrischen Voraussetzungen resultiert, dass Tris(pyrazolyl)borat-Liganden $[RB(pz^x)_3]^-$ in oktaedrischen Komplexen im Allgemeinen eine faciale κ^3N,N',N'' -Koordination aufweisen (Abbildung 3, III). Wie Cyclopentadienyl-Liganden handelt es sich um anionische Liganden, die formal Sechselektronendonoren sind. In oktaedrischen Komplexen weit weniger häufig beobachtet sind $\kappa^3N,N',B-H-$ (wenn $R = H$) oder κ^2N,N' -Koordinationsmodi [24].

In quadratisch-planaren Komplexen ist die bidentate κ^2N,N' -Koordination am weitesten verbreitet. Röntgenkristallographische Untersuchungen zeigen, dass sich der dritte Pyrazolylring im Festkörper quadratisch-planarer Platin-, Palladium- oder Rhodiumkomplexe in axialer Position der Bootstruktur befindet und somit in unmittelbarer Nähe zum Metallzentrum positioniert ist (Abbildung 3, IV) [27]. Das kann Reaktionen befördern, die einen Übergang von der quadratisch-planaren (κ^2N,N' -Koordinationsmodus) zur oktaedrischen Koordination (κ^3N,N',N'' -Koordinationsmodus) beinhalten. Erwähnenswert ist, dass in Rh(I)-Komplexen neben den quadratisch-planaren Strukturen auch quadratisch-pyramidalen bzw. trigonal-bipyramidalen Komplexen mit κ^3N,N',N'' -koordinierten Liganden gefunden worden sind [28]. Die bidentate Koordination von Tris(pyrazolyl)borat-Liganden in quadratisch-planaren Komplexen ist für Untersuchungen von oxidativen Additionsreaktionen mit Alkinylidonium-Verbindungen sehr interessant. Carty und Mitarbeiter konnten zeigen, dass durch formale Übertragung von $[C\equiv CR]^+$ unter gleichzeitiger Abspaltung von Phenylidod die hypervalenten Iodverbindungen $[IPh(C\equiv CR)]OTf$ mit Dimethylplatin(II)-Komplexen des Typs $[PtMe_2(N^+N)]$ oder $[PtMe_2(P^+P)]$ zu Alkinylplatin(IV)-Komplexen reagieren (Schema 5, a) [29]. Da die kationischen Alkinylidonium-Verbindungen nur in Gegenwart von schwach nukleophilen Anionen wie Triflat (OTf^-), Tosylat ($OTos^-$) oder Tetrafluoroborat stabil sind [30], mussten zur Besetzung der sechsten Koordinationsstelle zusätzliche, stärkere Donoren (Iodid, Pyridin) zugegeben werden, um hinreichend stabile Platin(IV)-Komplexe zu erhalten (Schema 5, b) [29, 31].



Schema 5.

Im Fall analoger Reaktionen von Verbindungen des Typs $[\text{PtL}_2\{(pz^x)_3\text{BH}\}]$ mit κ^2N,N' -gebundenen Skorpionatliganden sollte der dritte Pyrazolylring, welcher sich in unmittelbarer Nähe zum Metallzentrum befindet, nach Übertragung des $[\text{C}\equiv\text{CR}]^+$ -Fragments sofort die sechste Koordinationsstelle besetzen können, ohne dass ein „externer“ Donor zugegeben werden muss (Schema 6). Im Vergleich zu den Reaktionen an $[\text{PtMe}_2(\text{N}^\wedge\text{N})]$ mit bidentaten N -Donorliganden, würde so ein weiterer Reaktionsschritt entfallen.

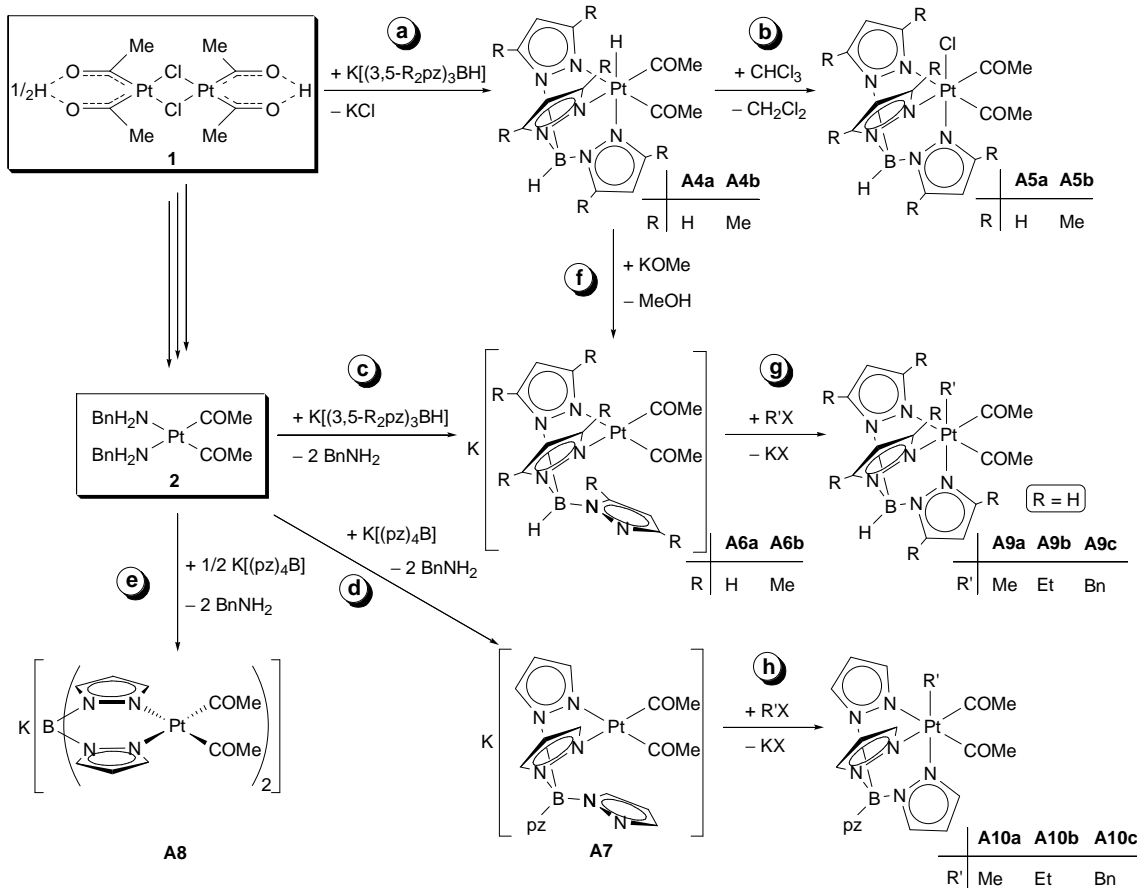


Schema 6.

2.1.2. Synthese und Reaktivität

Reaktionen des Platina- β -diketons **1** mit den Tris(pyrazolyl)boraten des Typs $\text{K}\{(\text{3,5-R}_2\text{pz})_3\text{BH}\}$ ($\text{R} = \text{H}, \text{Me}$) führten zur Bildung der thermisch stabilen Diacetyl(hydrido)platin(IV)-Komplexe **A4** mit κ^3 -koordinierten Skorpionatliganden (Schema 7, **a**). In analogen Umsetzungen von **1** mit Tetrakis(pyrazolyl)borat ($\text{K}\{(\text{pz})_4\text{B}\}$) wurden jedoch nur Produktgemische aus mehreren nicht identifizierten Verbindungen erhalten. Lösungen von $[\text{Pt}(\text{COMe})_2\text{H}\{(\text{3,5-R}_2\text{pz})_3\text{BH}\}]$ ($\text{R} = \text{H}, \text{A4a}; \text{Me}, \text{A4b}$) in Chloroform sind nicht stabil und reagierten innerhalb von zwei Tagen zu den entsprechenden Diacetyl(chlorido)platin(IV)-Komplexen **A5** (Schema 7, **b**). Längere Reaktionszeiten führten zu einer unspezifischen Zersetzung der gebildeten Chloridokomplexe $[\text{Pt}(\text{COMe})_2\text{Cl}\{(\text{3,5-R}_2\text{pz})_3\text{BH}\}]$ ($\text{R} = \text{H}, \text{A5a}; \text{Me}, \text{A5b}$). Da bei NMR-Versuchen in deuteriertem Chloroform CDHCl_2 detektiert wurde und die Reaktionszeiten durch Abdunkeln deutlich erhöht werden konnten, kann ein radikalischer Reaktionsmechanismus angenommen werden, welcher auch für die unter deutlich schärferen Bedingungen (CCl_4 , UV-Licht-Einstrahlung) ablaufende Reaktion des strukturell sehr ähnlichen Hydridokomplexes $[\text{PtMe}_2\text{Cl}\{(\text{3,5-Me}_2\text{pz})_3\text{BH}\}]$ zum entsprechenden Chloridokomplex diskutiert wird [32].

Anionische Diacetylplatin(II)-Komplexe mit κ^2 -gebundenen Tris- und Tetrakis(pyrazolyl)-borat-Liganden sind in Ligandenaustauschreaktionen mit dem Bis(benzylamin)platin(II)-Komplex **2** zugänglich (Schema 7, **c–e**). Während Umsetzungen von $[\text{Pt}(\text{COMe})_2(\text{NH}_2\text{Bn})_2]$ (**2**) mit äquimolaren Mengen des entsprechenden Skorpionatliganden zur Bildung der

**Schema 7.**

mononuklearen Komplexe $[\text{Pt}(\text{COMe})_2\{(3,5-\text{R}_2\text{pz})_3\text{BH}\}]$ ($\text{R} = \text{H}$, **A6a**; Me , **A6b**) und $\text{K}[\text{Pt}(\text{COMe})_2\{(\text{pz})_4\text{B}\}]$ (**A7**) führten (Schema 7, **c/d**), wurde bei der Reaktion von **2** mit einem halben Äquivalent $\text{K}[(\text{pz})_4\text{BH}]$ der schwerlösliche dinukleare Komplex **A8**, bei dem zwei Diacetylplatin-Fragmente über den Skorpionatliganden verbrückt sind, isoliert (Schema 7, **e**). Alle Verbindungen wurden als farblose, luft- und feuchtigkeitsempfindliche Feststoffe erhalten, wobei $\text{K}[\text{Pt}(\text{COMe})_2\{(\text{pz})_4\text{B}\}]$ (**A7**) eine deutliche höhere Stabilität gegenüber Luft und Feuchtigkeit aufweist als die Komplexe **A6** mit Tris(pyrazolyl)borat-Liganden. Die Umsetzung der Hydridokomplexe **A4** mit Kaliummethanolat gemäß Schema 7, **f** stellt eine alternative Syntheseroute für die Diacetylplatin(II)-Komplexe **A6** mit Tris(pyrazolyl)borat-Liganden dar. Dagegen sind die Verbindungen **A7** und **A8** nur in der Reaktionsfolge Platina-β-diketon (**1**) → Bis(benzylaminoplatin(II))-Komplex (**2**) → Diacetylplatin(II)-Komplex zugänglich.

Umsetzungen von $[\text{Pt}(\text{COMe})_2\{(\text{pz})_3\text{BH}\}]$ (**A6a**) und $\text{K}[\text{Pt}(\text{COMe})_2\{(\text{pz})_4\text{B}\}]$ (**A7**) mit Alkylhalogeniden führten gemäß Schema 7 **g/h** zur Bildung der neutralen Diacetylplatin(IV)-Komplexe $[\text{Pt}(\text{COMe})_2\text{R}\{(\text{pz})_3\text{BH}\}]$ ($\text{R} = \text{Me}$, **A9a**; Et , **A9b**; Bn , **A9c**) bzw. $[\text{Pt}(\text{COMe})_2\text{R}\{(\text{pz})_4\text{B}\}]$ ($\text{R} = \text{Me}$, **A10a**; Et , **A10b**; Bn , **A10c**), wobei die Reaktionen mit Methyliodid deutlich schneller abliefen als die Umsetzungen mit Ethyliodid bzw. Benzylbromid. Da alle

Komplexe luft- und feuchtigkeitsstabil sind, konnten die gebildeten Kaliumsalze mittels wässriger Extraktion abgetrennt werden. Die Konstitution der in Ausbeuten von 46% bis 87% isolierten farblosen Feststoffe wurde NMR- (^1H , ^{13}C , ^{195}Pt) und IR-spektroskopisch sowie durch Elementaranalyse (**A4**, **A9**, **A10**) bzw. hochauflösende Massenspektrometrie (HR-ESI-MS, **A5–A8**) und durch Röntgeneinkristallstrukturanalysen (**A4a**, **A5a**, **A7·(18C6)**, **A9c**) sichergestellt.

Bei Umsetzungen der Diacetylplatin(II)-Komplexe $[\text{Pt}(\text{COMe})_2\{(3,5-\text{R}_2\text{pz})_3\text{BH}\}]$ ($\text{R} = \text{H}$, **A6a**; Me, **A6b**) und $\text{K}[\text{Pt}(\text{COMe})_2\{(\text{pz})_4\text{B}\}]$ (**A7**) mit den Alkinylodonium-Verbindungen $[\text{IPh}(\text{C}\equiv\text{CSiMe}_3)]\text{OTf}$ und $[\text{IPh}(\text{C}\equiv\text{C}^t\text{Bu})]\text{OTos}$ wurden ausschließlich Produktgemische verschiedener nicht identifizierter Verbindungen isoliert. Da das bei oxidativen Additionsreaktionen mit Alkinylodonium-Verbindungen als Nebenprodukt gebildete Phenylidod mittels GC/MS detektiert wurde, kann angenommen werden, dass thermisch instabile Alkinylplatin(IV)-Komplexe gebildet wurden und diese sich bei der Isolierung zersetzen.

2.1.3. Spektroskopische Charakterisierung

In Tabelle 1 sind charakteristische spektroskopische Parameter der Komplexe **A4–A10** zusammengestellt. Aufgrund der Spiegelsymmetrie der Komplexe **A4–A10** in Lösung wird in den NMR-spektroskopischen Untersuchungen für die H- und C-Atome beider Acetylliganden jeweils nur ein Signal gefunden. Die Protonen der Pyrazolylringe der Komplexe mit Tris(pyrazolyl)borat-Liganden **A4–A6** und **A9** ergeben deshalb Signalsätze mit einem Intensitätsverhältnis von 2:1, während für den Diacetylplatin(II)-Komplex **A7** und die Diacetyl-(alkyl)platin(IV)-Komplexe **A10** mit Tetrakis(pyrazolyl)borat-Liganden dementsprechend Signalsätze im Verhältnis 2:2 (**A7**) bzw. 2:1:1 (**A10**) zu beobachten sind. Das Inversionszentrum am Boratom des Skorpionatliganden im dinuklearen Komplex **A8** führt zur chemischen und magnetischen Äquivalenz beider Diacetylplatin-Fragmente und somit nur zu einem Signalsatz sowohl für die Acetylgruppen als auch für alle vier Pyrazolylringe.

Die chemischen Verschiebungen der Carbonylkohlenstoffatome der Acetylgruppen werden in den Diacetylplatin(II)-Komplexen **A6–A8** im typischen Bereich [16, 19] bei ca. 230 ppm gefunden und sind damit im Vergleich zu den für die Diacetylplatin(IV)-Komplexe **A4**, **A5**, **A9** und **A10** (δ_{C} 187.5–196.2) beobachteten Werten signifikant um ca. 30–38 ppm zu tiefem Feld verschoben. Auch die δ_{C} -Resonanzen der Methylgruppen der Acetylgruppen in **A6–A8** weisen mit Ausnahme der Hydridokomplexe **A4** eine leichte Tieffeldverschiebung um ca. 7–10 ppm auf. Die δ_{H} -Resonanzen der Acetylgruppen in den Platin(II)-Komplexen

Tabelle 1. Charakteristische spektroskopische Parameter der Diacetylplatin(II)- (**A6–A8**) und Diacetylplatin(IV)-Komplexe (**A4, A5, A9, A10**) mit Skorpionatliganden (δ in ppm; J in Hz; ν in cm^{-1}).

	COCH_3 $\delta_{\text{H}} (^3J_{\text{Pt,H}})$	COCH_3 $\delta_{\text{C}} (^2J_{\text{Pt,C}})$	COCH_3 $\delta_{\text{C}} (^1J_{\text{Pt,C}})$	δ_{Pt}	$\nu(\text{B–H})$
Diacetylplatin(II)-Komplexe					
A6a	2.04	44.5	234.6	-3351.4	2454
A6b	1.73	44.0	235.3	-3372.7	2466
A7	1.85	44.1	234.5	-3371.4	–
A8	1.80	43.6	226.5	-3339.8	–
Diacetyl(hydrido)- (A4) und Diacetyl(chlorido)platin(IV)-Komplexe (A5)					
A4a	2.60 (23.9)	44.3 (255.3)	191.6	-1618.1	2481
A4b	2.32 (13.7)	40.4 (206.9)	195.5 (896.3)	-1740.0	2513
A5a	2.79 (8.9)	35.1 (91.5)	187.5 (736.6)	-762.9	2528
A5b	2.52 (6.6)	33.2 (94.6)	190.8 (736.6)	-763.0	2553
Diacetyl(alkyl)platin(IV)-Komplexe					
A9a	2.29 (10.7)	36.5 (184.0)	194.3 (936.6)	-1461.5	2483
A9b	2.25 (9.8)	36.7 (182.2)	194.6 (981.9)	-1396.5	2489
A9c	2.24 (8.9)	35.7 (168.6)	194.1 (956.8)	-1281.5	2481
A10a	2.36 (11.0)	36.7 (181.9)	196.2 (939.3)	-1489.2	–
A10b	2.31 (10.1)	35.5 (181.3)	194.8 (970.6)	-1436.4	–
A10c	2.29 (9.0)	36.5 (169.6)	194.9 (951.6)	-1314.8	–

A6–A8 liegen im Bereich von 1.73–2.04 ppm und sind damit im Vergleich zu den Verschiebungen in den Platin(IV)-Komplexen **A4, A5, A9** und **A10** um ca. 0.3–0.9 ppm zu höherem Feld verschoben.

Die ^{195}Pt -Verschiebungen der Platin(II)-Komplexe **A4–A6** liegen im Bereich anderer Diacetylplatin(II)-Komplexe mit zwei neutralen *N*-Donorliganden (δ_{Pt} ca. -3350) [16, 19] und sind, wie erwartet [33], im Vergleich zu den Platin(IV)-Komplexen **A4, A5, A9** und **A10** um mehr als 1600 ppm hochfeldverschoben. Die ^{195}Pt -Resonanzen der Platin(IV)-Komplexe sind des Weiteren in Korrelation mit der ansteigenden Elektronegativität des sechsten Liganden ($\chi_{\text{Cl}} > \chi_{\text{Alkyl}} > \chi_{\text{H}}$) immer stärker zu tiefen Feld verschoben und weisen keine signifikante Abhängigkeit von der Natur des Skorpionatliganden auf.

Wie bereits für quadratisch planare (κ^2) bzw. trigonal pyramidal (κ^3) Rhodiumkomplexe mit Tris(pyrazoyl)borat-Liganden gezeigt [28], ist auch im Fall der Komplexe **A4–A6** und **A9** die Frequenz der B–H-Valenzschwingung charakteristisch für den Koordinationsmodus des

Liganden. So liegen diese Absorptionsbanden in den Platin(II)-Komplexen mit κ^2 -koordinierten Tris(pyrazolyl)borat-Liganden (2454 cm^{-1} , **A6a**; 2466 cm^{-1} , **A6b**) bei niedrigeren Wellenzahlen ($\Delta\nu \geq 27\text{ cm}^{-1}$ bzw. $\Delta\nu \geq 47\text{ cm}^{-1}$) als bei den entsprechenden Platin(IV)-Komplexen **A4**, **A5** und **A9** mit κ^3 -koordinierten Liganden. Durch die Koordination des dritten Pyrazolylringes wird der Ligand deutlicher starrer, was zu einer erschwerten Schwingung führen könnte. Des Weiteren führt die Methylsubstitution in $(3,5\text{-Me}_2\text{pz})_3\text{BH}^-$ zu einer Verschiebung der B–H-Valenzschwingung zu höheren Wellenzahlen ($\Delta\nu 12\text{--}32\text{ cm}^{-1}$) im Vergleich zu den Komplexen mit dem unsubstituierten Liganden.

2.1.4. Strukturelle Charakterisierung

Von allen wesentlichen Typen der zuvor beschriebenen Skorpionatkomplexe konnte jeweils ein Vertreter (**A4a**, **A5a**, **A7**·(18C6), **A9c**) strukturell charakterisiert werden. So sind im Festkörper des Diacetyl(hydrido)platin(IV)-Komplexes **A4a** sowie des analogen Diacetyl(chlorido)platin(IV)-Komplexes **A5a** die Platinatome aufgrund des „Bisses“ des Tris(pyrazolyl)borat-Liganden [24] verzerrt oktaedrisch koordiniert: Alle N–Pt–N Winkel ($83.7(1)\text{--}87.4(1)^\circ$) sind kleiner als 90° . Die Pt–N-Bindungslänge *trans* zum Hydridoliganden ($2.162(6)$ Å, **A4a**) ist im Vergleich zur Bindungslänge *trans* zum Chloridoliganden ($2.060(4)$ Å, **A5a**) deutlich länger, was den höheren *trans*-Einfluss des Hydridoliganden widerspiegelt [34]. Die Pt–N-Bindungslängen *trans* zu den Acetylliganden liegen im Bereich von $2.174(4)$ Å bis $2.219(4)$ Å und lassen vermuten, dass der *trans*-Einfluss des Acetyl-liganden in einer vergleichbaren Größenordnung wie für einen Hydridoliganden liegt.

Die röntgeneinkristallographische Charakterisierung eines Diacetylplatin(II)-Komplexes gelang erst in Anwesenheit des Kronenethers 18C6 im Fall von $\text{K}[\text{Pt}(\text{COMe})_2\{(pz)_4\text{B}\}]$ (**A7**). Im Festkörper von **A7**·(18C6) ist das Kaliumkation neben dem Kronenether zusätzlich an den O-Atomen der Acetyl-liganden des Platinkomplexes koordiniert (Abbildung 4, **a**), was zu einer nahezu parallelen Anordnung (Interplanarwinkel $5.24(9)^\circ$) der Komplexebene und des Kronenethers führt (Abbildung 4, **b**). Der K···O₂ Abstand ($2.854(4)$ Å) liegt im Bereich der K···O-Abstände zwischen K- und O-Atomen des Kronenethers ($2.815(4)\text{--}2.992(3)$ Å), während der K···O₁-Abstand mit $2.770(5)$ Å sogar signifikant kürzer ist. Der kurze Pt···K-Abstand von $3.511(1)$ Å deutet auf eine zusätzliche attraktive Wechselwirkung unter Beteiligung des doppelt besetzten d_{z2} -Pt-Orbitals hin. Der Pt···K-Abstand ist vergleichbar mit den für $[\text{K}(18\text{C}6)]_2[\text{PtCl}_4]$ (3.668 Å) [35] bzw. $\text{K}[\text{PtCl}_3(\text{NH}_2^+\text{iPr})]\cdot\text{H}_2\text{O}$ (3.588 Å) [36] gefundenen Werten.

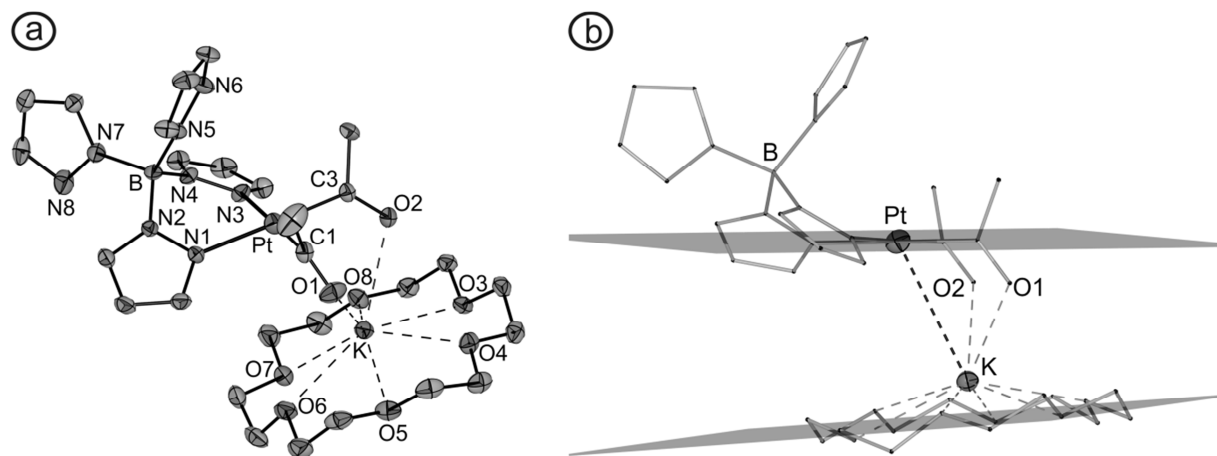


Abbildung 4. a) Molekülstruktur von $[K(18C_6)][Pt(\text{COMe})_2\{(pz)_4\text{B}\}]$ ($\text{A7}\cdot(18C_6)$). Die Ellipsoide sind mit einer Wahrscheinlichkeit von 30% dargestellt. Aus Gründen der Übersichtlichkeit sind keine H-Atome dargestellt. Ausgewählte strukturelle Parameter (Abstände in Å): $K\cdots O1$ 2.770(5), $K\cdots O2$ 2.854(4), $K\cdots O3$ 2.992(3), $K\cdots O4$ 2.815(4), $K\cdots O5$ 2.938(4), $K\cdots O6$ 2.900(4), $K\cdots O7$ 2.967(4), $K\cdots O8$ 2.922(4), $Pt\cdots K$ 3.511(1). b) Stabmodell des Komplexes, welches die relative Position der Komplexebene im Vergleich zur Ebene des Kronenethers, die durch die Lage Sauerstoffatome definiert wird, darstellt.

2.2. Diacetylplatin-Komplexe mit κ^2 - und κ^3 -koordinierten Tris(pyrazolyl)methan-Liganden

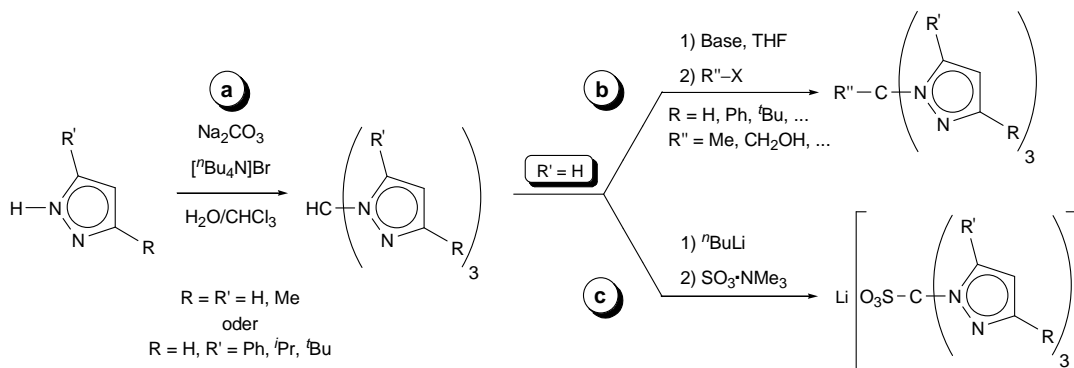
(siehe Publikation B im Anhang)

2.2.1. Einführung

Tris(pyrazolyl)methan-Verbindungen der allgemeinen Struktur $(\text{pz}^x)_3\text{CH}$ (pz^x = Pyrazol-1-yl mit nicht näher spezifiziertem Substitutionsmuster) sind die neutralen Analoga der in Kapitel 2.1.1. beschriebenen anionischen Tris(pyrazol)borate und leiten sich von diesen durch (formale) Substitution des B-Atoms durch ein C-Atom ab [37]. Im Vergleich zu den Skorpionenaten fand diese Ligandenklasse bis zum Beginn des neuen Jahrtausends aufgrund schwierigerer Synthesen mit geringen Ausbeuten nur wenig Beachtung als Coligand in der Koordinationschemie. Erst Fortschritte in der Synthese dieser Verbindungen und die Entwicklung neuer Möglichkeiten zur Derivatisierung bzw. Funktionalisierung führten zu einem merklichen Anstieg des Interesses an dieser Ligandenklasse [37].

Die Synthese der „Stammverbindung“ (Tris(pyrazolyl)methan, $(\text{pz})_3\text{CH}$) durch Umsetzung von Pyrazol mit Kalium und anschließender Zugabe von Chloroform wurde bereits im Jahre 1937 beschrieben [38]. In der heutigen Zeit stellt die Umsetzung von Pyrazol mit Na_2CO_3 und Chloroform in einer Zweiphasenreaktion (Wasser/Chloroform) die gebräuchlichste Methode zur Synthese von $(\text{pz})_3\text{CH}$ und verschiedenen an den Pyrazolyrringen substituierten Derivaten dar (Schema 8, a) [39]. Weiterhin kann – sofern die Position 5 der Pyrazolyrringe nicht substituiert ist ($R' = \text{H}$) – das acide Proton der C–H-Gruppe am Rückgrat des Liganden durch

geeignete Basen abstrahiert werden, was weitere Möglichkeiten zur Derivatisierung bzw. Funktionalisierung dieser Substanzklasse eröffnet (Schema 8, **b**) [40]. So konnten beispielsweise durch Umsetzung der lithiierten Verbindungen mit Schwefeltrioxid–Triethylamin auch hydrophile Substituenten eingeführt werden [37, 41]. Derartige Derivate könnten für die Synthese von Komplexen, die als Enzymmodelle unter physiologischen Bedingungen löslich und stabil sind, von großem Nutzen sein [40].



Schema 8.

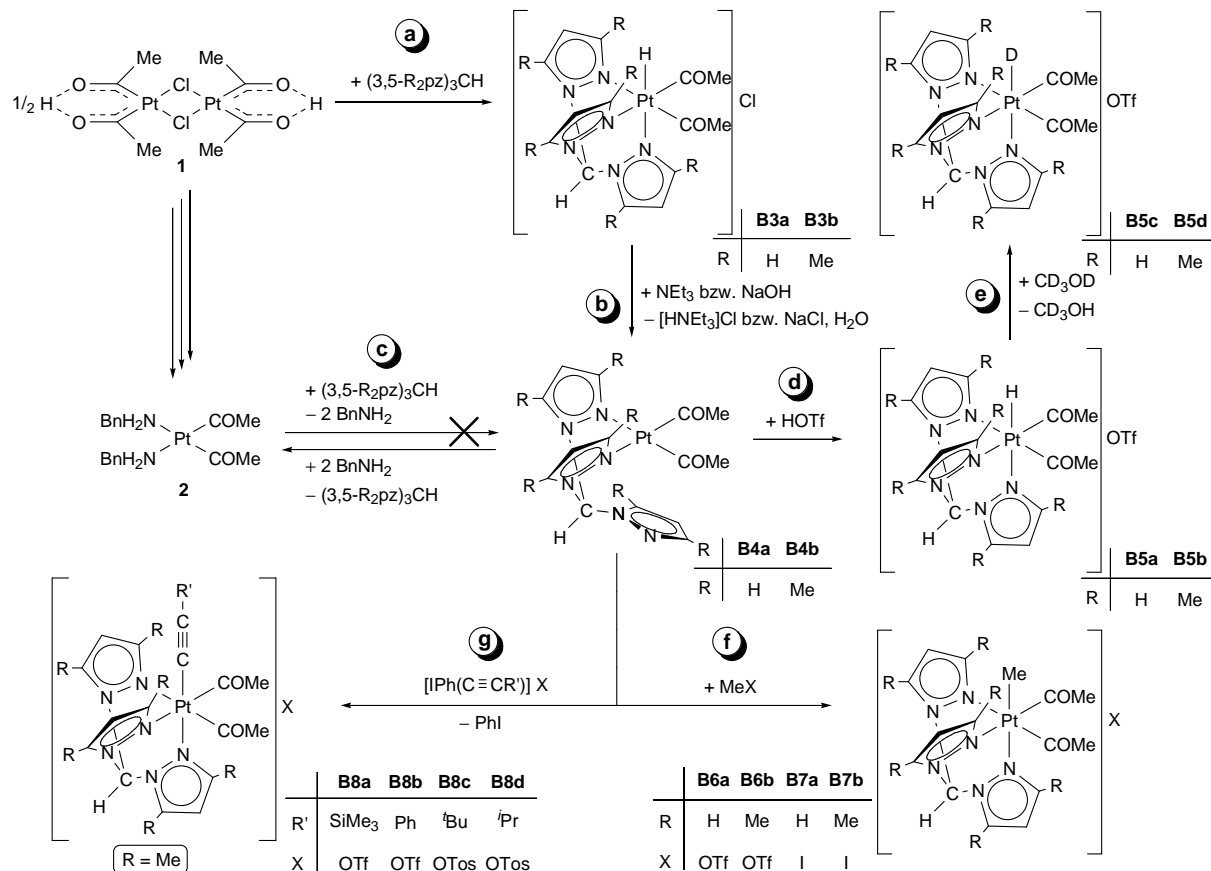
Tris(pyrazolyl)borat- und -methan-Liganden sind isoelektronisch zueinander und weisen, wie bereits in Kapitel 2.1.1. beschrieben, eine vergleichbare Struktur (Bootkonformation der $C(\mu\text{-pz})_2M$ -bzw. $B(\mu\text{-pz})_2M$ -Gruppe) und die gleichen geometrischen Einschränkungen (faciale κ^3N,N',N'' -Koordination in oktaedrischen und κ^2N,N' -Koordination in quadratisch-planaren Komplexen) auf. Aufgrund der anionischen Natur sind Skorpionate etwas basischer als die neutralen Tris(pyrazolyl)methane [42]. Nichtsdestotrotz können Tris(pyrazolyl)-methan-Liganden selbst Pd(IV)-Verbindungen stabilisieren [37] und der kationische Pd-Komplex $[Pd(\eta^3\text{-C}_3H_5)\{(R_2pz)_3CH\}]PF_6$ wird sogar als deutlich stabiler beschrieben als der analoge neutrale Komplex $[Pd(\eta^3\text{-C}_3H_5)\{(R_2pz)_3BH\}]$ mit Skorpionatliganden [43]. Dieses Beispiel zeigt, dass neben der Donorfähigkeit des Coliganden auch die Ladung der entsprechenden Komplexe (neutral vs. kationisch oder auch anionisch vs. neutral) einen Einfluss auf die Stabilität und/oder Reaktivität der Verbindungen haben kann.

In weiterführenden Untersuchungen sollte nun geklärt werden, ob sich Diacetylplatin(II)-bzw. -platin(IV)-Komplexe mit den Tris(pyrazolyl)methan-Liganden des Typs $(3,5\text{-R}_2pz)_3CH$ ($R = H, Me$) hinsichtlich Stabilität, Reaktivität und chemischer Eigenschaften von den analogen Komplexen mit Skorpionatliganden unterscheiden.

2.2.2. Synthese und Reaktivität

Umsetzungen des Platina- β -diketons **1** mit Tris(pyrazolyl)methanen des Typs $(3,5\text{-R}_2\text{pz})_3\text{CH}$ ($\text{R} = \text{H}, \text{Me}$) und anschließende Zugabe von Basen ($\text{NaOH}, \text{NEt}_3$) führten zur Bildung der Diacetylplatin(II)-Komplexe $[\text{Pt}(\text{COMe})_2\{(3,5\text{-R}_2\text{pz})_3\text{CH}\}]$ ($\text{R} = \text{H}, \text{B4a}; \text{Me}, \text{B4b}$) (Schema 9, **a/b**) mit κ^2 -koordinierten Tris(pyrazolyl)methan-Liganden. Beide Verbindungen sind in Lösung wenig stabil und weisen eine völlig unterschiedliche Löslichkeit auf: Während Komplex **B4a** (mit dem unsubstituierten Tris(pyrazolyl)methan-Liganden) nur in protischen Lösungsmitteln wie Methanol oder DMSO mäßig löslich ist, weist **B4b** aufgrund der zusätzlichen Methylgruppen an den Pyrazolylringen eine gute Löslichkeit in allen gängigen Lösungsmitteln auf. In nicht koordinierenden Lösungsmitteln läuft die Zersetzung von **B4b** deutlich schneller ab als in Methanol oder THF. Überraschenderweise waren die Diacetylplatin(II)-Komplexe **B4** nicht via Ligandenaustauschreaktionen ausgehend vom Bis(benzylamin)platin(II)-Komplex **2** zugänglich (Schema 9, **c**). Im Gegenteil: Die Umsetzungen der Verbindungen **B4** mit Benzylamin führten zur Bildung von **2**.

Die bei der Synthese von **B4** als Zwischenprodukt gebildeten kationischen Diacetyl(hydrido)-platin(IV)-Komplexe $[\text{Pt}(\text{COMe})_2\text{H}\{(3,5\text{-R}_2\text{pz})_3\text{CH}\}]\text{Cl}$ ($\text{R} = \text{H}, \text{B3a}; \text{Me}, \text{B3b}$) sind in Lösung thermisch instabil und konnten nicht isoliert werden. Die Konstitution dieser



Schema 9.

Verbindungen wurde aber mittels Tieftemperatur-NMR-Untersuchungen der Reaktionsansätze zweifelsfrei belegt. Die Stabilität kationischer Hydridoplatin(IV)-Komplexe dieses Typs hängt von der Natur des Anions ab, denn durch Protonierung der Diacetylplatin(II)-Komplexe **B4** mit Triflourmethansulfonsäure wurden die thermisch stabilen Hydridokomplexe $[\text{Pt}(\text{COMe})_2\text{H}\{(3,5-\text{R}_2\text{pz})_3\text{CH}\}]\text{OTf}$ ($\text{R} = \text{H}$, **B5a**; Me, **B5b**) mit Triflat als Anion erhalten (Schema 9, **d**). In Lösungen von **B5** in deuteriertem Methanol findet ein H/D-Austausch zwischen dem Lösungsmittel und dem Hydridoliganden statt (Schema 9, **e**). Die Komplexe $[\text{Pt}(\text{COMe})_2\text{D}\{(3,5-\text{R}_2\text{pz})_3\text{CH}\}]\text{OTf}$ ($\text{R} = \text{H}$, **B5c**; Me, **B5d**) mit Deuterido-liganden wurden isoliert und der H/D-Austausch durch ^1H - und ^2H -NMR-Spektroskopie belegt.

Weiterhin wurde die Reaktivität der Diacetylplatin(II)-Komplexe **B4** gegenüber Methyliodid, Trifluormethansulfonsäuremethylester und den Alkinyliodoium-Verbindungen $[\text{IPh}(\text{C}\equiv\text{CR})]\text{X}$ ($\text{R}/\text{X} = \text{SiMe}_3/\text{OTf}$, Ph/OTf , $^1\text{Bu}/\text{OTos}$, $^i\text{Pr}/\text{OTos}$) untersucht. Während das Substitutionsmuster der Tris(pyrazolyl)methan-Liganden ($(\text{pz})_3\text{CH}$ vs. $(\text{Me}_2\text{pz})_3\text{CH}$) keinen Einfluss auf die Stabilität der kationischen Diacetyl(methyl)platin(IV)-Komplexe $[\text{Pt}(\text{COMe})_2\text{Me}\{(3,5-\text{R}_2\text{pz})_3\text{CH}\}]\text{OTf}$ ($\text{R} = \text{H}$, **B6a**; Me, **B6b**) und $[\text{Pt}(\text{COMe})_2\text{Me}\{(3,5-\text{R}_2\text{pz})_3\text{CH}\}]\text{I}$ ($\text{R} = \text{H}$, **B7a**; Me, **B7b**) hat (Schema 9, **f**), wurden stabile Diacetyl(alkinyl)platin(IV)-Komplexe nur im Fall der Umsetzungen von $[\text{Pt}(\text{COMe})_2\{(3,5-\text{Me}_2\text{pz})_3\text{CH}\}]$ (**B4b**) mit Alkinyliodonium-Verbindungen erhalten (Schema 9, **g**). Die Beobachtungen bei den analogen Reaktionen des Diacetylplatin(II)-Komplexes $[\text{Pt}(\text{COMe})_2\{(\text{pz})_3\text{CH}\}]$ (**B4a**) mit dem unsubstituierten Tris(pyrazolyl)methan-Liganden lassen vermuten, dass auch in diesem Fall Alkinylplatin(IV)-Komplexe gebildet wurden, die jedoch thermisch instabil sind und sich im Verlauf der Isolierung zersetzen.

Bis auf die thermisch instabilen Hydridokomplexe **B3** wurden alle zuvor beschriebenen Verbindungen als farblose bis hellgelbe Feststoffe in Ausbeuten von 61 bis 90% isoliert und NMR- (^1H , ^{13}C , ^{195}Pt) und IR-spektroskopisch sowie durch hochauflösende Massenspektrometrie (HR-ESI-MS) und Röntgeneinkristallstrukturanalysen (**B4a**, **B4b**, **B7a**· CH_2Cl_2 , **B8a**·THF, **B8d**· CHCl_3) vollständig charakterisiert.

2.2.3. Strukturelle Charakterisierung

Neben den Diacetylplatin(II)-Komplexen **B4** und dem Diacetyl(methyl)platin(IV)-Komplex **B7a** konnten auch zwei Vertreter der Diacetyl(alkinyl)platin(IV)-Komplexe (**B8a**, **B8d**) strukturell charakterisiert werden. Die Moleküle im Festkörper von $[\text{Pt}(\text{COMe})_2\{(3,5-\text{R}_2\text{pz})_3\text{CH}\}]$ ($\text{R} = \text{H}$, **B4a**; Me, **B4b**) sind aufgrund schwacher intermolekularer

C–H···O-Wasserstoffbrückenbindungen zu eindimensionalen Strängen verknüpft. Im Fall von **B4a** liegen zwei Wasserstoffbrücken vor, bei denen jeweils das O-Atom eines Acetylliganden als H-Akzeptor und eine C–H-Gruppe der koordinierten Pyrazolylringe als H-Donor fungieren (C···O 3.016(6)–3.080(6) Å; H···O 2.13–2.25 Å; C–H···O 143–147°). Die strukturellen Parameter im Festkörper von **B4b** weisen auf eine Wasserstoffbrücke zwischen der C–H-Gruppe am Rückgrat des Tris(pyrazolyl)methan-Liganden und dem O-Atom eines Acetylliganden hin [44].

Im Festkörper von **B7a·CH₂Cl₂** liegt eine C–H···I Wasserstoffbrücke zwischen der C–H-Gruppe am Rückgrat des Tris(pyrazolyl)methan-Liganden und dem Iodidanion als H-Akzeptor vor (Abbildung 5). Sowohl der C···I- (3.716(5) Å) und H···I-Abstand (2.76 Å) als auch der C–H···I-Winkel (159°) liegen im Bereich solcher attraktiver Wechselwirkungen [45].

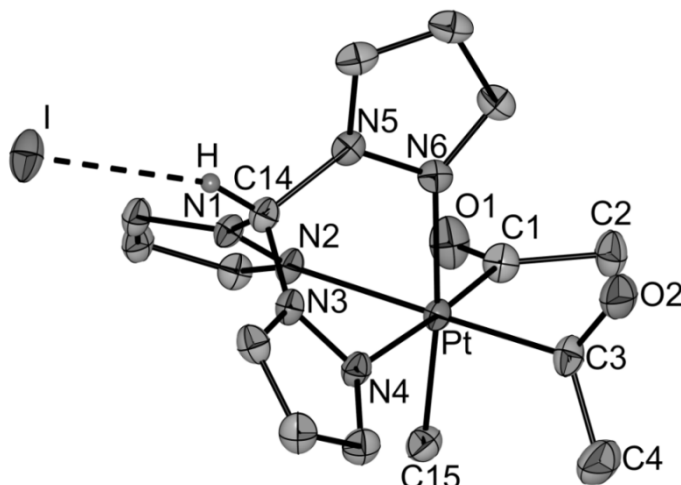


Abbildung 5. Molekülstruktur von $[\text{Pt}(\text{COMe})_2\text{Me}\{(\text{pz})_3\text{CH}\}]\text{I}$ (**B7a**) in Kristallen von $\mathbf{7a}\cdot\text{CH}_2\text{Cl}_2$. Die Ellipsoide sind mit einer Wahrscheinlichkeit von 30% dargestellt. Aus Gründen der Übersichtlichkeit sind keine H-Atome dargestellt. Ausgewählte strukturelle Parameter (Abstände in Å, Winkel in °): I···C14 3.716(5), I···H 2.76, I···H–C14 159.

In den Festkörperstrukturen der Diacetyl(alkinyl)platin(IV)-Komplexe $[\text{Pt}(\text{COMe})_2(\text{C}\equiv\text{CR})\{(\text{3,5-Me}_2\text{pz})_3\text{CH}\}]\text{X}$ ($\text{R/X} = \text{SiMe}_3/\text{OTf}$, **B8a**; $^i\text{Pr}/\text{OTos}$, **B8d**) sind die Pt–N-Bindungen *trans* zu den Acetyl-Liganden (2.208(3)–2.247(3) Å) im Vergleich zu den Bindungen *trans* zum Alkinyl-Liganden (2.100(3)/2.106(2) Å) signifikant länger, was für einen deutlich höheren *trans*-Einfluss der Acetyl-Liganden spricht. Die Pt–C≡C–R-Struktureinheiten sind annähernd linear (Pt–C≡C 177.7(4)/176.5(3)°, C≡C–Si/C≡C–C 174(4)/178.4(4)°) und die C≡C-Bindungslängen (1.180(6)/1.182(4) Å) liegen im Bereich von denen in anderen Alkinyl-platin(IV)-Komplexen [46] und typischen C–C-Dreifachbindungen [47].

2.2.4. Zur Moleküldynamik in Diacetylplatin(II)-Komplexen

Die bei Raumtemperatur aufgenommenen ^1H - und ^{13}C -NMR-Spektren der Diacetylplatin(II)-Komplexe $[\text{Pt}(\text{COMe})_2\{(3,5-\text{R}_2\text{pz})_3\text{CH}\}]$ ($\text{R} = \text{H}$, **B4a**; Me, **B4b**) deuten auf das Vorliegen eines dynamischen Prozesses, der zu einer chemischen und magnetischen Äquivalenz des nicht koordinierten mit den koordinierten Pyrazolylringen im Tris(pyrazolyl)methan-Liganden führt. So weist beispielsweise bei Raumtemperatur das ^1H -NMR-Spektrum von **B4a** für die Resonanzen der aromatischen Protonen jeweils nur ein, teilweise stark verbreitertes, Signal auf, welches bei tieferen Temperaturen in zwei Signalsätze mit einem Intensitätsverhältnis von 2:1 aufgespalten wird (Abbildung 6, a) [48]. In temperaturabhängigen ^1H -NMR-Messungen wurde beobachtet, dass die Koaleszenz der Signale der Pyrazolylprotonen im Komplex **B4b** generell bei höheren Temperaturen eintritt als bei **B4a** (Tabelle 2). Aus dem Zusammenhang $k_C = \pi \cdot \Delta v / \sqrt{2}$ (Δv = Shiftdifferenz der Signale bei eingefrorenem Austausch) und $\Delta G_C^\neq = 0.00458 \cdot T_C \cdot (10.32 + \log k_C/T_C)$ ließen sich die Gleichgewichtskonstanten am Koaleszenzpunkt abschätzen und die freien Aktivierungsenthalpien bei der Koaleszenztemperatur (T_C) berechnen (Tabelle 2) [49]. Komplex **B4b** mit dem methylsubstituierten Tris(pyrazolyl)methan-Liganden weist für die beobachtete Dynamik eine um ca. 2.5 kcal/mol höhere freie Aktivierungsenthalpie auf (15.9 vs. 13.4 kcal/mol), wobei sowohl diese Werte als auch die jeweiligen Koaleszenztemperaturen im Bereich von anderen dynamischen Prozessen in der Ligandensphäre von Palladium- und Platinkomplexen liegen [50, 51, 52, 53].

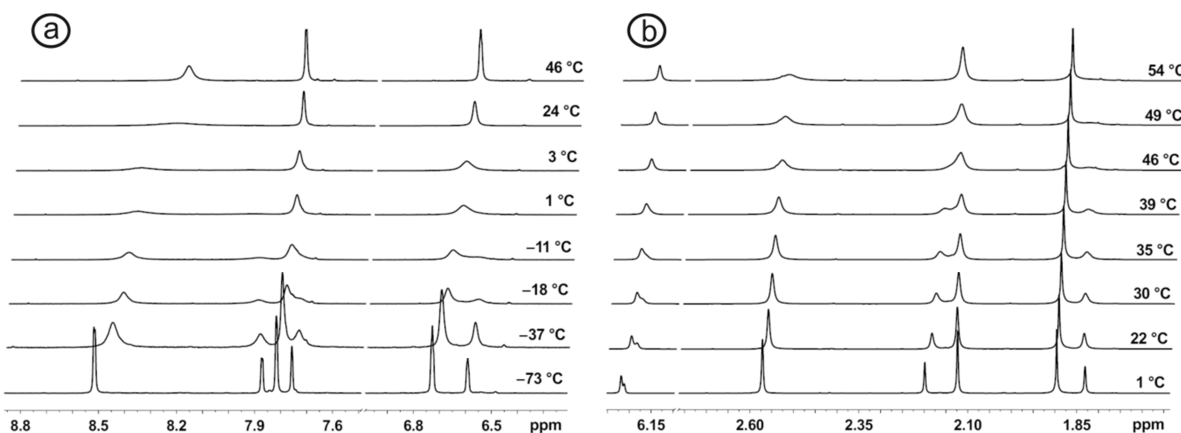


Abbildung 6. Relevante Bereiche der temperaturabhängigen ^1H -NMR-Spektren von **B4a** (a) und **B4b** (b).

Tabelle 2. Relevante Parameter der Dynamik und deren freie Aktivierungsenthalpien in Komplexen $[\text{Pt}(\text{COMe})_2\{(3,5-\text{R}_2\text{pz})_3\text{CH}\}]$ ($\text{R} = \text{H}$, **B4a**; Me, **B4b**).

	B4a			B4b	
	H3	H4	H5	H4	$\text{C}^3\text{-CH}_3$
T_C (in K)	262	276	297	312	322
Δv (in s^{-1})	28.3	62.7	268.9	14.9	68.2
k_C (in s^{-1})	62.9	139.3	597.3	33.1	151.5
ΔG_C^\ddagger (in kcal/mol)	13.2	13.4	13.6	16.2	15.7

Die Ergebnisse der NMR-spektroskopischen Untersuchungen sowie die geringe Stabilität der Komplexe **B4** in Lösung lassen vermuten, dass die κ^2N,N' -koordinierten Tris(pyrazolyl)-methan-Liganden nur relativ schwach gebunden sind. Der schnelle Austausch zwischen koordinierten und nicht koordinierten Pyrazolylringen könnte gemäß einem dissoziativen Mechanismus unter intermediärer Bildung eines T-förmigen Komplexes mit κN -koordinierten Liganden verlaufen. Alternativ ist auch ein assoziativer Mechanismus denkbar, der die Bildung eines Intermediates mit κ^3N,N',N'' -koordinierten Liganden beinhaltet.

Unter Einbeziehung dieser Überlegungen wurden quantenchemische Rechnungen auf DFT-Niveau durchgeführt. Die stabilsten Strukturen mit κ^2N,N' -koordinierten Liganden (Abbildung 7, **a** für **B4a**) sind sehr ähnlich den experimentell ermittelten Strukturen in Kristallen von **B4a** und **B4b**. Die berechneten T-förmigen Gleichgewichtsstrukturen (Intermediate beim dissoziativen Mechanismus) von **B4** weisen eine um 4.0 kcal/mol (**B4a**; Abbildung 7, **b**) bzw. 2.1 kcal/mol (**B4b**) höhere freie Aktivierungsenthalpie auf. Die Intermediate beim assoziativen Prozess mit κ^3N,N',N'' -gebundenen Tris(pyrazolyl)methan-Liganden konnten nicht als Gleichgewichtsstrukturen lokalisiert werden, wohl aber Strukturen, bei denen das N-Atom des nicht koordinierten Pyrazolylringes zum Platin gerichtet ist. Bei **B4a** (Abbildung 7, **c**) handelt es sich um eine Gleichgewichtsstruktur und bei **B4b** um einen Übergangszustand.

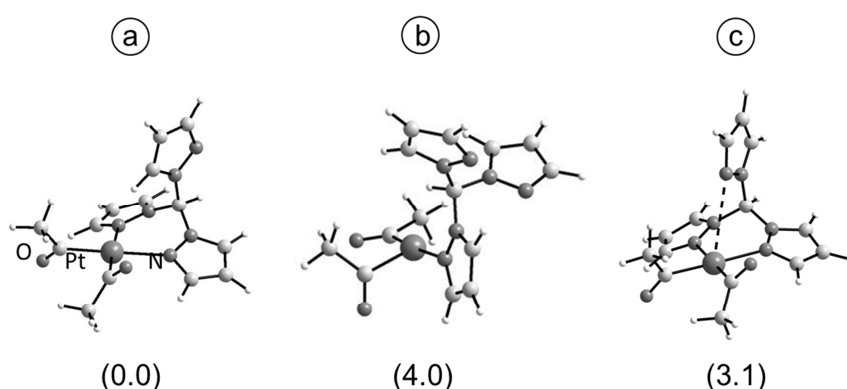


Abbildung 7. Berechnete Gleichgewichtsstrukturen von **B4a** mit einer κ^2N,N' - (a) und κN -Koordination (b) des Liganden. Die gestrichelte Linie (c) weist auf einen relativ kurzen, aber nichtbindenden $\text{Pt}\cdots\text{N}$ -Abstand von 3.535 Å hin. Die freien Standardaktivierungsenthalpien sind in Klammern bezogen auf das stabilste Isomer angegeben.

Weiterhin sind sowohl beim dissoziativen als auch beim assoziativen Mechanismus Rotationen innerhalb der Liganden und Ringinversionen der sechsgliedrigen Pt(N–N)₂C-Ringe zu berücksichtigen, damit sich die Dynamik ($pz_{\text{koord}} \rightleftharpoons pz_{\text{nichtkoord.}}$) vollziehen kann. Im Ergebnis dieser Analyse und unter Einbeziehung der Berechnungen zu den unterschiedlichen Koordinationsmodi der Liganden (vgl. Abbildung 7) kann geschlussfolgert werden, dass der dissoziative Mechanismus wahrscheinlicher ist als der assoziative und dass Komplex **B4b** mit methylsubstituiertem Tris(pyrazolyl)methan-Liganden eine höhere Aktivierungsbarriere für die Moleküldynamik aufweist als Verbindung **B4a** mit nichtsubstituierten Liganden. Letzteres steht im Einklang mit den NMR-spektroskopischen Ergebnissen.

2.2.5. Spektroskopische Charakterisierung von Diacetylplatin(IV)-Komplexen

Die Konstitution der Diacetylplatin(IV)-Komplexe **B3** sowie **B5–B8** wird durch ¹H-, ¹³C- und ¹⁹⁵Pt-NMR-spektroskopische Untersuchungen in vollem Umfang bestätigt (vgl. die Zusammenstellung von charakteristischen Parametern in Tabelle 3). Die Verschiebungen der Protonen der Acetylgruppen und die entsprechenden ³J_{Pt,H}-Kopplungskonstanten hängen

Tabelle 3. Charakteristische spektroskopische Parameter der kationischen Diacetylplatin(IV)-Komplexe **B3**, **B5–B8** (δ in ppm; J in Hz).

X	COCH ₃		$\delta_{\text{C}}(^1\text{J}_{\text{Pt,C}})$	HC(pz*) ₃ ^a	
	$\delta_{\text{H}}(^3\text{J}_{\text{Pt,H}})$	$\delta_{\text{C}}(^2\text{J}_{\text{Pt,C}})$		δ_{Pt}	
Diacetyl(hydrido)platin(IV)-Komplexe					
B3a^b	Cl	2.71	44.7 (257.1)	189.0	12.39
B3b^b	Cl	2.49	40.6 (209.3)	192.3	7.97
B5a	OTf	2.73 (28.5)	44.2 (263.9)	186.7	10.17
B5b	OTf	2.58 (17.7)	41.3 (222.0)	190.5	8.08
Diacetyl(methyl)platin(IV)-Komplexe					
B6a	OTf	2.48 (15.4)	35.8 (200.7)	189.5 (939.0)	10.30
B6b	OTf	2.31 (8.9)	34.1 (181.5)	193.3 (944.4)	8.20
B7a	I	2.47 (14.7)	35.8 (200.7)	189.2 (940.0)	12.22
B7b	I	2.31 (7.7)	34.2 (181.4)	193.2 (944.7)	8.18
Diacetyl(alkinyl)platin(IV)-Komplexe					
B8a	OTf	2.75 (13.6)	35.9 (187.1)	185.0 (787.9)	8.18
B8b	OTf	2.81 (14.0)	36.4 (181.2)	185.1 (780.2)	8.11
B8c	OTos	2.72 (13.3)	36.0 (186.1)	185.6 (795.1)	8.29
B8d	OTos	2.71 (13.6)	36.7 (181.9)	185.6 (795.1)	8.32

a) $pz^* = pz$ (**B3a**, **B5a**, **B6a**, **B7a**); 3,5-Me₂pz (**B3b**, **B5b**, **B6b**, **B7b**, **B8**) b) Bei –80°C in CD₂Cl₂ gemessen.

signifikant von der Art des Tris(pyrazolyl)methan-Liganden ab: So sind die Protonenresonanzen in Verbindungen mit dem unsubstituierten Liganden (**B3a**, **B5a–B7a**) um 0.15–0.22 ppm zu tieferem Feld verschoben und die $^3J_{\text{Pt},\text{H}}$ -Kopplungskonstanten sind um 6.5–9.8 Hz kleiner als in den jeweils analogen Komplexen mit dem methylsubstituierten Liganden (**B3b**, **B5b–B7b**). Im Gegensatz dazu weisen die δ_{C} der Acetyl-Liganden keine vergleichbare Differenzierung auf. Lediglich die $^2J_{\text{Pt},\text{C}}$ -Kopplungskonstanten sind in **B3a**, **B5a–B7a** um 19–46 Hz größer als in den entsprechenden Komplexen **B3b**, **B5b–B7b**. Weiterhin sind die ^{195}Pt -Resonanzen in Komplexen mit dem $(3,5\text{-Me}_2\text{pz})_3\text{CH}$ -Liganden um ca. 90–100 ppm zu höherem Feld verschoben als in den analogen Komplexen mit dem $(\text{pz})_3\text{CH}$ -Liganden, was auf eine größere Donorstärke des $(3,5\text{-Me}_2\text{pz})_3\text{CH}$ -Liganden bedingt durch den +I-Effekt der zusätzlichen Methylgruppen zurückzuführen sein könnte.

Während die Verschiebungen des Protons am Rückgrat des $(3,5\text{-Me}_2\text{pz})_3\text{CH}$ -Liganden sowohl im freien Liganden [54] als auch in den Verbindungen **B3b**, **B5b–B7b** und **B8** in einem engen Bereich um ca. 8 ppm liegt, ist δ_{H} im Fall der Diacetylplatin(IV)-Komplexe $[\text{Pt}(\text{COMe})_2\text{R}\{(\text{pz})_3\text{CH}\}]\text{X}$ ($\text{R}/\text{X} = \text{H}/\text{Cl}$, **A3a**; H/OTf , **B5a**; Me/OTf , **B6a**; Me/I , **B7a**) im Vergleich zum freien Liganden ($\delta_{\text{H}} 8.41$) [55] um 1.7–3.0 ppm zu tiefem Feld verschoben. Die Größe dieser Tieffeldverschiebung hängt dabei signifikant vom Anion ab ($\delta_{\text{H}} 12.39/12.22$ für $\text{X} = \text{Cl}/\text{I}$, $\delta_{\text{H}} 10.17/10.30$ für $\text{X} = \text{OTf}$), was auf das Vorliegen einer C–H \cdots X-Wasserstoffbrückenbindung in Lösung deutet [56], welche auch im Festkörper von **B7a**· CH_2Cl_2 gefunden wurde (vgl. Kapitel 2.2.2).

Die Signale der Pt–H-Wasserstoffatome (−17.98 bis −18.73 ppm) und auch die entsprechenden $^1J_{\text{Pt},\text{H}}$ -Kopplungskonstanten (1619.7–1659.2 Hz) in den Diacetyl(hydrido)platin(IV)-Komplexen **B3** und **B5** liegen im erwarteten Bereich von Hydridoplatin(IV)-Komplexen [57]. In Lösungen von $[\text{Pt}(\text{COMe})_2\text{H}\{(3,5\text{-R}_2\text{pz})_3\text{CH}\}]\text{OTf}$ ($\text{R} = \text{H}$, **B5a**; Me , **B5b**) in CD_3OD wurde ein H/D-Austausch zwischen dem Lösungsmittel und dem Hydridoliganden beobachtet, welcher zusätzlich durch ^2H -NMR-Spektren (Pt–D: $\delta_{\text{D}} -18.07/-18.53$) belegt werden konnte.

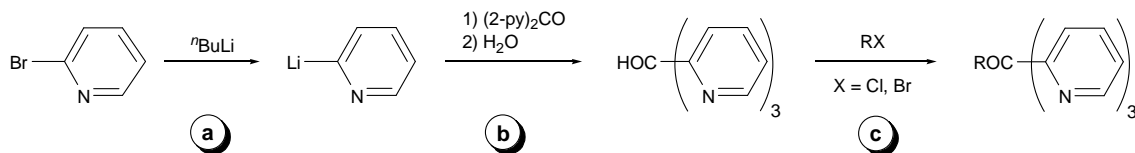
2.3. Diacetylplatin(II)-Komplexe mit κ^2 -koordinierten (2-py)₃COR-Liganden (siehe Publikationen C und D im Anhang)

2.3.1. Einführung

Bisher wurde durch formale Substitution der B–H-Gruppe in Tris(pyrazolyl)-Skorpionatliganden durch eine C–H-Gruppe der Einfluss der Ladung der tridentaten *N*-Donor-Liganden auf die Stabilität und Reaktivität von Diacetylplatin(II)- und -platin(IV)-Komplexen unter-

sucht. In weiteren Untersuchungen sollten nun die Donorgruppen variiert werden, weshalb Verbindungen des Typs $(py)_3COR$ in den Fokus rückten, deren Donorzentren Pyridin-N-Atome sind und die im „Rückgrat“ eine elektronegative OR-Gruppe ($R = H, Me, Et, Bn$) aufweisen. Im Vergleich zu Pyrazol weist Pyridin sowohl eine höhere σ -Donor- als auch eine höhere π -Akzeptorfähigkeit auf, was zu unterschiedlichen Eigenschaften und Reaktivitäten von Übergangsmetallkomplexen mit diesen Liganden führen kann [58].

Die „Stammverbindung“ (Tris(2-pyridyl)methanol; $(py)_3COR$, $R = H$) ist gemäß Schema 10 **a/b** durch Umsetzung von 2-Pyridyllithium mit Bis(2-pyridyl)keton darstellbar. Im Vergleich zu Pyrazol sind derivatisierte Pyridine schwieriger zugänglich, was die gezielte Beeinflussung der sterischen und elektronischen Eigenschaften dieser Liganden deutlich erschwert. Die C–OH-Gruppe am Rückgrat des Liganden kann aber relativ einfach durch Williamson-Veretherungen ($R = Me, Et, Bn$) modifiziert werden (Schema 10, **c**) [59, 60]. Auf die gleiche Weise ist auch eine Kopplung von $(py)_3COH$ an größere Moleküle (z. B. Dendrimere [61], Makrocyclen [60], Polymere [62]) möglich.



Schema 10.

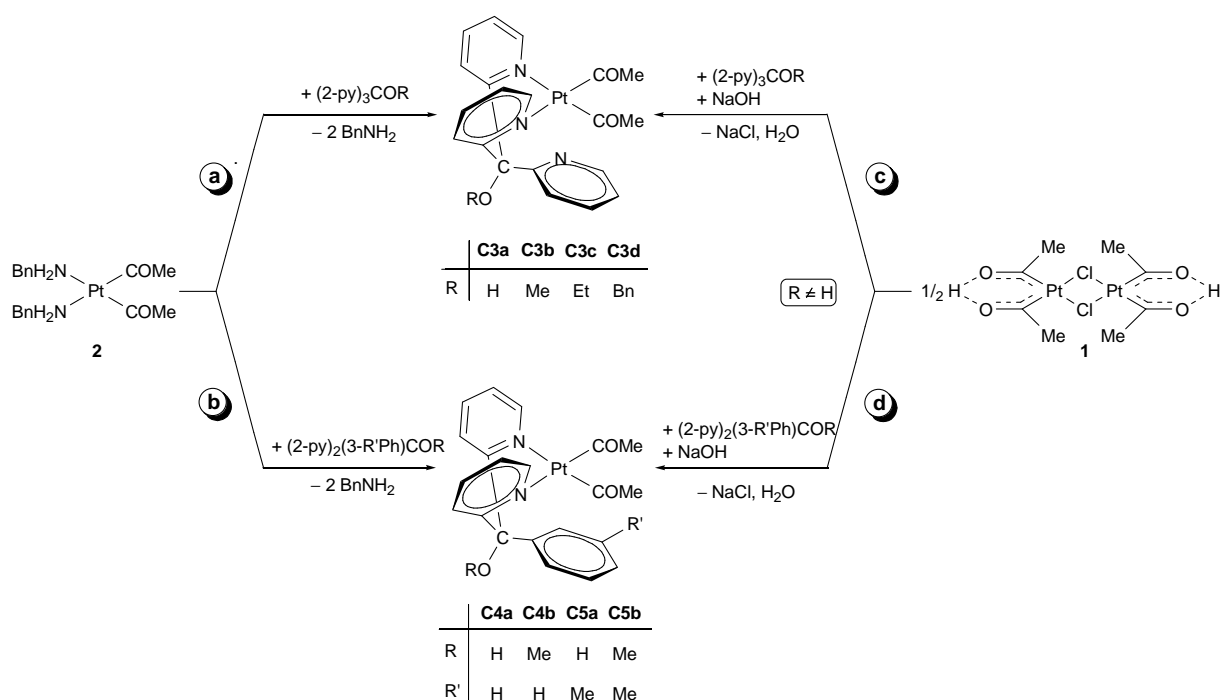
Wie Tris(pyrazolyl)borate und -methane koordinieren diese neutralen Liganden hauptsächlich facial (κ^3N,N',N'') in oktaedrischen Komplexen. Weiterhin sind – besonders im Fall von $(py)_3COH$ – auch $\kappa^2N,N',\kappa O$ - [58] bzw. $\kappa N,\kappa O$ -Koordinationsmodi [63] bekannt. In quadratisch-planaren Komplexen ist die Koordination dieser Liganden aus geometrischen Gründen auf den bidentaten κ^2N,N' -Modus beschränkt, wobei die $C(\mu-py)_2M$ -Gruppe auch hier eine Bootkonformation ausbildet [58]. Als einziges strukturell charakterisiertes Beispiel mit einem bidentat koordinierten $(py)_3COR$ -Liganden ist der Komplex $[Pd\{(2-py)_3COH\}_2](NO_3)_2$ in der Literatur beschrieben.

In der Organometallchemie des Palladiums und Platins gibt es bislang nur wenige Verbindungen mit dem Tris(pyridyl)methanol-Liganden. Arbeiten von Canty zum Studium von oxidativen Additionsreaktionen von Wasser an Komplexe des Typs $[PtR_2\{(2-py)_3COH\}]$ ($R = Me, Ph$) stellen hier den Schwerpunkt der bisherigen Forschung auf diesem Gebiet dar [64], während Pd- und Pt-Komplexe mit den veretherten Derivaten ($R \neq H$) überhaupt noch nicht beschrieben sind. Deshalb standen in den folgenden Untersuchungen die Synthese und vor allem die strukturelle Charakterisierung von Diacetylplatin(II)-Komplexen mit Liganden des Typs $(py)_3COR$ ($R = H, Me, Et, Bn$) im Mittelpunkt der Untersuchungen.

2.3.2. Synthese und Reaktivität

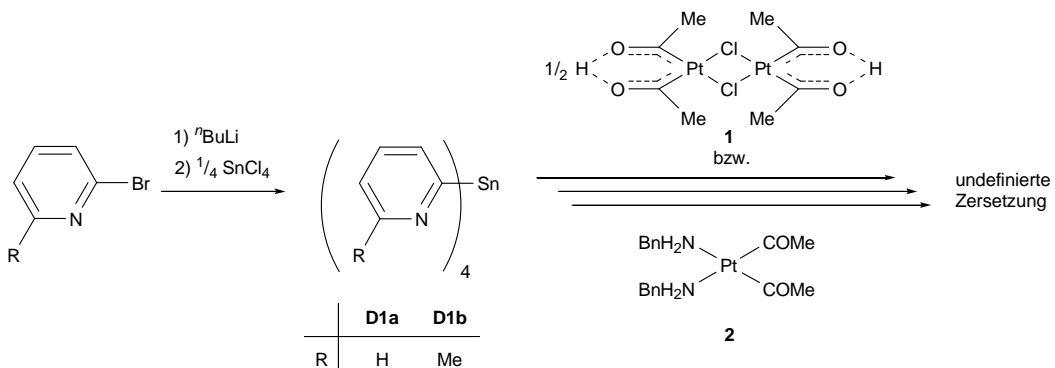
Diacetylplatin(II)-Komplexe des Typs $[\text{Pt}(\text{COMe})_2\{(2\text{-py})_3\text{COR}\}]$ ($\text{R} = \text{H}$, **C3a**; Me , **C3b**; Et , **C3c**; Bn , **C3d**) mit κ^2N,N' -gebundenen Tris(2-pyridyl)methanol- bzw. Tris(2-pyridyl)-methylether-Liganden sind gemäß Schema 11, **a** via Ligandenaustausch aus dem Bis(benzylamin)-Komplex **2** zugänglich. Auf analoge Weise konnten – zum Vergleich – auch die strukturell ähnlichen Verbindungen $[\text{Pt}(\text{COMe})_2\{(2\text{-py})_2\text{PhCOR}\}]$ ($\text{R} = \text{H}$, **C4a**; Me ; **C4b**) und $[\text{Pt}(\text{COMe})_2\{(2\text{-py})_2(m\text{-Tol})\text{COR}\}]$ ($\text{R} = \text{H}$, **C5a**; Me , **C5b**) synthetisiert werden (Schema 11, **b**), bei denen im Vergleich zu **C3a** und **C3b** der dritte nicht koordinierte Pyridinring durch eine Phenyl- (**C4**) bzw. *m*-Tolylgruppe (**C5**) ersetzt wurde. Die Komplexe **C3b–C3d**, **C4b** und **C5b** mit veretherten Liganden ($\text{R} \neq \text{H}$) konnten auch durch Reaktion des Platin- β -diketons **1** mit den entsprechenden Liganden und anschließender Zugabe von wässriger NaOH-Lösung dargestellt werden (Schema 11, **c/d**). Alle Verbindungen wurden als gelbe Feststoffe in Ausbeuten von 68 bis 90 % isoliert und NMR- (^1H , ^{13}C , ^{195}Pt) und IR-spektroskopisch sowie durch hochauflösende Massenspektrometrie (HR-ESI-MS) und durch Röntgeneinkristallstrukturanalysen (**C3a–C3d**) eindeutig identifiziert.

Rodriguez zeigte, dass die den oben beschriebenen Liganden des Typs $(2\text{-py})_3\text{COR}$ strukturell sehr ähnliche Zinnverbindung $^n\text{BuSn}(2\text{-py})_3$ ebenfalls als tridentater *N*-Donorligand in der Koordinationschemie agieren kann [65]. In eigenen Untersuchungen konnten durch Umsetzung von 2-Brompyridin bzw. 2-Brom-6-methylpyridin mit *n*-Butyllithium und anschließender Zugabe von SnCl_4 die entsprechenden Tetrakis(2-pyridyl)zinn-Verbindungen $\text{Sn}(6\text{-R-2-py})_4$ ($\text{R} = \text{H}$, **D1a**; Me , **D1b**) synthetisiert werden (Schema 12) [66]. Allerdings



Schema 11.

wurden bei Umsetzungen dieser Zinnverbindungen mit dem Bis(benzylamin)platin(II)-Komplex **2** und dem Platina- β -diketon **1** nur schnelle, nicht selektive Zersetzungreaktionen beobachtet. Die erhaltenen, in den üblichen Lösungsmitteln unlöslichen, Feststoffe wurden nicht charakterisiert (Schema 12).



Schema 12.

2.3.3. Strukturelle Charakterisierung

Alle Diacetylplatin(II)-Komplexe **C3** mit $(2\text{-py})_3\text{COR}$ -Liganden konnten strukturell charakterisiert werden, als Beispiel ist in Abbildung 8, a die Struktur von **C3b** ($R = \text{Me}$) gezeigt. In allen Strukturen bildet die $\text{C}(\mu\text{-py})_2\text{Pt}$ -Gruppe eine Bootstruktur mit den Pt- und den zentralen C-Atomen des Ligandengerüsts an den Spitzen. Die OR-Gruppe am Rückgrat des Liganden befindet sich dabei in äquatorialer und der nicht koordinierte dritte Pyridinring in axialer Position, womit dieser zum Platinatom zeigt. Der Substituent R ($R = \text{Me, Et, Bn}$) und die freie Pyridingruppe nehmen eine *gauche*-Position zueinander ein (Torsionswinkel $\text{C}-\text{O}-\text{C}-{}^i\text{C}_{\text{py}}$ 44.3(7), **C3b**; 47.9(7), **C3c**; 41.2(7), **C3d**).

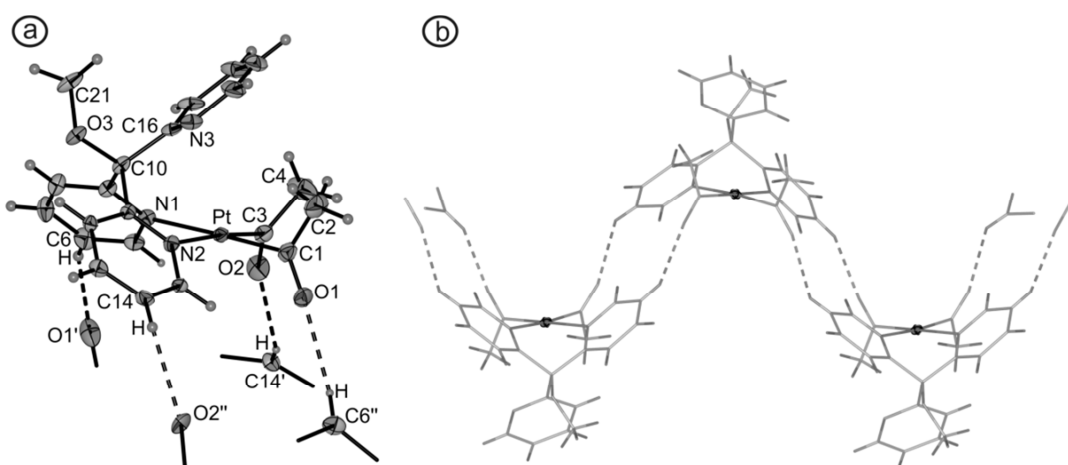


Abbildung 8. a) Molekülstruktur von $[\text{Pt}(\text{COMe})_2\{(2\text{-py})_3\text{COMe}\}]$ (**C3b**). Die gestrichelten Linien zeigen intermolekulare $\text{C}-\text{H}\cdots\text{O}$ -Wasserstoffbrückenbindungen in Kristallen von **C3b** an. Die Ellipsoide sind mit einer Wahrscheinlichkeit von 30% dargestellt. Ausgewählte strukturelle Parameter (Abstände in Å, Winkel in °): $\text{C}6\cdots\text{O}1'$ 3.35(1), $\text{H}\cdots\text{O}1'$ 2.49, $\text{C}6-\text{H}\cdots\text{O}1'$ 151, $\text{C}14'\cdots\text{O}2$ 3.277(8), $\text{H}\cdots\text{O}2$ 2.51, $\text{C}14'-\text{H}\cdots\text{O}2$ 139. b) Stabmodell, welches die zickzack-förmige Anordnung der Moleküle in Kristallen von **C3b** zeigt.

Aus Gründen der Minimierung von sterischer (COMe) und elektronischer (COMe) Wechselwirkung erscheint eine „*transoide*“ Anordnung der Acetylliganden (O-Atome auf unterschiedlichen Seiten der Komplexebene) energetisch günstiger. In allen Strukturen wurden jedoch „*cisoide*“ Anordnungen gefunden, was vermutlich auf intermolekulare Wasserstoffbrückenbindungen unter Beteiligung der O-Atome der Acetylgruppen als H-Akzeptor zurückzuführen ist. So sind beispielsweise im Festkörper von **C3b** die Moleküle durch Ausbildung von jeweils zwei intermolekularen C–H···O-Wasserstoffbrückenbindungen zu zickzack-Ketten verknüpft (Abbildung 8, **b**). Die relevanten strukturellen Parameter (C···O 3.35(1)/3.277(8) Å, H···O 2.49/2.52 Å, C–H···O 151/139°) liegen alle im Bereich solch schwacher attraktiven Wechselwirkungen [44].

2.3.4. Spektroskopische Charakterisierung

Die NMR-spektroskopische Analyse der strukturell ähnlichen Komplexe **C3–C5** zeigt, dass sowohl der Substituent R am Rückgrat der Liganden, als auch die nicht koordinierte aromatische Gruppe (**C3**: 2-py; **C4**: Ph; **C5**: *m*-Tol) maßgeblichen Einfluss auf die Symmetrie der Verbindungen in Lösung haben.

Der Komplex [Pt(COMe)₂{(2-py)₃COH}] (**C3a**) ist in Lösung spiegelsymmetrisch und weist, unabhängig von der Messtemperatur, in den NMR-Spektren sowohl für die beiden Acetylgruppen als auch für die beiden koordinierten Pyridinringe jeweils nur einen Signalsatz auf. Im Gegensatz dazu sind in den bei Raumtemperatur aufgenommenen Spektren der Verbindungen [Pt(COMe)₂{(2-py)₃COR}] mit veretherten Liganden (R = Me, **C3b**; Et, **C3c**; Bn, **C3d**) diese Signale stark verbreitert. In temperaturabhängigen NMR-Untersuchungen wurden bei höheren Temperaturen deutlich schärfere Signale und bei tieferen Temperaturen eine Aufspaltung in zwei Signalsätze beobachtet, was auf eine gehinderte Moleküldynamik und damit einhergehend den Verlust der Spiegelsymmetrie in Lösung deutet.

Die NMR-Spektren von [Pt(COMe)₂{(2-py)₂PhCOR}] (R = H, **C4a**; Me; **C4b**), bei denen der unsymmetrische Pyridinring durch eine symmetrische Phenylgruppe ersetzt wurde, weisen keine Abhängigkeit vom Substituenten R auf: Beide Verbindungen sind auch bei tiefen Temperaturen spiegelsymmetrisch in Lösung. Demgegenüber verhalten sich die Verbindungen mit unsymmetrischer nicht koordinierter *m*-Tolylgruppe [Pt(COMe)₂{(2-py)₂(*m*-Tol)-COR}] (R = H, **C5a**; Me; **C5b**) wie die analogen Komplexe **C3a/b** mit nicht koordinierten unsymmetrischen Pyridinring: Bei tieferen Temperaturen wird im Fall der Verbindung mit veretherten Liganden (R = Me, **C5b**) keine Spiegelsymmetrie in Lösung beobachtet.

Voraussetzung für eine Spiegelsymmetrie der Diacetylplatin(II)-Komplexe **C3–C5** in Lösung ist die freie Drehbarkeit der Acetylliganden, welche aufgrund zahlreicher experimenteller Befunde in allen Fällen als gegeben betrachtet werden kann [16, 19, 67]. Somit muss die beobachtete Dynamik mit einer gehinderten bzw. nicht gehinderten Rotation der unsymmetrischen nicht koordinierten Pyridin- (**C3**) bzw. *m*-Tolylgruppe (**C5**) und/oder der OR-Gruppe zusammenhängen. Die Beobachtungen lassen erkennen, dass der sterische Anspruch von R dabei eine entscheidende Rolle spielt.

Um die Aktivierungsparameter der potentiellen Rotationsbarrieren in den Verbindungen **C3b–d** und **C5b** experimentell zu bestimmen, wurden ^1H -NMR-Spektren bei verschiedenen Temperaturen im Bereich der Koaleszenztemperaturen ($T_C = 296 \text{ K}$, **C3b**; 301 K, **C3c**; 303 K, **C3d**; 302, **C5b**) aufgenommen. Durch Full-Lineshape-Analysen (gNMR [68], Abbildung 9) der Acetylsignale wurden die für die Eyring-Auftragung ($\ln(k/T)$ gegen $1/T$, Abbildung 10) benötigten Geschwindigkeitskonstanten berechnet. Die Aktivierungsenthalpien (ΔH^\ddagger) und -entropien (ΔS^\ddagger) der Verbindungen **C3b–d** sind mit 9.1 bis 9.3 kcal·mol $^{-1}$ bzw. –18.2 bis –19.1 cal·mol $^{-1}\cdot\text{K}^{-1}$ sehr ähnlich, während die für **C5b** ermittelte Aktivierungsenthalpie um ca. 2.5 kcal·mol $^{-1}$ und die Aktivierungsentropie um ca. 10.2 cal·mol $^{-1}\cdot\text{K}^{-1}$ größer ist.

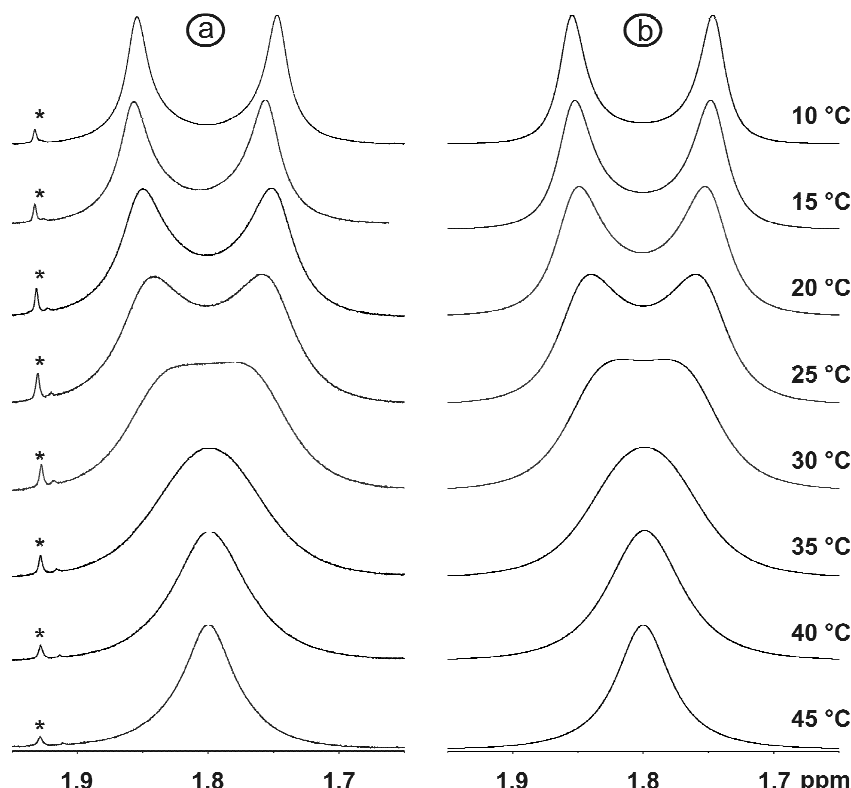


Abbildung 9. Temperaturabhängige ^1H -NMR-Spektren von **C3d** im Bereich der Acetylsignale (* Verunreinigung). a) Gemessen. b) Simulierte Spektren, aus denen die Geschwindigkeitskonstanten berechnet worden sind.

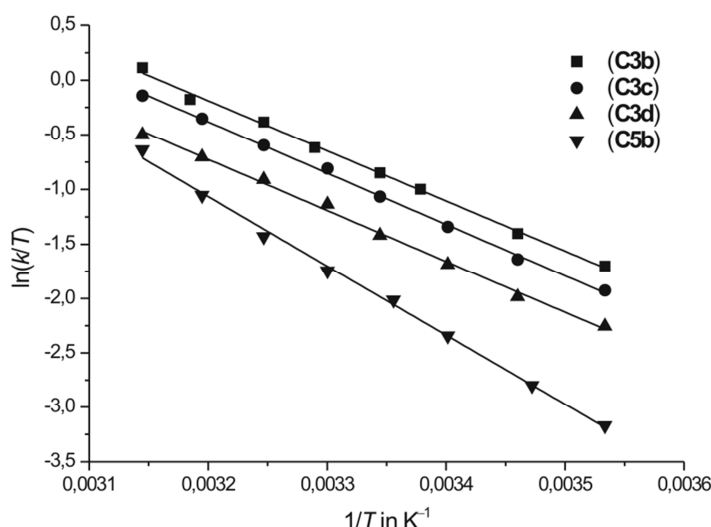


Abbildung 10. Eyring-Auftragung zur Bestimmung der Aktivierungsparameter der gehinderten Rotationen in den Komplexen **C3b–d** und **C5b**.

2.3.5. Zu dynamischen Prozessen in Diacetylplatin(II)-Komplexen

Um einen weiteren Einblick in diese Moleküldynamik zu erhalten, sind für $[\text{Pt}(\text{COMe})_2\{(2\text{-py})_3\text{COMe}\}]$ (**C3b**), $[\text{Pt}(\text{COMe})_2\{(2\text{-py})_2(m\text{-Tol})\text{COMe}\}]$ (**C5b**) und zum Vergleich auch für $[\text{Pt}(\text{COMe})_2\{(2\text{-py})_3\text{COH}\}]$ (**C3a**) umfangreiche quantenchemische Rechnungen auf DFT-Niveau¹ durchgeführt worden [69]. Berechnungen der Gleichgewichtsstrukturen verschiedener möglicher Isomere zeigten, dass das jeweils stabilste berechnete Isomer den experimentell ermittelten Strukturen mit Ausnahme der „*transoiden*“ Anordnung der Acetyl-liganden entspricht (vgl. die Röntgeneinkristallstrukturanalysen in Kapitel 2.3.2). Der nicht koordinierte Pyridinring in **C3a***, **C3b***² bzw. die *m*-Tolylgruppe in **C5b*** befinden sich in axialer Position der Bootstruktur der $\text{C}(\mu\text{-py})_2\text{Pt}$ -Gruppe und in *gauche*-Position zum Substituenten R (Abbildung 11, **a**).

Für die Drehung des nicht koordinierten Pyridinringes im *gauche*-Isomer von **C3a*** ($R = H$) wurden zwei verschiedene Rotationsbarrieren berechnet (4.2 vs. 13.7 kcal/mol; Abbildung 11, **a** → **c**). Somit ist keine vollständige Drehung um 360° zu erwarten, sondern eine flip-flop-Bewegung, bei der das N-Atom des Pyridinringes zum Substituenten $R = H$ zeigt. In Übereinstimmung mit dem Experiment lässt die berechnete Rotationsbarriere (4.2 kcal/mol) erwarten, dass diese (symmetrieerhaltende) Bewegung auch bei tieferen Temperaturen nicht eingefroren ist. Weiterhin wurde gezeigt, dass das *anti*-Isomer von **C3a*** keine Rolle spielt,

¹ Die quantenchemischen Rechnungen wurden dankenswerterweise von Dipl.-Chem. T. Kluge durchgeführt.

² Hier und im Folgenden sind berechnete Komplexe mit einem Stern gekennzeichnet. Grundsätzlich sind nachfolgend freie Enthalpien unter Standardbedingungen angegeben. Lösungsmitteneinflüsse (Methanol) sind im Rahmen des Polarisationsmodells von Tomasi (PCM = polarizable continuum model) berücksichtigt.

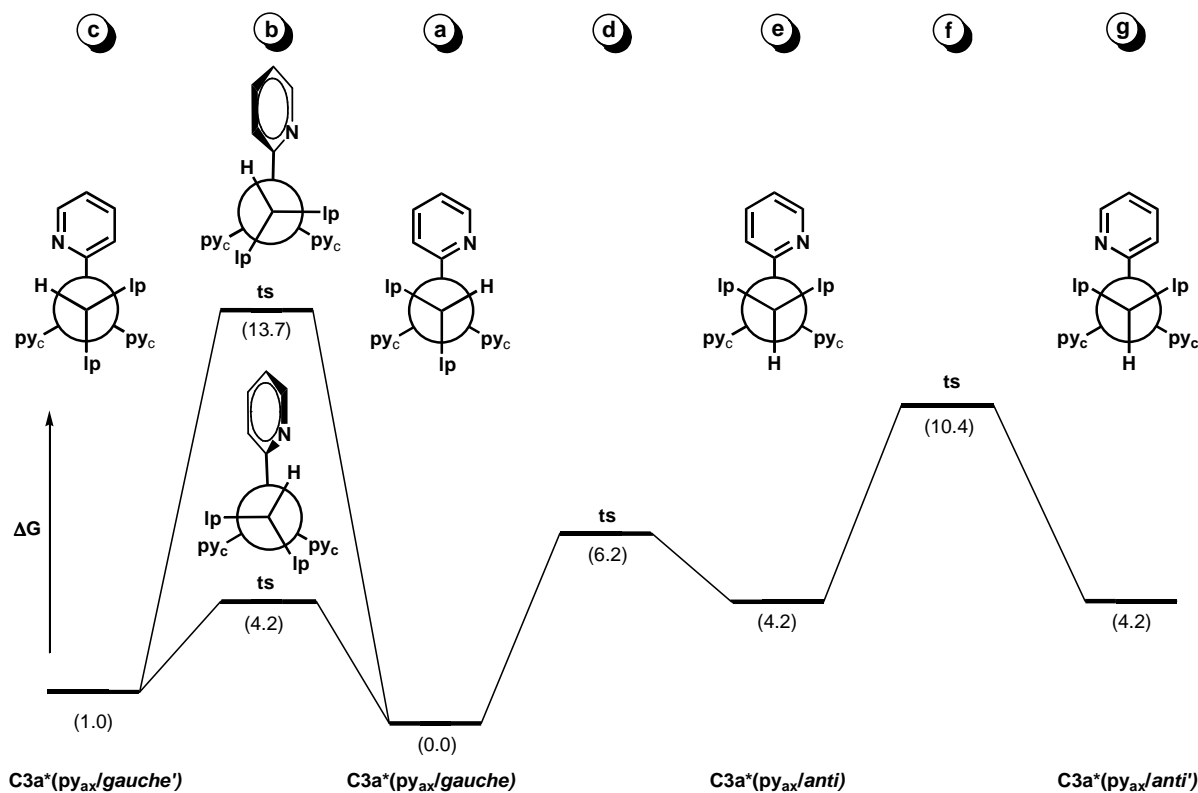


Abbildung 11. Diagramm für die freie Aktivierungsenthalpie (in kcal/mol in Relation zum stabilsten Isomer) verschiedener Molekülbewegungen in **C3a*** (ts = Übergangszustand; Ip = freies Elektronenpaar; py_c = koordinierter Pyridinring). Die Newman-Projektionen zeigen die Verbindung entlang der O–C-Bindung im Rückgrat des Liganden.

da zum einen die für die *gauche-anti*-Isomerisierung erforderliche Drehung des Substituenten R = H (Abbildung 11, **a** → **e**) eine höhere Aktivierungsbarriere als die flip-flop-Bewegung im *gauche*-Isomer aufweist (6.2 vs. 4.2 kcal/mol) und zum anderen die Drehung des Pyridinringes im *anti*-Konformer zusätzlich durch Rotationsbarrieren behindert ist (**e** → **g**).

Auch im Fall von Komplex **C3b*** mit einem veretherten Liganden (R = Me) wurden für die Drehung des nicht koordinierten Pyridinringes im *gauche*-Konformer zwei Rotationsbarrieren gefunden, die beide jedoch von vergleichbarer Größenordnung (17.8/19.5 kcal/mol; Abbildung 12, **a** → **c**) sind und deutlich höher liegen als in **C3a***. Somit kann sowohl eine flip-flop-Bewegung, als auch eine volle 360°-Rotation ausgeschlossen werden. Im Vergleich dazu ist die Barriere für den Übergang vom *gauche*- in das *anti*-Konformer um ca. 4 kcal/mol kleiner (Abbildung 12, **a** → **e**). Im *anti*-Konformer von **C3b*** ist, ähnlich wie oben für das *gauche*-Isomer von **C3a*** beschrieben, eine flip-flop-Bewegung des Pyridinringes möglich (Abbildung 12, **e** → **g**), wobei das N-Atom des nicht koordinierten Pyridinringes zum Platinatom zeigt (Abbildung 12, **f** unten).

Die Ergebnisse der Berechnungen für Komplex **C5b*** mit einer nicht koordinierten *m*-Tolylgruppe sind sehr ähnlich zu **C3b**. Der einzige wesentliche Unterschied ist eine nahezu

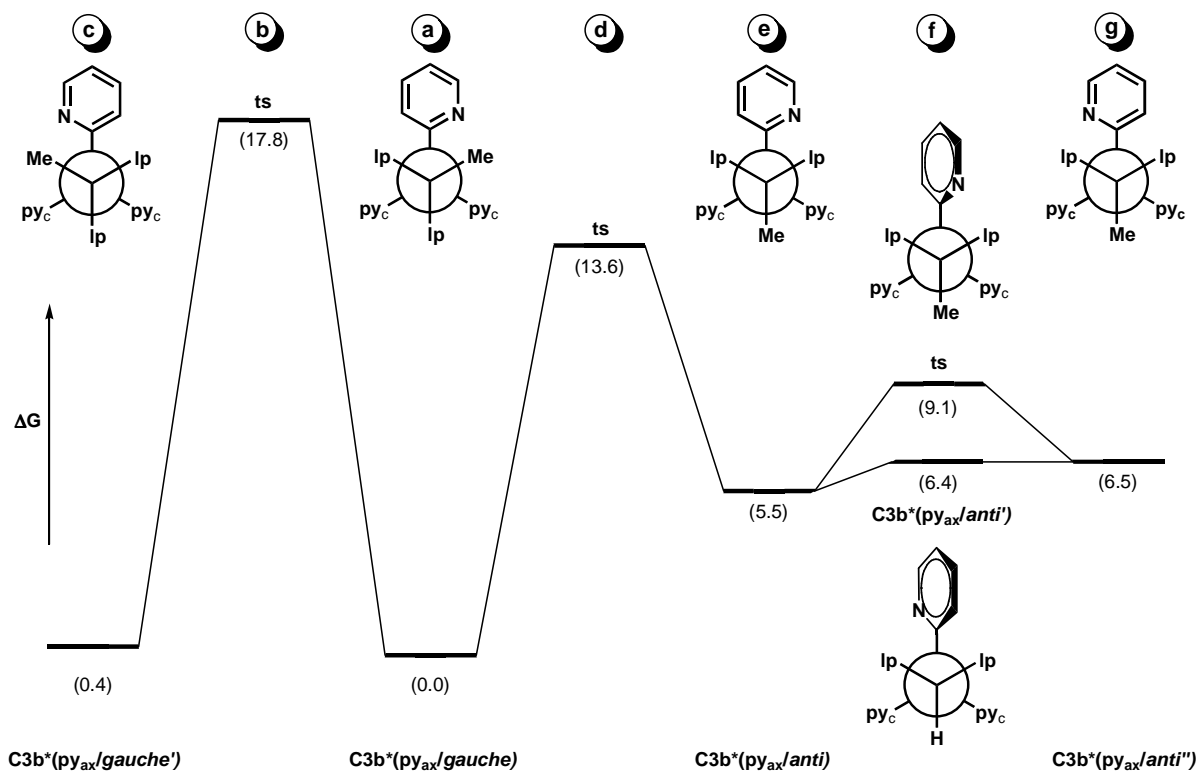
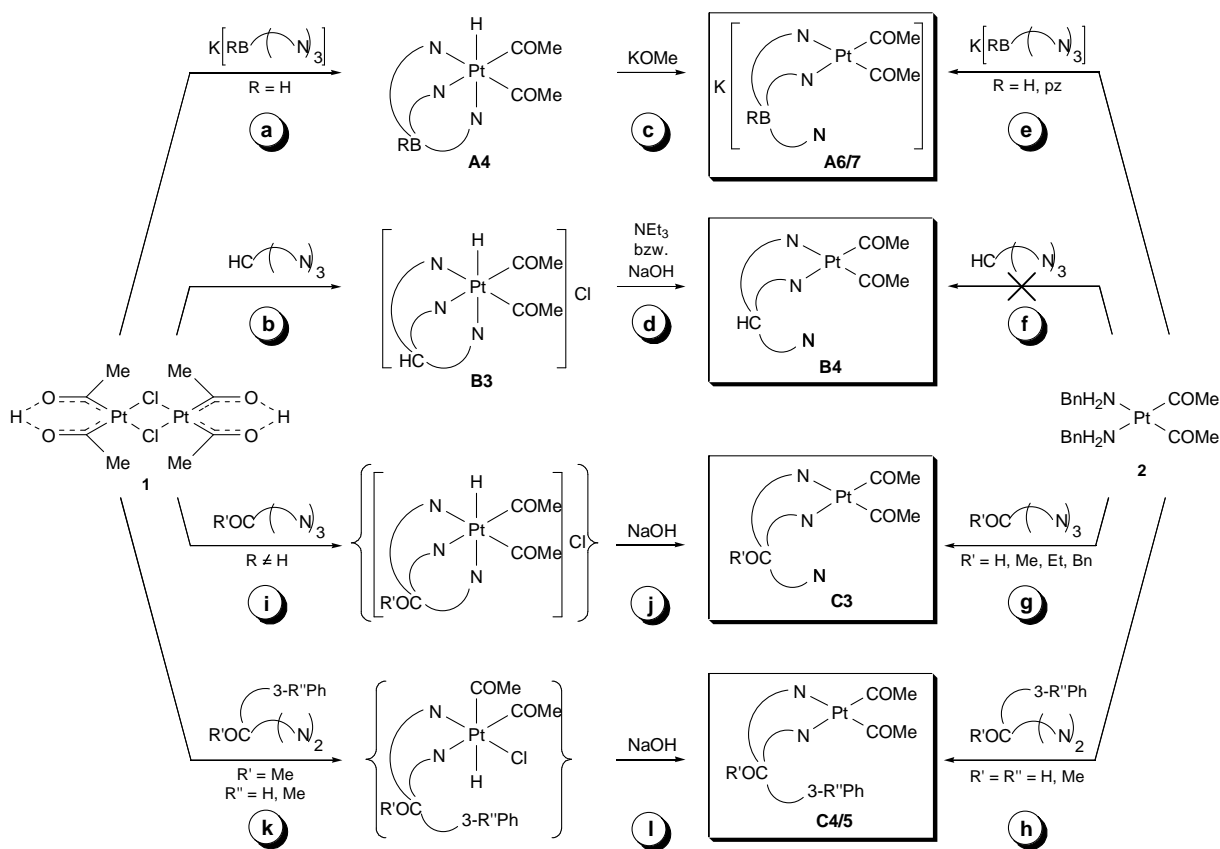


Abbildung 12. Diagramm für die freie Aktivierungsenthalpie (in kcal/mol in Relation zum stabilsten Isomer) verschiedener Molekülbewegungen in **C3b^{*}** (ts = Übergangszustand; Ip = freies Elektronenpaar; py_c = koordinierter Pyridinring). Die Newman-Projektionen zeigen die Verbindung entlang der O–C-Bindung im Rückgrat des Liganden.

barrierlose vollständige Drehbarkeit der *m*-Tolylgruppe im *anti*-Konformer. Während in **C3a^{*}** (R = H) die Symmetrie des Komplexes in Lösung durch eine flip-flop-Bewegung des nicht koordinierten Pyridinringes erhalten bleibt, muss in **C3b^{*}** (R = Me) und **C5b^{*}** (R = Me) erst eine *gauche-anti*-Isomerisierung stattfinden, um eine Bewegung des Pyridinringes bzw. der *m*-Tolylgruppe, die die Symmetrie in Lösung aufrecht erhält, zu ermöglichen. Das entspricht in vollem Umfang den experimentell ermittelten Beobachtungen: Die berechneten Aktivierungsbarrieren ($\Delta G_{298} = 13.6$ kcal/mol, **C3b^{*}**; 14.5 kcal/mol, **C5b^{*}**) für diese Isomerisierung liegen im Bereich der experimentell ermittelten Werte ($\Delta G_{298} = 14.6$ kcal/mol, **C3b**; 15.3 kcal/mol, **C5b**).

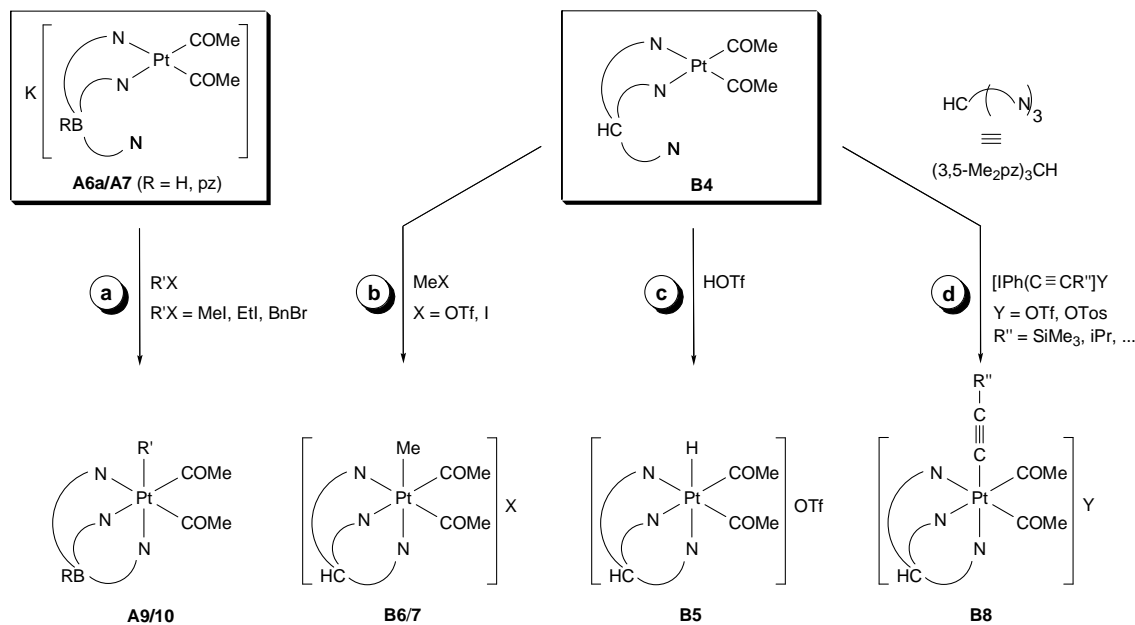
2.4. Diskussion der Ergebnisse

Im Rahmen der vorliegenden Arbeit sind Untersuchungen zur Synthese und Reaktivität sowie zu Eigenschaften von quadratisch-planaren Diacetylplatin(II)-Komplexen mit κ^2N,N' -koordinierten *N*-Donorliganden der Typen (pz^x)₃BR, (pz^x)₃CH und (py)₃COR' durchgeführt worden. Gemäß Schema 13 **a** → **c** bzw. **b** → **d** sind Diacetylplatin(II)-Komplexe mit κ^2 -koordinierten Tris(pyrazolyl)borat- (**A6**) und -methan-Liganden (**B4**) aus dem Platina-β-diketon **1** via Diacetyl(hydrido)platin(IV)-Komplexe **A4/B3** als Zwischenstufen zugänglich.

**Schema 13.**

Ligandenaustauschreaktionen ausgehend vom Bis(benzylamin)platin(II)-Komplex **2** gelangen dagegen nur für die Komplexe **A6/7**, nicht aber für die Verbindungen **B4** mit Tris(pyrazolyl)methan-Liganden (Schema 13, **e/f**). Diacetylplatin(II)-Komplexe mit κ^2 -koordinierten Liganden des Typs $(\text{py})_3\text{COR}'$ (**C3**) bzw. $(\text{py})_2(\text{Ph})\text{COR}'$ (**C4**) und $(\text{py})_2(m\text{-Tol})\text{COR}'$ (**C5**) waren ausgehend von **2** (Schema 13, **g/h**) zugänglich. Im Fall veretherter Liganden ($\text{R}' \neq \text{H}$) konnte gezeigt werden, dass die Verbindungen **C3–C5** auch in der Reaktionsfolge Platina- β -diketon **1** → Hydridoplatin(IV)-Komplex → Diacetylplatin(II)-Komplex zugänglich sind, wobei die Hydridokomplexe nicht isoliert wurden (Schema 13, **i** → **j** bzw. **k** → **l**).

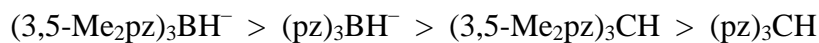
Untersuchungen zur oxidativen Addition an Diacetylplatin(II)-Komplexen mit Tris(pyrazolyl)borat-Liganden zeigten, dass die Komplexe **A6a** und **A7** mit Alkyhalogeniden zu den neutralen Diacetyl(alkyl)platin(IV)-Komplexen **A9** bzw. **A10** reagieren (Schema 14, **a**). Die Umsetzungen der Komplexe **B4** mit Methyliodid bzw. Trifluormethansulfonsäuremethylester führten zur Bildung der kationischen Diacetyl(methyl)platin(IV)-Komplexe **B6/B7** mit κ^3 -koordinierten Tris(pyrazolyl)methan-Liganden (Schema 14, **b**). Umsetzungen von **B4** mit Trifluormethansulfonsäure lieferten die Diacetyl(hydrido)platin(IV)-Komplexe **B5** (Schema 14, **c**), welche im Gegensatz zu den Hydridokomplexen **B3** (Schema 13) thermisch stabil sind. Reaktionen der Diacetylplatin(II)-Precursorkomplexe **A6**, **A7**

**Schema 14.**

und **B4** mit Alkinyliodonium-Verbindungen zeigten, dass stabile kationische Diacetyl-(alkinyl)platin(IV)-Komplexe (**B8**) nur bei Verwendung des $(3,5\text{-}Me_2pz)_3CH$ -Liganden zugänglich sind (Schema 14, **d**).

Über die Donorstärke von Tris(pyrazolyl)borat- und -methan-Liganden

Es kann davon ausgegangen werden, dass die anionischen $(3,5\text{-}R_2pz)_3BH^-$ -Liganden stärkere Donoren sind als die neutralen $(3,5\text{-}R_2pz)_3CH$ -Liganden. Des Weiteren sind die methylsubstituierten Derivate ($R = Me$) infolge des induktiven Effektes der Methylgruppen stärkere Donoren als die „Stammverbindungen“ ($R = H$). Damit in Übereinstimmung stehen die Größen der $^1J_{Pt,H}$ -Kopplungskonstanten in den Hydridoplatin(IV)-Komplexen $[Pt(COMe)_2H\{(3,5\text{-}R_2pz)_3BH\}]$ ($R = H$, **A4a**, 1522 Hz; Me , **A4b**, 1496 Hz) und $[Pt(COMe)_2H\{(3,5\text{-}R_2pz)_3CH\}]OTf$ ($R = H$, **B5a**, 1659 Hz; Me , **B5b**, 1637 Hz). Diese Werte spiegeln eine Abstufung im *trans*-Einfluss



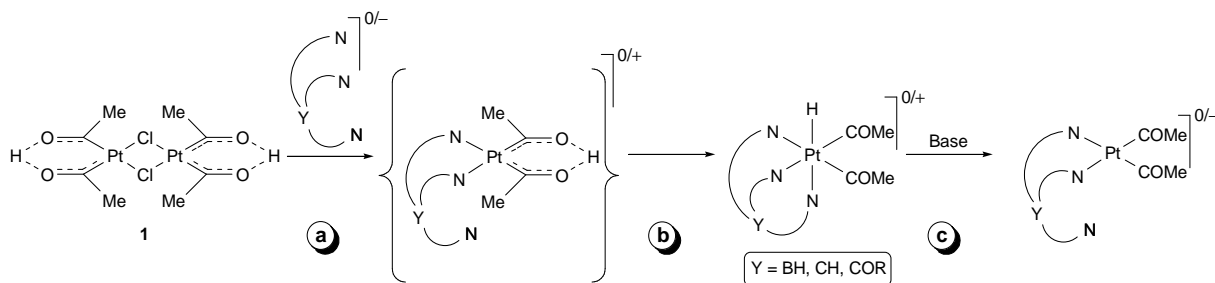
wider.

Eine Einordnung der Donorstärke des Tris(pyridyl)methanol-Liganden und seiner veretherten Derivate ist schwierig. Auf der einen Seite ist Pyridin ein stärkerer σ -Donor (und auch stärkerer π -Akzeptor) als Pyrazol [58], auf der anderen Seite bleibt offen, wie die OH- bzw. OR-Substitution am Rückgrat des Liganden die Donorstärke beeinflusst.

*Zur Synthese von Diacetylplatin(II)-Komplexen ausgehend vom Platina- β -diketon **1***

In Analogie zu zahlreichen Umsetzungen vom Platina- β -diketon **1** mit bidentaten und monodentaten *P*-, *N*-, *S*- und *O*-Liganden kann davon ausgegangen werden, dass sowohl die

Reaktionen mit tridentaten Tris(pyrazolyl)borat- und -methan-Liganden, als auch mit veretherten Tris(pyridyl)methanol-Liganden gemäß Reaktionsschema 15 abläuft.



Schema 15.

Im ersten Reaktionsschritt (Schema 15, **a**) werden die labilen Pt–Cl–Pt-Brücken des Platina- β -diketons **1** unter Bildung von mononukleären Platina- β -diketonen gespalten, die aber in der vorliegenden Arbeit nicht nachgewiesen wurden. Dem schließt sich eine H-Verschiebung an, die im Sinne einer oxidativen Addition zu Hydridoplatin(IV)-Komplexen führt (**b**). Es ist klar belegt, dass in diesen Komplexen der Ligand tridentat (κ^3N,N',N'') koordiniert ist. Das ist ein wesentlicher Unterschied zu den zuvor erwähnten Umsetzungen mit bidentaten Liganden, bei denen Hydrido(chlorido)platin(IV)-Komplexe wie $[\text{Pt}(\text{COMe})_2\text{Cl}(\text{H})(\text{N}^{\text{H}}\text{N})]$ gebildet werden [14, 16]. Eine baseninduzierte Abspaltung des Hydridoliganden führt schließlich zu Diacetylplatin(II)-Komplexen mit κ^2N,N' -koordinierten Liganden (Schema 15, **c**).

Die Umsetzung von **1** mit Alkoholderivaten $(\text{py})_3\text{COH}$ bzw. $(\text{py})_2\text{PhCOH}$ und $(\text{py})_2(m\text{-Tol})\text{COH}$ führte nur zu einem Gemisch aus nicht identifizierten Verbindungen. Weil für die Darstellung der entsprechenden Komplexe ein anderer nützlicher Syntheseweg zur Verfügung stand (vide infra), wurden die Ursachen dafür nicht weiter untersucht.

Zur Synthese von Diacetylplatin(II)-Komplexen ausgehend vom Bis(benzylamin)platin(II)-Komplex **2**

Umsetzungen von $[\text{Pt}(\text{COMe})_2(\text{NH}_2\text{Bn})_2]$ (**2**) mit den tridentaten Liganden verlaufen im Sinne eines einfachen Ligandenaustausches von zwei monodentaten Aminliganden (NH_2Bn) durch einen mehrzähligen Liganden, der in den gebildeten Komplexen **A6/7**, **B4** und **C3–5** (Schema 13, **e–h**) bidentat (κ^2N,N') koordiniert ist.

Diese Reaktionen verlaufen mit den anionischen Tris(pyrazolyl)borat- und den neutralen $(\text{py})_3\text{COR}$ -Liganden sehr schnell und führen im Allgemeinen zu hohen Ausbeuten der entsprechenden Diacetylplatin(II)-Komplexe. Im Gegensatz dazu sind bei analogen Umsetzungen mit Tris(pyrazolyl)methanol-Liganden keinerlei Reaktionen zu beobachten. Ursache dafür ist wahrscheinlich die vergleichsweise schwache Donorstärke dieser Liganden. Das wird eindrucksvoll durch folgenden Sachverhalt belegt: Zum einen bildet sich nicht ein-

mal der schwer lösliche Komplex $[\text{Pt}(\text{COMe})_2\{(pz)_3\text{CH}\}]$ (**B4a**) auf diesem Wege, zum anderen reagiert dieser mit Benzylamin unter Abspaltung des $(pz)_3\text{CH}$ -Liganden und Bildung von **2** (vgl. Kapitel 2.2.2.)

Zur Moleküldynamik in Diacetylplatin(II)-Komplexen mit Tris(pyrazolyl)methan-Liganden

Die Diacetylplatin(II)-Komplexe mit Tris(pyrazolyl)methan-Liganden zeigen bei Raumtemperatur eine ausgeprägte Moleküldynamik, die – trotz der κ^2N,N' -Koordination – zu einer chemischen und magnetischen Äquivalenz aller drei Pyrazolylringe führt. Quantenchemische Rechnungen auf DFT-Niveau zeigen, dass wahrscheinlich im ersten Schritt ein Übergang zu einem T-förmigen Komplex mit einem nur κN -koordinierten $(3,5-\text{R}_2\text{pz})_3\text{CH}$ -Liganden im Sinne eines dissoziativen Mechanismus erfolgt. Dem folgt eine erneute κ^2N,N' -Koordination des Liganden, nachdem durch interne Rotation der zuvor nicht koordinierte Pyrazolylring in die entsprechende Position gebracht worden ist (*syn-anti*-Isomerisierung, vgl. Kapitel 2.2.4.). Im Unterschied dazu zeigen die analogen Komplexe mit den anionischen Skorpionatliganden keinerlei Moleküldynamik. Das findet seine zwanglose Erklärung in der stärkeren Donorwirkung dieser Liganden, wodurch die Dissoziation eines Pyrazolylringes ($\kappa^2N,N' \rightarrow \kappa N$) erheblich erschwert ist.

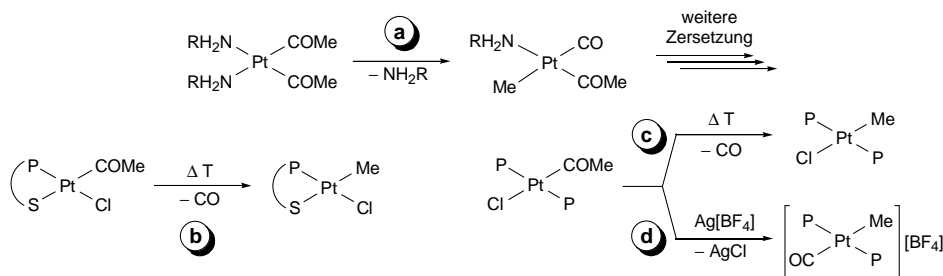
Interessanterweise treten bei den Diacetylplatin(II)-Komplexen mit $(py)_3\text{COR}$ -Liganden ebenfalls dynamische Prozesse auf, die aber NMR-spektroskopischen Untersuchungen und quantenchemischen Rechnungen zufolge ihren Ursprung nicht in einer Dekoordination/Rekoordination eines Pyridinringes haben, sondern auf (teilweise) gehinderte Rotationsbewegungen der (nicht koordinierten) Substituenten am zentralen C-Atom des Liganden zurückzuführen sind. Insgesamt steht dieser Sachverhalt mit einer relativ starken Koordination dieser Liganden im Einklang.

Zur Stabilität von Diacetylplatin(II)-Komplexen in Lösung

Während Diacetylplatin(II)-Komplexe mit $(3,5-\text{R}_2\text{pz})_3\text{BH}^-$ (**A6**) und $(py)_3\text{COR}$ -Liganden (**C3**) in Lösung und unter anaeroben Bedingungen über längere Zeit stabil sind, war in Lösungen von $[\text{Pt}(\text{COMe})_2\{(3,5-\text{R}_2\text{pz})_3\text{CH}\}]$ (**B4**) eine innerhalb weniger Stunden beginnende Zersetzung zu beobachten.

Diese Eigenschaft der Komplexe **B4** steht in Übereinstimmung mit den quantenchemischen Berechnungen bezüglich der Moleküldynamik. Diese zeigten, dass – infolge der vergleichsweise schwachen Koordination der Tris(pyrazolyl)methan-Liganden – T-förmige Komplexe mit κN -gebundenen Liganden leicht zugänglich sind, was aufgrund der freien Koordinationsstelle rasche Zersetzungsreaktionen ermöglichen kann. So konnte in früheren Untersuchungen

zur Reaktivität und Stabilität von Acetylplatin(II)-Komplexen gezeigt werden, dass – gemäß Schema 16 – die Extrusion von CO eine typische Reaktion von T-förmigen Intermediaten ist, die durch Dissoziation eines labilen (**a**) bzw. hemilabilen Liganden (**b**) oder durch Abspaltung eines Chloridoliganden (**d**) gebildet worden sind [19, 70]. Im Fall der Bis(amin)platin(II)-Komplexe stellt diese Reaktion dabei den einleitenden Schritt zur vollständigen Zersetzung dieser Verbindungen dar (Schema 16, **a**) [19], wobei dieser Prozess, wie auch für $[\text{Pt}(\text{COMe})_2\{(3,5-\text{Me}_2\text{pz})_3\text{CH}\}]$ (**A6b**) beobachtet, in Lösungsmitteln mit höherer Donorfähigkeit (z.B. Methanol, THF) aufgrund der Stabilisierung der T-förmigen Intermediate deutlich langsamer abläuft als in nicht koordinierenden Lösungsmitteln wie Methylchlorid oder Chloroform.



Schema 16.

Zur Stabilität von Alkinylplatin(IV)-Komplexen

Diacetyl(alkinyl)platin(IV)-Komplexe konnten nur in Anwesenheit von $(3,5-\text{Me}_2\text{pz})_3\text{CH}$ als Coligand isoliert werden (Schema 14, **d**). Die experimentellen Befunde lassen vermuten, dass die entsprechenden Komplexe $[\text{Pt}(\text{COMe})_2(\text{C}\equiv\text{CR})\{(3,5-\text{R}'_2\text{pz})_3\text{CH}\}]X$ mit unsubstituierten Tris(pyrazolyl)methan-Liganden und $[\text{Pt}(\text{COMe})_2(\text{C}\equiv\text{CR})\{(3,5-\text{R}'_2\text{pz})_3\text{BR}''\}]$ ($\text{R}'/\text{R}'' = \text{H}/\text{H}$, Me/H , H/pz) mit Skorpionatliganden zwar gebildet worden sind, aber thermisch instabil waren und sich bei der Isolierung zersetzen.

Der einleitende Schritt bei der Zersetzung von koordinativ gesättigten Organylplatin(IV)-Komplexen sind oftmals reduktive C–H- oder C–C-Eliminierungen, wobei in vielen Fällen die Schaffung einer freien Koordinationsstelle (d.h. die Bildung eines fünffach koordinierten Intermediates) die entscheidende Voraussetzung für das Ablauen dieser Reaktionen ist [71]. Übertragen auf Diacetyl(alkinyl)platin(IV)-Komplexe mit facial (κ^3N,N',N'') koordinierten Tris(pyrazolyl)borat und -methan-Liganden entspricht das der Dekoordination eines Pyrazolyrringes unter Ausbildung einer κ^2N,N' -Ligandkoordination. Während Diacetyl(alkinyl)platin(IV)-Komplexe mit Skorpionatliganden neutral sind, handelt es sich bei analogen Verbindungen mit Tris(pyrazolyl)methan-Liganden um kationische Komplexe. Die positive Ladung am Metallzentrum erschwert die Dissoziation eines Pyrazolyrringes, was

möglicherweise zu einer allgemein höheren Stabilität der Diacetyl(alkinyl)platin(IV)-Komplexe mit diesen Liganden führt. Die höhere Stabilität von $[\text{Pt}(\text{COMe})_2(\text{C}\equiv\text{CR}-\{(3,5-\text{Me}_2\text{pz})_3\text{CH}\})]$ (**B8**) im Vergleich zu den Verbindungen mit unsubstituierten $(\text{pz})_3\text{CH}$ -Liganden könnte in einer stärkeren Koordination des $(3,5-\text{Me}_2\text{pz})_3\text{CH}$ -Liganden aufgrund des +I-Effekts der zusätzlichen Methylgruppen und/oder in sterischen Effekten begründet sein.

Zum Einfluss der Methylgruppen auf Eigenschaften und Reaktivität der Verbindungen

Im Allgemeinen können durch eine Modifizierung der Pyrazolylringe Tris(pyrazolyl)borat-Liganden hinsichtlich ihrer sterischen und/oder elektronischen Eigenschaften variiert werden [24]. Die Analyse der C=O-Streckfrequenzen in Komplexen des Typs $[\text{Mn}(\text{CO})_3-\{(3,5-\text{RR}'\text{pz})_3\text{CH}\}]$ deutet hingegen darauf hin, dass es im Fall von Tris(pyrazolyl)methan-Liganden keinen signifikanten Einfluss des Substitutionsmusters der Pyrazolylringe auf die Donorfähigkeit dieser Liganden gibt [39].

Damit in Übereinstimmung hat die Einführung von Methylgruppen an Position 3 und 5 im Fall der Diacetylplatinkomplexe **A4–6** mit Skorpionatliganden einen geringen Einfluss auf NMR-spektroskopische Parameter. So deuten beispielsweise die schwache Hochfeldverschiebung der ^{195}Pt -Resonanzen und die kleineren $^3J_{\text{Pt},\text{H}}$ - und $^2J_{\text{Pt},\text{C}}$ -Kopplungskonstanten der Acetyl-Liganden in Verbindungen mit dem methylsubstituierten Liganden $(3,5-\text{Me}_2\text{pz})_3\text{BH}^-$ auf eine etwas höhere Donorstärke dieser Liganden um Vergleich zu $(\text{pz})_3\text{BH}^-$. Deutlich ausgeprägter dagegen sind bei den Komplexen $[\text{Pt}(\text{COMe})_2\{(3,5-\text{Me}_2\text{pz})_3\text{CH}\}]$ (**B4a**) und $[\text{Pt}(\text{COMe})_2\{(3,5-\text{Me}_2\text{pz})_3\text{CH}\}]$ (**B4b**) Unterschiede in der Löslichkeit (vgl. Kapitel 2.2.2), Reaktivität (Bildung stabiler Alkinylplatin(IV)-Komplexe) und Moleküldynamik (vgl. Kapitel 2.2.4). Letzteres ist aber nach quantenchemischen Untersuchungen eher auf sterische Effekte als auf induktive Effekte zurückzuführen.

Weiterhin wird die C–H-Gruppe am Rückgrat der Tris(pyrazolyl)methan-Liganden durch die Methylgruppen an Position 5 effektiv abgeschirmt (vgl. Abbildung 13), weshalb in den

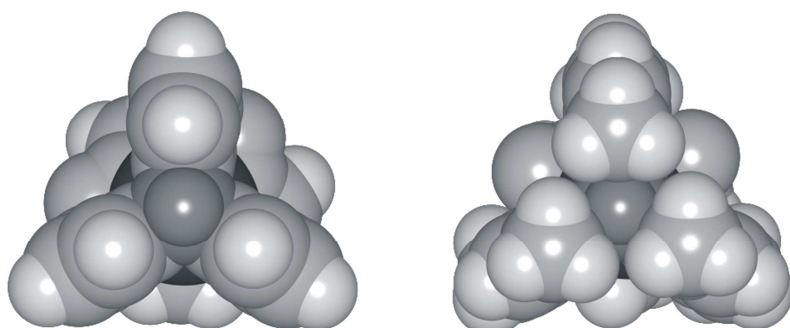


Abbildung 13. Raumfüllendes Modell der berechneten Kationen $[\text{Pt}(\text{COMe})_2\text{Me}\{(3,5-\text{Me}_2\text{pz})_3\text{CH}\}]^+$ (**B7a***, links) und $[\text{Pt}(\text{COMe})_2\text{Me}\{(3,5-\text{Me}_2\text{pz})_3\text{CH}\}]^+$ (**B7b***, rechts) mit Blick entlang des C–H–Pt-Vektors (dunkelgrau dargestellt).

kationischen Komplexen $[\text{Pt}(\text{COMe})_2\text{H}\{(3,5\text{-Me}_2\text{pz})_3\text{CH}\}]\text{Cl}$ und $[\text{Pt}(\text{COMe})_2\text{Me}\{(3,5\text{-Me}_2\text{pz})_3\text{CH}\}]\text{I}$ im Gegensatz zu den analogen Komplexen mit $(\text{pz})_3\text{CH}$ -Liganden keine C–H···Halogen-Wasserstoffbrücken ausgebildet werden können.

Zur oxidativen Addition von Alkylhalogeniden

Die Umsetzung von $[\text{Pt}(\text{COMe})_2\{(\text{pz})_3\text{BH}\}]$ (**A6a**) und $\text{K}[\text{Pt}(\text{COMe})_2\{(\text{pz})_4\text{B}\}]$ (**A7**) mit Alkylhalogeniden bzw. $[\text{Pt}(\text{COMe})_2\{(\text{pz})_3\text{CH}\}]$ (**B4a**) und $[\text{Pt}(\text{COMe})_2\{(3,5\text{-Me}_2\text{pz})_3\text{CH}\}]$ (**B4b**) mit Methyliodid führte zur Bildung von Alkylplatin(IV)-Komplexen mit κ^3N,N',N'' -koordinierten Tris(pyrazolyl)borat- bzw. -methan-Liganden (Schema 14, **a/b**). Es ist bekannt, dass derartige Reaktionen meistens über einen S_N2 -analogen Mechanismus verlaufen [72].

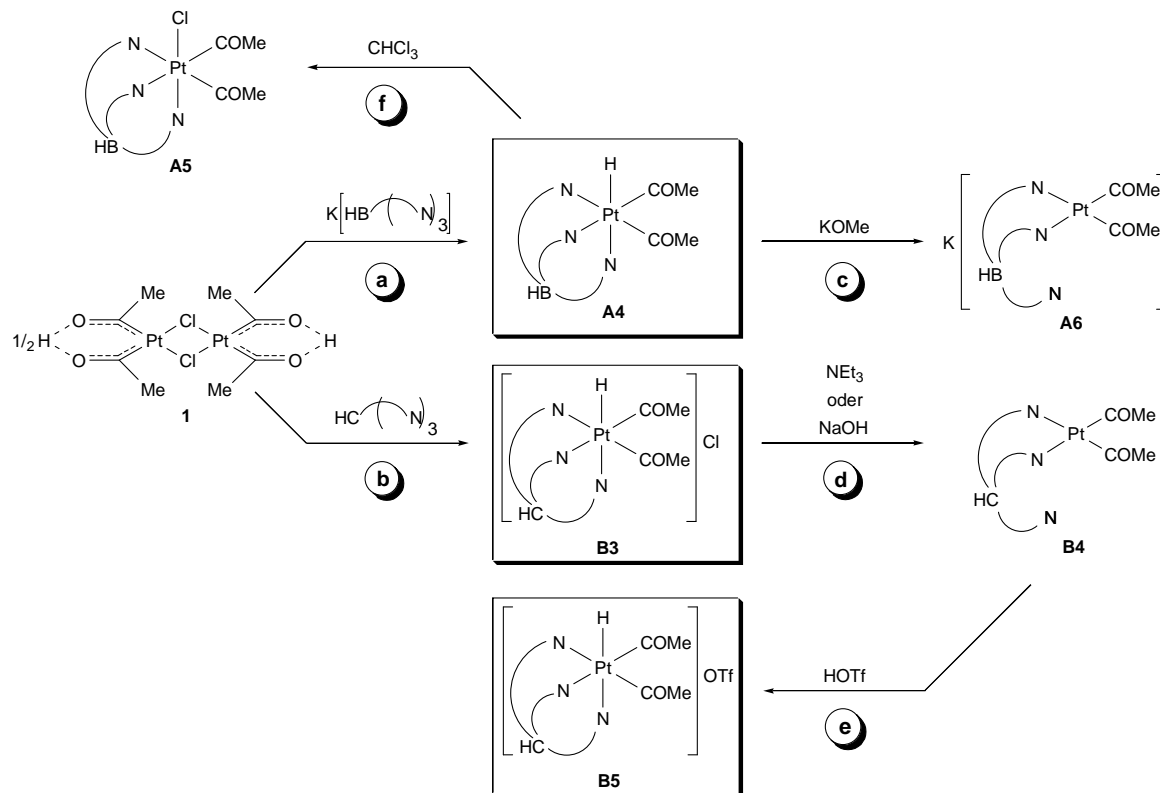
Diese Reaktionen können – obwohl keine Koordination des Halogenids erfolgt – als oxidative Additionen im erweiterten Sinne aufgefasst werden [1]. Prinzipiell wäre zwar auch eine „klassische“ oxidative Addition denkbar, der ein Ligandenaustausch ($\text{X}^- \rightarrow \text{pz}$) nachgelagert ist. Das ist aber wenig wahrscheinlich, da durch die Bootstruktur der $\text{B}(\mu\text{-pz})_2\text{Pt}$ - bzw. $\text{C}(\mu\text{-pz})_2\text{Pt}$ -Gruppe das Platinzentrum relativ gut abgeschirmt ist. Vielmehr ist anzunehmen, dass der in der Nähe des Platinzentrums positionierte dritte Pyrazolylring unmittelbar nach dem elektrophilen Angriff von R-X an Pt die freie sechste Koordinationsstelle besetzt oder die Übertragung des R^+ -Fragments und die Pyrazolylkoordination synchron ablaufen.

Im Rahmen der vorliegenden Arbeit wurden ausgehend vom Platina- β -diketon $[\text{Pt}_2\{(\text{COMe})_2\text{H}\}_2(\mu\text{-Cl})_2]$ (**1**) Diacetylplatin(II)-Komplexe mit bidentat koordinierten Liganden der Typen $(\text{pz}^x)_3\text{BR}$, $(\text{pz}^x)_3\text{CH}$ und $(\text{py})_3\text{COR}'$ synthetisiert und umfassend spektroskopisch und strukturell charakterisiert. Das typische strukturelle Merkmal dieser Verbindungen ist eine weitere Donorgruppe, die aufgrund der Ligandenstruktur in unmittelbarer Nähe des Platinzentrums positioniert ist. Die Rolle dieses „Ligandenarms“ in oxidativen Additionsreaktionen wurde ebenso wie der Einfluss der Ladung, des Substitutionsmusters und der Natur der Donorgruppe dieser potentiell tridentaten Liganden auf Eigenschaften, Stabilität und Reaktivität der Diacetylplatin-Komplexe untersucht. Die Ergebnisse dieser Untersuchungen belegen das außergewöhnliche Synthesepotential der Platina- β -diketone und damit einhergehend die großen Möglichkeiten zum Studium von Elementarschritten an Diacetylplatin-Komplexen, die sowohl in der metallorganischen Chemie als auch der homogenen Katalyse von grundsätzlicher Bedeutung sind.

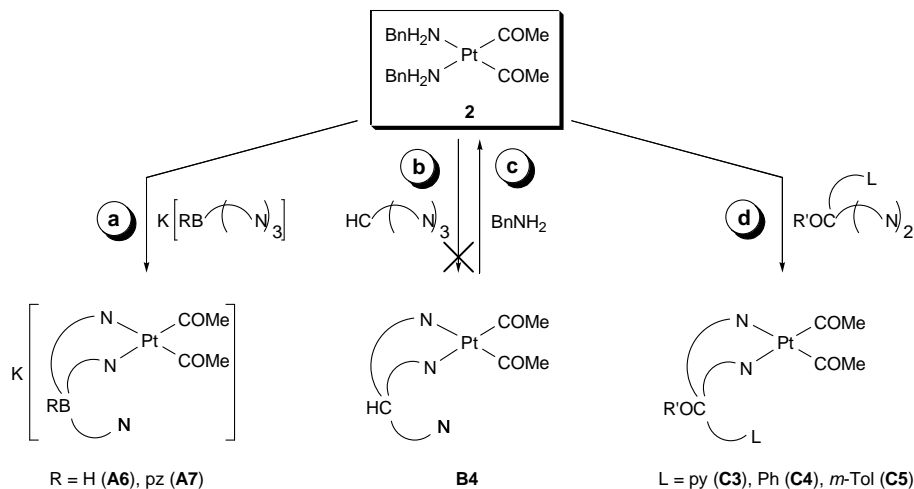
3. Zusammenfassung

Organoplatinkomplexe sind aufgrund ihrer thermodynamischen und/oder kinetischen Stabilität für die Untersuchung und Identifizierung reaktiver Zwischenstufen in homogen-katalytischen Reaktionen und für das Studium von Elementarschritten der Organometallchemie prädestiniert. So bietet beispielsweise das elektronisch (16 ve) und koordinativ ungesättigte Platina- β -diketon $[\text{Pt}_2\{(\text{COMe})_2\text{H}\}_2(\mu\text{-Cl})_2]$ (**1**) Zugang zu einer breiten Palette an Diacetylplatin-Komplexen mit bidentaten *N*-Donorliganden, welche zum Studium von oxidativen Additions- und reduktiven Eliminierungsreaktionen geeignet sind. Ziel der Arbeit war, ausgehend vom Platina- β -diketon **1**, die Synthese und umfassende Charakterisierung von Diacetylplatin-Komplexen mit potentiell tridentaten *N*-Donorliganden. Dabei sollten die Reaktivität, die Stabilität und die Eigenschaften dieser Verbindungen in Abhängigkeit der Ladung, des Substitutionsmusters und der Natur der Donorgruppe untersucht werden. Die dabei erzielten Ergebnisse lassen sich wie folgt zusammenfassen:

Über Hydridoplatin(IV)-Komplexe

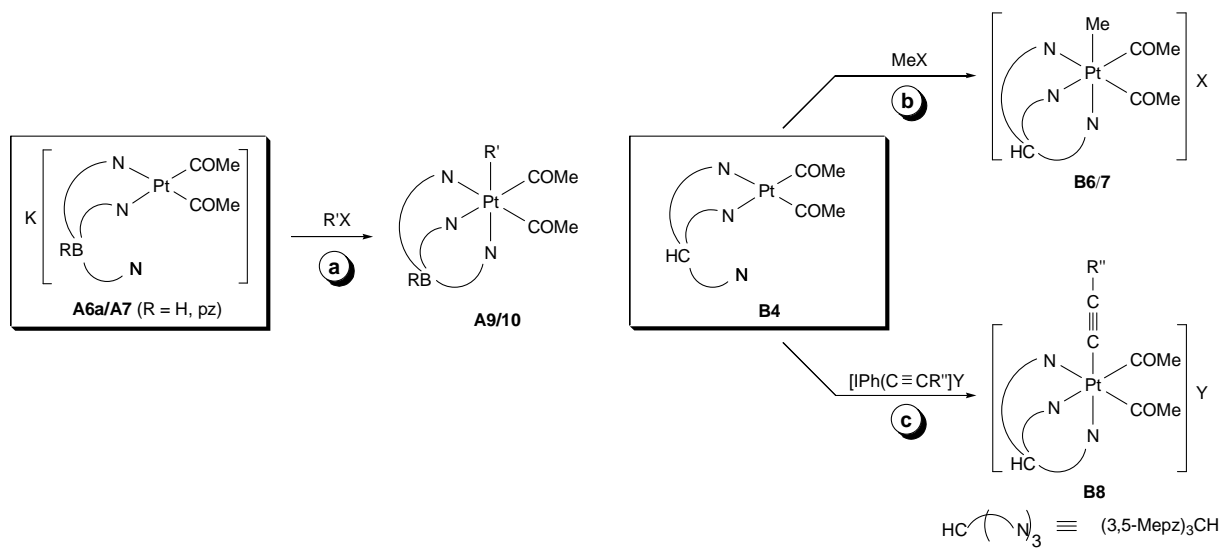


1. *Reaktionspfade a und b.* Die Umsetzungen des Platina- β -diketons **1** mit K[(3,5-R₂pz)BH] und (3,5-R₂pz)CH (R = H, Me) führte zur Bildung von Diacetyl(hydrido)platin(IV)-Komplexen der Typen **A4** bzw. **B3**. Während die neutralen Verbindungen **A4** mit Tris(pyrazolyl)borat-Liganden als sehr stabile Feststoffe isoliert und mittels Elementaranalyse, NMR- (¹H, ¹³C, ¹⁹⁵Pt) und IR-Spektroskopie sowie durch Röntgeneinkristallstrukturanalyse vollständig charakterisiert wurden, erwiesen sich die kationischen Hydridokomplexe **B3** mit Tris(pyrazolyl)methan-Liganden als thermisch labil. Die Konstitution dieser Verbindungen konnte jedoch durch Tieftemperatur-NMR-Untersuchungen sichergestellt werden.
2. *Reaktionspfade c und d.* Die Hydridoliganden der Komplexe **A4** und **B3** konnten durch Basen wie KOMe, NEt₃ oder NaOH abstrahiert werden, was zur Bildung der Diacetylplatin(II)-Komplexe **A6/B4** mit κ^2 -koordinierten Tris(pyrazolyl)borat- bzw. -methan-Liganden führte. Die Konstitution dieser Verbindungen wurde mittels hochauflösender Massenspektrometrie (HR-ESI-MS), NMR- und IR-Spektroskopie sowie durch Röntgeneinkristallstrukturanalyse (**B4**) belegt. Im Gegensatz zu den Verbindungen **A6** wurde bei den neutralen Komplexen **B4** ein schneller Austausch zwischen koordinierten und nicht koordinierten Pyrazolylringen beobachtet, dem wahrscheinlich ein dissoziativer Mechanismus zugrunde liegt.
3. *Reaktionspfad e.* Kationische Hydridokomplexe des Typs **B5** mit Tris(pyrazolyl)methan-Liganden konnten durch Umsetzung der Diacetylplatin(II)-Komplexe **B4** mit Trifluormethansulfonsäure erhalten werden. Die Konstitution dieser Verbindungen wurde massenspektrometrisch (HR-ESI-MS) und spektroskopisch sichergestellt. Im Vergleich zu den Hydridokomplexen **B3** waren diese Verbindungen sehr stabil, was den erheblichen Einfluss des Gegenions (OTf vs. Cl) auf die Stabilität dieser kationischen Hydridoplatin(IV)-Komplexe zeigt.
4. *Reaktionspfad f.* In chlorierten Lösungsmitteln wurde eine Zersetzung der Diacetyl(hydrido)platin(IV)-Komplexe **A4** und **B5** nach einem radikalischen Reaktionsmechanismus beobachtet. Im Fall von **A4** konnten die entsprechenden Chloridokomplexe **A5** in hoher Reinheit isoliert und vollständig charakterisiert werden.

Zur Reaktivität von $[Pt(\text{COMe})_2(\text{NH}_2\text{Bn})_2]$ (2)

5. *Reaktionspfad a.* Die Diacetylplatin(II)-Komplexe **A6/7** mit κ^2 -koordinierten Tris- und Tetrakis(pyrazolyl)borat-Liganden waren ausgehend vom Bis(benzylamin)platin(II)-Komplex **2** in Ligandenaustauschreaktionen zugänglich. Im Gegensatz zu den Verbindungen **A6** konnte Komplex **A7** mit Tetrakis(pyrazolyl)borat-Liganden nur gemäß dieser Syntheseroute dargestellt werden und wurde massenspektrometrisch (HR-ESI-MS), spektroskopisch und als Kronenetheraddukt auch strukturell charakterisiert.
6. *Reaktionspfade b und c.* Die Diacetylplatin(II)-Komplexe **B4** konnten nicht durch Umsetzung des Bis(benzylamin)platin(II)-Komplexes **2** mit Tris(pyrazolyl)methanen erhalten werden, weil das Gleichgewicht dieser Reaktion vollständig auf Seiten der Edukte liegt. Dementsprechend wurde gezeigt, dass die Komplexe **B4** mit Benzylamin zu **2** reagieren.
7. *Reaktionspfad d.* Die Umsetzungen von $[Pt(\text{COMe})_2(\text{NH}_2\text{Bn})_2]$ (**2**) mit $(\text{py})_3\text{COR}'$ ($\text{R}' = \text{H}, \text{Me}, \text{Et}, \text{Bn}$), $(2\text{-py})_2(\text{Ph})\text{COR}'$ bzw. $(2\text{-py})_2(m\text{-Tol})\text{COR}'$ ($\text{R}' = \text{H}, \text{Me}$) führte zur Bildung der Diacetylplatin(II)-Komplexe **C3–5** mit bidentat koordinierten Liganden. In Abhängigkeit von R' wurde eine gehinderte Moleküldynamik beobachtet, die auf sterische Wechselwirkungen zwischen der nicht koordinierten Pyridyl-/m-Tolylgruppe und dem Substituenten R' zurückzuführen ist.

Zur Reaktivität von Diacetylplatin(II)-Komplexen in oxidativen Additionsreaktionen



8. *Reaktionspfad a.* Die oxidative Addition von $\text{R}'\text{X}$ ($\text{R}'\text{X} = \text{MeI}$, EtI , BnBr) an die Diacetylplatin(II)-Komplexe **A6a** und **A7** lieferte die neutralen Alkylplatin(IV)-Komplexe **A9/10**. Die Konstitution dieser Verbindungen wurde elementaranalytisch, spektroskopisch sowie durch eine Röntgeneinkristallstrukturanalyse (**A9c**) sichergestellt.
9. *Reaktionspfad b.* Die kationischen Diacetyl(methyl)platin(IV)-Komplexe **B6** und **B7** sind durch Umsetzung der Diacetylplatin(II)-Komplexe **B4** mit Trifluormethansulfonsäure-methylester bzw. Methyliodid zugänglich. In $[\text{Pt}(\text{COMe})_2\text{Me}\{(3,5\text{-Me}_2\text{pz})_3\text{CH}\}] \text{I}$ (**B7a**) liegt sowohl im Festkörper als auch in Lösung ein C–H \cdots I-Wasserstoffbrücke zwischen der C–H-Gruppe am Rückgrat des Liganden und dem Gegenion (I^-) vor.
10. *Reaktionspfad c.* Umsetzungen von Diacetylplatin(II)-Komplexen mit Alkinyliodonium-Verbindungen ($[\text{IPh}(\text{C}\equiv\text{CR}'')] \text{X}$; $\text{R}'' = \text{SiMe}_3$, Ph , ${}^t\text{Bu}$, ${}^i\text{Pr}$) lieferten nur unter Verwendung von $(3,5\text{-Me}_2\text{pz})_3\text{CH}$ als Coligand stabile Diacetyl(alkinyl)platin(IV)-Komplexe. Die Konstitution der Komplexe **B8** ist massenspektrometrisch (HR-ESI-MS), NMR-spektroskopisch und auch durch Röntgeneinkristallstrukturanalysen belegt.

Die Ergebnisse dieser Arbeit belegen das herausragende Synthesepotential der Platina- β -diketone zur Darstellung von Diacetylplatin(II)- und -platin(IV)-Komplexen mit potentiell tridentaten *N*-Donorliganden. Weiterhin konnte gezeigt werden, wie vielfältig der Einfluss der Ladung, des Substitutionsmusters und der Natur der Donorgruppe dieser Liganden auf Eigenschaften, Reaktivität und Stabilität von Platin(II)- und Platin(IV)-Komplexen sein kann. Die vorliegenden Ergebnisse erweitern damit die Kenntnisse auf dem Gebiet der Koordinationschemie und Organometallchemie des Platins mit facial koordinierenden tridentaten *N*-Donorliganden.

4. Literaturverzeichnis

- [1] D. Steinborn, *Grundlagen der metallorganischen Komplexkatalyse*, Teubner, Wiesbaden 2007.
- [2] J. Smidt, W. Hafner, R. Jira, R. Sieber, J. Sedlmeier, A. Sabel, *Angew. Chem.* **1962**, *74*, 93.
- [3] (a) R. R. Schrock, A. H. Hoveyda, *Angew. Chem.* **2003**, *115*, 4740. (b) A. Fürstner, *Angew. Chem.* **2000**, *112*, 3140. (c) T. M. Trnka, R. H. Grubbs, *Acc. Chem. Res.* **2001**, *34*, 18.
- [4] F. Diederich, P. J. Stang, *Metal-catalyzed Cross-coupling Reactions*, Wiley-VCH Weinheim 1998.
- [5] (a) J. L. Speier, J. A. Webster, G. H. Barnes, *J. Am. Chem. Soc.* **1957**, *79*, 974. (b) B. D. Karstedt, *US 3.775.452*. **1973**. (c) G. Chandra, P. Y. Lo, P. B. Hitchcock, M. F. Lappert, *Organometallics* **1987**, *6*, 191. (d) P. B. Hitchcock, M. F. Lappert, N. J. W. Warhurst, *Angew. Chem., Int. Ed.* **1991**, *30*, 438.
- [6] (a) P. S. Pregosin, *Coord. Chem. Rev.* **1982**, *44*, 247. (b) R. G. Kidd, *Annu. Rep. NMR Spectrosc.* **1991**, *23*, 85.
- [7] (a) T. G. Appleton, H. C. Clark, L. E. Manzer, *Coord. Chem. Rev.* **1973**, *10*, 335. (b) T. G. Appleton, M. A. Bennett, *Inorg. Chem.* **1978**, *17*, 738.
- [8] (a) V. Guerchais, C. Lepinte, *J. Chem. Soc., Chem. Commun.* **1986**, 663 (b) A. Asdar, C. Lapinte, *J. Organomet. Chem.* **1987**, *327*, C33. (c) A. Asdar, C. Lapinte, L. Toupet, *Organometallics* **1989**, *8*, 2708. (d) D. H. Gibson, S. K. Mandal, K. Owens, J. F. Richardson, *Organometallics*, **1990**, *9*, 1936.
- [9] C. M. Lukehart, J. V. Zeile, *J. Am. Chem. Soc.* **1976**, *98*, 2365.
- [10] (a) C. M. Lukehart, *Acc. Chem. Res.* **1981**, *14*, 109. (b) C. M. Lukehart, *Adv. Organomet. Chem.* **1986**, *25*, 45.
- [11] D. Steinborn, *Dalton Trans.* **2005**, 2664.
- [12] (a) M. A. Garralda, R. Hernández, L. Ibarlucea, E. Pinilla M. R. Torres, *Organometallics* **2003**, *22*, 3600. (b) F. Acha, R. Ciganda, M. A. Garralda, R. Hernández, L. Ibarlucea, E. Pinilla M. R. Torres, *Dalton Trans.* **2008**, 4602.
- [13] (a) C. M. Lukehart, J. V. Zeile *J. Am. Chem. Soc.* **1978**, *100*, 2774. (b) C. M. Lukehart, J. V. Zeile *Inorg. Chem.* **1978**, *17*, 2369.
- [14] M. Gerisch, C. Bruhn, A. Vyater, J. A. Davies, D. Steinborn, *Organometallics* **1998**, *17*, 3101.

- [15] (a) M. Gerisch, F. W. Heinemann, C. Bruhn, J. Scholz, D. Steinborn, *Organometallics* **1999**, *18*, 564. (b) A. Vyater, C. Wagner, K. Merzweiler, D. Steinborn, *Organometallics* **2002**, *21*, 4369. (c) T. Gosavi, E. Rusanov, H. Schmidt, D. Steinborn, *Inorg. Chim. Acta* **2004**, *357*, 1781. (d) T. Gosavi, C. Wagner, H. Schmidt, D. Steinborn, *J. Organomet. Chem.* **2005**, *690*, 3229.
- [16] M. Werner, C. Bruhn, D. Steinborn, *J. Organomet. Chem.* **2008**, *693*, 2369.
- [17] C. Albrecht, C. Wagner, D. Steinborn, *Z. Anorg. Allg. Chem.* **2008**, *334*, 2858.
- [18] (a) M. Werner, C. Wagner, D. Steinborn, *J. Organomet. Chem.* **2009**, *694*, 190. (b) M. Werner, C. Bruhn, D. Steinborn, *Transition Met. Chem.* **2009**, *34*, 61.
- [19] T. Kluge, M. Bette, C. Vetter, J. Schmidt, D. Steinborn, *J. Organomet. Chem.* **2012**, *715*, 93.
- [20] (a) T. Kluge, *Diplomarbeit*, Martin-Luther-Universität Halle-Wittenberg, Halle (Saale) 2009. (b) E. Herrmann, *Masterarbeit*, Martin-Luther-Universität Halle-Wittenberg, Halle (Saale) 2011.
- [21] S. Richter, *Diplomarbeit*, Martin-Luther-Universität Halle-Wittenberg, Halle (Saale) 2011.
- [22] S. Schwieger, R. Herzog, C. Wagner, D. Steinborn, *J. Organomet. Chem.* **2009**, *694*, 3548.
- [23] S. Trofimenko, *J. Am. Chem. Soc.* **1967**, *89*, 3170.
- [24] (a) S. Trofimenko, *Scorpionates: The Coordination Chemistry of Polypyrazolylborate Ligands*; Imperial College Press: London, 1999. (b) Pettinari, C. *Scorpinate II: Chelating Borate Ligands*; Imperial College Press: London, 2008.
- [25] B. Domhöver, W. Kläui, A. Kremer-Ach, R. Bell, D. Mootz, *Angew. Chem.* **1998**, *110*, 3218.
- [26] (a) A. J. Canty, S. D. Fritsche, H. Jin, J. Patel, B. W. Skelton, A. D. White, *Organometallics* **1997**, *16*, 2175. (b) M. P. Jensen, D. D. Wick, S. Reinartz, P. S. White, J. L. Templeton, K. I. Goldberg, *J. Am. Chem. Soc.* **2003**, *125*, 8614. (c) C. N. Kostelansky, M. G. MacDonald, P. S. White, J. L. Templeton, *Organometallics* **2006**, *25*, 2993. (d) M. G. MacDonald, C. N. Kostelansky, P. S. White, J. L. *Organometallics* **2006**, *25*, 4560.
- [27] Cambridge Structural Database (ConQuest), Version 1.14, Cambridge University Chemical Laboratory, Cambridge 2011.
- [28] (a) U. E. Bucher, A. Curraro, R. Nesper, H. Rüegger, L. M. Venanzi, E. Younger, *Inorg. Chem.* **1995**, *34*, 64. (b) M. Akita, K. Ohta, Y. Takahashi, S. Hikichi, Y.

- Moro-oka, *Organometallics* **1997**, *16*, 4121. (c) M. Akita, M. Hashimoto, S. Hikichi, Y. Moro-oka, *Organometallics* **2000**, *19*, 3744.
- [29] (a) A. J. Canty, T. Rodemann, *Inorg. Chem. Commun.* **2003**, *6*, 1382. (b) A. J. Canty, T. Rodemann, B. W. Skelton, A. H. White, *Organometallics* **2006**, *25*, 3996. (c) A. J. Canty, M. G. Gardiner, R. C. Jones, T. Rodemann, M. Sharma, *J. Am. Chem. Soc.* **2009**, *131*, 7236.
- [30] V. V. Zhdankin, P. J. Stang, *Tetrahedron* **1998**, *54*, 10927.
- [31] A. J. Canty, R. P. Watson, S. S. Karpiniec, T. Rodemann, M. G. Gardiner, R. C. Jones, *Organometallics* **2008**, *27*, 3203.
- [32] J. L. Look, D. D. Wick, J. M. Mayer, K. I. Goldberg, *Inorg. Chem.* **2009**, *48*, 1356.
- [33] (a) P. S. Pregosin, *Coord. Chem. Rev.* **1982**, *44*, 247. (b) R. G. Kidd, *Annu. Rep. NMR Spectrosc.* **1991**, *23*, 85.
- [34] (a) T. G. Appleton, H. C. Clark, L. E. Manzer, *Coord. Chem. Rev.* **1973**, *10*, 335. (b) P. K. Sajith, C. S. Suresh, *J. Organomet. Chem.* **2011**, *696*, 2086.
- [35] B. R. D. Nayagam, S. R. Jebas, D. Kalavathy, R. Murugesan, D. Schollmeyer, *Acta Crystallogr. Sect. E* **2010**, *E66*, m667.
- [36] F. D. Rochon, R. Melanson, M. Doyon, *Inorg. Chem.* **1987**, *26*, 3065.
- [37] (a) H. R. Bigmore, S. L. Lawrence, P. Mounford, C. S. Tredget, *Dalton Trans.* **2005**, 635. (b) C. Pettinari, R. Pettinari, *Coord. Chem. Rev.* **2005**, *249*, 525.
- [38] W. Hückel, H. Bretschneider, *Chem. Ber.* **1937**, *9*, 2024.
- [39] D. L. Reger, T. C. Grattan, K. J. Brown, C. A. Little, J. J. S. Lamba, A. L. Rheingold, R. D. Sommer, *J. Organomet. Chem.* **2000**, *607*, 120.
- [40] D. L. Reger, T. C. Grattan, *Synthesis* **2003**, 350.
- [41] (a) W. Kläui, M. Berghahn, G. Rheinwald, H. Lang, *Angew. Chem., Int. Ed.*, **2000**, *39*, 2464. (b) W. Kläui, M. Berghahn, W. Frank, G. J. Reiß, T. Schönherr, G. Rheinwald, H. Lang, *Eur. J. Inorg. Chem.*, **2003**, 2059.
- [42] A. J. Hallett, K. M. Anderson, N. G. Conelly, M. F. Haddow, *Dalton Trans.* **2009**, 4181.
- [43] S. Trofimenko, *J. Am. Chem. Soc.*, **1970**, *92*, 5118.
- [44] T. Steiner, *Cryst. Rev.* **1996**, *6*, 1.
- [45] (a) T. Steiner, *Acta Cryst.* **1998**, *B54*, 456. (b) G. R. Desiraju, T. Steiner, *The Weak Hydrogen Bond In Structural Chemistry and Biology*, Oxford University Press, New York 1999.

- [46] (a) M. C. Janzen, H. A. Jenkins, M. C. Jennings, L. M. Rendina, R. J. Puddephatt, *J. Chem. Soc., Dalton Trans.* **1999**, 1713. (b) A. J. Canty, T. Rodemann, B. W. Skelton, A. H. White, *Inorg. Chem. Commun.* **2005**, 8, 55. (c) C. Munro-Leighton, Y. Feng, J. Zhang, N. M. Alsop, T. B. Gunnoe, P. D. Boyle, J. L. Petersen, *Inorg. Chem.* **2008**, 47, 6124.
- [47] P. Rademacher, *Strukturen organischer Moleküle*; VCH Verlagsgesellschaft, Weinheim 1987.
- [48] M. Bette, J. Schmidt, D. Steinborn, *Eur. J. Inorg. Chem.*, DOI: 10.1002/ejic.201201468.
- [49] (a) H. Kessler, *Angew. Chem., Int. Ed. Engl.* **1970**, 9, 219. (b) J. Sandström, *Dynamic NMR Spectroscopy*, Academic Press INC., London 1982.
- [50] F. A. Jalón, B. R. Manzano, A. Otero, M. C. Rodríguez-Pérez, *J. Organomet. Chem.* **1995**, 494, 179.
- [51] J. Elguero, A. Fruchier, A. de la Hoz, F. A. Jalón, B. R. Manzano, A. Otero, F. Gómez-de la Torre, *Chem. Ber.* **1996**, 129, 589.
- [52] C. Xu, G. K. Anderson, L. Brammer, J. Braddock-Wilking, N. P. Rath, *Organometallics* **1996**, 15, 3972.
- [53] L. E. Crascall, J. L. Spencer, *J. Chem. Soc., Dalton Trans.* **1992**, 3445.
- [54] C. Titze, J. Hermann, H. Vahrenkamp, *Chem. Ber.* **1995**, 128, 1095.
- [55] H. Pfeiffer, A. Rojas, J. Niesel, U. Schatzschneider, *Dalton Trans.* **2009**, 4292.
- [56] G. A. Jeffrey, *An Introduction to Hydrogen Bonding*, Oxford University Press, Oxford 1997.
- [57] (a) R. J. Puddephatt, *Coord. Chem. Rev.* **2001**, 219, 157. (b) S. A. O'Reilly, P. S. White, J. L. Templeton, *J. Am. Chem. Soc.* **1996**, 118, 5684.
- [58] L. F. Szczepura, L. M. Witham, K. J. Takeuchi, *Coord. Chem. Rev.* **1998**, 174, 5.
- [59] (a) D. L. White, J. W. Faller, *Inorg. Chem.* **1982**, 21, 3119. (b) R. T. Jonas, T. D. P. Stack, *Inorg. Chem.* **1998**, 37, 6615.
- [60] V. Levacher, H. Adolfson, C. Moberg, *Acta Chem. Scand.* **1996**, 50, 454.
- [61] M. J. Hannon, P. C. Mayers, P. C. Taylor, *J. Chem. Soc., Perkin Trans 1* **2000**, 1881.
- [62] H. Fujii, T. Yoshimura, H. Kamada, *Chem. Lett.* **1996**, 581.
- [63] R. Fandos, C. Hernández, A. Otero, A. Rodriguez, M. J. Ruiz, P. Terreros, *J. Chem. Soc., Dalton Trans.* **2000**, 2990.
- [64] A. J. Canty, S. D. Fritzsche, H. Jin, R. T. Honeyman, B. W. Skelton, A. H. White, *J. Organomet. Chem.* **1996**, 510, 281.

- [65] D. Morales, J. Perez, L. Riera, V. Riera, D. Miguel, *Organometallics* **2001**, *20*, 4517.
- [66] M. Bette, D. Steinborn, *Phosphorus, Sulfur, Silicon Relat. Elem.* **2012**, *187*, 1271.
- [67] M. Bette, T. Rüffer, C. Bruhn, J. Schmidt, D. Steinborn, *Organometallics* **2012**, *31*, 3700.
- [68] P. H. M. Budzelaar, *gNMR, NMR Simulation Program*; Version 5.0.6.0; Ivory Soft, 2006.
- [69] Gaussian09, weitere Details im Kapitel 3.10. „Computational Details“ der Publikation C.
- [70] M. Block, M. Bette, C. Wagner, D. Steinborn, *Z. Anorg. Allg. Chem.* **2011**, *637*, 206.
- [71] (a) U. Fekl, W. Kaminsky, K. I. Goldberg, *J. Am. Chem. Soc.* **2001**, *123*, 6423. (b) R. J. Puddephatt, *Angew. Chem., Int. Ed. Engl.* **2002**, *41*, 261.
- [72] (a) L. M. Rendina, R. J. Puddephatt, *Chem. Rev.* **1997**, *97*, 1735. (b) C. R. Baar, L. P. Carbray, M. C. Jennings, R. J. Puddephatt, *Organometallics* **2000**, *19*, 2482. (c) S. M. Nabavizadeh, S. J. Hoseini, B. Z. Momeni, N. Shahabadi, M. Rashidi, A. H. Pakiari, K. Eskandari, *Dalton Trans.* **2008**, 2414.

Anhang: Publikationen zur Arbeit

Veröffentlichungen als Erstautor und als Anlagen A–D beigelegt:

- A M. Bette, T. Rüffer, C. Bruhn, J. Schmidt, D. Steinborn, *Organometallics* **2012**, *31*, 3700–3710.

“*Synthesis, Characterization, and Reactivity of Diacetylplatinum(II) and -platinum(IV) Complexes Bearing κ^2 and κ^3 Coordinated Scorpionate Ligands*”

- B M. Bette, J. Schmidt, D. Steinborn, *Eur. J. Inorg. Chem.*, im Druck,
DOI: 10.1002/ejic.201201468.

„*Diacetylplatinum(II) and -platinum(IV) Complexes Bearing κ^2 - and κ^3 -Coordinated Tris(pyrazolyl)methane Ligands: Investigations on the Synthesis, Fluxionality and Reactivity in Dependence on the Substitution Pattern of the Ligands*”

- C M. Bette, T. Kluge, J. Schmidt, D. Steinborn, *Organometallics*, im Druck,
DOI: 10.1021/om400091h

„*Diacetylplatinum(II) Complexes with κ^2 Coordinated Tris(pyridyl)methanol and -methyl Ether Ligands: Structural Insight into the Ligand Dynamics in Solution*”

- D M. Bette, D. Steinborn, *Phosphorus, Sulfur, Silicon Relat. Elem.* **2012**, *187*, 1271–1277.

„*Synthesis, Characterization, and Structures of Tris(2-pyridyl)tin Compounds*”

Weitere Veröffentlichungen, zu denen durch Anfertigung von Röntgeneinkristallstrukturanalysen beigetragen wurde:

- H. Kommera, G. N. Kaluđerović, M. Bette, J. Kalbitz, P. Fuchs, S. Fulda, W. Mier, R. Paschke, *Chem.-Biol. Interact.* **2010**, *185*, 128.
“*In vitro anticancer studies of alpha- and beta-D-glucopyranose botulin anomers*”
- M. Block, M. Bette, C. Wagner, D. Steinborn, *Z. Anorg. Allg. Chem.* **2011**, *637*, 206.
“*On the reactivity of the platina- β -diketone $[Pt_2\{(COMe)_2H\}(\mu-Cl)_2]$ towards $Ph_2PCH_2CH_2CH_2SO_xPh$ ($x = 0, 2$)*”

- M. Block, T. Kluge, M. Bette, J. Schmidt, D. Steinborn, *Organometallics* **2010**, 29, 6749.
„On the reactivity of rhodium(I) complexes with κP -coordinated γ -phosphino functionalized propyl phenyl sulfide ligands: routes to cyclic rhodium complexes with $\kappa C,\kappa P$ - and $\kappa P,\kappa S$ -coordinated ligands as well as bis(diphenylphosphino)methanide ligands“
- M. Block, M. Bette, C. Wagner, J. Schmidt, D. Steinborn, *J. Organomet. Chem.* **2011**, 696, 1768.
„Rhodium(I) complexes with κP coordinated ω -phosphinofunctionalized alkyl phenyl sulfide, sulfoxide and sulfone ligands and their reactions with sodium bis(trimethylsilyl)amide and Ag[BF₄]“
- R. I. Yousef, M. Bette, G. N. Kaluderovic, R. Paschke, Y. R. Cui, D. Steinborn, H. Schmidt, *Polyhedron* **2011**, 30, 1990.
„Structure determination and investigations on cytotoxicity of potassium dichlorido(*L*-prolinato)platinate(II) versus chlorido(dimethyl sulfoxide)(*L*-prolinato)platinum(II) complex – In vitro antitumor deactivation by Cl-/DMSO ligand exchange“
- A. König, M. Bette, C. Wagner, R. Lindner, D. Steinborn, *Organometallics*, **2011**, 30, 5919.
„On the equilibrium between alkyne and olefin platinum(II) complexes of Zeise's Salt type: syntheses and characterization of [K(18C6)][PtCl₃(RC≡CR')]“
- A. König, C. Wagner, M. Bette, D. Steinborn, *Dalton Trans.* **2012**, 41, 7156.
„On the isomerization of cyclooctyne into cycloocta-1,3-diene: synthesis, characterization, and structure of a dinuclear platinum(II) complex with a $\mu\text{-}\eta^2\text{:}\eta^2\text{-}1,3\text{-COD}$ ligand“
- G. Ludwig, G. N. Kaluderovic, M. Bette, M. Block, R. Paschke, D. Steinborn, *J. Inorg. Biochem.* **2012**, 113, 77.
„Highly active neutral ruthenium(II) arene complexes: Synthesis, characterization, and investigations of their anticancer properties“
- T. Kluge, M. Bette, C. Vetter, J. Schmidt, D. Steinborn, *J. Organomet. Chem.* **2012**, 715, 93.
„Synthesis and characterization of diacetyl platiunum(II) complexes with two primary and secondary amine ligands“
- G. M. Rakić, S. Grugić-Šipka, G. N. Kaluđerović, M. Bette, L. Filipović, S. Aranđelović, S. Radulović, Z. Lj. Tešić, *Eur. J. Med. Chem.* **2012**, 55, 214.
„The Synthesis, spectroscopic, X-ray characterization and vitro cytotoxic testing results of activity of five new trans-platinum(IV) complexes with functionalized pyridines“

- A. König, M. Bette, C. Bruhn, D. Steinborn, *Eur. J. Inorg. Chem.* **2012**, 2012, 5881.
„Dinuclear Olefin and Alkyne Complexes of Platinum(II)“
- S. R. Chaudhuri, G. N. Kaluđerović, M. Bette, J. Schmidt, H. Schmidt, R. Paschke, D. Steinborn, *Inorg. Chim. Acta* **2013**, 394, 472.
„Synthesis, characterization, and cytotoxicity studies of platinum(II) complexes with amino acid ligands in various coordination modes“
- G. Ludwig, G. N. Kaluđerović, T. Rüffer, M. Bette, M. Korb, M. Block, R. Paschke, H. Lang, D. Steinborn, *Dalton Trans.* **2013**, 42, 3771.
„Cationic arene ruthenium(II) complexes with chelating P-functionalized alkyl phenyl sulfide und sulfoxide ligand as potent anticancer agents“

Synthesis, Characterization, and Reactivity of Diacetylplatinum(II) and -platinum(IV) Complexes Bearing κ^2 - and κ^3 -Coordinated Scorpionate Ligands

Martin Bette,[†] Tobias Rüffer,[‡] Clemens Bruhn,[§] Jürgen Schmidt,[⊥] and Dirk Steinborn^{*†}

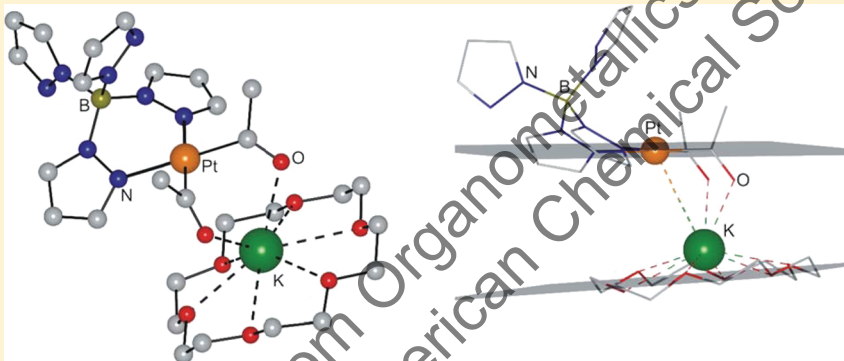
[†]Institute of Chemistry—Inorganic Chemistry, Martin Luther University of Halle-Wittenberg, Kurt-Mothes-Straße 2, D-06120 Halle, Germany

[‡]Institute of Chemistry, Chemnitz University of Technology, Straße der Nationen 62, D-09111 Chemnitz, Germany

[§]Institute of Chemistry, University of Kassel, Heinrich-Plett-Straße 40, D-34132 Kassel, Germany

[⊥]Department of Bioorganic Chemistry, Leibniz Institute of Plant Biochemistry, Weinberg 3, D-06120 Halle, Germany

Supporting Information



ABSTRACT: Reactions of the dinuclear platin- β -diketone $[\text{Pt}_2\{(\text{COR})_2\text{H}\}_2(\mu\text{-Cl})_2]$ (**1**) with $\text{K}[(\text{pz})_3\text{BH}]$ and $\text{K}[(3,5\text{-Me}_2\text{pz})_3\text{BH}]$ (pz = pyrazolyl; $3,5\text{-Me}_2\text{pz}$ = 3,5-dimethylpyrazolyl) afforded neutral diacetyl(hydrido)platinum(IV) complexes $[\text{Pt}(\text{COMe})_2\text{H}\{(\text{pz})_3\text{BH}\}]$ (**4a**) and $[\text{Pt}(\text{COMe})_2\text{H}\{(3,5\text{-Me}_2\text{pz})_3\text{BH}\}]$ (**4b**), bearing κ^3 -bonded tris(pyrazolyl)borate (scorpionate) ligands. These complexes were found to decompose in chloroform solution under formation of the respective chlorido complexes $[\text{Pt}(\text{COMe})_2\text{Cl}\{(\text{pz})_3\text{BH}\}]$ (**5a**) and $[\text{Pt}(\text{COMe})_2\text{Cl}\{(3,5\text{-Me}_2\text{pz})_3\text{BH}\}]$ (**5b**) as the initial step. Diacetylplatinum(II) complexes with κ^2 -coordinated scorpionate ligands ($\text{K}[\text{Pt}(\text{COMe})_2\{(\text{pz})_3\text{BH}\}]$, **6a**; $\text{K}[\text{Pt}(\text{COMe})_2\{(3,5\text{-Me}_2\text{pz})_3\text{BH}\}]$, **6b**; $\text{K}[\text{Pt}(\text{COMe})_2\{(\text{pz})_4\text{B}\}]$, **7**; $\text{K}[\{\text{Pt}(\text{COMe})_2\}_2\{(\text{pz})_4\text{B}\}]$, **8**) were obtained in ligand exchange reactions of $[\text{Pt}(\text{COMe})_2(\text{NH}_2\text{Bn})_2]$ (Bn = benzyl) with the respective potassium (pyrazolyl)borates. The deprotonation of the hydrido complexes **4** with potassium methoxide led also to the formation of **6**. Diacetylplatinum(II) complexes **6a** and **7** were found to react in oxidative addition reactions with alkyl halides to yield diacetylplatinum(IV) complexes of the type $[\text{Pt}(\text{COMe})_2\text{R}\{(\text{pz})_3\text{BH}\}]$ ($\text{R} \neq \text{Me}$, **9a**; Et , **9b**; Bn , **9c**) and $[\text{Pt}(\text{COMe})_2\text{R}\{(\text{pz})_4\text{B}\}]$ ($\text{R} = \text{Me}$, **10a**; Et , **10b**; Bn , **10c**), respectively, with κ^3 -bonded scorpionate ligands. The identities of all platinum complexes were unambiguously proved by microanalyses or by high-resolution mass spectrometric investigations, by NMR (^1H , ^{13}C , ^{195}Pt) and IR spectroscopies, and by single-crystal X-ray diffraction analyses (**4a**, **5a**, **7**·($18\text{C}6$), **9c**; $18\text{C}6$ = 18-crown-6). The reactivity of the complexes is discussed in terms of hemilability of the scorpionate ligands.

1. INTRODUCTION

Dinuclear platin- β -diketones $[\text{Pt}_2\{(\text{COR})_2\text{H}\}_2(\mu\text{-Cl})_2]$ (R = alkyl) can be considered as hydroxycarbene complexes being stabilized by intramolecular O—H···O hydrogen bonds to neighboring acyl ligands. Due to their electronic unsaturation (16 valence electron complexes) and their kinetically labile ligand sphere, platin- β -diketones exhibit a unique reactivity and thus are precursor complexes for the synthesis of a great variety of acetyl platinum(II) and platinum(IV) complexes with bidentate $\text{N}^{\wedge}\text{N}$, $\text{P}^{\wedge}\text{P}$, $\text{S}^{\wedge}\text{S}$, and $\text{N}^{\wedge}\text{O}$ ligands.¹ Platin- β -diketones are accessible by reactions of hexachloridoplatinic

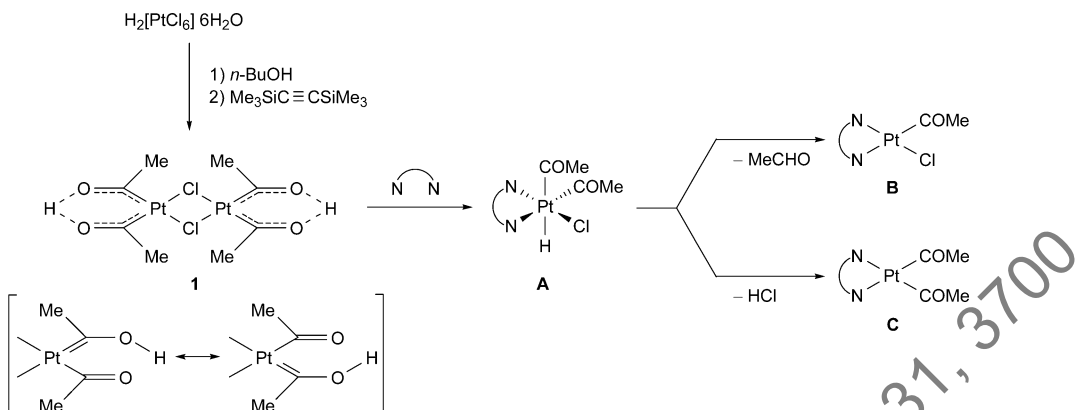
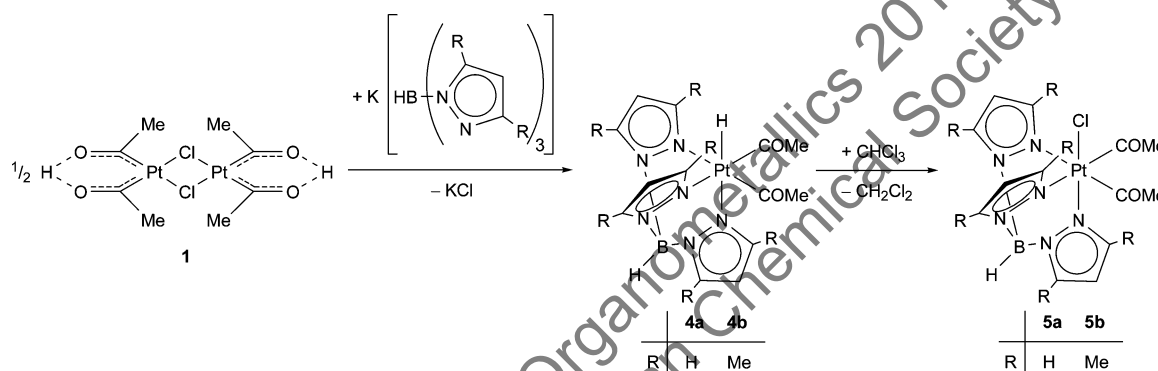
acid with *n*-butyl alcohol and trimethylsilyl-substituted alkynes, as shown in Scheme 1 for the formation of the parent complex **1** ($\text{R} = \text{Me}$).² Thus, the reaction of complex **1** with $\text{N}^{\wedge}\text{N}$ ligands leads to the formation of thermally extraordinarily stable diacetyl(hydrido)platinum(IV) complexes of type A (Scheme 1).³ Depending on the reaction conditions, these complexes were found to react under reductive elimination of acetaldehyde to yield acetyl(chlorido)platinum(II) complexes

Received: March 8, 2012

Published: April 30, 2012

Organometallics

Article

Scheme 1. Synthesis of the Platina- β -diketone **1** and Its Reactivity toward Bidentate N,N Ligands**Scheme 2.** Synthesis of Hydridoplatinum(IV) Complexes **4a** and **4b** and Their Reactivity toward CHCl_3 .

of type **B**.³ The selective formation of diacetylplatinum(II) complexes of type **C** can be induced by the addition of bases to complexes **A**.⁴ In summary, reactions of the platina- β -diketone **1** toward various bidentate nitrogen donor ligands and also reactions of the resulting type **C** diacetylplatinum(II) complexes with reagents that enable oxidative addition reactions such as alkyl halides or halogens are well investigated.⁵ In contrast, the reaction of bis(2-picoly)amine with $[\text{Pt}_2\{(\text{COMe})_2\text{H}\}_2(\mu\text{-Cl})_2]$ (**1**) yielding a hydridoplatinum(IV) complex is the only example of an investigation on the reactivity of platina- β -diketones toward tridentate nitrogen donor ligands.⁶

Tris(pyrazolyl)borates of the type $[(\text{pz}^X)_3\text{BH}]^-$ ($\text{pz}^X =$ pyrazolyl group with unspecified substituents) are versatile anionic tridentate nitrogen donor ligands that are well established in transition metal chemistry. These ligands belong to the large class of scorpionate ligands.⁷ Due to their tetrahedral geometry, tris(pyrazolyl)borates generally coordinate as facial-binding $\kappa^3\text{-N},\text{N}',\text{N}''$ ligands in octahedral complexes. For the same reason, the coordination is restricted to the $\kappa^2\text{-N},\text{N}'$ coordination mode with a pendant third pyrazolyl ring in square-planar complexes. However, also some other coordination modes (such as $\kappa\text{-N}$) and also agostic B–H interactions are reported.⁷ Furthermore, tris(pyrazolyl)borates can act as hemilabile ligands, as reported for some rhodium complexes, where a fast interconversion between $\kappa^3\text{-N},\text{N}',\text{N}''$ (trigonal-bipyramidal) and $\kappa^2\text{-N},\text{N}'$ coordination mode (square-planar) was observed.⁸

Here, we report on the reactivity of the platina- β -diketone $[\text{Pt}_2\{(\text{COMe})_2\text{H}\}_2(\mu\text{-Cl})_2]$ (**1**) toward pyrazolylborates $[(\text{pz}^X)_3\text{BH}]^-$, yielding stable hydridoplatinum(IV) complexes,

which convert into chloridoplatinum(IV) complexes in chloroform solution. Furthermore, we present the synthesis of type **C** complexes (see Scheme 1) bearing $\kappa^2\text{-N},\text{N}'$ -coordinated scorpionate ligands and their reactivity in oxidative addition reactions.

2. RESULTS AND DISCUSSION

2.1. Reactivity of Platina- β -diketone **1 toward Scorpionate Ligands.** **2.1.1. Synthesis and Reactivity of Diacetyl(hydrido)platinum(IV) Complexes.** The dinuclear platina- β -diketone $[\text{Pt}_2\{(\text{COMe})_2\text{H}\}_2(\mu\text{-Cl})_2]$ (**1**) was found to react with $\text{K}[(\text{pz})_3\text{BH}]$ and $\text{K}[(3,5\text{-Me}_2\text{pz})_3\text{BH}]$ under formation of diacetyl(hydrido)platinum(IV) complexes **4a/b** (Scheme 2). In contrast, in the reaction of **1** with $\text{K}[\text{B}(\text{pz})_4]$ only a mixture of unidentified products was obtained. Compounds **4a/b** were isolated in good yields of 70% and 85%, respectively, as white powders, which were characterized by NMR (^1H , ^{13}C , ^{195}Pt) and IR spectroscopy as well as by microanalyses and single-crystal X-ray diffraction analysis (**4a**). The reactions were performed in THF, and the workup procedure was done in methylene chloride. Due to a restricted stability in methylene chloride, the latter has to be done quickly. In chloroform complexes **4** are even less stable than in methylene chloride. It was found that the first step of this decomposition is the conversion of the hydridoplatinum(IV) complexes **4a/b** into the analogous chloridoplatinum(IV) complexes **5a/b** (Scheme 2). The best way to isolate them proved to be stirring chloroform solutions of **4a/b** at room temperature and under exposure to ambient light for two days. Longer reaction times (3–4 days) resulted in a further decomposition, yielding several unidentified products. Thus,

Organometallics

Article

complexes **5a/b** were obtained as white powders in good yields (80–85%) and characterized by NMR (^1H , ^{13}C , ^{195}Pt) and IR spectroscopy as well as by high-resolution mass spectrometric (HRMS-ESI) investigations and single-crystal X-ray diffraction analysis (**5a**).

An analogous reactivity of the hydridodimethylplatinum(IV) complex $[\text{PtMe}_2\text{H}\{(3,5-\text{Me}_2\text{pz})_3\text{BH}\}]$ in CCl_4 under UV radiation yielding $[\text{PtMe}_2\text{Cl}\{(3,5-\text{Me}_2\text{pz})_3\text{BH}\}]$ was found by Goldberg and was shown to be a radical reaction.⁹ However, the reaction of **4a/b** yielding **5a/b** proceeds under much milder reaction conditions. The formation of CHDCl_2 could be observed when these reactions were performed as an NMR experiment in CDCl_3 . Furthermore, in a darkened NMR tube the reaction was not finished after two days. Thus, a radical pathway can also be assumed here.

2.1.2. Spectroscopic Characterization. Selected ^1H , ^{13}C , and ^{195}Pt NMR spectroscopic parameters of complexes **4** and **5** are given in Table 1. The spectra confirm the identities of the

Table 1. Selected NMR Spectroscopic Parameters of $[\text{Pt}(\text{COMe})_2\text{L}\{(\text{pz})_3\text{BH}\}]$ ($\text{L} = \text{H}$, **4a; $\text{L} = \text{Cl}$, **5a**) and $[\text{Pt}(\text{COMe})_2\text{L}\{(3,5-\text{Me}_2\text{pz})_3\text{BH}\}]$ ($\text{L} = \text{H}$, **4b**; $\text{L} = \text{Cl}$, **5b**) (δ in ppm, J in Hz)**

	COCH_3		COCH_3	$\text{Pt}-\text{H}$	δ_{Pt}
	δ_{H} ($^3J_{\text{Pt},\text{H}}$)	δ_{C} ($^2J_{\text{Pt},\text{C}}$)	δ_{C} ($^1J_{\text{Pt},\text{C}}$)	δ_{H} ($^1J_{\text{Pt},\text{H}}$)	
4a	2.60 (23.9)	44.3 (255.3)	191.6 — ^a	−17.80 (1522)	−1618.1
4b	2.32 (13.7)	40.4 (206.9)	195.5 (896.3)	−18.22 (1496)	−1740.0
5a	2.79 (8.9)	35.1 (91.5)	187.5 (736.6)		−762.9
5b	2.52 (6.6)	33.2 (94.6)	190.8 (736.6)		−763.0

^aDue to poor solubility not observed.

complexes; all signals were found in the expected shift range with correct intensities in the ^1H NMR spectra. The two sets of signals with 2:1 intensity in the aromatic area and only one set of signals for the two acetyl ligands reflect the mirror symmetry of all compounds in solution. In the hydrido complexes **4a/b** the ^1H and ^{13}C chemical shifts of the acetyl ligands are in a comparable range, but the platinum–hydrogen and platinum–carbon coupling constants in complex **4a** are significantly larger than for **4b**. This could be explained by a higher *trans* influence of the methyl-substituted scorpionate ligand because of the electron-donating effect of the methyl groups. The resonances of the hydrido ligands and the $^1J_{\text{Pt},\text{H}}$ coupling constants are in the range of other hydridoplatinum(IV) complexes bearing κ^3 -bonded scorpionate ligands.¹⁰

Compared to the hydrido complexes **4**, the δ_{H} and δ_{C} of the acetyl ligands in the corresponding chlorido complexes **5** are shifted by about 0.2 ppm to lower field and by 4–9 ppm to higher field, respectively. The platinum coupling constants were found to be significantly lower in compounds **5** than in **4**. The shifts in the ^{195}Pt NMR spectra show a strong influence on the type of ligand. In accordance with the electronegativity $\chi(\text{H}) < \chi(\text{Cl})$ the ^{195}Pt chemical shifts of hydrido complexes **4** were found to be at much higher fields than those for the chlorido complexes **5** ($\Delta\delta_{\text{Pt}}$ ca. 1000 pm).

The hydrido and chlorido complexes can be easily identified by IR spectroscopy. The former ones exhibit a characteristic $\nu_{\text{Pt}-\text{H}}$ absorbance at 2230/2233 cm^{-1} (**4a/b**), and the latter

ones a $\nu_{\text{Pt}-\text{Cl}}$ absorbance at 331/328 cm^{-1} (**5a/b**).^{11,12} The B–H stretching frequencies of these complexes will be discussed in Section 2.2.2.

2.1.3. Structures of $[\text{Pt}(\text{COMe})_2\text{H}\{(\text{pz})_3\text{BH}\}]$ (4a**) and $[\text{Pt}(\text{COMe})_2\text{Cl}\{(\text{pz})_3\text{BH}\}]$ (**5a**).** Crystals of **4a** and **5a** suitable for X-ray diffraction analysis were obtained from saturated methylene chloride (**4a**) and chloroform (**5a**) solution at −40 °C. Both compounds crystallized as isolated molecules without unusual intermolecular interactions (shortest distance between non-hydrogen atoms: 3.25(1) Å, C8···O1', **4a**; 3.119(6) Å, C5···O1', **5a**). The molecular structures are shown in Figures 1

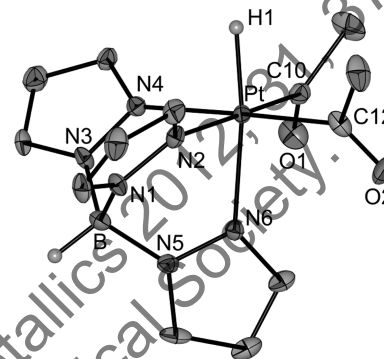


Figure 1. Molecular structure of $[\text{Pt}(\text{COMe})_2\text{H}\{(\text{pz})_3\text{BH}\}]$ (**4a**). The ellipsoids are shown with a probability of 30%. H atoms are omitted for clarity except that at the boron atom and the hydrido ligand. Selected structural parameters (distances in Å, angles in deg): Pt–C10 2.040(7), Pt–C12 2.027(8), Pt–N2 2.208(5), Pt–N4 2.182(6), Pt–N6 2.162(5), Pt–H1 1.61(2), C10–Pt–C12 87.2(3), C10–Pt–N6 93.8(3), C10–Pt–N4 93.3(3), C12–Pt–N6 92.8(3), C12–Pt–N2 95.2(3), N2–Pt–N4 84.2(2), N2–Pt–N6 85.3(2), N4–Pt–N6 85.8(2), C10–Pt–N2 177.5(3), C12–Pt–N4 178.5(3).

and 2; selected structural parameters are given in the figure captions. The platinum atoms adopt a distorted octahedral geometry and are coordinated by two acetyl ligands, the facial

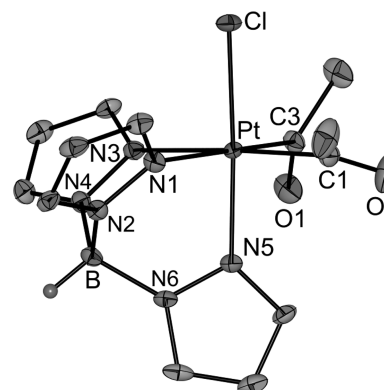
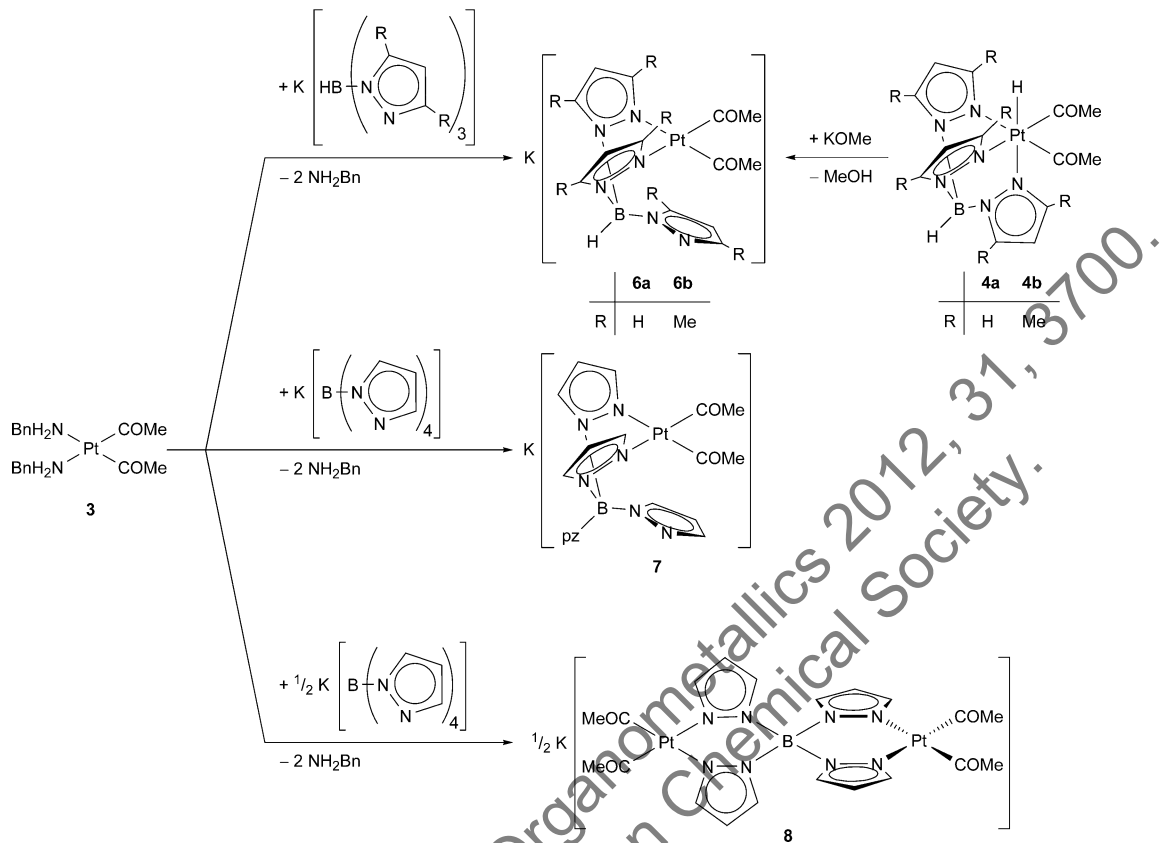


Figure 2. Molecular structure of $[\text{Pt}(\text{COMe})_2\text{Cl}\{(\text{pz})_3\text{BH}\}]$ (**5a**). The ellipsoids are shown with a probability of 30%. H atoms are omitted for clarity except that at the boron atom. Selected structural parameters (distances in Å, angles in deg): Pt–C1 2.048(5), Pt–C3 2.054(5), Pt–N1 2.219(4), Pt–N3 2.174(4), Pt–N5 2.060(4), Pt–Cl 2.331(1), C1–Pt–C3 89.0(2), C1–Pt–Cl 90.6(1), C3–Pt–Cl 92.8(1), C1–Pt–N1 98.6(2), C1–Pt–N5 89.7(2), C3–Pt–N3 88.7(2), C3–Pt–N5 92.2(2), N1–Pt–N3 83.7(1), N1–Pt–N5 86.3(2), N3–Pt–N5 87.4(1), N1–Pt–Cl 88.7(1), N3–Pt–Cl 92.5(1), C1–Pt–N3 176.2(2), C3–Pt–N1 172.3(2), N5–Pt–Cl 175.0(1).

Scheme 3. Synthesis of Diacetylplatinum(II) Complexes Bearing κ^2 -Bonded Scorpionate Ligands

κ^3 -coordinated tris(pyrazolyl)borate ligand, and one hydrido ligand (**4a**) or one chlorido ligand (**5a**). Due to the restricted bite of the facial-coordinated scorpionate ligand, the N–Pt–N angles are slightly diminished (84.2(2)–85.8(2) $^\circ$, **4a**; 83.7(1)–87.4(1) $^\circ$, **5a**). Although the hydrido ligand in the structure of **4a** could be located in the difference Fourier map, its location may be compromised by residual electron density near the platinum atom. Thus, no geometric parameters containing the hydrido ligand are discussed here.

In both structures, the carbonyl oxygen atoms of the two acetyl ligands were found on the same side of the complex plane. Thus, the diacetyl moieties represent a “*cisoid*” conformation. Within the 3 σ criterion, the Pt–C bond lengths in **4a** (2.040(7)/2.027(8) Å) are equal to those in **5a** (2.054(5)/2.048(5) Å). The lengths of the Pt–N bonds *trans* to the acetyl ligands are in the range 2.174(4)–2.219(4) Å (**4a**, **5a**). The Pt–N bond length of 2.162(5) Å *trans* to the hydrido ligand in complex **4a** is significantly longer than the respective bond *trans* to the chlorido ligand in complex **5a** (2.060(4) Å), reflecting a *trans* influence order Cl $^-$ < H $^-$ as expected.¹³

2.2. Synthesis and Characterization of Diacetylplatinum(II) Complexes Bearing κ^2 -Coordinated Scorpionate Ligands. **2.2.1. Synthesis.** Because of its substitution-labile benzylamine ligands, [Pt(COMe)₂(NH₂Bn)₂] (**3**) was found to be a useful precursor complex for synthesizing a variety of diacetylplatinum(II) complexes via facile ligand exchange reactions.¹⁴ The reactions of [Pt(COMe)₂(NH₂Bn)₂] (**3**) with tris- or tetrakis(pyrazolyl)-borates in a molar ratio of 1:1 led to the formation of the mononuclear diacetylplatinum(II) complexes **6a**, **6b**, and **7**, bearing κ^2 -bonded scorpionate ligands (Scheme 3). Furthermore, the reaction of **3** with K[(pz)₄B] in a molar ratio of 2:1

resulted in the formation of the dinuclear complex **8**, where two diacetylplatinum units are bridged by a tetrakis(pyrazolyl)-borate ligand in a $\mu\text{--}\kappa^2N,N'\text{--}\kappa^2N'',N'''$ mode. The white, moisture-sensitive complexes **6**–**8** were obtained in yields between 57% and 87% and characterized by NMR spectroscopy (¹H, ¹³C, ¹⁹⁵Pt), by IR spectroscopy, by high-resolution mass spectrometric (HRMS-ESI) investigations, and by a single-crystal X-ray measurement of the 18-crown-6 adduct of **7**. Complexes **6a**, **6b**, and **7** were soluble in THF, methylene chloride, and chloroform, but in chloroform and methylene chloride complexes **6a** and **6b** decomposed within a few hours. Compound **8** was only slightly soluble in methanol or DMSO, but decomposition occurred within about one hour.

An alternative route to prepare diacetylplatinum(II) complexes is, in general, the reduction of the diacetyl(hydrido)-platinum(IV) complexes via proton abstraction by a base.⁴ Having this in mind, the hydridoplatinum(IV) complexes **4a** and **4b**, bearing κ^3 -coordinated tris(pyrazolyl)borate ligands, were treated with potassium methoxide (Scheme 3). As anticipated, the reactions proceeded with deprotonation, yielding the platinum(II) complexes **6a** and **6b**, bearing κ^2 -bonded scorpionate ligands, whose identities were deduced from NMR spectra.

2.2.2. Spectroscopic Characterization. ¹H and ¹³C NMR spectra of complexes **6**–**8** proved to be fully consistent with the constitution of the complexes given in Scheme 3. Selected NMR spectroscopic data are given in Table 2. The ¹H NMR spectra of **6**–**8** displayed chemical equivalence of the acetyl ligands as well as a 2:1 (**6a**, **6b**) and, respectively, a 2:2 (**7**) pattern for the resonances in the aromatic area, which is indicative of a mirror symmetry. For all complexes δ_H and δ_C of the acetyl ligands are in a narrow range. Compared with the

Organometallics

Article

Table 2. Selected NMR Spectroscopic Parameters of Complexes 6–8 (δ in ppm)

	COCH ₃		COCH ₃	δ_{Pt}
	δ_{H}	δ_{C}	δ_{C}	
6a	2.04	44.5	234.6	-3351.4
6b	1.73	44.0	235.3	-3372.7
7	1.85	44.1	234.5	-3371.4
8	1.80	43.6	226.5	-3339.8

diacetylplatinum(IV) complexes 4 and 5, in the platinum(II) complexes 6–8 the carbonyl carbon atoms of the acetyl ligands were found to be low-field shifted by approximately 40 ppm, as it has been already observed for other diacetylplatinum(II) complexes.⁴ The ¹⁹⁵Pt resonances of all compounds are shifted to higher field in comparison to the hydridoplatinum(IV) (4a, 4b) and chloridoplatinum(IV) (5a, 5b) complexes, as expected.¹⁵

In complexes containing tris(pyrazolyl)borate ligands the B–H stretching frequencies proved to be indicative of the coordination mode of the scorpionate ligand and the substitution pattern of the pyrazolyl rings.⁸ The requisite values for complexes 4–6 are given in Table 3. The 3,5-

Table 3. B–H Stretching Vibrations of Complexes 4–6

complex	hapticity	$\nu(\text{B–H})$
[Pt(COMe) ₂ H{(pz) ₃ BH}] (4a)	κ^3	2481
[Pt(COMe) ₂ Cl{(pz) ₃ BH}] (5a)	κ^3	2513
K[Pt(COMe) ₂ {(pz) ₃ BH}] (6a)	κ^2	2454
[Pt(COMe) ₂ H{(3,5-Me ₂ pz) ₃ BH}] (4b)	κ^3	2528
[Pt(COMe) ₂ Cl{(3,5-Me ₂ pz) ₃ BH}] (5b)	κ^3	2553
K[Pt(COMe) ₂ {(3,5-Me ₂ pz) ₃ BH}] (6b)	κ^2	2466

dimethyl substitution of the pyrazolyl rings gave rise to a shift to higher wavenumbers by 12–47 cm⁻¹. Furthermore, in complexes 6, with κ^2 -coordinated tris(pyrazolyl) ligands, the $\nu_{\text{B–H}}$ absorbance was found at significantly lower wavenumbers than in complexes 4 and 5, bearing κ^3 -bonded ligands.

2.2.3. Structure of [K(18C6)][Pt(COMe)₂{(pz)₃B}] (7·(18C6)). Crystals of 7·(18C6) were obtained from a THF solution of [Pt(COMe)₂(NH₂Bn)₂] (3) and an equimolar amount of [K(18C6)][(pz)₃B] with a layer of diethyl ether at room temperature. In the solid state, 7·(18C6) forms discrete molecules without notable intermolecular interactions (shortest distance between non-hydrogen atoms: 3.31(1) Å, N8···C23'). The molecular structure is shown in Figure 3, and selected structural parameters are given in the figure caption. The platinum atom is square-planar coordinated by two acetyl ligands and a κ^2 -bonded tetrakis(pyrazolyl)borate ligand. The B(μ -pz)₂Pt unit adopts the typical boat conformation with the boron and platinum atoms at the apexes.¹⁶ The angles between neighboring ligands are all close to 90° (86.1(3)–94.5(3)°).

There are close contacts of the [K(18C6)]⁺ cation and the oxygen atoms of the two acetyl ligands, which lie on the same side of the coordination plane (“cisoid” conformation). The K···O2 distance (2.854(4) Å) is in the same range as the K···O distances between the potassium ion and the oxygen atoms of the crown ether (2.815(4)–2.992(3) Å), whereas the K···O1 distance (2.770(5) Å) is even slightly shorter. Furthermore, the potassium ion is located 0.845(1) Å outside the mean plane of the crown ether defined by its six oxygen atoms. This plane is nearly parallel (5.24(9)°) to the complex plane (see Figure 3B).

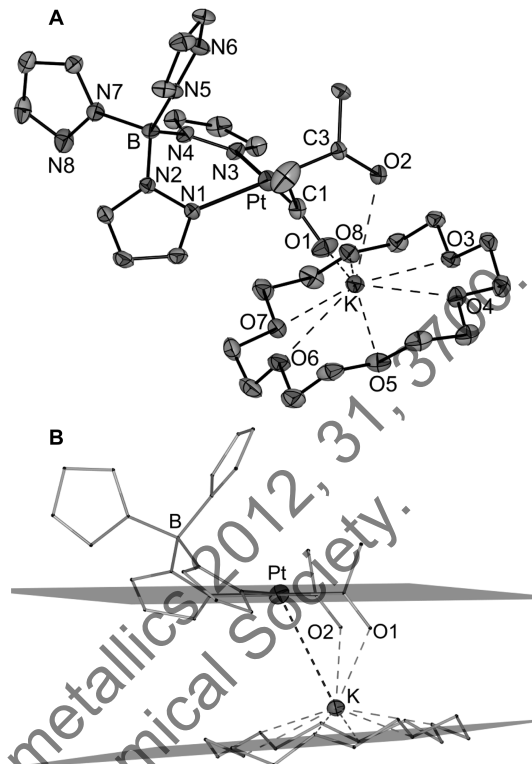


Figure 3. (A) Molecular structure of 7·(18C6). The ellipsoids are shown with a probability of 30%. H atoms are omitted for clarity. Selected structural parameters (distances in Å, angles in deg): Pt–C1 1.988(6), Pt–C3 1.984(4), Pt–N1 2.117(3), Pt–N3 2.115(4), C1–Pt–C3 86.1(3), C1–Pt–N1 92.8(2), C3–Pt–N3 94.5(3), N1–Pt–N3 86.6(2), C1–Pt–N3 179.4(2), C3–Pt–N1 178.0(3), K–O1 2.770(5), K–O2 2.854(4), K–O3 2.992(3), K–O4 2.815(4), K–O5 2.938(4), K–O6 2.900(4), K–O7 2.967(4), K–O8 2.922(4), Pt···K 3.511(1). (B) Wire model of the complex showing the relative position of the coordination plane (Pt,C1,C3,N1,N3) and the mean plane of the crown ether molecule defined by its oxygen atoms.

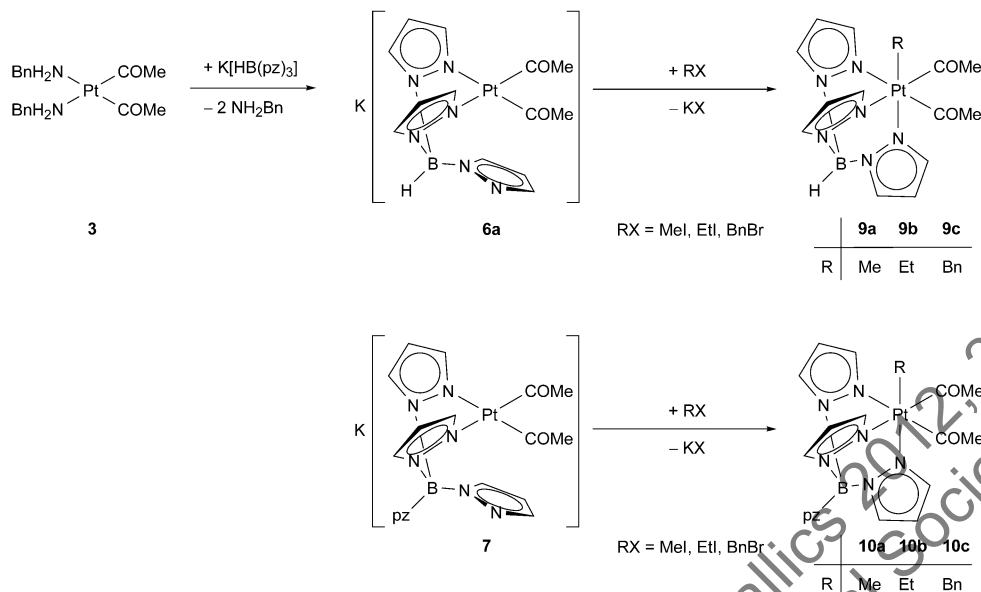
Thus, the potassium atom has a relatively short contact with the platinum atom (Pt···K 3.511(1) Å). Similar short distances were found, for instance, in [K(18C6)]₂[PtCl₄] (3.668 Å)¹⁷ and K[PtCl₃(NH₂Bn)]·H₂O (3.588 Å).¹⁸

2.3. Oxidative Addition Reactions to Diacetylplatinum(II) Complexes Bearing κ^2 -Coordinated Scorpionate Ligands. **2.3.1. Synthesis of Alkyl(diacetyl)-platinum(IV) Complexes.** Reactions of K[Pt(COMe)₂{(pz)₃BH}] (6a) and K[Pt(COMe)₂{(pz)₄B}] (7) with methyl iodide, ethyl iodide, and benzyl bromide resulted in the formation of neutral platinum(IV) complexes [Pt(COMe)₂R{(pz)₃BH}] (9a–c) and [Pt(COMe)₂R{(pz)₄B}] (10a–c), respectively (Scheme 4). The syntheses of 9a–c were performed in a one-pot procedure starting from the benzylamine complex 3 without isolation of compound 6a. The advantage is a higher overall yield because all side products (KX, benzylamine) could be easily removed by extracting the reaction solutions with an aqueous solution of HCl. On the other hand, the synthesis of complexes 10a–c started from the isolated complex 7 because the noncoordinated pyrazolyl ring of the tetrakis(pyrazolyl)borate ligand would be protonated upon workup of the reaction mixture with HCl. All complexes were isolated in 46–61% yield as colorless, moisture- and air-stable powders and were characterized by NMR spectroscopy

Organometallics

Article

Scheme 4. One-Pot Synthesis of $[\text{Pt}(\text{COMe})_2\text{R}\{(\text{pz})_3\text{BH}\}]$ (9a–c) Starting from $[\text{Pt}(\text{COMe})_2(\text{NH}_2\text{Bn})_2]$ (3) and Preparation of $[\text{Pt}(\text{COMe})_2\text{R}\{(\text{pz})_4\text{B}\}]$ (10a–c)



(^1H , ^{13}C , ^{195}Pt), elemental analysis, and single-crystal X-ray diffraction analysis (9c).

2.3.2. Spectroscopic Characterization. ^1H and ^{13}C NMR spectra of complexes 9 and 10 are fully consistent with the constitution of the complexes given in Scheme 4. Selected spectroscopic parameters are compiled in Table 4. The NMR

Table 4. Selected NMR Spectroscopic Parameters of $[\text{Pt}(\text{COMe})_2\text{R}\{(\text{pz})_3\text{BH}\}]$ (9) and $[\text{Pt}(\text{COMe})_2\text{R}\{(\text{pz})_4\text{B}\}]$ (10) (δ in ppm, J in Hz)

R	COCH_3		COCH_3		
	δ_{H} ($^3\text{J}_{\text{Pt},\text{H}}$)	δ_{C} ($^2\text{J}_{\text{Pt},\text{C}}$)	δ_{C} ($^1\text{J}_{\text{Pt},\text{C}}$)	δ_{Pt}	
9a	Me	2.29 (10.7)	36.5 (184.0)	194.3 (936.6)	-1461.5
9b	Et	2.25 (9.8)	36.7 (182.2)	194.6 (981.9)	-1396.5
9c	Bn	2.24 (8.9)	35.7 (168.6)	194.1 (956.8)	-1281.5
10a	Me	2.36 (11.0)	36.7 (181.9)	196.2 (939.3)	-1489.2
10b	Et	2.31 (10.1)	35.5 (181.3)	194.8 (970.6)	-1436.4
10c	Bn	2.29 (9.0)	36.5 (169.6)	194.9 (951.6)	-1314.8

spectroscopic parameters of the acetyl ligands do not depend significantly on the type of scorpionate ligand ($[(\text{pz})_3\text{BH}]^-$ vs $[(\text{pz})_4\text{B}]^-$). The platinum–hydrogen and platinum–carbon coupling constants of the acetyl ligands were found to be dependent on the nature of the alkyl ligand R, although the acetyl and the alkyl ligands are in a mutual *cis* position. Thus, for instance, for the $^1\text{J}_{\text{Pt},\text{C}}$ couplings the order Me < Bn < Et was found (Table 4). The ^{195}Pt resonances were found to be between -1490 and -1280 ppm and, thus, shifted approximately 2000 ppm to higher field in comparison to the respective platinum(II) precursor complexes $\text{K}[\text{Pt}(\text{COMe})_2\{(\text{pz})_3\text{BH}\}]$ (6a) and $\text{K}[\text{Pt}(\text{COMe})_2\{(\text{pz})_4\text{B}\}]$ (7), as expected.¹⁵

2.3.3. Structure of $[\text{Pt}(\text{COMe})_2\text{Bn}\{(\text{pz})_3\text{BH}\}]$ (9c). Crystals of 9c suitable for X-ray diffraction analysis were obtained from a toluene solution with a layer of *n*-pentane at 4 °C. Complex 9c crystallized as discrete molecules without unusual intermolecular interactions (shortest distance between non-hydrogen

atoms; 3.26(4) Å, O1–C3'). The molecular structure is shown in Figure 4, and selected structural parameters are given in the

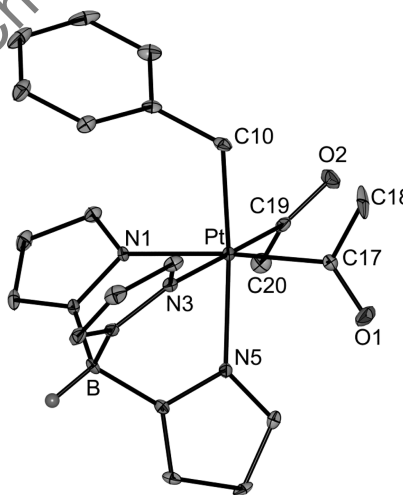
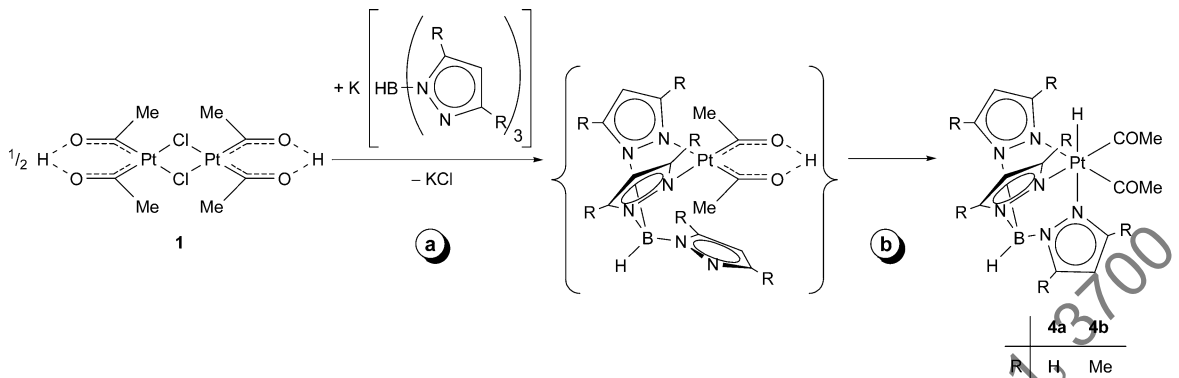


Figure 4. Molecular structure of $[\text{Pt}(\text{COMe})_2\text{Bn}\{(\text{pz})_3\text{BH}\}]$ (9c). The ellipsoids are shown with a probability of 30%. H atoms are omitted for clarity except the B–H proton. Selected structural parameters (distances in Å, angles in deg): Pt–C17 2.041(3), Pt–C19 2.030(3), Pt–C10 2.089(3), Pt–N1 2.176(3), Pt–N3 2.183(3), Pt–N5 2.177(3), C17–Pt–C19 85.3(1), C10–Pt–C17 90.6(1), C10–Pt–C19 90.1(1), C10–Pt–N1 94.7(1), C10–Pt–N3 89.7(1), C17–Pt–N3 94.8(1), C17–Pt–N5 91.7(1), C19–Pt–N1 92.6(1), C19–Pt–N5 96.0(1), N1–Pt–N3 87.4(1), N1–Pt–N5 83.3(1), N3–Pt–N5 84.20(9), C10–Pt–N5 173.7(1), C17–Pt–N1 174.3(1), C19–Pt–N3 179.8(1).

figure caption. The platinum atom is located in the center of a distorted octahedral environment and coordinated by a facially κ^3 -bonded tris(pyrazolyl)borate ligand and by two acetyl and one benzyl ligand. Due to the restricted bite of the scorpionate ligand, the N–Pt–N angles are slightly diminished (83.3(1)–87.4(1)°). Within the 3σ criterion, both Pt–N bonds (2.176(3)–2.183(3) Å) and the Pt–C bonds of the acetyl

Scheme 5. Reactivity of Platina- β -diketone 1 toward Tris(pyrazolyl)borates

ligands ($2.041(3)/2.030(3)$ Å) are of the same length each. In contrast, the Pt–C bond of the benzyl ligand ($2.089(3)$ Å) is significantly longer than those of the acetyl ligands.

The carbonyl oxygen atoms of the acetyl ligands are located on different sides of the Pt,C17,C19,N1,N3 complex plane, thus representing a “*transoid*” conformation. Whereas one acetyl ligand (C17,C18,O1) is almost perpendicular to the complex plane (interplanar angle $80.1(2)^\circ$), the other one (C19,C20,O2) is twisted significantly from the vertical position ($45.1(2)^\circ$).

2.4. Conclusions. Within this work, the synthesis and reactivity of diacetylplatinum complexes bearing κ^2 - and κ^3 -bonded tris- and tetrakis(pyrazolyl)borate ligands are described. The following conclusions can be drawn:

- (1) Reactions of the platina- β -diketone 1 with anionic tris(pyrazolyl)borate ligands afford thermally stable, neutral hydridoplatinum(IV) complexes 4, bearing κ^2 -coordinated scorpionate ligands (Schemes 2 and 5). It can be assumed that these reactions go along with a cleavage of the Cl–Pt–Cl bridges and κ^2 coordination of the tris(pyrazolyl)borate ligand, forming neutral mononuclear platina- β -diketon complexes as intermediates (Scheme 5, a). This reaction is instantaneously followed by an oxidation of the platinum center through a proton shift, forming, with coordination of the pendant pyrazolyl group, an octahedral diacetyl(hydrido)platinum(IV) complex (Scheme 5, b). This proposed reaction pathway is in compliance with observations made in reactions of platina- β -diketone 1 with various bidentate N–N donors.^{1,4}
- (2) Diacetylplatinum(II) complexes 6–8, with κ^2 -bonded tris- and tetrakis(pyrazolyl)borate ligands, are accessible in facile ligand exchange reactions with $[Pt(COMe)_2(NH_2Bn)_2]$ (3) and, alternatively for complexes 6a/b, by deprotonation of the respective hydridoplatinum(IV) complexes (Scheme 3). Thus, it has been demonstrated that $[Pt(COMe)_2(NH_2Bn)_2]$ (3) is a useful alternative for the synthesis of diacetylplatinum(II) complexes starting from the platina- β -diketone 1, especially if the conventional pathway hydridoplatinum(IV) type A complex → diacetylplatinum(II) type C complex failed (see Scheme 1).
- (3) The reactions of $K[Pt(COMe)_2\{(pz)_3BH\}]$ (6a) and $K[Pt(COMe)_2\{(pz)_3B\}]$ (7) with alkyl halides lead to the formation of the neutral alkylplatinum(IV) complexes $[Pt(COMe)_2R\{(pz)_3BH\}]$ (9) and $[Pt(COMe)_2R\{(pz)_3B\}]$ (10).

$(COMe)_2R\{(pz)_3B\}$] (10), with κ^3 -bonded scorpionate ligands (Scheme 4). In most cases, oxidative addition of primary alkyl halides to square-planar platinum(II) complexes occurs by a polar S_N2 mechanism.¹⁹ Thus, most likely, to complexes 6a/7 the organyl group R and the N atom of the pendant pyrazolyl group are coordinated to Pt, yielding complexes 9/10 without prior coordination of the halide X^- . A “classical” oxidative addition with coordination of X^- (prior to the N coordination of the pendant pyrazolyl group) is less likely and, in particular, with regard to the boat conformation of the $B(\mu-pz)_2Pt$ unit^{f6} in the starting platinum(II) complexes 6a/7, which sterically shield the platinum center.

For all these reactions the capability of κ^2 -coordinated scorpionate ligands to occupy an additional coordination site by the pendant pyrazolyl group and of κ^3 -coordinated scorpionate ligands to create a vacant coordination site forming a pendant pyrazolyl group, respectively, is of special importance. Thus, this chemistry is a further instructive example that scorpionates are versatile flexidentate ligands.

3. EXPERIMENTAL PART

3.1. General Comments. All reactions were performed in an argon atmosphere using the standard Schlenk techniques. Solvents were dried (diethyl ether, THF, and *n*-pentane over Na/benzophenone, CH_2Cl_2 over CaH_2 , acetone over phosphorus pentoxide followed by 4 Å molecular sieves) and distilled prior to use. NMR spectra were recorded at $27^\circ C$ with Varian Gemini 200, VXR 400, and Unity 500 spectrometers. Chemical shifts are relative to solvent signals ($CDCl_3$, δ_H 7.24, δ_C 77.0; $THF-d_8$, δ_H 3.58, δ_C 67.6; acetone- d_6 , δ_H 2.04, δ_C 29.8; $DMSO-d_6$, δ_H 2.49, δ_C 39.5) as internal references; $\delta^{(195)Pt}$ is referenced to $Na_2[PtCl_6]$. IR spectra were recorded on a Galaxy Mattson 5000 FT-IR spectrometer using KBr pellets. Microanalyses were performed by the University of Halle microanalytical laboratory using a CHNS-932 (LECO) elemental analyzer. The high-resolution ESI mass spectra were obtained from a Bruker Apex III Fourier transform ion cyclotron resonance (FT-ICR) mass spectrometer (Bruker Daltonics) equipped with an infinity cell, a 7.0 T superconducting magnet (Bruker), a rf-only hexapole ion guide, and an external APOLLO electrospray ion source (Agilent, off-axis spray). The sample solutions were introduced continuously via a syringe pump with a flow rate of $120 \mu L h^{-1}$. The complexes $[Pt_2\{(COMe)_2H\}_2(\mu-Cl)_2]$ (1) and $[Pt(COMe)_2(NH_2Bn)_2]$ (3) were prepared according to literature methods.^{2,14}

3.2. Synthesis of $[Pt(COMe)_2H\{(pz)_3BH\}]$ (4a). To a suspension of $[Pt_2\{(COMe)_2H\}_2(\mu-Cl)_2]$ (1) (200 mg, 0.31 mmol) in THF (5 mL) at $-78^\circ C$ was added dropwise a solution of $K[(pz)_3BH]$ (166 mg, 0.66 mmol) in THF (5 mL). After stirring for 30 min at this temperature, the reaction mixture was allowed to warm to room

Organometallics

Article

temperature and stirred for an additional 1 h, resulting in a clear, colorless solution. Then, the solvent was removed in vacuo, the residue was extracted with methylene chloride (5 mL) and filtered, and *n*-pentane (15 mL) was added to the solution. The precipitate formed was filtered off, washed with *n*-pentane (3 × 2 mL), and dried in vacuo. Yield: 218 mg (70%).

Anal. Calcd for $C_{13}H_{17}N_6O_2BPt$ (495.2 g/mol): C, 31.53; H, 3.46; N, 16.97. Found: C, 31.60; H, 3.66; N, 16.66. 1H NMR (400 MHz, acetone- d_6): δ -17.80 (s+d, 1H, $^1J_{Pt,H}$ = 1522 Hz, Pt-H), 2.60 (s+d, $^3J_{Pt,H}$ = 23.9 Hz, 6H, COCH₃), 6.30 (t, 2H, $H^{4/4'}$ pz), 6.37 (t, 1H, H^9 pz), 7.82 (d, 2H, $H^{3/3'}$ pz), 7.88 (d, 2H, $H^{5/5'}$ pz), 7.90 (d, 1H, H^{10} pz), 8.12 (d, 1H, H^8 pz). ^{13}C NMR (125 MHz, acetone- d_6): δ 44.3 (s+d, $^2J_{Pt,C}$ = 255.3 Hz, COCH₃), 106.2 (s, $C^{4/4'}$ pz), 106.8 (s, C^9 pz), 136.1 (s, C^{10} pz), 136.4 (s, $C^{5/5'}$ pz), 141.7 (s, C^8 pz), 143.3 (s, $C^{3/3'}$ pz), 191.6 (s, COCH₃). (Here and in the following, pyrazolyl rings are numbered consecutively 1–5, 6–10, ...; for chemically equivalent rings primed numbers are used.) ^{195}Pt NMR (86 MHz, acetone- d_6): δ -1618.1 (d, $^1J_{Pt,H}$ = 1506.9 Hz). IR: ν (BH) 2481, ν (PtH) 2230, ν (CO) 1695, ν (CO) 1656 cm⁻¹.

3.3. Synthesis of $[Pt(COMe)_2H\{(3,5-Me_2pz)_3BH\}]$ (4b). To a suspension of $[Pt_2\{(COCH_3)_2H\}_2(\mu-Cl)_2]$ (1) (84 mg, 0.13 mmol) in THF (5 mL) at -78 °C was added dropwise a solution of K[(3,5-Me₂pz)₃BH] (93.7 mg, 0.28 mmol) in THF (5 mL). After stirring for 30 min at this temperature, the reaction mixture was allowed to warm to room temperature and stirred for 2 h, resulting in a clear, colorless solution. Then, the solvent was removed in vacuo, and the residue extracted with methylene chloride (5 mL). After evaporation to dryness in vacuo, the residue was dissolved in toluene (5 mL), *n*-pentane (10 mL) was added, and a white precipitate was obtained, which was filtered off, washed with *n*-pentane (3 × 2 mL), and dried in vacuo. Yield: 130 mg (85%).

Anal. Calcd for $C_{19}H_{29}N_6O_2BPt$ (579.4 g/mol): C, 39.39; H, 5.05; N, 14.51. Found: C, 39.64; H, 5.18; N, 14.28. 1H NMR (400 MHz, THF- d_8): δ -18.22 (s+d, 1H, $^1J_{Pt,H}$ = 1496 Hz, Pt-H), 1.85 (s, 3H, CO⁸-CH₃), 2.03 (s, 6H, $C^{3/3'}$ -CH₃), 2.32 (s+d, $^3J_{Pt,H}$ = 13.7 Hz, 6H, COCH₃), 2.37 (s, 6H, $C^{5/5'}$ -CH₃), 2.45 (s, 3H, C^{10} -CH₃), 5.79 (s, 2H, $H^{4/4'}$ pz), 5.91 (s, 1H, H^9 pz). ^{13}C NMR (125 MHz, THF- d_8): δ 12.5 (s, $C^{5/5'}$ -CH₃), 12.8 (s, C^{10} -CH₃), 14.8 (s, C^8 -CH₃), 14.9 (s, $C^{3/3'}$ -CH₃) 40.4 (s+d, $^2J_{Pt,C}$ = 206.9 Hz, COCH₃), 106.7 (s, $C^{4/4'}$ pz), 107.4 (s, C^9 pz), 145.0 (s, C^{10} pz), 145.4 (s, $C^{5/5'}$ pz), 149.7 (s, C^8 pz), 150.1 (s, $C^{3/3'}$ pz), 195.5 (s+d, $^1J_{Pt,C}$ = 896.3 Hz, COCH₃). ^{195}Pt NMR (86 MHz, THF- d_8): δ -1740.0 (d, $^1J_{Pt,H}$ = 1500.0 Hz). IR: ν (BH) 2528, ν (PtH) 2233, ν (CO) 1667 cm⁻¹.

3.4. Synthesis of $[Pt(COMe)_2Cl\{(pz)_3BH\}]$ (5a). A solution of $[Pt(COMe)_2H\{(pz)_3BH\}]$ (4a) (60 mg, 0.12 mmol) in chloroform was stirred two days at room temperature. Then, the solvent was reduced to approximately 2 mL in vacuo, and *n*-pentane (5 mL) was added. The obtained white solid was filtered off, washed with *n*-pentane (3 × 2 mL), and dried in vacuo. Yield: 51 mg (80%).

HRMS(ESI): m/z calcd for $[C_{13}H_{16}O_2N_6BClPtNa]^+$ 552.06563, found for $[M + Na]^+$ 552.06562. 1H NMR (400 MHz, CDCl₃): δ 2.79 (s+d, $^3J_{Pt,H}$ = 8.9 Hz, 6H, COCH₃), 6.28 (t, 2H, $H^{4/4'}$ pz), 6.31 (t, 1H, H^9 pz), 7.67 (m, 2H, $H^{3/3'}$ pz), 7.71 (m, 2H, $H^{5/5'}$ pz), 7.80 (d, 1H, H^8 pz), 7.89 (d, 1H, H^{10} pz). ^{13}C NMR (100 MHz, CDCl₃): δ 35.1 (s+d, $^2J_{Pt,C}$ = 91.5 Hz, COCH₃), 106.3 (s+d, $^3J_{Pt,C}$ = 11.5 Hz, $C^{4/4'}$ pz), 106.4 (s, $^3J_{Pt,C}$ = 43.0 Hz, C^9 pz), 135.5 (s, $C^{5/5'}$ pz), 136.6 (s+d, $^3J_{Pt,C}$ = 30.0 Hz, C^{10} pz), 139.6 (s+d, $^2J_{Pt,C}$ = 44.4 Hz, C^8 pz), 140.7 (s+d, $^2J_{Pt,C}$ = 17.7 Hz, $C^{3/3'}$ pz), 187.5 (s+d, $^1J_{Pt,C}$ = 736.6 Hz, COCH₃). ^{195}Pt NMR (86 MHz, CDCl₃): δ -762.9 (s). IR: ν (BH) 2513, ν (CO) 1725, ν (CO) 1700, ν (CO) 1676, ν (PtCl) 331 cm⁻¹.

3.5. Synthesis of $[Pt(COMe)_2Cl\{(3,5-Me_2pz)_3BH\}]$ (5b). A solution of $[Pt(COMe)_2H\{(3,5-Me_2pz)_3BH\}]$ (4b) (60 mg, 0.1 mmol) in chloroform was stirred for two days at room temperature.

The clear, colorless solution was evaporated to dryness, and a white solid was obtained. Yield: 53 mg (85%).

HRMS(ESI): m/z calcd for $[C_{19}H_{28}O_2N_6BClPtNa]^+$ 636.15953, found for $[M + Na]^+$ 636.16029. 1H NMR (500 MHz, CDCl₃): δ 1.82 (s, 3H, CO⁸-CH₃), 2.29 (s, 6H, $C^{3/3'}$ -CH₃), 2.36 (s, 6H, $C^{5/5'}$ -CH₃), 2.43 (s, 3H, C^{10} -CH₃), 2.52 (s+d, $^3J_{Pt,H}$ = 6.6 Hz, 6H, COCH₃), 5.82 (s, 2H, $H^{4/4'}$ pz), 5.91 (s+d, $^4J_{Pt,H}$ = 20.5 Hz, 1H, H^9 pz). ^{13}C NMR (125 MHz, CDCl₃): δ 12.4 (s, $C^{5/5'}$ -CH₃), 13.3 (s, C^{10} -CH₃), 13.8 (s, $C^{3/3'}$ -CH₃), 15.5 (s, CO⁸-CH₃), 33.2 (s+d, $^2J_{Pt,C}$ = 94.6 Hz, COCH₃), 107.9 (s, $C^{4/4'}$ pz), 108.1 (s, C^9 pz), 144.1 (s, COCH₃), 145.3 (s, CO¹⁰ pz), 148.0 (s, C^8 pz), 151.1 (s, $C^{3/3'}$ pz), 190.8 (s+d, $^1J_{Pt,C}$ = 736.6 Hz, COCH₃). ^{195}Pt NMR (86 MHz, CDCl₃): δ -763.0 (s). IR: ν (BH) 2553, ν (CO) 1718, ν (CO) 1703, ν (PtCl) 328 cm⁻¹.

3.6. Synthesis of $K[Pt(COME)_2\{(pz)_3BH\}]$ (6a) and $K[Pt(COME)_2\{(3,5-Me_2pz)_3BH\}]$ (6b). Route A. $[Pt(COME)_2(NH_2Bn)_2]$ (3) (100 mg, 0.20 mmol) and K[(*p*z)₃BH] (50 mg, 0.20 mmol) or K[(3,5-Me₂pz)₃BH] (67.9 mg, 0.20 mmol) were dissolved in THF (5 mL), and the solution was stirred for 30 min. The solvent was reduced to approximately 1 mL in vacuo. After the addition of diethyl ether (3 mL) and *n*-pentane (3 mL) a white precipitate was obtained, which was filtered off, washed with cold diethyl ether (3 × 1 mL), and dried in vacuo.

Route B. A solution of potassium methoxide (14.7 mg, 0.21 mmol) in methanol (5 mL) was added to a suspension of $[Pt(COME)_2H-\{(pz)_3BH\}]$ (4a) (100 mg, 0.20 mmol) or $[Pt(COME)_2H\{(3,5-Me_2pz)_3BH\}]$ (4b) (116 mg, 0.20 mmol) in methanol (3 mL). The reaction mixture was stirred for 2 h at room temperature, resulting in a clear, colorless solution. Then, the solvent was removed in vacuo, and the residue was dissolved in methylene chloride (2 mL). After the addition of *n*-pentane (6 mL) a white precipitate was obtained, which was filtered off, washed with *n*-pentane (3 × 1 mL), and dried in vacuo.

$K[Pt(COME)_2\{(pz)_3BH\}]$ (6a). Yield: 93 mg (87%, route A). HRMS(ESI): m/z calcd for $[C_{13}H_{16}O_2N_6BptNa]^-$ 494.10810, found for $[M]^-$ 494.10688. 1H NMR (400 MHz, THF- d_8): δ 2.04 (s, 6H, COCH₃), 6.12 (s, br, 2H, $H^{4/4'}$ pz), 6.19 (s, br, 1H, H^9 pz), 7.24 (s, br, 2H, $H^{3/3'}$ pz), 7.53 (m, 1H, H^8 pz), 7.62 (m, 3H, $H^{5/5'}$ + H^{10} pz). ^{13}C NMR (100 MHz, THF- d_8): δ 44.5 (s+d, $^2J_{Pt,C}$ = 333.0 Hz, COCH₃), 103.9 (s, C^9 pz), 105.0 (s, $C^{4/4'}$ pz), 134.2 (s, C^{10} pz), 136.7 (s, $C^{5/5'}$ pz), 140.5 (s, C^8 pz), 141.7 (s, $C^{3/3'}$ pz), 234.6 (s+d, $^1J_{Pt,C}$ = 1245.6 Hz, COCH₃). ^{195}Pt NMR (107 MHz, THF- d_8): δ -3351.4 (s). IR: ν (BH) 2454, ν (CO) 1607, ν (CO) 1571 cm⁻¹.

$K[Pt(COME)_2\{(3,5-Me_2pz)_3BH\}]$ (6b). Yield: 58 mg (58%, route A). HRMS(ESI): m/z calcd for $[C_{19}H_{28}O_2N_6BptNa]^-$ 579.20066, found for $[M]^-$ 578.20091. 1H NMR (500 MHz, THF- d_8): δ 1.70 (s, 3H, CO⁸-CH₃), 1.73 (s, 6H, COCH₃), 1.98 (s, 6H, $C^{3/3'}$ -CH₃), 2.09 (s, 3H, C^{10} -CH₃), 2.37 (s, 6H, $C^{5/5'}$ -CH₃), 5.69 (s, 1H, H^9 pz), 5.70 (s, 2H, H^4/H^4' pz). ^{13}C NMR (125 MHz, THF- d_8): δ 12.2 (s, C^{10} -CH₃), 13.7 (s, $C^{5/5'}$ -CH₃), 14.3 (s, C^8 -CH₃), 14.6 (s, $C^{3/3'}$ -CH₃), 44.0 (s, COCH₃), 105.8 (s, C^9 pz), 106.0 (s, C^4/C^4'), 141.9 (s, C^{10} pz), 145.9 (s, C^8 pz), 146.0 (s, C^5/C^5' pz), 150.3 (s, C^3/C^3' pz), 235.3 (s, COCH₃). ^{195}Pt NMR (107 MHz, THF- d_8): δ -3372.7 (s). IR: ν (BH) 2466, ν (CO) 1596, ν (CO) 1542 cm⁻¹.

3.7. Synthesis of $K[Pt(COME)_2\{(pz)_4B\}]$ (7). $[Pt(COME)_2(NH_2Bn)_2]$ (3) (100 mg, 0.20 mmol) and K[(*p*z)₄B] (64 mg, 0.20 mmol) were dissolved in THF (5 mL), and the solution was stirred for 30 min. The resulting suspension was filtered, and the solution was reduced to 1 mL. After addition of diethyl ether (5 mL) a white precipitate was formed, which was filtered off, washed with diethyl ether (3 × 2 mL), and dried in vacuo. Yield: 80 mg (67%).

HRMS(ESI): m/z calcd for $[C_{16}H_{18}O_2N_8Bpt]^+$ 560.12990, found for $[M]^-$ 560.12878. 1H NMR (500 MHz, THF- d_8): δ 1.85 (s, 6H, COCH₃), 6.13 (t, 2H, $H^{4/4'}$ pz), 6.25 (t, 2H, $H^{9/9'}$ pz), 6.92 (d, 2H,

$H^{8/8'}$ pz), 7.24 (m, 4H, $H^{3/3'} + H^{5/5'}$ pz), 7.64 (d, 2H, $H^{10/10'}$ pz). ^{13}C NMR (125 MHz, THF- d_8): δ 44.1 (s+d, $^2J_{Pt,C} = 326.7$ Hz, COCH₃), 104.9 (s, C^{4/4'} pz), 105.0 (s, C^{9/9'} pz), 134.8 (s, C^{8/8'} pz), 137.3 (s, C^{3/3'} pz), 141.7 (s, C^{10/C^{10'}), 142.3 (s, C^{5/C^{5'}), 234.5 (s, COCH₃). ^{195}Pt NMR (107 MHz, THF- d_8): δ -3371.4 (s). IR: ν (CO) 1614, ν (CO) 1577 cm⁻¹.}}

3.8. Synthesis of K[Pt(COMe)₂{(pz)₄B}] (8). [Pt(COMe)₂(NH₂Bn)₂] (3) (81 mg, 0.16 mmol) and K[(pz)₄B] (26 mg, 0.08 mmol) were dissolved in THF (8 mL), and the solution was stirred at room temperature for 3 h. The volume of the resulting suspension was reduced to 1 mL, and *n*-pentane (5 mL) was added. The gray solid was filtered off, washed with acetone (3 \times 1 mL), and dried in vacuo. Yield: 40 mg (57%).

HRMS (ESI): *m/z* calcd for [C₂₀H₂₄O₄N₈BPt₂]⁻ 841.13145, found for [M]⁻ 841.13058. 1H NMR (400 MHz, DMSO- d_6): δ 1.80 (s, 6H, COCH₃), 6.48 (t, 4H, $H^{4/4'/4''/4'''}$ pz), 7.56 (d, 4H, $H^{3/3'/3''/3'''}$ pz), 7.65 (d, 4H, $H^{5/5'/5''/5'''}$ pz). ^{13}C NMR (125 MHz, DMSO- d_6): δ 43.6 (s, COCH₃), 106.8 (s, C^{4/4'/4''/4'''} pz), 137.9 (s, C^{5/5'/5''/5'''} pz), 144.5 (s, C^{3/3'/3''/3'''} pz), 226.5 (s, COCH₃). ^{195}Pt NMR (107 MHz, DMSO- d_6): δ -3339.8 (s). IR: ν (CO) 1617, ν (CO) 1580 cm⁻¹.

3.9. Synthesis of [Pt(COMe)₂R{(pz)₃BH}] (9a-c). [Pt(COMe)₂(NH₂Bn)₂] (3) (100 mg, 0.20 mmol) and K[(pz)₃BH] (50 mg, 0.20 mmol) were dissolved in methylene chloride (5 mL), and the solution was stirred for 30 min. After the addition of methyl iodide (68.4 mg, 0.48 mmol), ethyl iodide (77.2 mg, 0.49 mmol), or benzyl bromide (72.0 mg, 0.42 mmol), the reaction mixture was stirred for a further 30 min, resulting in a pale yellow suspension. Then, an aqueous solution of HCl (0.2 M, 5 mL) was added, and the reaction mixture was stirred vigorously for 15 min. The phases were separated, and the aqueous layer was extracted with methylene chloride (2 \times 5 mL). The combined organic extracts were dried (Na_2SO_4), and the solvent was removed in vacuo. The residue was dissolved in methylene chloride (1 mL), and *n*-pentane (ca. 5 mL) was added. The white precipitate obtained was filtered off, washed with *n*-pentane (2 \times 2 mL), and dried in vacuo over P₄O₁₀.

[Pt(COMe)₂Me{(pz)₃BH}] (9a). Yield: 50 mg (49%). Anal. Calcd for C₁₄H₁₉N₆O₂BPT (509.2 g/mol): C, 33.02; H, 3.76; N, 16.50. Found: C, 33.46; H, 3.96; N, 16.02. 1H NMR (500 MHz, acetone- d_6): δ 1.48 (s+d, $^2J_{Pt,H} = 75.1$ Hz, 3H, CH₃), 2.29 (s+d, $^3J_{Pt,H} = 10.7$ Hz, 6H, COCH₃), 6.33 (t, 2H, $H^{4/4'}$ pz), 6.40 (t, 1H, H^9 pz), 7.79 (d, 2H, $H^{3/3'}$ pz), 7.90 (d, 2H, $H^{5/5'}$ pz), 7.97 (d, 1H, H^{10} pz), 7.98 (d, 1H, H^8 pz). ^{13}C NMR (100 MHz, acetone- d_6): δ -2.4 (s+d, $^1J_{Pt,C} = 731.6$ Hz, CH₃), 36.5 (s+d, $^2J_{Pt,C} = 184.0$ Hz, COCH₃), 106.7 (s, C^{4/4' + C⁹ pz), 136.7 (s, C^{5/5' + C¹⁰ pz), 140.8 (s+d, $^2J_{Pt,C} = 16.0$ Hz, C^{3/3'} pz), 142.1 (s, $^2J_{Pt,C} = 19.9$ Hz, C⁸ pz), 194.3 (s+d, $^1J_{Pt,C} = 936.6$ Hz, COCH₃). ^{195}Pt NMR (86 MHz, acetone- d_6): δ -1461.5 (s). IR: ν (BH) 2483, ν (CO) 1686, ν (CO) 1655 cm⁻¹.}}

[Pt(COMe)₂Et{(pz)₃BH}] (9b). Yield: 53 mg (51%). Anal. Calcd for C₁₅H₂₁N₆O₂BPT (523.3 g/mol): C, 34.43; H, 4.04; N, 16.06. Found: C, 34.25; H, 4.13; N, 15.91. 1H NMR (400 MHz, acetone- d_6): δ 0.75 (t+dt, $^3J_{Pt,H} = 60.4$ Hz, 3H, CH₂CH₃), 2.25 (s+d, $^3J_{Pt,H} = 9.8$ Hz, 3H, COCH₃), 2.31 (q+dq, $^2J_{Pt,H} = 76.0$ Hz, 2H, CH₂CH₃), 6.33 (m, 2H, $H^{4/4'}$ pz), 6.38 (m, 1H, H^9 pz), 7.83 (m, 2H, $H^{3/3'}$ pz), 7.91 (m, 2H, $H^{5/5'}$ pz), 7.93 (m, 1H, H^8 pz), 7.95 (m, 1H, H^{10} pz). ^{13}C NMR (125 MHz, acetone- d_6): δ 12.8 (s+d, $^1J_{Pt,C} = 729.3$ Hz, CH₂CH₃), 16.6 (s+d, $^2J_{Pt,C} = 31.8$ Hz, CH₂CH₃), 36.7 (s+d, $^2J_{Pt,C} = 182.2$ Hz, COCH₃), 106.4 (s+d, $^3J_{Pt,C} = 10.0$ Hz, C^{4/4'} pz), 106.8 (s, C⁹ pz), 136.7 (s, C^{5/5'} pz), 136.8 (s, C¹⁰ pz), 141.3 (s+d, $^2J_{Pt,C} = 12.5$ Hz, C^{3/3'} pz), 142.3 (s+d, $^2J_{Pt,C} = 19.9$ Hz, C⁸ pz), 194.6 (s+d, $^1J_{Pt,C} = 981.9$ Hz, COCH₃). ^{195}Pt NMR (86 MHz, acetone- d_6): δ -1396.5 (s). IR: ν (BH) 2489, ν (CO) 1682, ν (CO) 1660 cm⁻¹.

[Pt(COMe)₂Bn{(pz)₃BH}] (9c). Yield: 54 mg (46%). Anal. Calcd for C₂₀H₂₃N₆O₂BPT (585.3 g/mol): C, 41.04; H, 3.96; N, 14.36. Found: C, 41.41; H, 4.06; N, 14.39. 1H NMR (400 MHz, acetone- d_6):

δ 2.24 (s+d, $^3J_{Pt,H} = 8.9$ Hz, 6H, COCH₃), 3.78 (s+d, $^2J_{Pt,H} = 93.9$ Hz, 2H, CH₂Ph), 6.16 (m, 2H, $H^{4/4'}$ pz), 6.39 (m, 1H, H^9 pz), 6.77 (m, 2H, o-CH Ph), 6.86 (m, 2H, m-CH Ph), 6.96 (m, 1H, p-CH Ph), 7.08 (m, 2H, $H^{3/3'}$ pz), 7.86 (m, 2H, $H^{5/5'}$ pz), 7.97 (m, 2H, $H^8 + H^{10}$ pz). ^{13}C NMR (125 MHz, acetone- d_6): δ 24.5 (s+d, $^1J_{Pt,C} = 711.6$ Hz, CH₂Ph), 35.7 (s+d, $^2J_{Pt,C} = 168.6$ Hz, COCH₃), 105.3 (s+d, $^3J_{Pt,C} = 9.7$ Hz, C^{4/4'} pz), 106.1 (s+d, $^3J_{Pt,C} = 14.5$ Hz, C⁹ pz), 124.5 (s+d, $^5J_{Pt,C} = 15.1$ Hz, p-CH Ph), 127.7 (s+d, $^4J_{Pt,C} = 13.1$ Hz, m-CH Ph), 129.0 (s+d, $^3J_{Pt,C} = 21.7$ Hz, o-CH Ph), 135.7 (s, C^{5/5'} pz), 136.1 (s, C¹⁰ pz), 140.3 (s+d, $^3J_{Pt,C} = 11.1$ Hz, C^{3/3'} pz), 141.8 (s+d, $^3J_{Pt,C} = 23.6$ Hz, C⁸ pz), 145.5 (s+d, $^2J_{Pt,C} = 50.0$ Hz, i-C Ph), 194.1 (s+d, $^1J_{Pt,C} = 956.8$ Hz, COCH₃). ^{195}Pt NMR (86 MHz, acetone- d_6): δ -1281.5 (s). IR: ν (BH) 2481, ν (CO) 1690, ν (CO) 1653 cm⁻¹.

3.10. Synthesis of [Pt(COMe)₂R{(pz)₃B}] (10a-c). To a solution of K[Pt(COMe)₂{(pz)₄B}] (6) (100 mg, 0.17 mmol) in THF (5 mL) was added methyl iodide (68.4 mg, 0.48 mmol), ethyl iodide (77.2 mg, 0.49 mmol), or benzyl bromide (72.0 mg, 0.42 mmol). After stirring for 1 h, the solvent was removed in vacuo from the resulting pale yellow suspension. The residue was dissolved in methylene chloride (10 mL), water (5 mL) was added, and the reaction mixture was stirred vigorously for 15 min. The phases were separated, and the aqueous layer was extracted with methylene chloride (2 \times 5 mL). The combined organic extracts were dried (Na_2SO_4), and the solvent was removed in vacuo. The residue was dissolved in methylene chloride (1 mL), and *n*-pentane (ca. 5 mL) was added. The precipitate obtained was filtered off, washed with *n*-pentane (2 \times 2 mL), and dried in vacuo over P₄O₁₀.

[Pt(COMe)₂Me{(pz)₄B}] (10a). Yield: 60 mg (61%). Anal. Calcd for C₁₇H₂₁N₆O₂BPT (575.3 g/mol): C, 35.49; H, 3.68; N, 19.48. Found: C, 34.88; H, 3.89; N, 18.79. 1H NMR (400 MHz, CDCl₃): δ 1.48 (s+d, $^2J_{Pt,H} = 73.3$ Hz, 3H, CH₃), 2.36 (s+d, $^3J_{Pt,H} = 11.0$ Hz, 6H, COCH₃), 6.27 (t, 2H, $H^{4/4'}$ pz), 6.29 (t, 1H, H^9 pz), 6.61 (t, 1H, H^{14} pz), 7.27 (d, 1H, H^{10} pz), 7.67 (d, 2H, $H^{3/3'}$ pz), 7.88 (d, 1H, H^8 pz), 7.95 (m, 3H, $H^{5/5'} + H^{13}$ pz), 8.00 (d, 1H, H^{15} pz). ^{13}C NMR (125 MHz, CDCl₃): δ -1.8 (s+d, $^1J_{Pt,C} = 722.6$ Hz, CH₃), 36.7 (s+d, $^2J_{Pt,C} = 181.9$ Hz, COCH₃), 106.2 (s, C^{4/4'} pz), 106.4 (s, C⁹ pz), 107.3 (s, C¹⁴ pz), 135.2 (s, C¹⁰ pz), 135.8 (s, C^{5/5'} pz), 136.1 (s, C¹⁵ pz), 140.8 (s, C^{3/3'} pz), 142.0 (s+d, $^2J_{Pt,C} = 18.4$ Hz, C⁸ pz), 142.2 (s, C¹³ pz), 196.2 (s+d, $^1J_{Pt,C} = 939.3$ Hz, COCH₃). ^{195}Pt NMR (107 MHz, acetone- d_6): δ -1489.2 (s). IR: ν (CO) 1690, ν (CO) 1653 cm⁻¹.

[Pt(COMe)₂Et{(pz)₄B}] (10b). Yield: 56 mg (56%). Anal. Calcd for C₁₈H₂₃N₆O₂BPT (589.4 g/mol): C, 36.68; H, 3.93; N, 19.02. Found: C, 36.28; H, 4.00; N, 18.66%. 1H NMR (400 MHz, acetone- d_6): δ 0.82 (t+dt, $^3J_{Pt,H} = 60.5$ Hz, 3H, CH₂CH₃), 2.31 (s+d, $^3J_{Pt,H} = 10.1$ Hz, 6H, COCH₃), 2.34 (q+dq, $^2J_{Pt,H} = 76.0$ Hz, 2H, CH₂CH₃), 6.39 (t, 2H, $H^{4/4'}$ pz), 6.41 (t, 1H, H^9 pz), 6.68 (t, 1H, H^{14} pz), 7.79 (d, 1H, H^{10} pz), 7.86 (d, 2H, $H^{5/5'}$ pz), 7.93 (d, 2H, $H^{3/3'}$ pz), 7.96 (d, 1H, H^{13} pz), 8.01 (d, 1H, H^8 pz), 8.22 (d, 1H, H^{15} pz). ^{13}C NMR (125 MHz, acetone- d_6): δ 11.9 (s+d, $^1J_{Pt,C} = 723.8$ Hz, CH₂CH₃), 15.6 (s+d, $^2J_{Pt,C} = 31.5$ Hz, CH₂CH₃), 35.5 (s+d, $^2J_{Pt,C} = 181.3$ Hz, COCH₃), 105.8 (s, C^{4/4'} pz), 106.1 (s, C⁹ pz), 107.1 (s, C¹⁴ pz), 135.6 (s, C¹⁰ pz), 135.7 (s, C^{5/5'} pz), 136.7 (s, C¹⁵ pz), 141.7 (s, C^{3/3'} pz), 141.9 (s, C¹³ pz), 142.6 (s, C⁸ pz), 194.8 (s+d, $^2J_{Pt,C} = 970.6$ Hz, COCH₃). ^{195}Pt NMR (107 MHz, acetone- d_6): δ -1436.4 (s). IR: ν (CO) 1690, ν (CO) 1653 cm⁻¹.

[Pt(COMe)₂Bn{(pz)₄B}] (10c). Yield: 65 mg (59%). Anal. Calcd for C₂₃H₂₅N₆O₂BPT (651.4 g/mol): C, 42.40; H, 3.87; N, 17.21. Found: C, 42.04; H, 3.78; N, 17.16. 1H NMR (400 MHz, acetone- d_6): δ 2.29 (s+d, $^3J_{Pt,H} = 9.0$ Hz, 6H, COCH₃), 3.80 (s+d, $^2J_{Pt,H} = 93.6$ Hz, 2H, CH₂Ph), 6.19 (t, 2H, $H^{4/4'}$ pz), 6.42 (t, 1H, H^9 pz), 6.67 (t, 1H, H^{14} pz), 6.80 (m, 2H, o-CH Ph), 6.89 (m, 2H, m-CH Ph), 7.00 (m, 1H, p-CH Ph), 7.18 (d, 2H, $H^{3/3'}$ pz), 7.78 (d, 1H, H^{10} pz), 7.82 (m, 2H, $H^{5/5'}$ pz), 7.95 (d, 1H, H^{13} pz), 8.04 (d, 1H, H^8 pz), 8.18 (d, 1H,

Organometallics

Article

Table 5. Crystal Data and Structure Refinement for 4a, 5a, 7·(18C6), and 9c

	4a	5a	7·(18C6)	9c
empirical formula	C ₁₃ H ₁₇ B ₁ N ₆ O ₂ Pt ₁	C ₁₃ H ₁₆ B ₁ Cl ₁ N ₆ O ₂ Pt ₁	C ₂₈ H ₄₂ B ₁ K ₁ N ₈ O ₈ Pt ₁	C ₂₀ H ₂₃ B ₁ N ₆ O ₂ Pt ₁
fw	495.2	529.7	664.3	585.3
cryst syst	orthorhombic	monoclinic	monoclinic	triclinic
space group	P2 ₁ 2 ₁ 2 ₁	P2 ₁ /c	P2 ₁	P $\bar{1}$
a (Å)	7.798(1)	9.794(2)	9.7876(5)	9.1821(4)
b (Å)	12.786(3)	12.800(5)	16.6534(6)	9.5744(4)
c (Å)	16.615(3)	12.055(4)	11.7754(6)	12.9873(4)
α (deg)				85.422(3)
β (deg)		115.63(2)	108.631(4)	84.808(3)
γ (deg)				64.466(4)
V (Å ³)	1656.6(6)	1701.6(9)	1818.8(2)	1024.95(7)
Z	4	4	2	2
D_{calc} (g·cm ⁻³)	1.986	2.068	1.577	1.897
$\mu(\text{Mo K}\alpha)$ (mm ⁻¹)	8.487	8.422	4.027	6.875
F(000)	944	1008	864	568
θ range (deg)	2.45–25.00	2.19–25.89	2.66–28.00	2.84–26.17
reflns collected	11 823	12 272	15 350	11 981
reflns obsd [$I > 2\sigma(I)$]	2696	2637	7891	3581
indep reflns	2807 [$R_{\text{int}} = 0.0384$]	3241 [$R_{\text{int}} = 0.0602$]	8718 [$R_{\text{int}} = 0.0321$]	4042 [$R_{\text{int}} = 0.0257$]
data/restrains/params	2807/1/216	3241/0/219	8718/1/427	4042/0/271
goodness-of-fit on F^2	1.048	1.031	0.974	1.045
final R indices [$I > 2\sigma(I)$]	$R_1 = 0.0242$ $wR_2 = 0.0589$	$R_1 = 0.0228$ $wR_2 = 0.0533$	$R_1 = 0.0279$ $wR_2 = 0.0677$	$R_1 = 0.0187$ $wR_2 = 0.0420$
R indices (all data)	$R_1 = 0.0261$ $wR_2 = 0.0601$	$R_1 = 0.0321$ $wR_2 = 0.0560$	$R_1 = 0.0316$ $wR_2 = 0.0687$	$R_1 = 0.0236$ $wR_2 = 0.0433$
largest diff peak and hole (e·Å ⁻³)	0.996 and -1.299	1.148 and -1.344	1.061 and -1.220	1.300 and -1.016

H^{15} pz). ^{13}C NMR (125 MHz, acetone- d_6): δ 25.4 (s+d, $^1J_{\text{Pt,C}} = 708.9$ Hz, CH_2Ph), 36.5 (s+d, $^2J_{\text{Pt,C}} = 169.6$ Hz, COCH_3), 106.3 (s, $C^{4/4'}$ pz), 107.2 (s, C^9 pz), 108.0 (s, C^{14} pz), 125.3 (s+d, $^5J_{\text{Pt,C}} = 14.5$ Hz, $p\text{-CH Ph}$), 128.8 (s+d, $^4J_{\text{Pt,C}} = 13.5$ Hz, $m\text{-CH Ph}$), 130.0 (s+d, $^4J_{\text{Pt,C}} = 21.8$ Hz, $o\text{-CH Ph}$), 136.5 (s, $C^{5/5'}$ pz), 136.6 (s, C^{10} pz), 137.6 (s, C^{15} pz), 142.4 (s, $C^{3/3'}$ pz), 142.8 (s, C^{13} pz), 143.9 (s, C^8 pz), 146.1 (s+d, $^2J_{\text{Pt,C}} = 49.5$ Hz, $i\text{-C Ph}$), 194.9 (s+d, $^1J_{\text{Pt,C}} = 951.6$ Hz, COCH_3). ^{195}Pt NMR (107 MHz, acetone- d_6): δ -1314.8 (s). IR: $\nu(\text{CO})$ 1683, $\nu(\text{CO})$ 1662 cm⁻¹.

3.11. X-ray Crystallography. Data for X-ray diffraction analysis of single crystals were collected on a Stoe-IPDS diffractometer (4a/5a) at 220 K, on a Stoe-IPDS 2T diffractometer (7·(18C6)) at 200 K, and on an Oxford Gemini S diffractometer (9c) at 105 K using Mo K α radiation ($\lambda = 0.71073$ Å, graphite monochromator). A summary of the crystallographic data, the data collection parameters, and the refinement parameters is given in Table 5. Absorption corrections were applied numerically with X-RED32²⁰ ($T_{\min}/T_{\max} = 0.30/0.34$, 4a; 0.24/0.67, 5a) and empirically with the PLATON program package²¹ ($T_{\min}/T_{\max} = 0.20/0.33$, 7·(18C6)) and CrysAlis RED²² ($T_{\min}/T_{\max} = 0.60/1.00$, 9c), respectively. The structures were solved with direct methods using SHELXS-97²³ and refined using full-matrix least-squares routines against F^2 with SHELXL-97.²⁴ All non-hydrogen atoms were refined with anisotropic displacement parameters and hydrogen atoms with isotropic ones. H atoms were placed in calculated positions according to the riding model.

ASSOCIATED CONTENT

Supporting Information

CIF files containing X-ray crystallographic data for 4a, 5a, 7·(18C6), and 9c. This material is available free of charge via the Internet at <http://pubs.acs.org>. Supplementary crystallographic data (4a, CCDC 870385; 5a, CCDC 870386; 7·(18C6), CCDC 870387; 9c, CCDC 870388) can also be obtained free of charge via <http://www.ccdc.cam.ac.uk/deposit>.

AUTHOR INFORMATION

Notes

The authors declare no competing financial interest.

REFERENCES

- Steinborn, D. *Dalton Trans.* **2005**, 2664.
- Steinborn, D.; Gerisch, M.; Merzweiler, K.; Schenzel, K.; Pelz, K.; Bögel, H.; Magull, J. *Organometallics* **1996**, 15, 2454.
- (a) Gerisch, M.; Bruhn, C.; Vyater, A.; Davies, J. A.; Steinborn, D. *Organometallics* **1998**, 17, 3101. (b) Vyater, A.; Wagner, C.; Merzweiler, K.; Steinborn, D. *Organometallics* **2002**, 21, 4369.
- Werner, M.; Bruhn, C.; Steinborn, D. *J. Organomet. Chem.* **2008**, 693, 2369.
- (a) Werner, M.; Wagner, C.; Steinborn, D. *J. Organomet. Chem.* **2009**, 694, 190. (b) Werner, M.; Bruhn, C.; Steinborn, D. *Transition Met. Chem.* **2009**, 34, 61.
- Schwieger, S.; Herzog, R.; Wagner, C.; Steinborn, D. *J. Organomet. Chem.* **2009**, 694, 3548.
- (a) Trofimenko, S. *Scorpionates: The Coordination Chemistry of Polypyrazolylborate Ligands*; Imperial College Press: London, 1999. (b) Pettinari, C. *Scorpionates II: Chelating Borate Ligands*; Imperial College Press: London, 2008.
- (a) Akita, M.; Ohta, K.; Takahashi, Y.; Hikichi, S.; Moro-oka, Y. *Organometallics* **1997**, 16, 4121. (b) Akita, M.; Hashimoto, M.; Hikichi, S.; Moro-oka, Y. *Organometallics* **2000**, 19, 3744.
- Look, J. L.; Wick, D. D.; Mayer, J. M.; Goldberg, K. I. *Inorg. Chem.* **2009**, 48, 1356.
- O'Reilly, S. A.; White, P. S.; Templeton, J. L. *J. Am. Chem. Soc.* **1996**, 118, 5684.
- Canty, A. J.; Fritsche, S. D.; Jin, H.; Patel, J.; Skelton, B. W.; White, A. H. *Organometallics* **1997**, 16, 2175.
- Nakamoto, K. *Infrared and Raman Spectra of Inorganic and Coordination Compounds*, 4th ed.; Wiley: New York, 1986.
- (a) Appleton, T. G.; Clark, H. C.; Manzer, L. E. *Coord. Chem. Rev.* **1973**, 10, 335. (b) Sajith, P. K.; Suresh, C. S. *J. Organomet. Chem.* **2011**, 696, 2086.

Organometallics

Article

- (14) (a) Schwieger, S.; Heinemann, F. W.; Wagner, C.; Kluge, R.; Damm, C.; Israel, G.; Steinborn, D. *Organometallics* **2009**, *28*, 2485.
(b) Kluge, T.; Bette, M.; Vetter, C.; Schmidt, J.; Steinborn, D. Publication in preparation.
- (15) Pregosin, P. S. *Coord. Chem. Rev.* **1982**, *44*, 247.
- (16) Trofimenko, S. *Chem. Rev.* **1993**, *93*, 943.
- (17) Nayagam, B. R. D.; Jebas, S. R.; Kalavathy, D.; Murugesan, R.; Schollmeyer, D. *Acta Crystallogr. Sect. E* **2010**, *E66*, m667.
- (18) Rochon, F. D.; Melanson, R.; Doyon, M. *Inorg. Chem.* **1987**, *26*, 3065.
- (19) (a) Rendina, L. M.; Puddephatt, R. J. *Chem. Rev.* **1997**, *97*, 1735.
(b) Baar, C. R.; Carbray, L. P.; Jennings, M. C.; Puddephatt, R. J. *Organometallics* **2000**, *19*, 2482. (c) Nabavizadeh, S. M.; Hoseini, S. J.; Momeni, B. Z.; Shahabadi, N.; Rashidi, M.; Pakiari, A. H.; Eskandari, K. *Dalton Trans.* **2008**, 2414.
- (20) X-RED32 (Version 1.07), Stoe Data Reduction Program; Stoe & Cie GmbH: Darmstadt, 2002.
- (21) (a) *MULscanABS*, PLATON for Windows v1.15; University of Glasgow, 2008. (b) Spek, A. L. *J. Appl. Crystallogr.* **2003**, *36*, 7.
- (22) *CrysAlis RED* (Version 1.171.32.5): SCALE3 ABSPACK; Oxford Diffraction Ltd.: Oxford, 2007.
- (23) Sheldrick, G. M. *SHELXS-97, Program for Crystal Structure Solution*; University of Göttingen: Göttingen, 1998.
- (24) Sheldrick, G. M. *SHELXL-97, Program for the Refinement of Crystal Structures*; University of Göttingen: Göttingen, 1997.

Reprint with permission from Organometallics
Copyright 2012 American Chemical Society. 31, 3700.

DOI:10.1002/ejic.201201468

Diacetylplatinum(II) and -platinum(IV) Complexes Bearing κ^2 - and κ^3 -Coordinated Tris(pyrazolyl)methane Ligands: Investigations on the Synthesis, Fluxionality, and Reactivity in Relation to the Substitution Pattern of the Ligands

Martin Bette,^[a] Jürgen Schmidt,^[b] and Dirk Steinborn^{*[a]}**Keywords:** Platinum / Tridentate ligands / Hydrogen bonds / Fluxionality / Ab initio calculations

Reactions of the dinuclear platina- β -diketone $[\text{Pt}_2\{(\text{COMe})_2\text{H}\}_2(\mu\text{-Cl})_2]$ (**1**) with $\text{HC}(\text{pz})_3$ and $\text{HC}(3,5\text{-Me}_2\text{pz})_3$ (pz = pyrazol-1-yl; $3,5\text{-Me}_2\text{pz}$ = 3,5-dimethylpyrazol-1-yl) afforded cationic, thermally labile diacetyl(hydrido)platinum(IV) complexes $[\text{Pt}(\text{COMe})_2\text{H}\{(\text{pz})_3\text{CH}\}] \text{Cl}$ (**3a**) and $[\text{Pt}(\text{COMe})_2\text{H}\{(\text{3,5-Me}_2\text{pz})_3\text{CH}\}] \text{Cl}$ (**3b**) with κ^3 -coordinated tris(pyrazolyl)methane ligands, which were found to react with NaOH or NEt_3 to yield neutral diacetylplatinum(II) complexes with κ^2 -coordinated tris(pyrazolyl)methane ligands $\{[\text{Pt}(\text{COMe})_2\{(\text{pz})_3\text{CH}\}]\}$ (**4a**); $\{[\text{Pt}(\text{COMe})_2\{(\text{3,5-Me}_2\text{pz})_3\text{CH}\}]\}$ (**4b**)). In **4a/b**, a molecular rearrangement (decoordination of a pyrazolyl ring and coordination of the originally pendant one) has been found that has been investigated by variable-temperature ^1H NMR spectroscopic measurements (coalescence method) as well as by DFT calculations. Diacetylplatinum(II) complexes **4** were found to react in oxidative addition reactions with ROTf ($\text{R} = \text{H, Me}$; OTf = trifluoromethanesulfonate) and methyl iodide to yield cationic diacetylplatinum(IV) complexes of the type $[\text{Pt}(\text{COMe})_2\text{R}\{(\text{pz})_3\text{CH}\}] \text{X}$ ($\text{R/X} = \text{H/OTf, }$

5a; Me/OTf, **6a**; Me/I, **7a** and $[\text{Pt}(\text{COMe})_2\text{R}\{(\text{3,5-Me}_2\text{pz})_3\text{CH}\}] \text{X}$ [$\text{R/X} = \text{H/OTf, }$ **5b**, Me/OTf, **6b**, Me/I, **7b**] with κ^3 -bonded tris(pyrazolyl)methane ligands. Treatment of **4b** with alkynyl iodine(II) reagents of the type $[\text{IPh}(\text{C}\equiv\text{CR})] \text{X}$ ($\text{R/X} = \text{SiMe}_3/\text{OTf, Ph/OTf, } t\text{Bu/OTos, } i\text{Pr/OTos, OTos} = p\text{-toluenesulfonate}$) led to the formation of cationic diacetyl(alkynyl)-platinum(IV) complexes $[\text{Pt}(\text{COMe})_2(\text{C}\equiv\text{CR})\{(\text{3,5-Me}_2\text{pz})_3\text{CH}\}] \text{X}$ [$\text{R/X} = \text{SiMe}_3/\text{OTf, }$ **8a**, Ph/OTf, **8b**, $t\text{Bu/OTos, }$ **8c**, $i\text{Pr/OTos, }$ **8d**]. The identities of all platinum complexes were unambiguously proven by high-resolution mass spectrometric investigations, by NMR ($^1\text{H, } ^{13}\text{C, } ^{195}\text{Pt}$) and IR spectroscopy, as well as by single-crystal X-ray diffraction analyses (**4a, 4b, 7a, 8a/d**). The constitution of the thermally labile complexes **3a/b** has been confirmed by low-temperature (-80°C) NMR ($^1\text{H, } ^{13}\text{C}$) spectroscopic measurements. The electronic and steric influence of the additional methyl groups in $\text{HC}(3,5\text{-Me}_2\text{pz})_3$ on reactivity, stability, and properties of the investigated compounds will be discussed.

Introduction

Dinuclear platina- β -diketones $[\text{Pt}_2\{(\text{COR})_2\text{H}\}_2(\mu\text{-Cl})_2]$ ($\text{R} = \text{alkyl}$) can be considered hydroxycarbene complexes, which are stabilized by intramolecular O–H \cdots O hydrogen bonds to neighboring acyl ligands. Due to their electronic unsaturation (16-valence-electron complexes) and their kinetically labile ligand sphere, platina- β -diketones exhibit a unique reactivity and thus can be precursor complexes for the synthesis of a great variety of acyl platinum(II) and platinum(IV) complexes with bidentate $\text{N}^{\text{A}}\text{N}$, $\text{P}^{\text{A}}\text{P}$, $\text{S}^{\text{A}}\text{S}$, $\text{N}^{\text{A}}\text{O}$ ligands.^[1] Platina- β -diketones are accessible by reactions of hexachloridoplatinic acid with *n*-butyl alcohol and

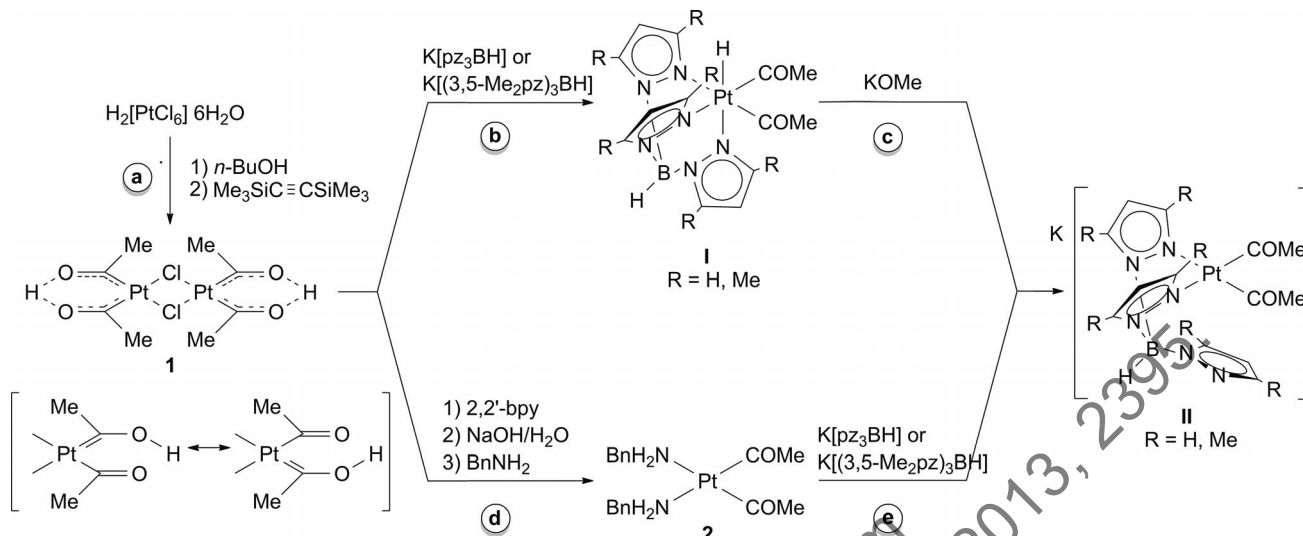
trimethylsilyl-substituted alkynes, as shown in Scheme 1 (reaction path a) for the synthesis of the parent complex **1** ($\text{R} = \text{Me}$).^[2]

Recently we reported the reactivity of the platina- β -diketone **1** toward tris(pyrazolyl)borates $[(\text{pz})_3\text{BH}]^-$ and $[(3,5\text{-Me}_2\text{pz})_3\text{BH}]^-$, which are known as versatile anionic tridentate nitrogen-donor ligands (Scheme 1).^[3] This type of ligand is well established in transition-metal chemistry and belongs to the manifold class of the scorpionate ligands.^[4] Owing to their tetrahedral structure, tris(pyrazolyl)borates generally coordinate in octahedral complexes as facial binding $\kappa^3\text{N,N',N''}$ ligands, as also found for the diacetyl(hydrido)platinum(IV) complexes **I** formed by the reaction of **1** with tris(pyrazolyl)borates (Scheme 1, reaction path b). Diacetylplatinum(II) complexes **II** bearing κ^2 -coordinated tris(pyrazolyl)borate ligands were found to be accessible by the reaction of the respective hydridoplatinum(IV) complexes **I** with potassium methoxide (Scheme 1c) as well as by means of facile ligand-exchange reactions with the diacetyl bis(benzylamine)platinum(II) complex $[\text{Pt}(\text{COMe})_2$

[a] Institute of Chemistry–Inorganic Chemistry,
Martin Luther University Halle-Wittenberg,
Kurt-Mothes-Strasse 2, 06120 Halle, Germany
Homepage: <http://www.chemie.uni-halle.de>

[b] Department of Bioorganic Chemistry,
Leibniz Institute of Plant Biochemistry,
Weinberg 3, 06120 Halle, Germany

Supporting information for this article is available on the WWW under <http://dx.doi.org/10.1002/ejic.201201468>.



Scheme 1. Synthesis of diacetylhydridoplatinum(IV) complexes with κ^3 -bonded and diacetylplatinum(II) complexes with κ^2 -bonded tris(pyrazolyl)borate ligand.

$(\text{NH}_2\text{Bn})_2$ (2) (Scheme 1e), which can be prepared in a multistep synthesis starting from the platina- β -diketone **1** (Scheme 1d).^[5] Because of the ligand structure described above, the coordination of the tris(pyrazolyl)borates in type **II** square-planar complexes is restricted to an κ^2N,N' -coordination mode with a pendant third pyrazolyl ring.

The isoelectronic neutral tris(pyrazolyl)methane ligands of the type $(\text{pz}^X)_3\text{CH}$ (pz^X = pyrazolyl group with unspecified substituents) are formally derived from the corresponding anionic tris(pyrazolyl)borate ligands by replacing the central boron atom by a carbon atom and, thus, exhibit the same geometric restrictions such as the tris(pyrazolyl)borates as described above.^[6] In contrast, tris(pyrazolyl)methane ligands have received much less attention than the scorpionates. In part, this has been due to the more difficult synthesis of ring-substituted tris(pyrazolyl)methane ligands in particular than the tris(pyrazolyl)borate analogues. Since the beginning of the new millennium, the preparation of the tris(pyrazolyl)methane ligands has been greatly improved,^[7,8] and chemistry in this area is expanding rapidly.^[6,9]

Herein, we report the synthesis and characterization of diacetylplatinum(II) complexes bearing κ^2N,N' -coordinated tris(pyrazolyl)methane ligands as well as the molecular rearrangements in these complexes. Furthermore, we present investigations on the reactivity of these compounds in oxidative addition reactions including those with alkynylidine(III) reagents.

Results and Discussion

Synthesis and Characterization of Diacetylplatinum(II) Complexes Bearing κ^2 -Coordinated Tris(pyrazolyl)methane Ligands

Synthesis

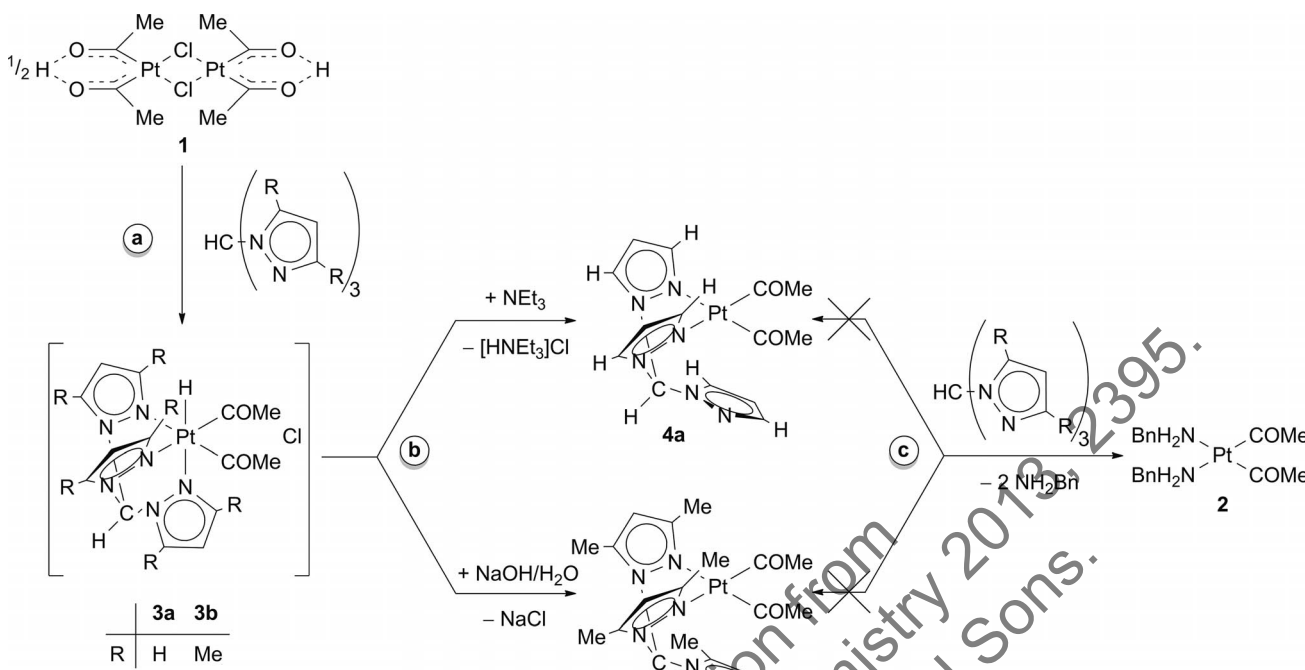
The reactions of the dinuclear platina- β -diketone $[\text{Pt}_2\{\text{COMe}\}_2\text{H}]_2(\mu\text{-Cl})_2$ (**1**) with tris(pyrazolyl)methane

and tris(3,5-dimethylpyrazolyl)methane at -78°C followed by the addition of a base such as NEt_3 or NaOH led to the formation of the diacetylplatinum(II) complexes $[\text{Pt}(\text{COMe})_2\{(\text{pz})_3\text{CH}\}]$ (**4a**) and $[\text{Pt}(\text{COMe})_2\{(3,5\text{-Me}_2\text{pz})_3\text{CH}\}]$ (**4b**), with κ^2 -coordinated tris(pyrazolyl)methane ligands (Scheme 2, a and b). Both compounds were isolated in good yields of 81% (**4a**) and 66% (**4b**) as white solids, which were characterized by NMR (^1H , ^{13}C , ^{195}Pt) and IR spectroscopy, as well as by high-resolution mass spectrometric (HRMS-ESI) investigations and single-crystal X-ray diffraction analyses.

Owing to their thermal instability, the hydridoplatinum(IV) complexes **3a/b**, formed as intermediates, could not be isolated (Scheme 2, a). Nevertheless, their identities were unambiguously proven by low-temperature NMR spectroscopic studies, which will be discussed below.

In principle, reactions of **3a** and **3b** both with NEt_3 and NaOH led to the formation of the respective platinum(II) complex **4a/b** (Scheme 2, b). The base given in Scheme 2 was chosen to properly separate the complex from the by-products. $[\text{Pt}(\text{COMe})_2\{(\text{pz})_3\text{CH}\}]$ (**4a**) is only slightly soluble in protic solvents like methanol and almost insoluble in dichloromethane, chloroform, acetone, or THF, as already observed for the analogous dimethylplatinum(II) complex $[\text{Pt}(\text{Me}_2)\{(\text{pz})_3\text{CH}\}]$.^[10] Thus, by using NEt_3 as base and dichloromethane as solvent, the soluble triethylammonium salt formed can be easily separated from the insoluble complex **4a**. In contrast, $[\text{Pt}(\text{COMe})_2\{(3,5\text{-Me}_2\text{pz})_3\text{CH}\}]$ (**4b**) is very soluble in dichloromethane and chloroform, so that using an aqueous solution of NaOH as base offers the possibility to extract the complex with dichloromethane.

However, in any case, the workup procedure has to be done quickly, because the two complexes were found to decompose in solution. At room temperature and under anaerobic conditions, colorless solutions of **4a** in methanol turned pale yellow within several hours, and the start of decomposition can even be detected by NMR spectroscopy after one hour. In the case of **4b**, the stability depends on



Scheme 2. Synthesis of the diacetylplatinum(II) complexes **4a/b**.

the type of solvent. At room temperature, solutions in dichloromethane were found to decompose within three hours, whereas solutions in methanol were stable for a couple of days.

As reported recently, the analogous complexes **II** (Scheme 1) bearing κ^2 -coordinated scorpionate ligands can also be synthesized in facile ligand exchange reactions starting from $[\text{Pt}(\text{COMe})_2(\text{NH}_2\text{Bn})_2]$ (**2**) (Scheme 1, e).^[3] In contrast, the benzylamine complex **2** was found not to react with $\text{HC}(\text{pz})_3$ and $\text{HC}(3,5\text{-Me}_2\text{pz})_3$ (Scheme 2, c). It has been shown by ^1H NMR spectroscopy that in THF at room temperature no reactions occur over several hours.

Spectroscopic Characterization

The ^1H , ^{13}C , and ^{195}Pt NMR spectra of the diacetylplatinum(II) complexes **4a** and **4b** give proof of their identities. At room temperature, ^1H and ^{13}C NMR spectra, some signals are broadened, which points to a dynamic process. Thus, low-temperature (-73°C) and temperature-dependent NMR spectroscopic measurements were also performed.

At room temperature, the ^1H NMR spectrum of $[\text{Pt}(\text{COMe})_2\{(\text{pz})_3\text{CH}\}]$ (**4a**) displayed one signal for both acetyl ligands at $\delta = 2.08$ ppm, which reflects the mirror-symmetric structure of the complex in solution. Surprisingly, the three protons of the pyrazolyl rings of the tris(pyrazolyl)methane ligand are represented by only three signals at $\delta = 6.62$, 7.76, and 8.25 ppm, in which the signal at $\delta = 8.25$ ppm is very broad. The ^{13}C NMR spectrum exhibits also only one (partially broadened) resonance for each of the aromatic carbon atoms. All this implies a dynamic process that leads to chemical and magnetic equivalence of all three pyrazolyl rings. An intramolecular rearrangement, which involves the dissociation of one of the two coordi-

nated rings followed by the coordination of the third prior noncoordinated pyrazolyl ring in the sense of a fluxional behavior, might be an explanation. A fluxional behavior of bis- and tris(pyrazolyl)methane ligands is described by Rodríguez-Pérez and co-workers for allylpalladium(II) complexes.^[11]

In contrast, at room temperature in the ^1H NMR spectrum of $[\text{Pt}(\text{COMe})_2\{(3,5\text{-Me}_2\text{pz})_3\text{CH}\}]$ (**4b**), two signals with 2:1 intensity were found for the protons of the tris(pyrazolyl)methane ligand. The ^{13}C NMR spectrum of **4b** also displayed two sets of signals for the carbon atoms of the pyrazolyl rings. Nevertheless, these signals are slightly broadened relative to the signals of the acetyl carbon atoms, which suggests the presence of a dynamic process for this compound too (Figure 1).

Thus, both complexes were analyzed by variable-temperature NMR spectroscopic measurements. The relevant parts of the ^1H NMR spectra of **4a/b** are shown in Figures 2 and 3. At -73°C , in the ^1H and ^{13}C spectra of **4a** all δ_{H} and δ_{C} of the three pyrazolyl rings were found to be split into two resonances, as expected for diacetylplatinum(II) complexes with only bidentately coordinated ligands of this type (Table 1 and Figure 2).^[3,12] At 54°C , the ^1H NMR spectrum of **4b** exhibits one signal at $\delta = 6.17$ ppm that represents the protons at the 4-position of the pyrazolyl rings. The methyl groups at the 3-position are represented by one broad signal at $\delta = 2.15$ ppm, whereas the resonances for the methyl groups at the 5-position were found to be still split into two very broad signals at $\delta = 1.85$ and 2.55 ppm. Thus, the coalescence of this signal was not achieved at this temperature (Figure 3). Owing to the low boiling point of the solvent, measurements at higher temperatures could not be performed.

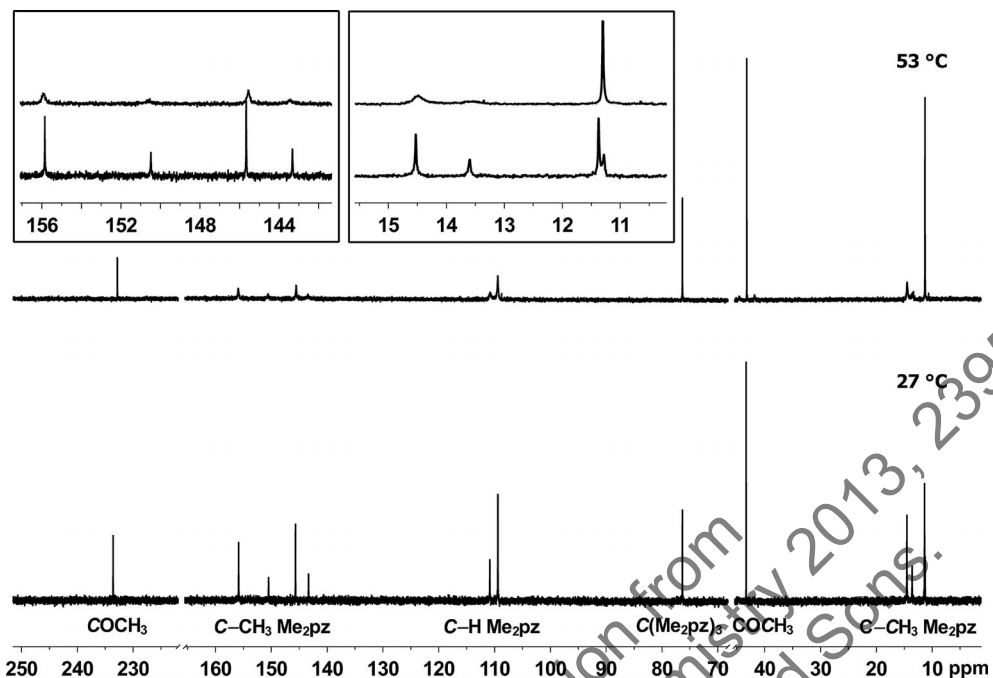


Figure 1. ¹³C NMR spectra of **4b** at 27 and 53 °C showing the range around $\delta = 13$ and 150 ppm as insets.

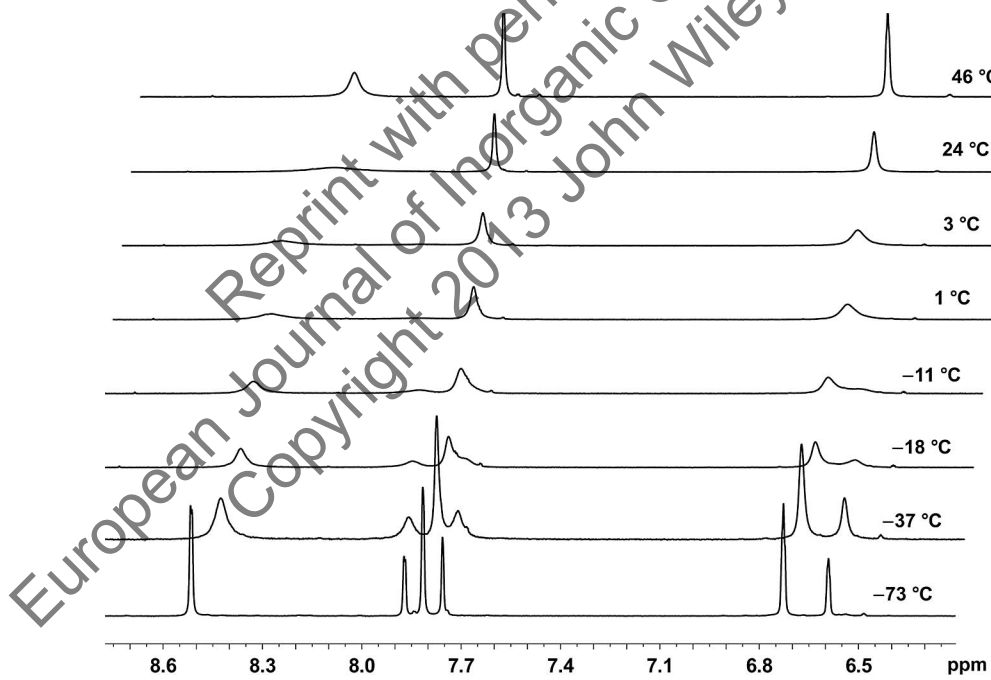


Figure 2. Aromatic region of variable-temperature ¹H NMR spectra of complex **4a**.

At 53 °C in the ¹³C NMR spectrum of **4b**, the carbon atoms of the methyl groups at the 5-position of the pyrazolyl rings are represented by one quite sharp signal at $\delta = 11.4$ ppm. The other pyrazolyl C atoms were found to be still split into two very broad signals (Figure 1). Although, in comparison to the spectrum recorded at 27 °C, these signals are broader, but the coalescence is not yet achieved in this case.

Furthermore, the variable-temperature ¹H NMR spectroscopic studies were used for an estimation of the Gibbs free energies of activation at the coalescence temperature for these dynamics. They were calculated according to $\Delta G_C^\neq = 0.00458 \cdot T_C \cdot (10.32 + \log k_C/T_C)$, for which the rate constant is determined by $k_C = \pi^* \Delta v / \sqrt{2}$ by using Δv of the frozen spectra at -73 °C.^[13] The compilation of ΔG_C^\neq and related parameters in Table 2 shows that for [Pt(COMe)₂-

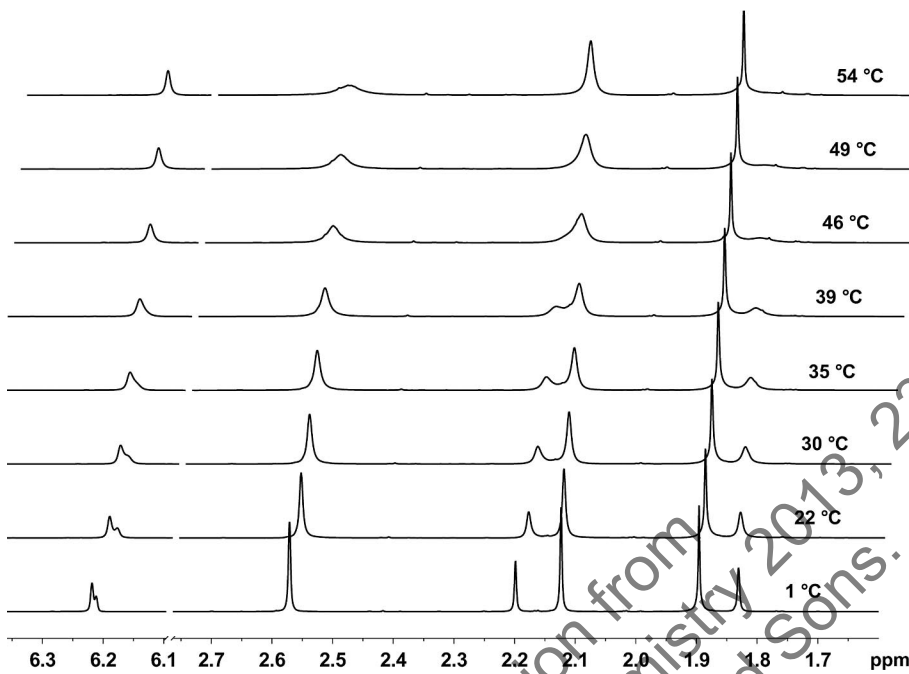


Figure 3. Variable-temperature ^1H NMR spectra of complex **4b**. The signal of the proton at the backbone C atom of the ligand at around $\delta = 8.4$ ppm is not shown.

Table 1. NMR spectroscopic parameters of the pyrazolyl rings in complex **4a** (δ in ppm).

T [°C]	$\delta_{\text{H}3}$	$\delta_{\text{H}4}$	$\delta_{\text{H}5}$	$\delta_{\text{C}3}$	$\delta_{\text{C}4}$	$\delta_{\text{C}5}$
23	7.76	6.62	8.25	145.2	108.8	135.0
-73 ^[a]	7.76	6.59	7.87	143.1	108.0	131.8
	7.81	6.73	8.52	146.2	109.3	137.2

[a] Resonances of noncoordinated pyrazolyl ring are given first.

$\{(pz)_3\text{CH}\}$ (**4a**) the Gibbs free energy of activation was calculated to be about 2.5 kcal mol $^{-1}$ lower (13.4 versus 15.9 kcal mol $^{-1}$) than that of $[\text{Pt}(\text{COMe})_2(3,5-\text{Me}_2\text{pz})_3\text{CH}]$ (**4b**). The higher activation barrier of **4b** might be caused by the higher donor ability of the $\text{HC}(3,5-\text{Me}_2\text{pz})_3$ ligand or by steric reasons due to the additional methyl groups.

Table 2. Gibbs free energies of activation and related parameters for the dynamics in complexes **4a/b**.

	4a			4b	
	H3	H4	H5	H4	C3-CH ₃
T_C [K]	262	276	297	312	322
Δv [s $^{-1}$]	28.3	62.7	268.9	14.9	68.2
k_C [s $^{-1}$]	62.9	139.3	597.3	33.1	151.5
ΔG_C^\neq [kcal mol $^{-1}$]	13.2	13.4	13.6	16.2	15.7

In general, NMR spectroscopy activation parameters are accessible in the range between 5 and 25 kcal mol $^{-1}$.^[13] By taking the well-studied dimethylformamide as a benchmark ($\Delta G_C^\neq = 21.5$ kcal mol $^{-1}$ at $T_C = 114$ °C), the dynamics in complexes **4a/b** are much faster, but in a comparable range with other molecular rearrangements in palladium and platinum complexes ($\Delta G_C^\neq = 10.6$ –15.3 kcal mol $^{-1}$ at $T_C = -43$ to 68 °C).^[11,14–16]

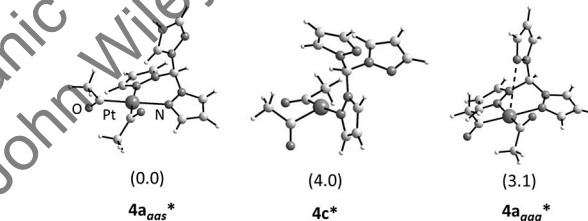


Figure 4. Equilibrium structures (calcd.) of complexes $[\text{Pt}(\text{COMe})_2\{(pz)_3\text{CH}\}]$ with the ligand $\kappa^2\text{N},\text{N}'$ -coordinated in an *anti-anti-syn* (**4a_{aas}***) and *anti-anti-anti* (**4a_{aaa}***) conformation, respectively, as well as κN -coordinated (**4c***). The standard Gibbs free energies [kcal mol $^{-1}$] are given in parentheses relative to the most stable isomer. In **4a_{aaa}*** the broken line indicates the nonbonding Pt...N'' distance (3.535 Å).

DFT Calculations

To gain insight into the dynamics of complexes **4**, quantum chemical calculations at the DFT level of theory were performed using the B3LYP functional and high-quality basis sets for all atoms and a pseudopotential for Pt considering relativistic effects (for details, see the Experimental Section). In all calculations, solvent effects (MeOH) were considered according to Tomasi's polarized continuum model (PCM). Please note that throughout this paper calculated complexes are marked with a star. All Gibbs energies given refer to standard conditions (298 K).

The structure of the calculated complex $[\text{Pt}(\text{COMe})_2\{(pz)_3\text{CH}-\kappa^2\text{N},\text{N}'\}]$ (**4a_{aas}***; Figure 4) is very close to that of the complex in crystals of **4a** except – as will be discussed below – that the arrangement of the two acetyl ligands is *transoid*. The analogous T-shaped complex **4c*** (Figure 4), which has only bound the tris(pyrazolyl)methane ligand in

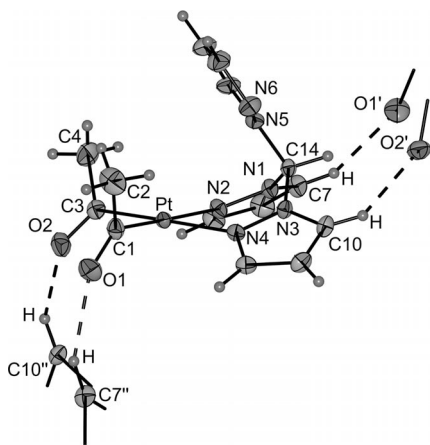


Figure 6. Molecular structure of $[\text{Pt}(\text{COMe})_2\{(\text{pz})_3\text{CH}\}]$ (**4a**). The ellipsoids are shown with a probability of 30%. Broken lines indicate intermolecular $\text{C}-\text{H}\cdots\text{O}$ hydrogen bonds in crystals of **4a**. Selected structural parameters (distances in Å, angles in °): Pt–C1 1.973(3), Pt–C3 1.978(4), Pt–N2 2.139(3), Pt–N4 2.118(3); Cl–Pt–C3 87.4(2), C1–Pt–N4 92.5(1), C3–Pt–N2 94.9(1), N2–Pt–N4 85.2(1), C1–Pt–N2 177.3(1), C3–Pt–N4 179.1(1); C7…O1' 3.080(6), H…O1' 2.25, C7–H…O1' 145, C10…O2' 3.036(5), H…O2' 2.22, C10–H…O2' 143.

a κN -coordinated fashion, is 4.0 kcal mol^{-1} higher in the standard Gibbs free energy. For the analogous complexes bearing the tris(3,5-dimethylpyrazolyl)methane ligand, the difference in the Gibbs energies amounts only to 2.1 kcal mol^{-1} ; the structures of these complexes are given in the Supporting Information.

To get an impression of the energy demand for rotation of pyrazolyl rings in these ligands (which must precede the coordination of the originally pendant pyrazolyl group), the rotational barriers in the free (noncoordinated) ligands were calculated. For $\text{HC}(\text{pz})_3$ the results are shown in the diagram in Figure 5 [for $(3,5\text{-Me}_2\text{pz})_3\text{CH}$, see the Supporting Information]. Two equilibrium structures have been calculated. The one with an *anti-anti-syn* conformation represents the global minimum, and the one with the *anti-anti-anti* conformation is 2.7 kcal mol^{-1} higher in the Gibbs energy. Here and in the following sections, the conformations are described with respect to the $\text{H}-\text{C}-\text{N}-\text{N}$ angles. The *anti-anti-syn* conformation was found in crystals of complexes **4a/b** (see Figures 6 and 7) bearing the ligand in an κ^2N,N' -coordinated fashion, whereas the *anti-anti-anti* conformation would permit an κ^3N,N',N'' coordination. The Gibbs free energy of activation for the *syn-anti* transformation according to Figure 5 amounts to 4.1 kcal mol^{-1} . In the case of the dimethyl-substituted derivative, both conformers have the same energy, but the activation barrier is significantly higher (5.9 kcal mol^{-1}).

An alternate process for the fluxional behavior of the complexes would be via an intermediate complex with the tripodal ligand κ^3N,N',N'' -coordinated, but we failed to localize such a complex, $[\text{Pt}(\text{COMe})_2\{(\text{pz})_3\text{CH}-\kappa^3N,N',N''\}]$, as an equilibrium structure. Nevertheless, it cannot be strictly ruled out that at first the pendant pyrazolyl ring in the complex $[\text{Pt}(\text{COMe})_2\{(\text{pz})_3\text{CH}-\kappa^2N,N'\}]$ (**4a_{aas}**) is ro-

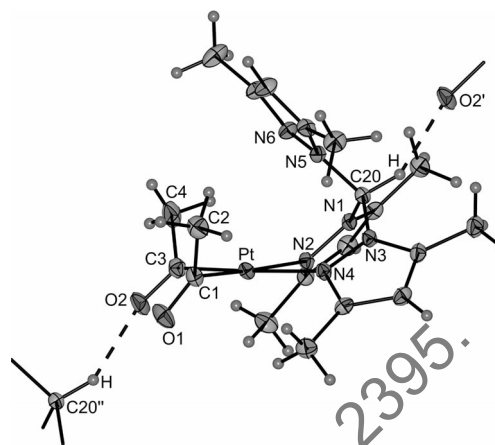


Figure 7. Molecular structure of $[\text{Pt}(\text{COMe})_2\{(\text{3,5-Me}_2\text{pz})_3\text{CH}\}]$ (**4b**). The ellipsoids are shown with a probability of 30%. Broken lines indicate intermolecular $\text{C}-\text{H}\cdots\text{O}$ hydrogen bonds in crystals of **4b**. Selected structural parameters (distances in Å, angles in °): Pt–C1 2.008(5), Pt–C3 1.994(5), Pt–N2 2.176(4), Pt–N4 2.134(4); C1–Pt–C3 88.1(2), C1–Pt–N4 94.9(2), C3–Pt–N2 94.6(2), N2–Pt–N4 82.4(1), C1–Pt–N2 176.4(2), C3–Pt–N4 176.7(2); C20…O2' 3.016(6), H…O2' 2.13, C20–H…O2' 147.

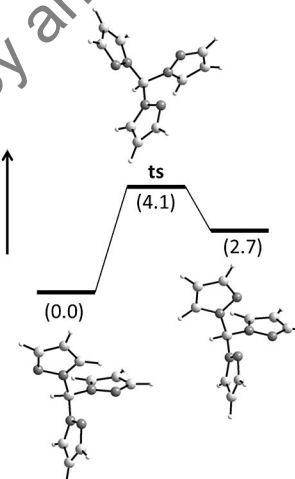


Figure 5. Gibbs free-energy diagram for the rotation of one pyrazolyl group in $\text{HC}(\text{pz})_3$. The Gibbs energies [kcal mol^{-1}] are given in parentheses relative to the most stable isomer (left: *anti-anti-syn* conformation; right: *anti-anti-anti* conformation; ts = transition state).

tated such that the ligand adopts an *anti-anti-anti* conformation. The Gibbs energy of this complex (**4a_{aaa}***; Figure 4) is 3.1 kcal mol^{-1} higher than that of complex **4a_{aas}***. The Pt…N'' distance (3.535 Å) indicates that there are no bonding interactions. The Gibbs free energy of activation is 3.8 kcal mol^{-1} . In the case of the complex with the dimethyl-substituted ligand, the situation is different. Here, the structure in which the N atom from the pendant pyrazolyl ring is pointed toward the central platinum atom is a transition state (Pt…N'' 3.215 Å) that lies 6.5 kcal mol^{-1} above the equilibrium structure.

Because the decoordination of one of the two N atoms in the starting complexes **4a_{aas}***/**4b_{aas}*** can be assumed to proceed with a low activation barrier (**4a_{aas}*** → **4c***;

4b_{aus}* → 4d*), the conformational changes of κ^1N -coordinated ligands (such that the previous pendant pyrazolyl groups are ready for coordination) are the processes that determine the activation barrier. The calculations show that – in accordance with the experiments – the barrier is less for the $\text{HC}(\text{pz})_3$ ligand. Although less likely, the process in which the conformational change of the ligand precedes the decoordination of one of the two N atoms, gives the same result.

Structures of $[\text{Pt}(\text{COMe})_2\{(\text{pz})_3\text{CH}\}]$ (**4a**) and $[\text{Pt}(\text{COMe})_2\{(3,5-\text{Me}_2\text{pz})_3\text{CH}\}]$ (**4b**)

Crystals of **4a/b** were obtained from saturated solutions in methanol at -7°C . The molecular structures are shown in Figures 6 and 7; selected structural parameters are given in the figure captions. The platinum atoms are square-planar-coordinated by two acetyl ligands and an κ^2 -bonded tris(pyrazolyl)- (**4a**) or tris(3,5-dimethylpyrazolyl)methane (**4b**) ligand. The angles between neighboring ligands are all close to 90° [85.2(1)–94.9(1) $^\circ$, **4a**; 82.4(1)–94.9(2) $^\circ$, **4b**]. The $\text{HC}(\mu\text{-pz})_2\text{Pt}$ units adopt a boat conformation with the backbone carbon atom of the tris(pyrazolyl)methane ligand (C14, **4a**; C20, **4b**) and the platinum atom at the apices. The noncoordinated pyrazolyl rings are orientated pseudoparallel to the coordination plane (Pt,C1,C3,N2,N4). The angles between the complex plane and the plane of the noncoordinated ring are 55.0(1) (**4a**) and 52.0(2) $^\circ$ (**4b**), which results in a distance of 3.722 (**4a**) and 3.692 Å (**4b**) between the platinum atom and the center of gravity of the noncoordinated rings.

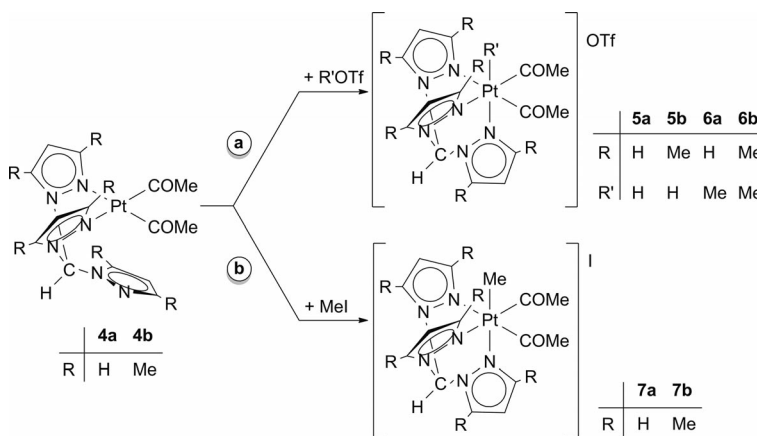
In both structures, the carbonyl oxygen atoms of the two acetyl ligands were found to lie on the same side of the complex plane. Thus, the diacetyl moieties represent a *cisoid* conformation. In *cis*-diacetyl complexes, a *transoid* conformation (which means that the carbonyl O atoms lie on different sides of the complex plane) should be favored, clearly due to a reduced repulsion between the negatively charged O atoms and the space-demanding methyl groups. Here, the *cisoid* conformations are stabilized by weak intermolecular C–H…O hydrogen bonds such that the crystals are three-

aded by one-dimensional strands (Figure 6 and Figure 7). The structural parameters of these hydrogen bonds in which the O atoms of the acetyl ligands act as hydrogen acceptors, and C–H groups of pyrazolyl rings (**4a**) and of backbone of the ligand (**4b**) act as hydrogen donors [C…O 3.016(6)–3.080(6) Å; H…O 2.13–2.25 Å; C–H…O 143–147 $^\circ$] are in the range of such attractive interactions.^[17] In full accord with this argumentation, DFT calculations that represent the molecules in the gas phase or in solution (methanol) without intermolecular interactions exhibit the *transoid* conformation as the most stable ones (see above).

Reactivity of $[\text{Pt}(\text{COMe})_2\{(\text{pz})_3\text{CH}\}]$ (**4a**) and $[\text{Pt}(\text{COMe})_2\{(3,5-\text{Me}_2\text{pz})_3\text{CH}\}]$ (**4b**) toward R'OTf (R' = H, Me) and Methyl Iodide

Synthesis

As described previously, the hydridoplatinum(IV) complexes $[\text{Pt}(\text{COMe})_2\text{H}\{(\text{pz})_3\text{CH}\}] \text{Cl}$ (**3a**) and $[\text{Pt}(\text{COMe})_2\text{H}\{(3,5-\text{Me}_2\text{pz})_3\text{CH}\}] \text{Cl}$ (**3b**) formed by the reaction of $[\text{Pt}(\text{COMe})_2\text{H}]_2(\mu\text{-Cl})_2$ (**1**) and the respective ligand as intermediates were found to be highly temperature-sensitive (Scheme 2, a). Keeping in mind that hydridoplatinum(IV) complexes can also be prepared by protonation of platinum(II) compounds,^[18] the reactivity of complexes **4a/b** toward trifluoromethanesulfonic acid was investigated. As shown in Scheme 3 (reaction pathway a), the reactions resulted in the formation of hydrido complexes **5a/b** of the type **3a/b**, but with triflate instead of chloride as counteranion. The compounds were isolated in good yields of 87% and identified by NMR (^1H , ^{13}C , ^{19}F , ^{195}Pt) and IR spectroscopy as well as by high-resolution mass spectrometric (HRMS-ESI) investigations. In contrast to **3a/b**, compounds **5a/b** were found to be stable in acetone or methanol at room temperature, thus exhibiting a pronounced dependence of the stability of the hydridoplatinum(IV) complexes on the counteranion. Solutions of **5a/b** in chloroform and dichloromethane showed a restricted stability. At room temperature and under ambient light, solutions of **5a/b** in



Scheme 3. Reactivity of $[\text{Pt}(\text{COMe})_2\{(\text{pz})_3\text{CH}\}]$ (**4a**) and $[\text{Pt}(\text{COMe})_2\{(3,5-\text{Me}_2\text{pz})_3\text{CH}\}]$ (**4b**) toward R'OTf (R' = H, Me) and methyl iodide.

dichloromethane were found to be stable for approximately 1 day, whereas decomposition in chloroform can be observed after just 2 h. It can be assumed that the initial step of this decomposition is a conversion of the hydrido- into chloridoplatinum(IV) complexes along a radical pathway as described for similar hydridoplatinum(IV) complexes ($[\text{PtMe}_2\text{H}\{(3,5-\text{Me}_2\text{pz})_3\text{BH}\}]$,^[19] $[\text{Pt}(\text{COMe})_2\text{H}\{(\text{pz})_3\text{BH}\}]$ / $[\text{Pt}(\text{COMe})_2\text{H}\{(3,5-\text{Me}_2\text{pz})_3\text{BH}\}]$ ^[3]) that bear scorpionate ligands. Here, starting from **5a/b**, the selective synthesis of the respective chlorido complexes failed and substances with a high content of impurities were always obtained.

Furthermore, the reactivity of $[\text{Pt}(\text{COMe})_2\{(\text{pz})_3\text{CH}\}]$ (**4a**) and $[\text{Pt}(\text{COMe})_2\{(3,5-\text{Me}_2\text{pz})_3\text{CH}\}]$ (**4b**) in oxidative addition reactions toward methyl trifluoromethanesulfonate (Scheme 3, a) and methyl iodide (Scheme 3, b) was investigated. The reactions with methyl trifluoromethanesulfonate proceeded significantly faster than those with methyl iodide. In both cases, white or pale yellow solids of cationic diacetylplatinum(IV) complexes with triflate (**6a/b**) and iodide (**7a/b**) as counterion were obtained and unambiguously identified by NMR (^1H , ^{13}C , ^{19}F (**6**), ^{195}Pt) and IR spectroscopy, as well as by high-resolution mass spectrometric (HRMS-ESI) investigations and single-crystal X-ray diffraction analysis (**7a**). All compounds proved to be air- and moisture-stable and soluble in dichloromethane, chloroform, and acetone without decomposition over several days. Thus, in this case, no significant effect of the counterion on the stability of the compounds was observed.

Spectroscopic Characterization

Selected ^1H , ^{13}C , and ^{195}Pt NMR spectroscopic parameters of complexes **3** and **5–7** are given in Tables 3 and 4. The spectra confirm the identities of the complexes; all signals were found in the expected shift ranges with correct intensities in the ^1H NMR spectra. The ^1H NMR spectra of the hydridoplatinum(IV) complexes **3** and **5** exhibit the characteristic, far-upfield-shifted ($\delta = -17.98$ to -18.73 ppm) hydride resonances with $^{1}\text{J}_{\text{Pt},\text{H}}$ coupling constants between 1619.7 and 1659.2 Hz as found for other hydridoplatinum(IV) complexes too.^[18,20] In ^1H NMR spectra of **5a/b** recorded in CD_3OD no signal for the hydrido ligand was observed. However, the resonances and intensities of the other protons did not change significantly, which suggests an H/D exchange between the hydrido ligands and the solvent. To prove it definitively, compounds **5a/b** were dissolved in CD_3OD , and after removal of the solvent ^2H NMR spectra of the obtained solids (dissolved in CH_2Cl_2) were recorded. Both spectra displayed a singlet signal at higher fields ($\delta_{\text{D}} = -18.07$ – -18.53 ppm) very close to δ_{H} for the hydrido ligands in the respective complexes **5a/b**. Thus, these results give proof for the formation of the complexes $[\text{Pt}(\text{COMe})_2\text{D}\{(\text{pz})_3\text{CH}\}]\text{OTf}$ (**5c**) and $[\text{Pt}(\text{COMe})_2\text{D}\{(3,5-\text{Me}_2\text{pz})_3\text{CH}\}]\text{OTf}$ (**5d**) in CD_3OD bearing deuterido instead of hydrido ligands.

In $[\text{Pt}(\text{COMe})_2\text{H}\{(\text{pz})_3\text{CH}\}]\text{Cl}$ (**3a**), the δ_{H} of the methine proton of the $\text{HC}(\text{pz})_3$ ligand was found at much lower field ($\delta_{\text{H}} = 12.39$ ppm) relative to the free ligand ($\delta_{\text{H}} = 8.41$ ppm)^[21] and to the corresponding diacetylplatinum(II)

Table 3. Selected NMR spectroscopic parameters (δ in ppm, J in Hz) of the hydridoplatinum(IV) complexes $[\text{Pt}(\text{COMe})_2\text{H}\{(\text{pz})_3\text{CH}\}]\text{X}$ [$\text{X} = \text{Cl}$ (**3a**), OTf (**5a**)] and $[\text{Pt}(\text{COMe})_2\text{H}\{(3,5-\text{Me}_2\text{pz})_3\text{CH}\}]\text{Cl}$ [$\text{X} = \text{Cl}$ (**3b**), OTf (**5b**)].

	COCH_3	COCH_3	$\text{Pt}-\text{H}$	$\frac{\text{HC}(\text{pz})_3}{\text{HC}(\text{Me}_2\text{pz})_3}$	
	δ_{H} ($^3\text{J}_{\text{Pt},\text{H}}$)	δ_{C} ($^2\text{J}_{\text{Pt},\text{C}}$)	δ_{C} [d]	δ_{H} ($^1\text{J}_{\text{Pt},\text{H}}$)	
3a ^[a]	2.71 [c] (257.1)	44.7 [c] (209.3)	189.0 [d] (263.9)	-17.98 [c] (1637.2) -18.54 [c] (1619.7)	12.39 7.97
3b ^[a]	2.49 [c] (28.5)	40.6 [c] (263.9)	192.3 [d] (222.0)	-18.30 [c] (1659.2) -18.73 [c] (1636.1)	10.17 8.08
5a ^[b]	2.73 [c] (28.5)	44.2 [c] (263.9)	186.7 [d] (222.0)	-18.30 [c] (1659.2) -18.73 [c] (1636.1)	10.17 8.08
5b ^[b]	2.58 [c] (17.7)	41.3 [c] (222.0)	190.5 [d] (222.0)	-18.73 [c] (1636.1)	8.08

[a] Measured at -80°C in CD_2Cl_2 . [b] Measured at $+27^\circ\text{C}$ in CD_2Cl_2 . [c] Observed as shoulders. [d] $^1\text{J}_{\text{Pt},\text{C}}$ coupling constants were not observed due to poor intensity.

Table 4. Characteristic NMR spectroscopic data of $[\text{Pt}(\text{COMe})_2\text{Me}\{(\text{pz})_3\text{CH}\}]\text{X}$ [$\text{X} = \text{OTf}$ (**6a**, **1** (**7a**)) and $[\text{Pt}(\text{COMe})_2\text{Me}\{(3,5-\text{Me}_2\text{pz})_3\text{CH}\}]\text{X}$ [$\text{X} = \text{OTf}$ (**6b**, **1** (**7b**))].

	COCH_3		COCH_3	
	δ_{H} ($^3\text{J}_{\text{Pt},\text{H}}$)	δ_{C} ($^2\text{J}_{\text{Pt},\text{C}}$)	δ_{C} ($^1\text{J}_{\text{Pt},\text{C}}$)	$\frac{\text{HC}(\text{pz})_3}{\text{HC}(\text{Me}_2\text{pz})_3}$ δ_{H} δ_{Pt}
6a	2.48 (15.4)	35.8 (200.7)	189.5 (939.0)	10.30 -1495.5
6b	2.31 (8.9)	34.1 (181.5)	193.3 (944.4)	8.20 -1584.4
7a	2.47 (14.7)	35.8 (200.7)	189.2 (940.0)	12.22 -1491.2
7b	2.31 (7.7)	34.2 (181.4)	193.2 (944.7)	8.18 -1583.2

complex **4a** ($\delta_{\text{H}} = 9.14$ ppm), whereas the analogous compound **5a** with triflate as counterion exhibits this resonance at $\delta = 10.17$ ppm. The same tendency was also observed for the methylplatinum(IV) complexes $[\text{Pt}(\text{COMe})_2\text{Me}\{(\text{pz})_3\text{CH}\}]\text{I}$ (**7a**, $\delta_{\text{H}} = 12.22$ ppm) and $[\text{Pt}(\text{COMe})_2\text{Me}\{(\text{pz})_3\text{CH}\}]\text{OTf}$ (**6a**, $\delta_{\text{H}} = 10.30$ ppm), thus indicating a significant influence of the type of counterion on this resonance (Table 4). A comparable downfield shift ($\delta_{\text{H}} = 12.49$ ppm) was detected for the similar cationic platinum(IV) compound $[\text{PtPh}_2\text{Me}\{(\text{pz})_3\text{CH}\}]\text{I}$ with iodide as counterion in relation to the corresponding platinum(II) complex $[\text{PtPh}_2\{(\text{pz})_3\text{CH}\}]$ ($\delta_{\text{H}} = 9.27$ ppm).^[12] Furthermore, the cationic platinum(IV) compound $[\text{PtMe}_2\text{I}\{(\text{pz})_3\text{CH}-\kappa^3\text{N},\text{N}',\text{N}''\}]\text{I}$ exhibits the resonance of the methine proton at $\delta = 12.60$ ppm and, thus, shifted about $\delta = 2.5$ ppm to lower field relative to the neutral isomer $[\text{PtMe}_2\text{I}_2\{(\text{pz})_3\text{CH}-\kappa^2\text{N},\text{N}'\}]$ ($\delta_{\text{H}} = 10.10$ ppm).^[22] Thus, downfield shifts of the methine proton at about $\delta = 10$ ppm might be due to the coordination of the ligand at a platinum(IV) center, whereas the downfield shifts above $\delta = 12$ ppm as in **3a** and **7a** suggest the presence of hydrogen bonds between the methine proton and the halide counterions even in solution.^[23] Furthermore, the geometric parameters found in the single-crystal X-ray diffraction analysis of **7a**, which will be discussed below, also confirm the

presence of these interactions. In the case of a cationic palladium(II) complex, the interaction between the $\text{HC}(\text{pz})_3$ ligand and the PF_6^- counterion through an assembly of hydrogen bonds is already proven both for the solid state and in solution.^[24]

In contrast, the methine proton of the dimethyl-substituted tris(pyrazolyl)methane ligand exhibits no dependence either on the oxidation state of the platinum center or on the type of counterion in cationic platinum(IV) complexes **3b**, **5b**, **6b**, and **7b** (Tables 3 and 4). The ^1H resonances in complexes **3b** and **5b–7b** and in the free ligand ($\delta_{\text{H}} = 8.00$ ppm)^[25] were all found at about $\delta = 8$ ppm. This might be due to steric protection of the methine proton by the methyl groups at the 5-position and/or the electron-donating effect of the methyl groups.

The ^1H and ^{13}C chemical shifts of the acetyl ligands in compounds **3** and **6** are very similar to those in the corresponding compounds **5** and **7**, which shows that, as expected, the counteranion has practically no influence on these chemical shifts. Overall, the ^1H and ^{13}C chemical shifts and corresponding coupling constants of the acetyl ligands in complexes **3** and **5–7** exhibit significant differences depending on the substitution pattern of the tris(pyrazolyl)methane ligand (Tables 3 and 4). In complexes **3a** and **5a–7a**, the δ_{H} and δ_{C} of the methyl groups of the acetyl ligands are shifted slightly ($\Delta\delta_{\text{H}} = 0.15\text{--}0.22$ ppm, $\Delta\delta_{\text{C}} = 1.6\text{--}4.1$ ppm) to lower fields relative to the corresponding compounds **3b** and **5b–7b**, whereas δ_{C} of the carbonyl carbon atoms is shifted by about 4 ppm to higher fields. The corresponding $^3J_{\text{Pt},\text{H}}$ as well as the $^2J_{\text{Pt},\text{C}}$ coupling constants in complexes with the $\text{HC}(\text{pz})_3$ ligand are significantly larger than those found in the analogous complexes bearing the $\text{HC}(3,5\text{-Me}_2\text{pz})_3$ ligand. Furthermore, owing to a higher *trans* influence, because of the electron-donating effect of the additional methyl groups, the ^{195}Pt shifts were found to be at higher fields in the hydridoplatinum(IV) complex **5b** and in the methylplatinum(IV) complexes **6b–7b** ($\Delta\delta_{\text{Pt}} \approx 90\text{--}100$) than in the corresponding complexes **5a**, **6a**, and **7a** bearing the unsubstituted tris(pyrazolyl)methane ligand.

Structure of $[\text{Pt}(\text{COMe})_2\text{Me}\{\text{(pz)}_3\text{CH}\}\text{I}\cdot\text{CH}_2\text{Cl}_2$ (**7a**· CH_2Cl_2)

Crystals of **7a**· CH_2Cl_2 suitable for X-ray diffraction analysis were obtained from a solution in dichloromethane in which the solvent was allowed slowly to evaporate at 4 °C. The molecular structure is shown in Figure 8, and selected structural parameters are given in the figure caption. In crystals of **7a**· CH_2Cl_2 , the complex cation and the iodide counterion are connected by a C–H···I hydrogen bond. The C···I [3.716(5) Å] and H···I (2.76 Å) distances as well as the C–H···I angle of 159° are in the range of such interactions.^[26] Other notable intermolecular interactions [shortest distance between non-hydrogen atoms: 3.325(7) Å, O1···C7'] were not found.

The platinum atom is located in the center of a distorted-octahedral environment and coordinated by a facially κ^3 -bonded tris(pyrazolyl)methane ligand, by two acetyl li-

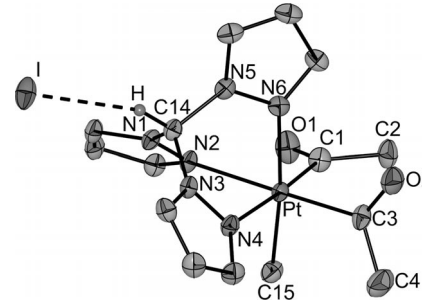


Figure 8. Structure of $[\text{Pt}(\text{COMe})_2\text{Me}\{\text{(pz)}_3\text{CH}\}\text{I}]$ (**7a**) in crystals of **7a**· CH_2Cl_2 . The ellipsoids are shown with a probability of 30%. Hydrogen atoms are omitted for clarity, except that at C14. The broken line indicates an C–H···I hydrogen bond in crystals of **7a**· CH_2Cl_2 . Selected structural parameters (distances in Å, angles in °): Pt–C1 2.014(6), Pt–C3 2.029(6), Pt–C15 2.053(6), Pt–N2 2.193(4), Pt–N4 2.206(5), Pt–N6 2.181(4), C1–Pt–C3 92.8(3), C1–Pt–C15 84.2(3), C3–Pt–C15 93.0(0), C1–Pt–N2 93.0(2), C1–Pt–N6 97.6(2), C3–Pt–N4 91.6(2), C3–Pt–N6 92.6(2), C15–Pt–N2 91.6(2), C15–Pt–N4 95.3(2), N2–Pt–N4 82.6(2), N2–Pt–N6 82.7(2), N4–Pt–N6 82.5(2), C1–Pt–N4 175.6(2), C3–Pt–N2 172.9(2), C15–Pt–N6 174.1(2), I–C14 3.716(5), I···H 2.76, I···C14 159.

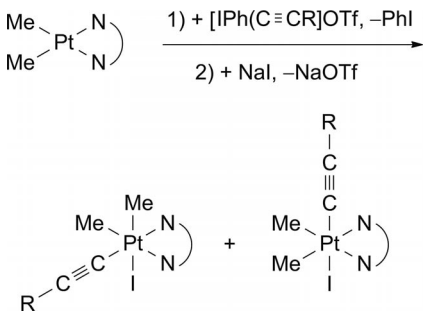
gands, and one methyl ligand. N–Pt–N [82.5(2)–82.7(2)°] and C–Pt–N [91.6(2)–97.6(2)°] angles are noticeably smaller and larger, respectively, than 90°. The Pt–N bond lengths are in the range 2.181(4)–2.206(5) Å. Within the 3σ criterion there is no significant difference in the Pt–N bond lengths *trans* to the methyl and acetyl ligands, whereas the differences in the lengths of the Pt–C_{Ac} [2.014(6)/2.029(6) Å] and Pt–C_{Me} [2.053(6) Å] bonds reflect the differences in the atomic radii of sp³- and sp²-hybridized C atoms.^[27]

Synthesis and Characterization of Alkynylplatinum(IV) Complexes

Synthesis

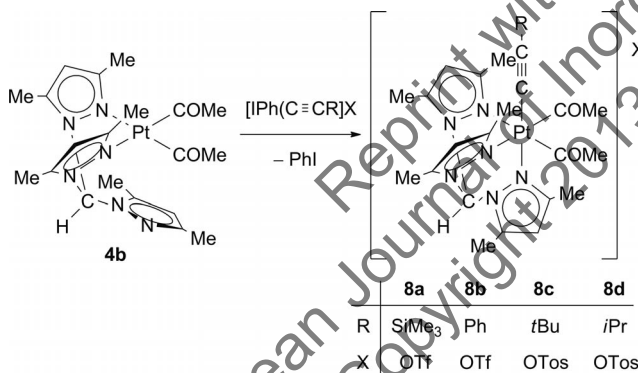
Canty and co-workers reported that alkynyl groups can be transferred (formally as $[\text{C}\equiv\text{CR}]^+$) from hypervalent alkynyl iodine(III) reagents such as $[\text{IPh}(\text{C}\equiv\text{CR})]\text{OTf}$ to platinum(II) complexes of the type $[\text{PtMe}_2(\text{N}^\wedge\text{N})]$ or $[\text{PtMe}_2(\text{P}^\wedge\text{P})]$ to form alkynyl(dimethyl)platinum(IV) complexes with release of iodobenzene (Scheme 4).^[28] To obtain more thermally stable complexes, the sixth coordination site of the platinum(IV) center has to be occupied by an additionally added anionic donor like iodide^[28] or an neutral N donor like pyridine^[29] because the anionic part of the alkynyl iodonium salts requires the incorporation of non-nucleophilic anions like triflate, tetrafluoridoborate, or tosylate.^[30] The use of diacetylplatinum(II) complexes with κ^2 -coordinated tris(pyrazolyl)methane ligands in such reactions should open the possibility to synthesize cationic alkynyl platinum(IV) complexes when the pendant pyrazolyl ring coordinates to the sixth coordination site.

Reactions of $[\text{Pt}(\text{COMe})_2\{\text{(3,5-Me}_2\text{pz})_3\text{CH}\}]$ (**4b**) with $[\text{IPh}(\text{C}\equiv\text{CR})]\text{X}$ (R/X = SiMe₃/OTf, Ph/OTf, tBu/OTos, iPr/OTos) led to the formation of the cationic diacetyl(alkynyl



Scheme 4. Synthesis of alkynyl(dimethyl)platinum(IV) complexes.^[28]

yl)platinum(IV) complexes **8** (Scheme 5). The reactions were performed at -78°C in dichloromethane, and after addition of the first drops of the alkynyl iodine(III) reagent, the color of the reaction mixture immediately turned dark red. After warming to room temperature, compounds **8** were isolated from henceforth clear, colorless solutions in good yields between 61 and 80%. Complexes **8** were fully characterized by NMR [^1H , ^{13}C , ^{19}F (**8a/b**), ^{195}Pt] and IR spectroscopy, as well as by high-resolution mass spectrometric (HRMS-ESI) investigations and single-crystal X-ray diffraction measurements (**8a/d**). The colorless, moisture- and air-stable complexes are soluble in chloroform, dichloromethane, and THF. At room temperature they are stable in solution for several days.



Scheme 5. Synthesis of diacetyl(alkynyl)platinum(IV) complexes **8**.

In contrast, in the corresponding reactions of $[\text{Pt}(\text{COMe})_2\{\text{(pz)}_3\text{CH}\}]$ (**4a**) with $[\text{IPh}(\text{C}\equiv\text{CR})]\text{X}$, only mixtures of unidentified products were obtained. After the addition of the iodine(III) reagents, the same characteristic color change into dark red was observed, but no complete decolorization occurred when the reaction mixtures were slowly warmed to room temperature, and the resulting solutions remained yellow. Thus, it can be assumed that the methyl groups at the pyrazolyl rings by their donor and/or steric effects are essential for the stability of alkynylplatinum(IV) complexes **8**.

Spectroscopic Characterization

^1H and ^{13}C NMR spectra of complexes **8** are fully consistent with the constitution of the complexes given in

Scheme 5. Selected spectroscopic parameters are compiled in Table 5. In all complexes, δ_{H} and δ_{C} values of the acetyl ligands and corresponding coupling constants are in a narrow range. The ^{195}Pt resonances were found to be between $\delta = -1366.5$ and -1380.9 ppm and, thus, shifted by approximately $\delta = 2100$ ppm to higher field relative to the respective platinum(II) precursor complex $[\text{Pt}(\text{COMe})_2\{\text{(3,5-Me}_2\text{pz)}_3\text{CH}\}]$ (**4b**), as expected.^[31]

Table 5. Selected NMR spectroscopic parameters (δ in ppm, J in Hz) of $[\text{Pt}(\text{COMe})_2(\text{C}\equiv\text{CR})\{\text{(3,5-Me}_2\text{pz)}_3\text{CH}\}] \text{X}$ [$\text{R/X} = \text{SiMe}_3/\text{OTf}$ (**8a**), Ph/OTf (**8b**), $t\text{Bu}/\text{OTos}$ (**8c**), $i\text{Pr}/\text{OTos}$ (**8d**)].

	COCH_3 δ_{H} ($^3\text{J}_{\text{Pt},\text{H}}$)	COCH_3 δ_{C} ($^1\text{J}_{\text{Pt},\text{C}}$)	$\text{Pt}-\text{C}_{\alpha}=\text{C}_{\beta}\text{R}$ $\delta_{\alpha\text{C}}/\delta_{\beta\text{C}}$	δ_{Pt}	
8a	2.75 (13.6)	35.9 (187.1)	185.0 (78.9)	80.6/103.6	-1366.5
8b	2.81 (14.0)	36.4 (181.2)	185.1 (780.2)	62.3/97.2	-1376.6
8c	2.72 (13.3)	36.0 (186.1)	185.6 (795.1)	46.5/104.4	-1380.9
8d	2.71 (13.6)	36.0 (184.9)	185.6 (795.1)	47.1/104.4	-1371.1

The chemical shifts of the α -carbon atoms of the alkynyl ligand were found to be strongly dependent on the substituent R, which results in the order $t\text{Bu}/i\text{Pr}$ ($\delta_{\text{C}} = 46.5/47.1$ ppm, **8c/d**) $<$ Ph ($\delta_{\text{C}} = 62.3$ ppm, **8b**) $<$ SiMe_3 ($\delta_{\text{C}} = 80.6$ ppm, **8a**), thus, they are strongly low-field-shifted ($\Delta\delta_{\text{C}} = 19/37$) relative to the corresponding alkynylidonium salts. On the contrary, the β -carbon atoms are high-field-shifted by $\delta = 8$ to 17 ppm.

Structures of Alkynylplatinum(IV) Complexes

Crystals of $[\text{Pt}(\text{COMe})_2(\text{C}\equiv\text{CSiMe}_3)\{\text{(3,5-Me}_2\text{pz)}_3\text{CH}\}]\text{OTf} \cdot \text{THF}$ (**8a**·THF) and $[\text{Pt}(\text{COMe})_2(\text{C}\equiv\text{C}i\text{Pr})\{\text{(3,5-Me}_2\text{pz)}_3\text{CH}\}]\text{OTos} \cdot \text{CHCl}_3$ (**8d**·CHCl₃) suitable for X-ray diffraction analyses were obtained from a THF solution layered with *n*-pentane (**8a**·THF) and from a chloroform solution (**8d**·CHCl₃), respectively. Both compounds crystallized as discrete cations and anions without unusual intermolecular interactions [shortest distance between non-hydrogen atoms: 3.136(6) Å, C18···O4', **8a**·THF; 3.037(5), O5···C33', **8d**·CHCl₃]. The molecular structures are shown in Figures 9 and 10. Selected structural parameters are given in the figure captions.

The platinum atoms adopt a distorted-octahedral geometry and are coordinated by the facially κ^3 -coordinated tris(3,5-dimethylpyrazolyl)methane ligand, two acetyl ligands, as well as one alkynyl ligand. Due to the restricted bite of the facially coordinated tris(pyrazolyl)methane ligand, the N–Pt–N angles are slightly diminished [81.9(1)–84.7(1) $^\circ$ (**8a**), 81.88(8)–85.77(8) $^\circ$ (**8d**)]. Whereas in the structure of **8a** the carbonyl oxygen atoms of the two acetyl ligands were found on different sides of the complex plane, thus representing a *transoid* conformation, in the structure of **8d**, the *cisoid* conformation can be observed. The differences in the lengths of the Pt–C_{Ac} bonds [2.040(3)–2.059(4) Å] and the Pt–C_{C≡CR} bonds [1.979(3)/1.996(4) Å] reflect the smaller atomic radius of a C(sp) than a C(sp²)

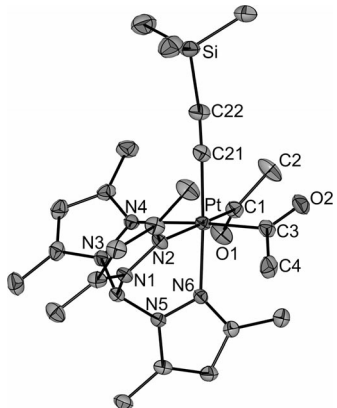


Figure 9. Structure of the cation in crystals of $[\text{Pt}(\text{COMe})_2(\text{C}\equiv\text{CSiMe}_3)\{(3,5-\text{Me}_2\text{pz})_3\text{CH}\}]\text{OTf}\cdot\text{THF}$ (**8a**·THF). The ellipsoids are shown with a probability of 30%. Hydrogen atoms are omitted for clarity. Selected structural parameters (distances in Å, angles in °): Pt–C1 2.059(4), Pt–C3 2.050(4), Pt–C21 1.996(4), Pt–N2 2.247(3), Pt–N4 2.208(3), Pt–N6 2.100(3); C1–Pt–C3 93.7(2), C1–Pt–C21 90.7(2), C3–Pt–C21 89.4(2), C1–Pt–N4 90.7(1), C1–Pt–N6 91.6(1), C3–Pt–N2 93.6(1), C3–Pt–N6 92.4(1), C21–Pt–N2 92.7(1), C21–Pt–N4 93.5(1), N2–Pt–N4 81.9(1), N2–Pt–N6 84.7(1), N4–Pt–N6 84.5(1), C1–Pt–N2 172.0(1), C3–Pt–N4 174.8(1), C21–Pt–N6 177.0(1), C21–C22 1.180(6), Pt–C21–C22 177.7(4), C21–C22–Si 174.4(4).

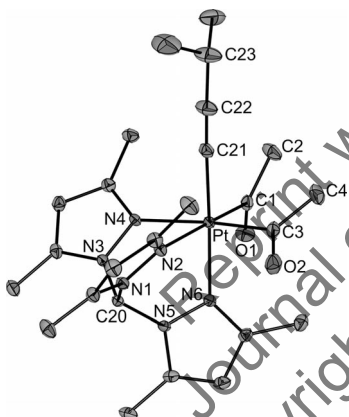


Figure 10. Structure of the cation in crystals of $[\text{Pt}(\text{COMe})_2(\text{C}\equiv\text{CIPr})\{(3,5-\text{Me}_2\text{pz})_3\text{CH}\}]\text{OTos}\cdot\text{CHCl}_3$ (**8d**· CHCl_3). The ellipsoids are shown with a probability of 30%. Hydrogen atoms are omitted for clarity. Selected structural parameters (distances in Å, angles in °): Pt–C1 2.050(3), Pt–C3 2.040(3), Pt–C21 1.979(3), Pt–N2 2.220(2), Pt–N4 2.223(2), Pt–N6 2.106(2); C1–Pt–C3 95.7(1), C1–Pt–C21 92.0(1), C3–Pt–C21 87.4(1), C1–Pt–N4 90.33(9), C1–Pt–N6 93.1(1), C3–Pt–N2 91.3(1), C3–Pt–N6 91.3(1), C21–Pt–N2 93.2(1), C21–Pt–N4 95.0(1), N2–Pt–N4 82.49(8), N2–Pt–N6 81.88(8), N4–Pt–N6 85.77(8), C1–Pt–N2 171.47(9), C3–Pt–N4 173.4(1), C21–Pt–N6 174.9(1), C21–C22 1.182(4), Pt–C21–C22 176.5(3), C21–C22–C23 178.4(4).

atom.^[27] The Pt–N bonds *trans* to the acetyl ligands [2.208(3)–2.247(3) Å] are significantly longer than those *trans* to the alkynyl ligands [2.100(3)/2.106(2) Å], thus indicating a higher *trans* influence of the acetyl ligands than the alkynyl ligands. The alkynyl fragments in both structures are slightly bent [Pt–C21–C21/C21–C22–Si 177.7(4)/174(4)[°] (**8a**), Pt–C21–C21/C21–C22–C23 176.5(3)/178.4(4)[°] (**8d**)], and the lengths of the carbon–carbon triple bonds

[1.180(6)/1.182(4) Å] are comparable with other ones found in platinum(IV) complexes with alkynyl ligands.^[32]

Conclusion

Within this work, the synthesis, reactivity, and dynamics of diacetylplatinum(II) and -platinum(IV) complexes bearing κ^2 - and κ^3 -bonded tris(pyrazolyl)- and tris(3,5-dimethylpyrazolyl)methane ligands are described. With particular regard to the different substitution patterns of these ligands, and in comparison with the corresponding isoelectronic tris(pyrazolyl)borate ligands,^[3] the following conclusions can be drawn:

(1) Reactions of the platinum-β diketone **1** with $(3,5-\text{R}_2\text{pz})_3\text{CH}$ ($\text{R} = \text{H}, \text{Me}$) followed by the addition of bases afforded neutral diacetylplatinum(II) complexes **4** with κ^2 -bonded tris(pyrazolyl)methane ligands (Scheme 2). Intermediates are thermally extraordinarily labile cationic hydridoplatinum(IV) complexes **3**. In contrast, the corresponding hydrido complexes (type **I** in Scheme 1) bearing the anionic isoelectronic scorpionate ligands $\{[\text{Pt}(\text{COMe})_2\text{H}\{(3,5-\text{R}_2\text{pz})_3\text{BH}\}]\}$, $\text{R} = \text{H}, \text{Me}\}$ proved to be thermally stable up to 150 °C.^[3] The same trend was found for the stability of the diacetylplatinum(II) complexes in solution $\{[\text{Pt}(\text{COMe})_2\{(3,5-\text{R}_2\text{pz})_3\text{CH}\}]\}$ (**4a/b**) < $\text{K}[\text{Pt}(\text{COMe})_2\{(3,5-\text{R}_2\text{pz})_3\text{BH}\}]\}$ (**II**), $\text{R} = \text{H}, \text{Me}\}$.

(2) Whereas the tris(pyrazolyl)borates were found to undergo facile ligand-substitution reactions with $[\text{Pt}(\text{COMe})_2(\text{NH}_2\text{Bn})_2]$ (**2**) to form type **II** complexes (Scheme 1), no such reactions proceeded with the tris(pyrazolyl)methanes (Scheme 2, path c). This indicates a higher donor ability of the anionic borate ligands than the neutral tris(pyrazolyl)methane ligands, as expected.

(3) As established by NMR spectroscopic experiments and DFT calculations, complexes **4a/b**, which bear κ^2 -coordinated tris(pyrazolyl)methane ligands, showed in solution a fluxional behavior, which involves decoordination of one pyrazolyl group to form T-shaped complexes with κ^1 -bonded ligands, rotation, and coordination of the original pendant pyrazolyl group. These dynamics are more pronounced in complex **4a**, which can be explained in terms of lower donor ability and/or less steric hindrance of the nonmethylated pyrazolyl groups. In accordance with this, in the corresponding type **II** complexes bearing the stronger coordinated tris(pyrazolyl)borate ligands, no such dynamics were observed at all.

(4) In the cationic complexes $[\text{Pt}(\text{COMe})_2\text{R}\{(\text{pz})_3\text{CH}\}]X$ ($\text{R}/\text{X} = \text{H}/\text{Cl}$, **3a**; Me/I , **7a**) with halides as counteranions between the backbone C–H protons and the halide anions, C–H···X hydrogen bonds were found both in the solid state and in solution. In contrast, the corresponding complexes **3b** and **7b** bearing the dimethyl-substituted ligand exhibited no such hydrogen bonds, which seems to be caused by steric shielding of the C–H group by the methyl groups (Figure 11).

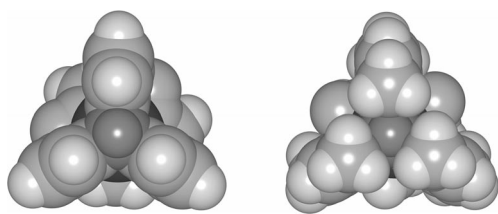


Figure 11. Space-filling model of the calculated cation in $[\text{Pt}(\text{COMe})_2\text{Me}\{(\text{pz})_3\text{CH}\}] \text{I}$ (**7a***, left) and $[\text{Pt}(\text{COMe})_2\text{Me}\{(3,5\text{-Me}_2\text{pz})_3\text{CH}\}] \text{I}$ (**7b***, right). The projection is shown along the C–H (dark gray) Pt (black) vector.

(5) The stability of diacetyl(alkynyl)platinum(IV) complexes, obtained by oxidative addition of alkynyl iodine(III) reagents $[\text{IPh}(\text{C}\equiv\text{CR})]\text{X}$ ($\text{R} = \text{SiMe}_3$, Ph, $t\text{Bu}$, $i\text{Pr}$; $\text{X} = \text{OTf}$, OTos) to complexes **4a/b** (Scheme 5), depends on the type of the tris(pyrazolyl) ligand. The reaction course indicates that when starting from both complex **4a** and **4b**, the respective alkynylplatinum(IV) complexes are formed, but only compounds **8** bearing the dimethyl-substituted ligand can be isolated as stable products, whereas, in the other case, decomposition occurred during the isolation.

To sum up, the present study shows how subtle the chemistry of platina- β -diketones with potentially tridentately binding tris(pyrazolyl)methane ligands, relative to tris(pyrazolyl)borate ligands, is dependent both on the total charge of these ligands (neutral methanes versus anionic borates) and on the substitution pattern of the pyrazolyl groups (pz versus 3,5-Me₂pz), which can be traced back to differences in electronic and steric effects.

Experimental Section

General Comments: All reactions were performed in an argon atmosphere using the standard Schlenk techniques. Solvents were dried (diethyl ether and THF over Na/benzophenone; CH_2Cl_2 over CaH_2 ; acetone over phosphorus pentoxide followed by molecular sieves (4 Å); methanol over magnesium methoxide) and distilled prior to use. If not otherwise stated, NMR spectra were recorded at 27 °C with Varian Gemini 200, VXR 400, and Unity 500 spectrometers. Chemical shifts are relative to solvent signals (CDCl_3 , $\delta_{\text{H}} = 7.24$ ppm, $\delta_{\text{C}} = 77.0$ ppm; CD_2Cl_2 , $\delta_{\text{H}} = 5.32$ ppm, $\delta_{\text{C}} = 53.8$ ppm; CD_3OD ($\delta_{\text{H}} = 3.31$ ppm, $\delta_{\text{C}} = 49.0$ ppm) as internal references; $\delta^{19}\text{Pt}$) is referenced to $\text{Na}_2[\text{PtCl}_6]$; $\delta^{19}\text{F}$) is relative to external CCl_4F . If necessary, 2D NMR spectroscopic techniques (H,H C,H COSY, HMBC, and NOESY) were used to assign the signals in ¹H and ¹³C NMR spectra. Temperature calibration for variable-temperature measurements was performed by using $\text{CH}_3\text{OH}/\text{CD}_3\text{OD}$ ($T < 282$ K)^[33] and CD_3OD ($T \geq 282$ K).^[34] IR spectra were recorded with a Bruker Tensor 28 spectrometer with a platinum ATR unit. The high-resolution ESI mass spectra were obtained with a Bruker Apex III Fourier transform ion cyclotron resonance (FT-ICR) mass spectrometer (Bruker Daltonics) equipped with an infinity cell, a 7.0 T superconducting magnet (Bruker), an rf-only hexapole ion guide, and an external APOLLO electrospray ion source (Agilent, off-axis spray). The sample solutions were introduced continuously with a syringe pump at a flow rate of 120 $\mu\text{L h}^{-1}$. Complexes $[\text{Pt}_2\{(\text{COMe})_2\}_2(\mu\text{-Cl})_2]$ (**1**)^[2] and $[\text{Pt}(\text{COMe})_2(\text{NH}_2\text{Bn})_2]$ (**2**),^[5] ligands (pz)₃CH and (3,5-Me₂pz)₃CH,^[8] as well as the alkynyl iodonium compounds $[\text{IPh}(\text{C}\equiv\text{CR})]\text{X}$

($\text{R} = \text{SiMe}_3$, Ph, $\text{X} = \text{OTf}$; $\text{R} = t\text{Bu}$, $i\text{Pr}$, $\text{X} = \text{OTos}$)^[35] were prepared according to literature methods.

Synthesis of $[\text{Pt}(\text{COMe})_2\text{H}\{(\text{pz})_3\text{CH}\}] \text{Cl}$ (3a**) and $[\text{Pt}(\text{COMe})_2\text{H}\{(3,5\text{-Me}_2\text{pz})_3\text{CH}\}] \text{Cl}$ (**3b**) at NMR Spectroscopy Scale:** At -78 °C in an NMR spectroscopy tube, **1** (32 mg, 0.05 mmol) and the respective ligand [(pz)₃CH, (3,5-Me₂pz)₃CH; 0.10 mmol] were dissolved in CD_2Cl_2 (1 mL). After 1 h, the NMR spectra of the henceforth colorless solutions were recorded, whereby it should be noted that the NMR spectroscopic tubes were kept at -78 °C at all times.

[(Pt(COMe)2H{pz}3CH)]Cl (3a**):** ¹H NMR (500 MHz, CD_2Cl_2 , -80 °C): $\delta = -17.98$ (s + d, $^1J_{\text{Pt},\text{H}} = 1637.2$ Hz, 1 H, Pt–H), 2.71 (s, 6 H, COCH_3), 6.46 (m, 2 H, $H^{4/4'}$ pz), 6.53 (m, 1 H, H^9 pz), 7.83 (m, 2 H, $H^{3/3'}$ pz), 8.18 (s, 1 H, H^8 pz), 8.70 (m, 1 H, H^{10} pz), 8.82 (m, 2 H, $H^{5/5'}$ pz), 12.39 [s, 1 H, (pz)₃C–H] ppm. ¹³C NMR (125 MHz, CD_2Cl_2 , -80 °C): $\delta = 44.7$ (s + d, $^2J_{\text{Pt},\text{C}} = 257.1$ Hz, COCH_3), 74.1 [s, (pz)₃C–H], 107.3 (s, C^4 pz), 107.7 (s, $C^{4/4'}$ pz), 133.3 (s, C^{10} pz), 134.1 (s, $C^{5/5'}$ pz), 142.0 (s, C^8 pz), 143.5 (s, $C^{3/3'}$ pz), 189.0 (s, COCH_3) ppm. (Here and in the following, pyrazolyl rings are numbered consecutively 1–5 and 6–10; for chemically equivalent nuclei primed numbers are used.)

[(Pt(COMe)2H{(3,5-Me2pz)}3CH)]Cl (3b**):** ¹H NMR (500 MHz, CD_2Cl_2 , -80 °C): $\delta = -18.54$ (s + d, $^1J_{\text{Pt},\text{H}} = 1619.7$ Hz, 1 H, Pt–H), 1.97 (s, 3 H, $C^8\text{--CH}_3$ pz), 2.11 (s, 6 H, $C^{3/3'}\text{--CH}_3$ pz), 2.49 (s, 6 H, COCH_3), 2.70 (s, 6 H, $C^{5/5'}\text{--CH}_3$ pz), 2.76 (s, 3 H, $C^{10}\text{--CH}_3$ pz), 6.18 (s, 2 H, $H^{4/4'}$ pz), 6.30 (s, 1 H, H^9 pz), 7.97 [s, 1 H, (Me₂pz)₃O–H] ppm. ¹³C NMR (125 MHz, CD_2Cl_2 , -80 °C): $\delta = 11.5$ (s, $C^{5/5'}\text{--CH}_3$ pz), 11.5 (s, $C^{10}\text{--CH}_3$ pz), 14.4 (s, $C^{3/3'}\text{--CH}_3$ + $C^8\text{--CH}_3$ pz), 40.6 (s + d, $^2J_{\text{Pt},\text{C}} = 209.3$ Hz, COCH_3), 69.0 [s, (Me₂pz)₃CH], 108.0 (s, $C^{4/4'}$ pz), 108.5 (s, C^9 pz), 142.4 (s, C^{10} pz), 142.9 (s, $C^{5/5'}$ pz), 152.4 (s, C^8 pz), 153.2 (s, $C^{3/3'}$ pz), 192.3 (s, COCH_3) ppm.

[(Pt(COMe)2{(pz)}3CH)] (4a**):** A solution of tris(pyrazolyl)methane (190 mg, 0.89 mmol) in dichloromethane (5 mL) was added dropwise at -78 °C to a suspension of **1** (276 mg, 0.43 mmol) in dichloromethane (15 mL). The reaction mixture was stirred for 30 min at this temperature to result in a clear and colorless solution. Then NEt_3 (146 mg, 1.4 mmol) was added. After stirring for an additional 15 min, the reaction mixture was warmed to room temperature and stirred for a further 30 min as a white solid precipitated. The volume of the suspension was reduced to approximately 10 mL. The solid was filtered off, washed with acetone (3 × 1 mL), and dried under vacuum. Yield 350 mg (81%). HRMS (ESI): m/z calcd. for $[\text{C}_{14}\text{H}_{17}\text{O}_2\text{N}_2\text{Pt}]^+$ 496.10552; found 496.10587 [$\text{M} + \text{H}]^+$. ¹H NMR (500 MHz, CD_3OD , 23 °C): $\delta = 2.08$ (s, 6 H, COCH_3), 6.62 (s, 3 H, $H^{4/4'}$ pz), 7.76 (s, 3 H, $H^{3/3'}$ pz), 8.25 [br. s, 3 H, $H^{5/5'}$ pz], 9.14 [s, 1 H, (pz)₃C–H] ppm. ¹H NMR (500 MHz, CD_3OD , -73 °C): $\delta = 2.05$ (s, 6 H, COCH_3), 6.59 (s, 1 H, H^9 pz), 6.73 (s, 1 H, $H^{4/4'}$ pz), 7.76 (s, 1 H, H^8 pz), 7.81 (s, 2 H, $H^{3/3'}$ pz), 7.87 (s, 1 H, H^{10} pz), 8.52 (s, 2 H, $H^{10/10'}$ pz), 9.31 [s, 1 H, (pz)₃C–H] ppm. ¹³C NMR (50 MHz, CD_3OD , 27 °C): $\delta = 43.8$ (s, COCH_3), 81.6 [s, (pz)₃C–H], 108.8 (s, $C^{4/4'}$ pz), 135.0 [br. s, $C^{5/5'}$ pz], 145.2 [br. s, $C^{3/3'}$ pz] 232.8 (s, COCH_3) ppm. ¹³C NMR (50 MHz, CD_3OD , -73 °C): $\delta = 44.0$ (s, COCH_3), 81.2 [s, (pz)₃C–H], 108.0 (s, C^9 pz), 109.3 (s, $C^{4/4'}$ pz), 131.8 (s, C^{10} pz), 137.2 (s, $C^{5/5'}$ pz), 143.1 (s, C^8 pz), 146.2 (s, $C^{3/3'}$ pz), 232.8 (s, COCH_3) ppm. ¹⁹⁵Pt NMR (107 MHz, CD_3OD , 27 °C): $\delta = -3138.6$ (s) ppm. IR: $\nu = 1623$ [v(CO)], 1573 [v(CO)] cm^{-1} .

[(Pt(COMe)2{(3,5-Me2pz)}3CH)] (4b**):** At -78 °C, a solution of tris(3,5-dimethylpyrazolyl)methane (245 mg, 0.82 mmol) in dichloromethane (5 mL) was added dropwise to a suspension of **1** (254 mg, 0.40 mmol) in dichloromethane (8 mL). After stirring for 30 min at this temperature, the clear and colorless solution was

warmed to about -20 °C and an aqueous solution of NaOH (800 mg in 30 mL) was added. The reaction mixture was stirred vigorously for a further 10 min at this temperature. The phases were separated quickly, and the aqueous phase was extracted with dichloromethane (2 × 10 mL). The combined organic extracts were dried with Na₂SO₄. The solvent was reduced to approximately 3 mL, and diethyl ether (20 mL) was added. The precipitation obtained was filtered off, washed with diethyl ether (2 × 2 mL), and dried under vacuum over P₄O₁₀. Yield 308 mg (66%). HRMS (ESI): *m/z* calcd. for [C₂₀H₂₉O₂N₆Pt]⁺ 580.19942; found 580.19954 [M + H]⁺. ¹H NMR (500 MHz, CD₃OD, 54 °C): δ = 1.85 [br. s, 3 H, C¹⁰-CH₃], 1.90 (s, 6 H, COCH₃), 2.15 (s, 9 H, C^{3/3'/13'}-CH₃), 2.55 [br. s, 6 H, C^{5/5'}-CH₃], 6.17 (s, 3 H, H^{4/4'/4''} pz), 8.34 [s, (Me₂pz)₃C-H] ppm. ¹H NMR (500 MHz, CD₃OD, 22 °C): δ = 1.84 (s, 3 H, C¹⁰-CH₃), 1.90 (s, 6 H, COCH₃), 2.13 (s, 6 H, C^{3/3'}-CH₃), 2.19 (s, 3 H, C⁸-CH₃), 2.56 (s, 6 H, C^{5/5'}-CH₃), 6.19 (s, 1 H, H⁹ pz), 6.20 (s, 2 H, H^{4/4'} pz), 8.47 [s, (Me₂pz)₃C-H] ppm. ¹H NMR (500 MHz, CD₃OD, -73 °C): δ = 1.81 (s, 3 H, C¹⁰-CH₃), 1.90 (s, 6 H, COCH₃), 2.11 (s, 6 H, C^{3/3'}-CH₃), 2.42 (s, 3 H, C⁸-CH₃), 2.60 (s, 6 H, C^{5/5'}-CH₃), 6.29 (s, 2 H, H^{4/4'} pz), 6.32 (s, 1 H, H⁹ pz), 8.84 [s, (Me₂pz)₃C-H] ppm. ¹³C NMR (125 MHz, CD₃OD, 53 °C): δ = 11.4 [(s, C^{5/5'}-CH₃ pz], 13.6 [br. s, C⁸-CH₃ pz], 14.5 [br. s, C^{3/3'}-CH₃ pz], 43.2 (s, COCH₃), 76.3 [s, (Me₂pz)₃CH], 109.4 [br. s, C^{4/4'} pz], 110.8 [br. s, C⁹ pz], 143.4 [br. s, C¹⁰ pz], 145.6 (s, C^{5/5'} pz), 150.5 [br. s, C⁸ pz], 155.9 [br. s, C^{3/3'} pz], 232.8 (s, COCH₃) ppm. ¹³C NMR (125 MHz, CD₃OD, 27 °C): δ = 11.3 [br. s, C¹⁰-CH₃ pz], 11.4 [br. s, C^{5/5'}-CH₃ pz], 13.6 [br. s, C⁸-CH₃ pz], 14.5 [br. s, C^{3/3'}-CH₃ pz], 43.3 (s, COCH₃), 76.3 [s, (Me₂pz)₃CH], 109.4 [br. s, C^{4/4'} pz], 110.9 [br. s, C⁹ pz], 143.3 [br. s, C¹⁰ pz], 145.7 [br. s, C^{5/5'} pz], 150.5 [br. s, C⁸ pz], 155.9 [br. s, C^{3/3'} pz], 233.6 (s, COCH₃) ppm. ¹³C NMR (125 MHz, CD₃OD, -73 °C): δ = 11.4 (s, C¹⁰-CH₃ pz), 11.5 (s, C^{5/5'}-CH₃ pz), 13.6 (s, C⁸-CH₃ pz), 14.5 (s, C^{3/3'}-CH₃ pz), 43.8 (s, COCH₃), 76.3 [s, (Me₂pz)₃CH], 108.0 (s, C^{4/4'} pz), 110.9 (s, C⁹ pz), 143.1 (s, C¹⁰ pz), 146.1 (s, C^{5/5'} pz), 150.4 (s, C⁸ pz), 155.7 (s, C^{3/3'} pz), 235.7 (s, COCH₃) ppm. ¹⁹⁵Pt NMR (86 MHz, CD₃OD, 27 °C): δ = -3486.3 (s) ppm. IR: ν = 1641 [v(CO)], 1600 [v(CO)] cm⁻¹.

[Pt(COMe)₂H{(pz)₃CH}]OTf (5a) and [Pt(COMe)₂H{(3,5-Me₂pz)₃CH}]OTf (5b): At -78 °C trifluoromethanesulfonic acid (33 mg, 0.22 mmol) was added to a suspension of **4a** (99 mg, 0.20 mmol) and **4b** (120 mg, 0.20 mmol), respectively, in THF (20 mL). The reaction mixture was warmed to room temperature and stirred for about 20 min until a clear colorless solution was obtained. The volume of the solvent was reduced to 3 mL, and diethyl ether (10 mL) was added. The white precipitate formed after 2 h at -6 °C was removed by filtration, washed with diethyl ether (2 × 5 mL), and dried under vacuum.

[Pt(COMe)₂H{(pz)₃CH}]OTf (5a): Yield 112 mg (87%). HRMS (ESI): *m/z* calcd. for [C₁₄H₁₆O₂N₆PtNa]⁺ 518.08747; found 518.08763 [M - H + Na]⁺. ¹H NMR (500 MHz, CD₂Cl₂): δ = -18.30 (s + d, ¹J_{Pt,H} = 1659.2 Hz, 1 H, Pt-H), 2.73 (s + d, ³J_{Pt,H} = 28.5 Hz, 6 H, COCH₃), 6.55 (m, 2 H, H^{4/4'} pz), 6.62 (m, 1 H, H⁹ pz), 7.87 (m, 2 H, H^{3/3'} pz), 8.26 (s, 1 H, H⁸ pz), 8.60 (m, 3 H, H^{5/5'} + H¹⁰ pz), 10.17 [s, 1 H, (pz)₃C-H] ppm. ¹³C NMR (125 MHz, CD₂Cl₂): δ = 44.2 (s + d, ²J_{Pt,C} = 263.9 Hz, COCH₃), 77.1 [s, (pz)₃C-H], 108.8 (s, C⁹ pz), 109.2 (s, C^{4/4'} pz), 121.1 (q, CF₃), 134.5 (s, C¹⁰ pz), 135.0 (s, C^{5/5'} pz), 143.9 (s, C⁸ pz), 145.0 (s + d, ²J_{Pt,C} = 18.5 Hz, C^{3/3'} pz), 186.7 (s, COCH₃) ppm. ¹⁹⁵Pt NMR (86 MHz, [D₆]acetone): δ = -1705.2 (s + d, ¹J_{Pt,H} = 1564.0 Hz) ppm. IR: ν = 2240 [v(PtH)], 1724 [v(CO)], 1678 [v(CO)] cm⁻¹.

[Pt(COMe)₂H{(3,5-Me₂pz)₃CH}]OTf (5b): Yield 127 mg (87%). HRMS (ESI): *m/z* calcd. for [C₂₀H₂₈O₂N₆PtNa]⁺ 602.18137; found

602.18172 [M - H + Na]⁺. ¹H NMR (500 MHz, CD₂Cl₂): δ = -18.73 (s + d, ¹J_{Pt,H} = 1636.7 Hz, 1 H, Pt-H), 2.06 (s, 3 H, C⁸-CH₃ pz), 2.19 (s, 6 H, C^{3/3'}-CH₃ pz), 2.58 (s + d, ³J_{Pt,H} = 17.7 Hz, 6 H, COCH₃), 2.68 (s, 6 H, C^{5/5'}-CH₃ pz), 2.75 (s, 3 H, C¹⁰-CH₃ pz), 6.18 (s, 2 H, H^{4/4'} pz), 6.30 (s, 1 H, H⁹ pz), 8.08 [s, 1 H, (Me₂pz)₃C-H] ppm. ¹³C NMR (100 MHz, [D₆]acetone): δ = 11.6 (s, C^{5/5'}-CH₃ pz), 11.7 (s, C¹⁰-CH₃ pz), 14.9 (s, C⁸-CH₃ pz), 15.0 (s, C^{3/3'}-CH₃ pz), 41.3 (s + d, ²J_{Pt,C} = 222.0 Hz, COCH₃), 70.3 [s, (Me₂pz)₃CH], 109.2 (s, C^{4/4'} pz), 109.8 (s, C⁹ pz), 122.5 (q, CF₃), 143.4 (s, C¹⁰ pz), 144.0 (s, C^{5/5'} pz), 154.0 (s, C⁸ pz), 154.6 (s, C^{3/3'} pz), 190.5 (s, COCH₃) ppm. ¹⁹F NMR (376 MHz, [D₆]acetone): δ = -78.2 (s) ppm. ¹⁹⁵Pt NMR (86 MHz, [D₆]acetone): δ = -1805.0 (s + d, ¹J_{Pt,H} = 1527.1 Hz) ppm. IR: ν = 2256 [v(PtH)], 1699 [v(CO)], 1680 [v(CO)] cm⁻¹.

[Pt(COMe)₂D{(pz)₃CH}]OTf (5c) and [Pt(COMe)₂D{(3,5-Me₂pz)₃CH}]OTf (5d) by H/D Exchange: At room temperature, a solution of **5a** (30 mg, 0.045 mmol) or **5b** (30 mg, 0.040 mmol) in CD₃OD (1 mL) was stirred for 10 min. Then the solvent was removed under vacuum and the residue was dissolved in dichloromethane. Complex **5c**: ²H NMR (614 MHz, CH₂Cl₂): δ = -18.07 (s) ppm. Complex **5d**: ²H NMR (614 MHz, CH₂Cl₂): δ = -18.53 (s) ppm.

[Pt(COMe)₂Me{(pz)₃CH}]OTf (6a) and [Pt(COMe)₂Me{(3,5-Me₂pz)₃CH}]OTf (6b): At >20 °C, methyl trifluoromethanesulfonate (30 mg, 0.18 mmol) was added to a suspension of **4a** (85 mg, 0.17 mmol) or **4b** (99 mg, 0.17 mmol) in THF (15 mL). After warming to room temperature, a clear, pale yellow solution was obtained within 15 min. The reaction mixture was concentrated under reduced pressure to approximately 3 mL. Then, diethyl ether (10 mL) was added. The resulting pale yellow solid was removed by filtration, washed with diethyl ether (3 × 5 mL), and dried under vacuum.

Complex 6a: Yield 77 mg (69%). HRMS (ESI): *m/z* calcd. for [C₁₅H₁₉O₂N₆Pt]⁺ 510.12117; found 510.12194 [M]⁺. ¹H NMR (400 MHz, CDCl₃): δ = 1.61 (s + d, ²J_{Pt,H} = 76.3 Hz, 3 H, Pt-CH₃), 2.48 (s + d, ³J_{Pt,H} = 15.4 Hz, 6 H, COCH₃), 6.54 (m, 2 H, H^{4/4'} pz), 6.59 (m, 1 H, H⁹ pz), 7.83 (m, 2 H, H^{3/3'} pz), 8.11 (s, 1 H, H⁸ pz), 8.65 (m, 3 H, H^{5/5'} pz), 8.68 (m, 1 H, H¹⁰ pz), 10.30 [s, 1 H, (pz)₃C-H] ppm. ¹³C NMR (125 MHz, CDCl₃): δ = -3.6 (s + d, ¹J_{Pt,C} = 748.9 Hz, Pt-CH₃), 35.8 (s + d, ²J_{Pt,C} = 200.7 Hz, COCH₃), 76.6 [s, (pz)₃C-H], 108.8 (s, C^{4/4'} pz), 108.9 (s, C⁹ pz), 120.5 (q, CF₃), 134.8 (s, C¹⁰ pz), 134.9 (s, C^{5/5'} pz), 142.3 (s + d, ²J_{Pt,C} = 10.4 Hz, C^{3/3'} pz), 143.4 (s + d, ²J_{Pt,C} = 12.3 Hz, C⁸ pz), 189.5 (s + d, ¹J_{Pt,C} = 939.0 Hz, COCH₃) ppm. ¹⁹F NMR (376 MHz, CDCl₃): δ = -78.3 (s) ppm. ¹⁹⁵Pt NMR (107 MHz, CDCl₃): δ = -1495.5 (s) ppm. IR: ν = 1719 [v(CO)], 1669 [v(CO)] cm⁻¹.

Complex 6b: Yield 78 mg (62%). HRMS (ESI): *m/z* calcd. for [C₂₁H₃₁O₂N₆Pt]⁺ 594.21507; found 594.21538 [M]⁺. ¹H NMR (400 MHz, CDCl₃): δ = 1.61 (s + d, ²J_{Pt,H} = 77.7 Hz, 6 H, Pt-CH₃), 1.95 (s, 3 H, C⁸-CH₃ pz), 2.17 (s, 6 H, C^{3/3'}-CH₃ pz), 2.31 (s + d, ³J_{Pt,H} = 8.9 Hz, 6 H, COCH₃), 2.75 (s, 6 H, C^{5/5'}-CH₃ pz), 2.79 (s, 3 H, C¹⁰-CH₃ pz), 6.14 (s, 2 H, H^{4/4'} pz), 6.22 (s, 1 H, H⁹ pz), 8.20 [s, 1 H, (Me₂pz)₃C-H] ppm. ¹³C NMR (100 MHz, CDCl₃): δ = -3.0 (s + d, ¹J_{Pt,C} = 747.5 Hz, Pt-CH₃), 11.6 (s, C^{5/5'}-CH₃ pz), 11.8 (s, C¹⁰-CH₃ pz), 13.7 (s, C^{3/3'}-CH₃ pz), 15.1 (s + d, ³J_{Pt,C} = 10.9 Hz, C⁸-CH₃ pz), 34.1 (s + d, ²J_{Pt,C} = 181.5 Hz, COCH₃), 70.1 [s, (Me₂pz)₃CH], 109.6 (s, C⁹ pz), 109.8 (s, C^{4/4'} pz), 120.8 (q, CF₃), 143.6 (s, C^{5/5'} pz), 143.7 (s, C¹⁰ pz), 152.3 (s + d, ³J_{Pt,C} = 13.8 Hz, C⁸ pz), 153.9 (s + d, ³J_{Pt,C} = 10.7 Hz, C^{3/3'} pz), 193.3 (s + d, ¹J_{Pt,C} = 944.4 Hz, COCH₃) ppm. ¹⁹F NMR (376 MHz, CDCl₃): δ = -78.3 (s) ppm. ¹⁹⁵Pt NMR (107 MHz, CDCl₃): δ = -1805.0 (s) ppm.

CDCl_3): $\delta = -1584.4$ (s) ppm. IR: $\nu = 1696$ [v(CO)], 1674 [v(CO)] cm^{-1} .

[Pt(COMe)₂Me{(pz)₃CH}]I (**7a**) and **[Pt(COMe)₂Me{(3,5-Me₂pz)₃CH}]I** (**7b**): At room temperature, methyl iodide (68 mg, 0.20 mmol) was added to a suspension of **4a** (100 mg, 0.20 mmol) or to a solution of **4b** (100 mg, 0.17 mmol) in dichloromethane (15 mL), and the mixture was stirred for 30 min until a clear, pale yellow solution was obtained. The solution was concentrated under reduced pressure almost to dryness. The residue was dissolved in dichloromethane (2 mL), and diethyl ether (10 mL) was added. The white precipitate formed was removed by filtration, washed with diethyl ether (3×5 mL), and dried under vacuum.

Complex 7a: Yield 103 mg (81%). HRMS (ESI): m/z calcd. for $[\text{C}_{15}\text{H}_{19}\text{O}_2\text{N}_6\text{Pt}]^+$ 510.12117; found 510.12190 [M]⁺. ¹H NMR (500 MHz, CDCl_3): $\delta = 1.61$ (s + d, ${}^2J_{\text{Pt},\text{H}} = 76.3$ Hz, 3 H, Pt- CH_3), 2.47 (s + d, ${}^3J_{\text{Pt},\text{H}} = 14.7$ Hz, 6 H, COCH_3), 6.54 (m, 2 H, $\text{H}^{4/4'}$ pz), 6.59 (m, 1 H, H^9 pz), 7.92 (m, 2 H, $\text{H}^{3/3'}$ pz), 8.07 (s, 1 H, H^8 pz), 9.10 (m, 3 H, $\text{H}^{5/5'} + \text{H}^{10}$ pz), 12.22 [s, 1 H, {(pz)₃C-H}] ppm. ¹³C NMR (125 MHz, CDCl_3): $\delta = -3.5$ (s + d, ${}^1J_{\text{Pt},\text{C}} = 752.4$ Hz, Pt- CH_3), 35.8 (s + d, ${}^2J_{\text{Pt},\text{C}} = 200.7$ Hz, COCH_3), 74.2 [s, {(pz)₃C-H}], 108.4 (s, $\text{C}^{4/4'}$ pz), 108.5 (s, C^9 pz), 134.1 (s, C^{10} pz), 134.2 (s, $\text{C}^{5/5'}$ pz), 141.9 (s + d, ${}^2J_{\text{Pt},\text{C}} = 10.0$ Hz, $\text{C}^{3/3'}$ pz), 142.9 (s + d, ${}^2J_{\text{Pt},\text{C}} = 12.1$ Hz, C^8 pz), 189.2 (s + d, ${}^1J_{\text{Pt},\text{C}} = 940.0$ Hz, COCH_3) ppm. ¹⁹⁵Pt NMR (107 MHz, CDCl_3): $\delta = -1491.2$ (s) ppm.

Complex 7b: Yield 110 mg (90%). HRMS (ESI): m/z calcd. for $[\text{C}_{21}\text{H}_{31}\text{O}_2\text{N}_6\text{Pt}]^+$ 594.21507; found 594.21516 [M]⁺. ¹H NMR (500 MHz, CDCl_3): $\delta = 1.60$ (s + d, ${}^2J_{\text{Pt},\text{H}} = 77.7$ Hz, 6 H, Pt- CH_3), 1.95 (s, 3 H, C^8-CH_3 pz), 2.16 (s, 6 H, $\text{C}^{3/3'}-\text{CH}_3$ pz), 2.31 (s + d, ${}^3J_{\text{Pt},\text{H}} = 7.7$ Hz, 6 H, COCH_3), 2.89 (s, 6 H, $\text{C}^{5/5'}-\text{CH}_3$ pz), 2.93 (s, 3 H, $\text{C}^{10}-\text{CH}_3$ pz), 6.18 (s, 2 H, $\text{H}^{4/4'}$ pz), 6.26 (s, 1 H, H^9 pz), 8.18 [s, 1 H, {(Me₂pz)₃C-H}] ppm. ¹³C NMR (100 MHz, CDCl_3): $\delta = -3.0$ (s + d, ${}^1J_{\text{Pt},\text{C}} = 748.1$ Hz, Pt- CH_3), 13.7 (s, $\text{C}^{3/3'}-\text{CH}_3$ pz), 13.8 (s, $\text{C}^{5/5'}-\text{CH}_3$ pz), 13.9 (s, $\text{C}^{10}-\text{CH}_3$ pz), 15.1 (s, C^8-CH_3 pz), 34.2 (s + d, ${}^2J_{\text{Pt},\text{C}} = 184.4$ Hz, COCH_3), 70.0 [s, {(Me₂pz)₃CH}], 109.7 (s, C^9 pz), 110.0 (s, $\text{C}^{4/4'}$ pz), 143.4 (s, $\text{C}^{5/5'}$ pz), 143.5 (s, C^{10} pz), 152.3 (s, C^8 pz), 153.9 (s, $\text{C}^{3/3'}$ pz), 193.2 (s + d, ${}^1J_{\text{Pt},\text{C}} = 944.7$ Hz, COCH_3) ppm. ¹⁹⁵Pt NMR (107 MHz, CDCl_3): $\delta = -1583.2$ (s) ppm. IR: $\nu = 1705$ [v(CO)], 1676 [v(CO)] cm^{-1} .

Diacetyl(alkynyl)platinum(IV) Complexes 8: At -78°C , **[IPh(C≡CR)]X** (SiMe₃/OTf, Ph/OTf, tBu/OTos, iPr/OTos; 0.12 mmol) in dichloromethane (3 mL) was added to a colorless solution of **[Pt(COMe)₂{(3,5-Me₂pz)₃CH}]** (70 mg, 0.12 mmol) in dichloromethane (5 mL). The reaction mixture turned red, and after stirring for 10 min at this temperature, was warmed to room temperature, thereby resulting in a colorless solution. After stirring for an additional 30 min, the solvent was reduced to approximately 1 mL, and diethyl ether (6 mL) was added. The colorless precipitate obtained was removed by filtration, washed with diethyl ether (2×2 mL), and dried under vacuum.

[Pt(COMe)₂(C≡CSiMe₃) $\{(3,5\text{-Me}_2\text{pz})_3\text{CH}\}]$ OTf (**8a**): Yield 73 mg (73%). HRMS (ESI): m/z calcd. for $[\text{C}_{25}\text{H}_{37}\text{O}_2\text{N}_6\text{SiPt}]^+$ 676.23895; found 676.23752 [M]⁺. ¹H NMR (400 MHz, CDCl_3): $\delta = 0.12$ [s, 9 H, Si(CH₃)₃], 1.93 (s, 3 H, C^8-CH_3 pz), 2.38 (s, 6 H, $\text{C}^{3/3'}-\text{CH}_3$ pz), 2.72 (s, 6 H, $\text{C}^{5/5'}-\text{CH}_3$ pz), 2.75 (s + d, ${}^3J_{\text{Pt},\text{H}} = 13.6$ Hz, 6 H, COCH_3), 2.80 (s, 3 H, $\text{C}^{10}-\text{CH}_3$ pz), 6.12 (s, 2 H, $\text{H}^{4/4'}$ pz), 6.22 (s + d, ${}^4J_{\text{Pt},\text{H}} = 10.4$ Hz, 1 H, H^9 pz), 8.18 [s, 1 H, {(Me₂pz)₃C-H}] ppm. ¹³C NMR (100 MHz, CDCl_3): $\delta = 0.34$ [s, Si(CH₃)₃], 11.3 (s, $\text{C}^{5/5'}-\text{CH}_3$ pz), 11.8 (s, $\text{C}^{10}-\text{CH}_3$ pz), 14.0 (s + d, ${}^4J_{\text{Pt},\text{C}} = 8.2$ Hz, $\text{C}^{3/3'}-\text{CH}_3$ pz), 14.9 (s, ${}^4J_{\text{Pt},\text{C}} = 13.2$ Hz, C^8-CH_3 pz), 35.9 (s + d, ${}^2J_{\text{Pt},\text{C}} = 187.1$ Hz, COCH_3), 69.8 [s, {(Me₂pz)₃CH}], 80.6 (s, Pt-C≡CSiMe₃), 103.6 (s, Pt-C≡C-SiMe₃), 109.5 (s, $\text{C}^{4/4'}$ pz), 109.6

(s, C^9 pz), 120.6 (q, CF₃), 143.3 (s, $\text{C}^{5/5'}$ pz), 144.0 (s, C^{10} , pz), 152.8 (s, C^8 pz), 154.6 (s, $\text{C}^{3/3'}$ pz), 185.0 (s + d, ${}^1J_{\text{Pt},\text{C}} = 787.9$ Hz, COCH_3) ppm. ¹⁹F NMR (376 MHz, CDCl_3): $\delta = -78.3$ (s) ppm. ¹⁹⁵Pt NMR (107 MHz, CDCl_3): $\delta = -1366.5$ (s) ppm. IR: $\nu = 2092$ [v(C≡C)], 1725 [v(CO)], 1698 [v(CO)] cm^{-1} .

For Comparison, [IPh(C≡CSiMe₃)]OTf: (¹H NMR spectroscopic data are reported in the literature^[35]). ¹³C NMR (100 MHz, CDCl_3): $\delta = -0.9$ [s, Si(CH₃)₃], 44.0 (s, C≡CSiMe₃), 116.8 (C, i-C Ph), 119.7 (s, C≡CSiMe₃), 119.8 (q, CF₃), 132.5, 132.6, 133.9 (s, C-H Ph) ppm.

[Pt(COMe)₂(C≡CPh){(3,5-Me₂pz)₃CH}]OTf (**8b**): Yield 63 mg (61%). HRMS (ESI): m/z calcd. for $[\text{C}_{28}\text{H}_{33}\text{O}_2\text{N}_6\text{Pt}]^+$ 680.23072; found 680.23012 [M]⁺. ¹H NMR (400 MHz, CD_2Cl_2): $\delta = 0.12$ [s, 9 H, Si(CH₃)₃], 2.01 (s, 3 H, C^8-CH_3 pz), 2.47 (s, 6 H, $\text{C}^{3/3'}-\text{CH}_3$ pz), 2.69 (s, 6 H, $\text{C}^{5/5'}-\text{CH}_3$ pz), 2.77 (s, 3 H, $\text{C}^{10}-\text{CH}_3$ pz), 2.81 (s + d, ${}^3J_{\text{Pt},\text{H}} = 14.0$ Hz, 6 H, COCH_3), 6.20 (s, 2 H, $\text{H}^{4/4'}$ pz), 6.32 (s + d, ${}^4J_{\text{Pt},\text{H}} = 10.8$ Hz, 1 H, H^9 pz), 7.26–7.39 (m, 5 H, C₆H₅), 8.11 [s, 1 H, {(Me₂pz)₃C-H}] ppm. ¹³C NMR (100 MHz, CD_2Cl_2): $\delta = 11.6$ (s, $\text{C}^{5/5'}-\text{CH}_3$ pz), 12.0 (s, $\text{C}^{10}-\text{CH}_3$ pz), 14.4 (s + d, ${}^4J_{\text{Pt},\text{C}} = 7.9$ Hz, $\text{C}^{3/3'}-\text{CH}_3$ pz), 15.5 (s, ${}^4J_{\text{Pt},\text{C}} = 13.2$ Hz, C^8-CH_3 pz), 36.4 (s + d, ${}^2J_{\text{Pt},\text{C}} = 181.2$ Hz, COCH_3), 62.3 (s, Pt-C≡C-SiMe₃), 70.2 [s, {(Me₂pz)₃CH}], 97.2 (s, Pt-C≡C-SiMe₃), 110.0 (s, $\text{C}^{4/4'}$ pz), 110.2 (s, C^9 pz), 121.3 (q, CF₃), 125.9 (s, i-C Ph), 127.8 (s, p-C Ph), 128.6 (s, m-C Ph), 131.7 (s + d, ${}^4J_{\text{Pt},\text{C}} = 12.5$ Hz, o-C Ph), 143.3 (s, $\text{C}^{5/5'}$ pz), 144.0 (s, C^{10} , pz), 153.8 (s, C^8 pz), 155.3 (s, $\text{C}^{3/3'}$ pz), 185.1 (s + d, ${}^1J_{\text{Pt},\text{C}} = 780.2$ Hz, COCH_3) ppm. ¹⁹F NMR (376 MHz, CD_2Cl_2): $\delta = -18.9$ (s) ppm. ¹⁹⁵Pt NMR (107 MHz, CD_2Cl_2): $\delta = -1376.6$ (s) ppm. IR: $\nu = 2164$ [v(C≡C)], 1721 [v(CO)], 1698 [v(CO)] cm^{-1} .

For Comparison, [IPh(C≡CPh)]OTf: ¹³C NMR (100 MHz, CDCl_3): $\delta = 39.3$ (s, C≡CPh), 105.3 (s, C≡CPh), 119.1, 120.2 (C, i-C Ph), 119.9 (q, CF₃), 128.5, 130.9, 131.7, 131.9, 133.0, 133.9 (s, C-H Ph) ppm.

[Pt(COMe)₂(C≡CtBu){(3,5-Me₂pz)₃CH}]OTos (**8c**): Yield 80 mg (80%). HRMS (ESI): m/z calcd. for $[\text{C}_{26}\text{H}_{37}\text{O}_2\text{N}_6\text{Pt}]^+$ 660.26202; found 660.26148 [M]⁺. ¹H NMR (500 MHz, CDCl_3): $\delta = 1.20$ [s, 9 H, C(CH₃)₃], 1.90 (s, 3 H, C^8-CH_3 pz), 2.30 (s, 3 H, CH₃ OTos), 2.36 (s, 6 H, $\text{C}^{3/3'}-\text{CH}_3$ pz), 2.72 (s + d, ${}^3J_{\text{Pt},\text{H}} = 13.3$ Hz, 6 H, COCH_3), 2.79 (s, 6 H, $\text{C}^{5/5'}-\text{CH}_3$ pz), 2.87 (s, 3 H, $\text{C}^{10}-\text{CH}_3$ pz), 6.05 (s, 2 H, $\text{H}^{4/4'}$ pz), 6.14 (s, 1 H, H^9 pz), 7.09 (d, 2 H, C-H OTos), 7.75 (d, 2 H, C-H OTos), 8.29 [s, 1 H, {(Me₂pz)₃C-H}] ppm. ¹³C NMR (125 MHz, CDCl_3): $\delta = 11.8$ (s, $\text{C}^{5/5'}-\text{CH}_3$ pz), 12.2 (s, $\text{C}^{10}-\text{CH}_3$ pz), 14.1 (s, $\text{C}^{3/3'}-\text{CH}_3$ pz), 15.1 (s, C^8-CH_3 pz), 21.2 (s, CH₃ OTos), 29.3 (s + d, ${}^3J_{\text{Pt},\text{C}} = 23.6$ Hz, CMe₃), 31.5 [s, C(CH₃)₃], 36.0 (s + d, ${}^2J_{\text{Pt},\text{C}} = 186.1$ Hz, COCH_3), 46.5 (s + d, ${}^1J_{\text{Pt},\text{C}} = 1556.7$ Hz, Pt-C≡C-CMe₃), 70.2 [s, {(Me₂pz)₃CH}], 104.4 (s + d, ${}^2J_{\text{Pt},\text{C}} = 324.8$ Hz, Pt-C≡C-CMe₃), 109.4 (s, $\text{C}^{4/4'}$ pz), 109.5 (s, C^9 pz), 126.0 (s, C-H OTos), 128.4 (s, C-H OTos), 138.7 (s, C-SO₃ OTos), 144.0 (s, $\text{C}^{5/5'}$ pz), 144.3 (s, C-CH₃ OTos), 144.7 (s, C^{10} , pz), 152.7 (s, C^8 pz), 154.5 (s, $\text{C}^{3/3'}$ pz), 185.6 (s + d, ${}^1J_{\text{Pt},\text{C}} = 795.1$ Hz, COCH_3) ppm. ¹⁹⁵Pt NMR (107 MHz, CDCl_3): $\delta = -1380.9$ (s) ppm. IR: $\nu = 1727$ [v(CO)], 1711 [v(CO)] cm^{-1} .

For Comparison, [IPh(C≡CtBu)]OTos: ¹³C NMR (100 MHz, CDCl_3): $\delta = 21.3$ (s, CH₃ OTos), 27.6 (s, C≡CtBu), 29.6 (s, CMe₃), 30.1 [s, C(CH₃)₃], 116.8 (C, C≡CtBu), 119.7 (s, i-C Ph), 126.0, 128.7 (s, C-H OTos), 131.6, 131.8, 133.4 (s, C-H Ph), 140.2, 141.5 (s, i-C OTos) ppm.

[Pt(COMe)₂(C≡CiPr){(3,5-Me₂pz)₃CH}]OTos (**8d**): Yield 73 mg (73%). HRMS (ESI): m/z calcd. for $[\text{C}_{25}\text{H}_{35}\text{O}_2\text{N}_6\text{Pt}]^+$ 646.24637; found 646.24700 [M]⁺. ¹H NMR (400 MHz, CDCl_3): $\delta = 1.15$ [d, 7 H, CH(CH₃)₂], 1.91 (s, 3 H, C^8-CH_3 pz), 2.30 (s, 3 H, CH₃ OTos),

2.37 (s, 6 H, C^{3/3'}-CH₃ pz), 2.71 (s + d, ³J_{Pt,H} = 13.6 Hz, 6 H, COCH₃), 2.70–2.80 [m, 1 H, CH(Me)₂], 2.80 (s, 6 H, C^{5/5'}-CH₃ pz), 2.90 (s, 3 H, C¹⁰-CH₃ pz), 6.05 (s, 2 H, H^{4/4'} pz), 6.15 (s, 1 H, H⁹ pz), 7.10 (d, 2 H, C-H OTos), 7.75 (d, 2 H, C-H OTos), 8.32 [s, 1 H, (Me₂Pz)₃C-H] ppm. ¹³C NMR (100 MHz, CDCl₃): δ = 11.9 (s, C^{5/5'}-CH₃ pz), 12.5 (s, C¹⁰-CH₃ pz), 14.1 (s, ³J_{Pt,C} = 8.0 Hz, C^{3/3'}-CH₃ pz), 15.1 (s, ³J_{Pt,C} = 13.0 Hz, C⁸-CH₃ pz), 21.3 (s, CH₃ OTos), 29.3 [s + d, ³J_{Pt,C} = 24.1 Hz, CH(CH₃)₂], 23.7 [s, ⁴J_{Pt,C} = 12.1 Hz, CH(CH₃)₂], 36.0 (s + d, ²J_{Pt,C} = 184.9 Hz, COCH₃), 47.1 [s + d, ¹J_{Pt,C} = 1558.8 Hz, Pt-C≡C-CH(CH₃)₂], 70.3 [s, (Me₂Pz)₃CH], 104.4 [s + d, ²J_{Pt,C} = 324.8 Hz, Pt-C≡C-CH(CH₃)₂], 109.4 (s, C^{4/4'} pz), 109.6 (s, C⁹ pz), 126.1 (s, C-H OTos), 128.3 (s, C-H OTos), 138.6 (s, C-SO₃ OTos), 144.1 (s, C^{5/5'} pz), 144.5 (s, C-CH₃ OTos), 144.9 (s, C¹⁰, pz), 152.7 (s, ²J_{Pt,C} = 26.1 Hz, C⁸ pz), 154.5 (s, ³J_{Pt,C} = 8.0 Hz, C^{3/3'} pz), 185.6 (s + d, ¹J_{Pt,C} = 795.1 Hz, COCH₃] ppm. ¹⁹⁵Pt NMR (107 MHz, CDCl₃): δ = -1371.1 (s) ppm. IR: ν = 1727 [v(CO)], 1711 [v(CO)] cm⁻¹. IR: ν = 2050 [v(C≡C)], 1727 [v(CO)], 1711 [v(CO)] cm⁻¹.

For Comparison, [IPh(C≡CiPr)OTos]: ¹³C NMR (100 MHz, CDCl₃): δ = 21.3 (s, CH₃ OTos), 22.0 [s, CH(CH₃)₂], 22.4 [s, CH(CH₃)₂], 28.0 (s, C≡CiPr), 113.8 (C, C≡CiPr), 118.4 (s, i-C Ph), 126.0, 128.7 (s, C-H OTos), 131.7, 131.8, 133.5 (s, C-H Ph), 140.1, 141.6 (s, i-C OTos) ppm.

X-ray Crystallography: Data for X-ray diffraction analyses of single crystals were collected with a Stoe-IPDS 2T diffractometer at 200 K using Mo-K_α radiation ($\lambda = 0.71073 \text{ \AA}$, graphite monochromator). A summary of the crystallographic data, the data collection parameters, and the refinement parameters is given in Table 6. Absorption corrections were applied empirically with the PLATON program package [$T_{\min}/T_{\max} = 0.04/0.15$ (**4a**), 0.23/0.47 (**4b**), 0.10/0.17 (**7a**·CH₂Cl₂), 0.45/0.71 (**8a**·THF), 0.17/0.33 (**8d**·CHCl₃)].^[36] The structures were solved with direct methods using SHELXS-97^[37] and refined using full-matrix least-squares cycles against F^2

with SHELXL-97.^[38] All non-hydrogen atoms were refined with anisotropic displacement parameters and hydrogen atoms with isotropic ones. Hydrogen atoms were placed in calculated positions according to the riding model. In the structure of complex **8a**, DFIX, DANG, SIMU, and DELU instructions have been used for the refinement of the THF molecule as packing solvent.

Computational Details: DFT calculations were performed by the Gaussian 09 program package^[39] using the functional B3LYP.^[40] The 6-311++G(d,p) basis sets as implemented in Gaussian 09 were employed for main group atoms, whereas the relativistic pseudopotential of the Ahlrichs group and related basis functions of TZVPP quality were employed for the Pt atom.^[41] The appropriateness of the functional in combination with the basis sets and effective core potential used for reliable interpretation of structural and energetic aspects of related platinum complexes has been demonstrated.^[42] All systems were fully optimized without any symmetry restrictions. The resulting geometries were characterized as equilibrium structures and transition states, respectively, by the analysis of the force constants of normal vibrations. Solvent effects were considered according to Tomasi's polarized continuum model.^[43] The method was used as implemented in Gaussian 09,^[39] which is much more sophisticated than in previous Gaussian versions, especially because solvent effects are considered in each optimization step.

Associated Content: CIF files containing X-ray crystallographic data for **4a**, **4b**, **7a**·CH₂Cl₂, **8a**·THF, and **8d**·CHCl₃.

CCDC 913033 (**4a**), -913034 (**4b**), -913035 (**7a**·CH₂Cl₂), -913036 (**8a**·THF), -913037 (**8d**·CHCl₃) contain the supplementary crystallographic data for this paper. These data can be obtained free of charge from The Cambridge Crystallographic Data Centre via www.ccdc.cam.ac.uk/data_request/cif.

Supporting Information (see footnote on the first page of this article): Structures of the complexes bearing the tris(3,5-dimethylpyr-

Table 6. Crystal data and structure refinement for **4a**, **4b**, **7a**·CH₂Cl₂, **8a**·THF, and **8d**·CHCl₃.

	4a	4b	7a ·CH ₂ Cl ₂	8a ·THF	8d ·CHCl ₃
Empirical formula	C ₁₄ H ₁₆ N ₆ O ₃ Pt	C ₂₀ H ₂₈ N ₆ O ₂ Pt	C ₁₆ H ₂₁ Cl ₂ I ₁ N ₆ O ₂ Pt	C ₃₀ H ₄₅ F ₃ N ₆ O ₆ S ₁ Si ₁ Pt ₁	C ₃₃ H ₄₃ Cl ₃ N ₆ O ₅ S ₁ Pt ₁
M _r	495.4	579.6	722.3	898.0	937.2
Crystal system	monoclinic	triclinic	triclinic	monoclinic	triclinic
Space group	<i>P</i> 2 ₁ / <i>c</i>	<i>P</i> 1	<i>P</i> 1	<i>P</i> 2 ₁ / <i>c</i>	<i>P</i> 1
<i>a</i> [Å]	8.5882(5)	8.7125(6)	8.9243(5)	12.6276(9)	10.6080(5)
<i>b</i> [Å]	12.5718(7)	10.2503(8)	10.5230(6)	14.403(1)	11.7491(5)
<i>c</i> [Å]	16.375(1)	12.3813(9)	12.0383(7)	20.857(1)	15.2227(7)
α [°]	—	94.630(6)	79.963(4)	—	86.367(4)
β [°]	112.442(5)	97.557(6)	82.496(5)	97.526(6)	89.996(4)
γ [°]	—	99.195(6)	85.120(5)	—	80.532(4)
<i>V</i> [Å ³]	1634.1(2)	1076.2(1)	1101.4(1)	3760.8(5)	1867.6(2)
<i>Z</i>	4	2	2	4	2
<i>D</i> _{calcd.} [g cm ⁻³]	2.014	1.789	2.178	1.586	1.667
μ (Mo-K _α) [mm ⁻¹]	8.605	6.547	8.038	3.880	4.075
<i>F</i> (000)	944	568	680	1800	936
θ range [°]	4.03–28.00	2.71–28.00	3.93–27.00	2.72–26.00	3.85–28.00
Reflections collected	13540	10412	11249	38538	21168
Reflections observed	3021	4345	4178	6789	7822
[<i>I</i> > 2σ(<i>I</i>)]					
Independent reflections	3939 [<i>R</i> _{int} = 0.0400]	5162 [<i>R</i> _{int} = 0.0459]	4754 [<i>R</i> _{int} = 0.0417]	7397 [<i>R</i> _{int} = 0.0282]	8993 [<i>R</i> _{int} = 0.0411]
Data/restraints/parameters	3939/0/210	5162/0/270	4178/0/256	7397/45/445	8993/0/453
GoF on <i>F</i> ²	0.929	0.979	1.030	1.034	0.941
Final <i>R</i> indices [<i>I</i> > 2σ(<i>I</i>)]	<i>R</i> ₁ = 0.0207, <i>wR</i> ₂ = 0.0453	<i>R</i> ₁ = 0.0279, <i>wR</i> ₂ = 0.0683	<i>R</i> ₁ = 0.0320, <i>wR</i> ₂ = 0.0784	<i>R</i> ₁ = 0.0300, <i>wR</i> ₂ = 0.0772	<i>R</i> ₁ = 0.0228, <i>wR</i> ₂ = 0.0506
<i>R</i> indices (all data)	<i>R</i> ₁ = 0.0309, <i>wR</i> ₂ = 0.0466	<i>R</i> ₁ = 0.0353, <i>wR</i> ₂ = 0.0711	<i>R</i> ₁ = 0.0377, <i>wR</i> ₂ = 0.0796	<i>R</i> ₁ = 0.0334, <i>wR</i> ₂ = 0.0793	<i>R</i> ₁ = 0.0282, <i>wR</i> ₂ = 0.0512
Largest difference peak/hole [e Å ⁻³]	0.957/-1.920	1.669/-1.898	1.420/-2.027	1.032/-1.133	1.076/-1.780

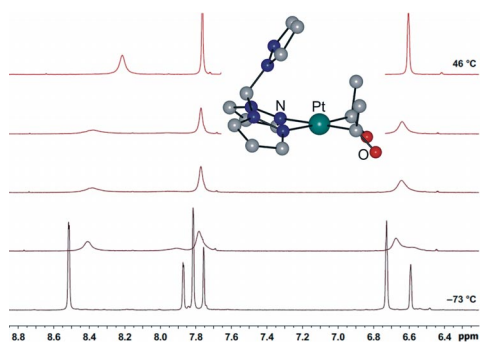
azolyl)methane ligand as well as energies and Cartesian coordinates of all calculated molecules is given.

- [1] D. Steinborn, *Dalton Trans.* **2005**, 2664–2671.
- [2] D. Steinborn, M. Gerisch, K. Merzweiler, K. Schenzel, K. Pelz, H. Bögel, J. Magull, *Organometallics* **1996**, *15*, 2454–2457.
- [3] M. Bette, T. Rüffer, C. Bruhn, J. Schmidt, D. Steinborn, *Organometallics* **2012**, *31*, 3700–3710.
- [4] a) S. Trofimenko, *Scorpionates: The Coordination Chemistry of Polypyrazolylborate Ligands*, Imperial College Press, London, **1999**; b) C. Pettinari, *Scorpionates II: Chelating Borate Ligands*, Imperial College Press, London, **2008**.
- [5] T. Kluge, M. Bette, C. Vetter, J. Schmidt, D. Steinborn, *J. Organomet. Chem.* **2012**, *715*, 93–101.
- [6] C. Pettinari, R. Pettinari, *Coord. Chem. Rev.* **2005**, *249*, 525–543.
- [7] a) C. Pettinari, M. Pellei, A. Cingolani, D. Martini, A. Drozdov, S. Troyanov, W. Panzeri, A. Mele, *Inorg. Chem.* **1999**, *38*, 5777–5787; b) D. L. Reger, *Comments Inorg. Chem.* **1999**, *21*, 1–28.
- [8] D. L. Reger, T. C. Grattan, K. J. Brown, C. A. Little, J. J. S. Lamba, A. L. Rheingold, R. D. Sommer, *J. Organomet. Chem.* **2000**, *607*, 120–128.
- [9] H. R. Bigmore, S. L. Lawrence, P. Mounford, C. S. Tredget, *Dalton Trans.* **2005**, 635–651.
- [10] A. J. Canty, N. J. Minchin, *J. Organomet. Chem.* **1982**, *226*, C14–C16.
- [11] F. A. Jalón, B. R. Manzano, A. Otero, M. C. Rodríguez-Pérez, *J. Organomet. Chem.* **1995**, *494*, 179–185.
- [12] A. J. Canty, R. T. Honeyman, *J. Organomet. Chem.* **1990**, *387*, 247–263.
- [13] a) H. Kessler, *Angew. Chem.* **1970**, *82*, 237; *Angew. Chem. Int. Ed. Engl.* **1970**, *9*, 219–253; b) J. Sandström, *Dynamic NMR Spectroscopy*, Academic Press, London **1982**, pp. 93–123.
- [14] J. Elguero, A. Fruchier, A. de la Hoz, F. A. Jalon, B. R. Manzano, A. Otero, F. Gómez-de la Torre, *Chem. Ber.* **1996**, *129*, 589–594.
- [15] C. Xu, G. K. Anderson, L. Brammer, J. Braddock-Wilking, N. P. Rath, *Organometallics* **1996**, *15*, 3972–3979.
- [16] L. E. Crascall, J. L. Spencer, *J. Chem. Soc., Dalton Trans.* **1992**, 3445–3452.
- [17] T. Steiner, *Cryst. Rev.* **1996**, *6*, 1–57.
- [18] R. J. Puddephatt, *Coord. Chem. Rev.* **2001**, *219*, 157–185.
- [19] J. L. Look, D. D. Wick, J. M. Mayer, K. T. Goldberg, *Inorg. Chem.* **2009**, *48*, 1356–1369.
- [20] S. A. O'Reilly, P. S. White, J. L. Templeton, *J. Am. Chem. Soc.* **1996**, *118*, 5684–5689.
- [21] H. Pfeiffer, A. Rojas, J. Niesel, U. Schatzschneider, *Dalton Trans.* **2009**, 4292–4298.
- [22] A. J. Canty, R. T. Honeyman, *J. Organomet. Chem.* **1990**, *396*, 105–113.
- [23] G. A. Jeffrey, *An Introduction to Hydrogen Bonding*, Oxford University Press, Oxford, **1997**.
- [24] B. Binotti, G. Bellachoma, G. Cardaci, A. Macchioni, C. Zuccaccia, E. Foresti, P. Sabatino, *Organometallics* **2002**, *21*, 346–354.
- [25] C. Titze, J. Hermann, H. Vahrenkamp, *Chem. Ber.* **1995**, *128*, 1095–1103.
- [26] a) T. Steiner, *Acta Crystallogr., Sect. B* **1998**, *54*, 456–463; b) G. R. Desiraju, T. Steiner, *The Weak Hydrogen Bond in Structural Chemistry and Biology*, Oxford University Press, New York, **1999**, pp. 246–253.
- [27] J. E. Huheey, E. A. Keiter, R. L. Keiter, *Inorganic Chemistry: Principles of Structure and Reactivity*, Harper Collins College Publishers, New York, **1993**, pp. 138–152.
- [28] a) A. J. Canty, T. Rodemann, *Inorg. Chem. Commun.* **2003**, *6*, 1382–1384; b) A. J. Canty, T. Rodemann, B. W. Skelton, A. H. White, *Organometallics* **2006**, *25*, 3996–4001; c) A. J. Canty, M. G. Gardiner, R. C. Jones, T. Rodemann, M. Sharma, *J. Am. Chem. Soc.* **2009**, *131*, 7236–7237.
- [29] A. J. Canty, R. P. Watson, S. S. Karpiniec, T. Rodemann, M. G. Gardiner, R. C. Jones, *Organometallics* **2008**, *27*, 3203–3209.
- [30] V. V. Zhdankin, P. J. Stang, *Tetrahedron* **1998**, *54*, 10927–10966.
- [31] a) P. S. Pregosin, *Coord. Chem. Rev.* **1982**, *44*, 247–291; b) R. G. Kidd, *Annu. Rep. NMR Spectrosc.* **1991**, *23*, 85–139.
- [32] a) M. C. Janzen, H. A. Jenkins, M. C. Jennings, L. M. Rendina, R. J. Puddephatt, *J. Chem. Soc., Dalton Trans.* **1999**, 1713–1715; b) A. J. Canty, T. Rodemann, B. W. Skelton, A. H. White, *Inorg. Chem. Commun.* **2005**, *8*, 55–57; c) C. Munro-Leighton, Y. Feng, J. Zhang, N. M. Alson, T. B. Gunnoe, P. D. Boyle, J. L. Petersen, *Inorg. Chem.* **2008**, *47*, 6124–6126.
- [33] S. Berger, S. Braun, *200 and More NMR Experiments, A Practical Course*, Wiley-VCH, Weinheim, Germany, **2004**.
- [34] M. Findeisen, T. Brand, S. Berger, *Magn. Reson. Chem.* **2007**, *45*, 175–178.
- [35] a) T. Kitamura, M. Kotani, Y. Fujiwara, *Synthesis* **1998**, 1416–1418; b) L. Rebrovic, G. F. Koser, *J. Org. Chem.* **1984**, *49*, 4700–4702.
- [36] a) *MULscanABS*, PLATON for Windows Taskbar v1.15, University of Glasgow, **2008**; b) A. L. Spek, *J. Appl. Crystallogr.* **2003**, *36*, 7–13.
- [37] G. M. Sheldrick, *SHELXS-97, Program for Crystal Structure Solution*, University of Göttingen, Göttingen, **1998**.
- [38] G. M. Sheldrick, *SHELXL-97, Program for the Refinement of Crystal Structures*, University of Göttingen, Germany, **1997**.
- [39] M. J. Frisch, J. G. W. Trucks, H. B. Schlegel, G. E. Scuseria, M. A. Robb, J. R. Cheeseman, G. Scalmani, V. Barone, B. Mennucci, G. A. Petersson, H. Nakatsuji, M. Caricato, X. Li, H. P. Hratchian, A. F. Izmaylov, J. Bloino, G. Zheng, J. L. Sonnenberg, M. Hada, M. Ehara, K. Toyota, R. Fukuda, J. Hasegawa, M. Ishida, T. Nakajima, Y. Honda, O. Kitao, H. Nakai, T. Vreven, J. A. Montgomery Jr., J. E. Peralta, F. Ogliaro, M. Bearpark, J. J. Heyd, E. Brothers, K. N. Kudin, V. N. Staroverov, T. Keith, R. Kobayashi, J. Normand, K. Raghavachari, A. Rendell, J. C. Burant, S. S. Iyengar, J. Tomasi, M. Cossi, N. Rega, J. M. Millam, M. Klene, J. E. Knox, J. B. Cross, V. Bakken, C. Adamo, J. Jaramillo, R. Gomperts, R. E. Stratmann, O. Yazyev, A. J. Austin, R. Cammi, C. Pomelli, J. W. Ochterski, R. L. Martin, K. Morokuma, V. G. Zakrzewski, G. A. Voth, P. Salvador, J. J. Dannenberg, S. Dapprich, A. D. Daniels, O. Farkas, J. B. Foresman, J. V. Ortiz, J. Cioslowski, D. J. Fox, *Gaussian 09*, rev. B.01, Gaussian, Inc., Wallingford CT, **2009**.
- [40] A. D. Becke, *J. Chem. Phys.* **1993**, *98*, 5648–5652.
- [41] a) F. Weigend, M. Häser, H. Patzelt, R. Ahlrichs, *Chem. Phys. Lett.* **1998**, *294*, 143–152; b) T. Leininger, A. Nicklass, W. Küchle, H. Stoll, M. Dolg, A. Bergner, *Chem. Phys. Lett.* **1996**, *255*, 274–280; c) D. Andrae, U. Häussermann, M. Dolg, H. Stoll, H. Preuss, *Theor. Chim. Acta* **1990**, *77*, 123–141.
- [42] a) D. Steinborn, S. Schwieger, *Chem. Eur. J.* **2007**, *13*, 9668–9678; b) M. Werner, T. Lis, C. Bruhn, R. Lindner, D. Steinborn, *Organometallics* **2006**, *25*, 5946–5954; c) C. Vetter, G. N. Kaluderović, R. Paschke, S. Gómez-Ruiz, D. Steinborn, *Polyhedron* **2009**, *28*, 3699–3706; d) S. Schwieger, F. W. Heinemann, C. Wagner, R. Kluge, C. Damm, G. Israel, D. Steinborn, *Organometallics* **2009**, *28*, 2485–2493.
- [43] a) E. Cancès, B. Mennucci, J. Tomasi, *J. Chem. Phys.* **1997**, *107*, 3032–3041; b) M. Cossi, V. Barone, B. Mennucci, J. Tomasi, *Chem. Phys. Lett.* **1998**, *286*, 253–260; c) B. Mennucci, J. Tomasi, *J. Chem. Phys.* **1997**, *106*, 5151–5158.

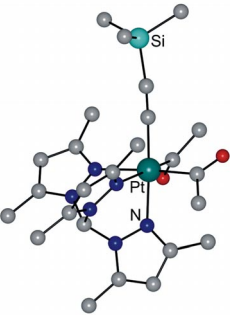
Received: December 5, 2012

Published Online: ■

Tridentate Ligands



The influence of the substitution pattern of tris(pyrazolyl)methane ligands (*pz* versus 3,5-Me₂*pz*) on the reactivity and fluxional-
ity of diacetylplatinum(II) complexes as



well as the synthesis of diacetyl(alkynyl)-
platinum(IV) complexes by means of
oxidative addition reactions using alkynyl-
iodine(III) reagents is described.

M. Bette, J. Schmidt,
D. Steinborn* 1–18

Diacetylplatinum(II) and -platinum(IV)
Complexes Bearing κ^2 - and κ^3 -Coordinated
Tris(pyrazolyl)methane Ligands: In-
vestigations on the Synthesis, Fluxionality,
and Reactivity in Relation to the Substi-
tution Pattern of the Ligands

Keywords: Platinum / Tridentate ligands /
Hydrogen bonds / Fluxionality / Ab initio
calculations

Reprint with permission from
European Journal of Inorganic Chemistry
Copyright 2013 John Wiley and Sons.

Diacetylplatinum(II) Complexes with κ^2 -Coordinated Tris(pyridyl)methanol and Tris(pyridyl)methyl Ether Ligands: Structural Insight into the Ligand Dynamics in Solution

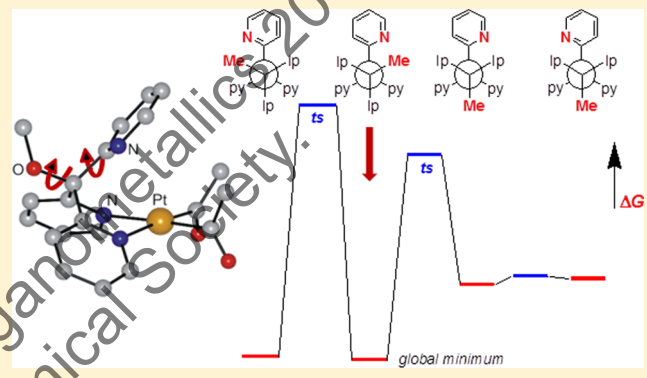
Martin Bette,[†] Tim Kluge,[†] Jürgen Schmidt,[‡] and Dirk Steinborn*,[†]

[†]Institute of Chemistry-Inorganic Chemistry, Martin Luther University of Halle-Wittenberg, Kurt-Mothes-Straße 2, D-06120 Halle, Germany

[‡]Department of Bioorganic Chemistry, Leibniz Institute of Plant Biochemistry, Weinberg 3, D-06120 Halle, Germany

Supporting Information

ABSTRACT: Reactions of the bis(benzylamine)platinum(II) complex $[\text{Pt}(\text{COMe})_2(\text{NH}_2\text{Bn})_2]$ (**2**; Bn = benzyl) with (2-py)₃COR (2-py = 2-pyridyl), (2-py)₂PhCOR, and (2-py)₂(*m*-Tol)COR (*m*-Tol = 3-methylphenyl) afforded the neutral diacetylplatinum(II) complexes $[\text{Pt}(\text{COMe})_2\{(2\text{-py})_3\text{COR}\}]$ (*R* = H (**3a**), Me (**3b**), Et (**3c**), Bn (**3d**)), $[\text{Pt}(\text{COMe})_2\{(2\text{-py})_2\text{PhCOR}\}]$ (*R* = H (**4a**), Me (**4b**)), and $[\text{Pt}(\text{COMe})_2\{(2\text{-py})_2(m\text{-Tol})\text{COR}\}]$ (*R* = H (**5a**), Me (**5b**))), respectively, having, due to a κ^2 coordination of the ligands, a 2-pyridyl (**3**), a phenyl (**4**), or a *m*-tolyl (**5**) ring as the pendant group. The identities of all complexes were unambiguously proved by high-resolution mass spectrometric investigations and by NMR (¹H, ¹³C, ¹⁹⁵Pt) and IR spectroscopy as well as by single-crystal X-ray diffraction analyses (**3a–d**). In methanol solution, complexes **3b–d** and **5b** show a dynamic behavior. The thermodynamic parameters of these dynamics have been determined by variable-temperature ¹H NMR measurements (Eyring plots). Furthermore, extensive DFT calculations will be presented, which indicate that the dynamics are caused by the interplay of hindered and respectively unhindered rotations of the substituent R and/or the pendant group.



1. INTRODUCTION

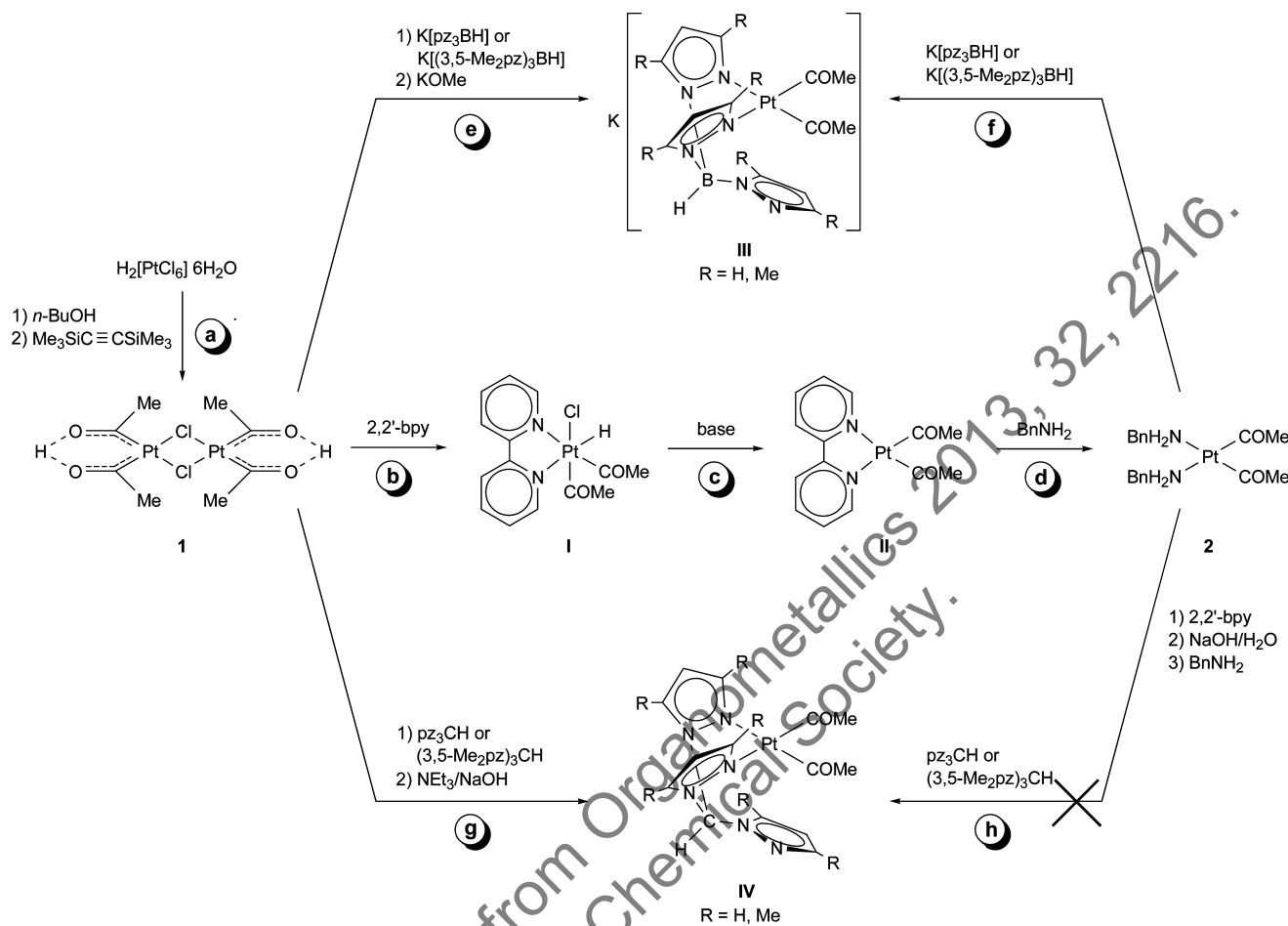
The dinuclear platina- β -diketone $[\text{Pt}_2\{(\text{COMe})_2\text{H}\}_2(\mu\text{-Cl})_2]$ (**1**), being accessible by the reaction of hexachloroplatinic acid with *n*-butyl alcohol and bis(trimethylsilyl)acetylene, can be considered as a hydroxycarbene complex, where the hydroxycarbene ligands are stabilized by intramolecular O–H...O hydrogen bonds to neighboring acetyl ligands (Scheme 1, **a**).¹ Due to its electronic unsaturation (16 valence electrons) and kinetically labile ligand sphere, the platina- β -diketone **1** exhibits a unique reactivity and thus is a suitable precursor complex for the synthesis of a great variety of acetyl platinum(II) and platinum(IV) complexes with bidentate N,N',P,P',S,S', and N,O ligands.² Thus, the reaction of complex **1** with the bidentate *N*-donor 2,2'-bipyridine leads to the formation of the thermally extraordinarily stable diacetyl-(hydrido)platinum(IV) complex **I** (Scheme 1, **b**), which affords with NaOH a reductive elimination of HCl to form the respective diacetylplatinum(II) complex **II** (Scheme 1, **c**).³ Reactions of **1** with tris(pyrazolyl)borates (so-called scorpionates)⁴ and tris(pyrazolyl)methanes, which represent examples of tridentate *N*-donor ligands, followed by the addition of a base led in an analogous manner to the formation of the diacetylplatinum(II) complexes **III** and **IV** bearing the tripodal ligand only κ^2N,N' coordinated with a pendant pyrazolyl ring

(Scheme 1, **d** and **e**).^{5,6} Due to its substitution-labile benzylamine ligands, the bis(benzylamine)platinum(II) complex **2**, accessible by the reaction of **II** in neat benzylamine (Scheme 1, **f**), was found to be another useful precursor complex for the synthesis of diacetylplatinum(II) complexes.⁷ In this reaction pathway diacetylplatinum(II) complexes **III** bearing scorpionate ligands could also be synthesized but, unexpectedly, not the type **IV** complexes (Scheme 1, **g** and **h**).^{5,6}

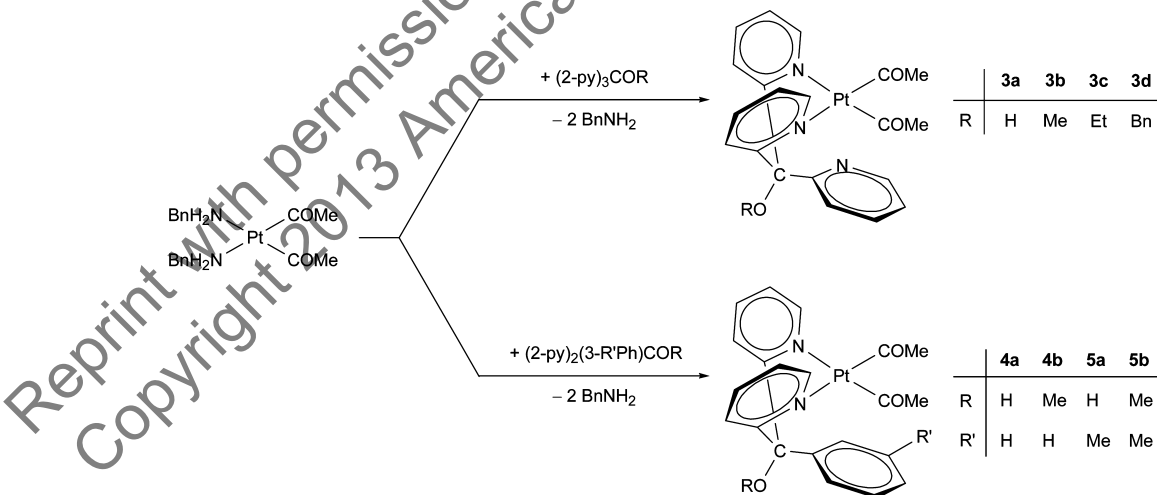
Both types of ligands, the anionic tris(pyrazolyl)borates as well as the isoelectronic neutral tris(pyrazolyl)methanes, are—due to the tetrahedral geometry at their central B or C backbone atom—restricted to a facial κ^2N,N',N'' coordination in octahedral complexes. For the same reason the coordination mode of these ligands in type **III** and **IV** square-planar complexes is κ^2N,N' with a pendant third pyrazolyl ring.^{4,8} Although these ligands are isoelectronically and structurally very similar, their diacetylplatinum(II) and -platinum(IV) complexes may exhibit great differences in reactivity and chemical behavior.^{5,6}

Received: February 1, 2013

Scheme 1. Synthesis of Diacetylplatinum(II) Complexes Bearing κ^2 -Bonded Scorpionate (III) and Tris(pyrazolyl)methane Ligands (IV)



Scheme 2. Syntheses of the Diacetylplatinum(II) Complexes 3–5



Another class of facially coordinating tripodal ligands, which has received considerable attention in both coordination and organometallic chemistry in recent years, are the neutral tris(2-pyridyl)methanol ligands ($(2\text{-py})_3\text{COH}$) and the respective tris(2-pyridyl)methyl ether ligands ($(2\text{-py})_3\text{COR}$).⁹ The main difference from the aforementioned ligand classes is the change of the donating group from pyrazole to pyridine, which is reported to be both a better σ donor and π acceptor ligand than

pyrazole.^{9,10} Here, we report on the synthesis and characterization of diacetylplatinum(II) complexes bearing κ^2N,N' -coordinated tris(2-pyridyl)methanol and tris(2-pyridyl)methyl ether ligands as well as on the molecular dynamics of these complexes. Furthermore, for comparison, ligands are included which bear a phenyl or *m*-tolyl group instead of the pendant third pyridine ring.

2. RESULTS AND DISCUSSION

2.1. Synthesis of Diacetylplatinum(II) Complexes.

Reactions of $[\text{Pt}(\text{COMe})_2(\text{NH}_2\text{Bn})_2]$ (**2**) with $(2\text{-py})_3\text{COR}$ afforded in facile ligand exchange reactions the diacetylplatinum(II) complexes $[\text{Pt}(\text{COMe})_2\{(2\text{-py})_3\text{COR}\}]$ ($\text{R} = \text{H}$ (**3a**), Me (**3b**), Et (**3c**), Bn (**3d**)) bearing κ^2 bonded tris(2-pyridyl)methanol (**3a**) and tris(2-pyridyl)methyl ether (**3b–d**) ligands (Scheme 2). By the same pathway the structurally similar complexes $[\text{Pt}(\text{COMe})_2\{(2\text{-py})_2\text{PhCOR}\}]$ ($\text{R} = \text{H}$ (**4a**), Me (**4b**)) and $[\text{Pt}(\text{COMe})_2\{(2\text{-py})_2(m\text{-Tol})\text{COR}\}]$ ($\text{R} = \text{H}$ (**5a**), Me (**5b**))) were prepared, where the pendant pyridyl group of type **3** complexes is replaced by a phenyl (**4**) and a *m*-tolyl group (**5**), respectively (Scheme 2). Thus, in type **4** and **5** complexes the pendant group is symmetrically and unsymmetrically replaced, respectively. All compounds were isolated in good yields between 68 and 90% as yellow solids, which were characterized by NMR (^1H , ^{13}C , ^{195}Pt) and IR spectroscopy as well as by high-resolution mass spectrometric (HRMS-ESI) investigations and single-crystal X-ray diffraction analyses (3). All complexes are soluble in methanol, methylene chloride, and chloroform. At room temperature under anaerobic conditions, solutions of compounds **3** are stable for several days, while for solutions of complexes **4** and **5** the start of decomposition can be detected by NMR spectroscopy within 2 days.

As an alternative route to prepare diacetylplatinum(II) complexes, in general, reactions of the respective bi- or tridentate ligands with the platina- β -diketone **1** followed by the reduction of the formed diacetyl(hydrido)platinum(IV) complexes induced by proton abstraction by a base can be envisioned. This is shown in Scheme 1 for the analogous diacetylplatinum(II) complexes bearing scorpionate (**III**) or tris(pyrazolyl)methane ligands (**IV**). Here, in this pathway, only complexes bearing etherified ligands ($\text{R} = \text{Me}$, Et, Bn; **3b–d**, **4b**, **5b**) could be synthesized. Reactions with the alcohol derivatives ($\text{R} = \text{H}$) failed. Due to, in general, poorer yields and a more time-consuming workup procedure, this pathway was not further pursued.

2.2. Structures of $[\text{Pt}(\text{COMe})_2\{(2\text{-py})_3\text{COR}\}]$ ($\text{R} = \text{H}$ (3a**), Me (**3b**), Et (**3c**), Bn (**3d**)), Crystals of $[\text{Pt}(\text{COMe})_2\{(2\text{-py})_3\text{COR}\}]$ ($\text{R} = \text{H}$ (**3a**), Me (**3b**), Et (**3c**), Bn (**3d**))) suitable for X-ray diffraction analyses were obtained from a saturated methylene chloride solution at -7°C (**3a**· CH_2Cl_2) and from THF solutions layered with *n*-pentane (**3b–d**). The molecular structures are shown in Figures 1–4, respectively. Selected structural parameters are given in the figure captions. The platinum atoms are coordinated in a square-planar fashion by two acetyl ligands and the κ^2N,N' -coordinated $(2\text{-py})_3\text{COR}$ ligand. The angles between neighboring ligands are all close to 90° ($84.3(1)$ – $95.9(1)^\circ$, **3a**; $84.4(2)$ – $93.2(2)^\circ$, **3b**; $84.2(2)$ – $93.7(2)^\circ$, **3c**; $84.2(2)$ – $94.0(2)^\circ$, **3d**). The $\text{C}(\mu\text{-py})_2\text{Pt}$ units adopt a boat conformation with the backbone carbon atom of the $(2\text{-py})_3\text{COR}$ ligand ($\text{C}10$) and the platinum atom at the apexes. The noncoordinated pyridine ring is situated in an axial position of this boat structure and oriented pseudo-parallel to the coordination plane ($\text{Pt}, \text{C}1, \text{C}3, \text{N}2, \text{N}4$). The angles between the complex plane and the plane of the noncoordinated pyridine ring are between $46.2(2)$ and $50.7(2)^\circ$, resulting in distances of 3.769 \AA (**3a**), 3.656 \AA (**3b**), 3.681 \AA (**3c**), and 3.770 \AA (**3d**) between the platinum atom and the center of gravity of the noncoordinated ring. In crystals of complexes **3b–d**, the torsion angles $\text{C}21\text{--O}3\text{--C}10\text{--C}16$ ($44.3(7)^\circ$, **3b**,**

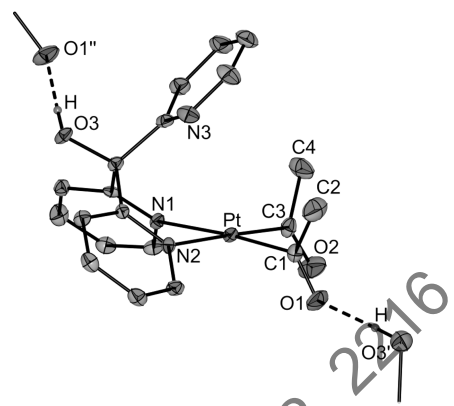


Figure 1. Structure of $[\text{Pt}(\text{COMe})_2\{(2\text{-py})_3\text{COH}\}]$ (**3a**) in crystals of **3a**· CH_2Cl_2 . Ellipsoids are shown at the 30% probability level. H atoms are omitted for clarity, except for that at O3. The broken line indicates an intermolecular O–H···O hydrogen bond in crystals of **3a**· CH_2Cl_2 . Selected structural parameters (distances in Å, angles in deg): Pt–C1 = $1.975(4)$, Pt–C3 = $1.997(4)$, Pt–N1 = $2.140(3)$, Pt–N2 = $2.139(3)$, C1–Pt–C3 = $87.1(2)$, C1–Pt–N2 = $92.7(1)$, C3–Pt–N1 = $95.9(1)$, N1–Pt–N2 = $84.3(1)$, C1–Pt–N1 = $175.4(1)$, C3–Pt–N2 = $178.4(2)$, O1···O3 = $2.652(4)$.

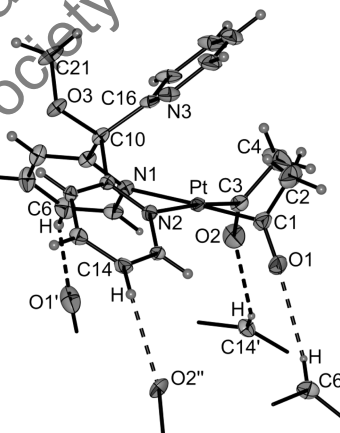


Figure 2. Molecular structure of $[\text{Pt}(\text{COMe})_2\{(2\text{-py})_3\text{COMe}\}]$ (**3b**). Ellipsoids are shown at the 30% probability level. Broken lines indicate intermolecular C–H···O hydrogen bonds in crystals of **3b**. Selected structural parameters (distances in Å, angles in deg): Pt–C1 = $2.016(7)$, Pt–C3 = $2.014(6)$, Pt–N1 = $2.140(5)$, Pt–N2 = $2.147(4)$, C1–Pt–C3 = $91.2(3)$, C1–Pt–N2 = $91.1(2)$, C3–Pt–N1 = $93.2(2)$, N1–Pt–N2 = $84.4(2)$, C1–Pt–N1 = $175.5(2)$, C3–Pt–N2 = $174.0(4)$, C21–O3–C10–C16 = $44.3(7)$, C6–O1' = $3.35(1)$, H···O1' = 2.49 , C6–H···O1' = 151 , C14'···O2 = $3.277(8)$, H···O2 = 2.51 , C14'–H···O2 = 139 .

$47.8(7)^\circ$, **3c**; $41.2(7)^\circ$, **3d**) demonstrated that the noncoordinated pyridine rings and the substituents R at the oxygen atoms O3 are *gauche* to each other.

In all structures, the carbonyl oxygen atoms of the two acetyl ligands were found to lie on the same side of the complex plane. Thus, the diacetyl moieties represent a “*cisoid*” conformation as a result of intermolecular hydrogen bonds: in crystals of the complex **3a**· CH_2Cl_2 the O1···O3' distance of $2.652(4)$ Å indicates the presence of an intermolecular O–H···O hydrogen bond¹¹ between the acetyl ligand and the hydroxyl group at the backbone C atom of the $(2\text{-py})_3\text{COH}$ ligand (Figure 1), such that the crystals are threaded by one-dimensional strands. In crystals of **3b,c** the oxygen atoms of the acetyl ligands were found to act as H acceptors in weak

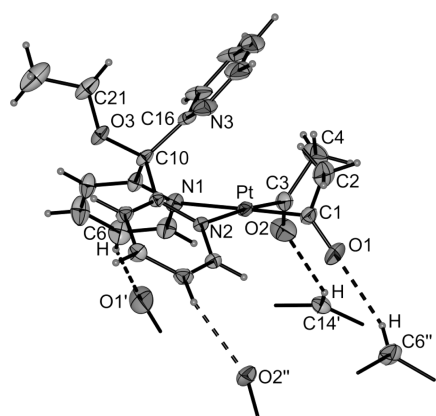


Figure 3. Molecular structure of $[\text{Pt}(\text{COMe})_2\{(2\text{-py})_3\text{COEt}\}]$ (**3c**). Ellipsoids are shown at the 30% probability level. Broken lines indicate intermolecular C—H···O hydrogen bonds in crystals of **3c**. Selected structural parameters (distances in Å, angles in deg): Pt—C1 = 1.998(6), Pt—C3 = 2.009(6), Pt—N1 = 2.143(4), Pt—N2 = 2.157(4), C1—Pt—C3 = 89.8(2), C1—Pt—N2 = 92.3(2), C3—Pt—N1 = 93.7(2), N1—Pt—N2 = 84.2(2), C1—Pt—N1 = 176.5(2), C3—Pt—N2 = 174.3(4), C21—O3—C10—C16 = 47.8(7), C6···O1' = 3.25(1), H···O1' = 2.37, C6—H···O1' = 155, C14''···O2 = 3.189(9), H···O2 = 2.43, C14''—H···O2 = 137.

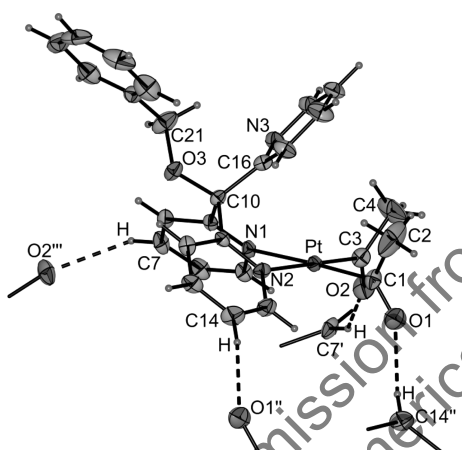


Figure 4. Molecular structure of $[\text{Pt}(\text{COMe})_2\{(2\text{-py})_3\text{COBn}\}]$ (**3d**). Ellipsoids are shown at the 30% probability level. Broken lines indicate intermolecular C—H···O hydrogen bonds in crystals of **3d**. Selected structural parameters (distances in Å, angles in deg): Pt—C1 = 2.007(6), Pt—C3 = 2.010(6), Pt—N1 = 2.142(4), Pt—N2 = 2.156(4), C1—Pt—C3 = 88.6(2), C1—Pt—N2 = 93.2(2), C3—Pt—N1 = 94.0(2), N1—Pt—N2 = 84.2(2), C1—Pt—N1 = 176.9(2), C3—Pt—N2 = 177.9(2), C21—O3—C10—C16 = 41.2(7), C7''···O2 = 3.272(8), H···O2 = 2.44, C7''—H···O2 = 147, C14''···O1 = 3.313(8), H···O1 = 2.38, C14''—H···O1 = 170.

intermolecular $\text{C}_{\text{py}}\text{—H}\cdots\text{O}$ hydrogen bonds, so that the crystals are built up by strands in a zigzag manner, as shown in Figure 5 for complex **3b** as an example. The structural parameters of all these hydrogen bonds ($\text{C}\cdots\text{O} = 3.189(9)\text{--}3.35(1)$ Å, $\text{O}\cdots\text{H} = 2.37\text{--}2.51$ Å, $\text{C—H}\cdots\text{O} = 137\text{--}170^\circ$) are in the range expected for such attractive interactions.¹² In contrast, in crystals of **3d** the $\text{C}_{\text{py}}\text{—H}\cdots\text{O}$ hydrogen bonds built up a three-dimensional network.

2.3. Spectroscopic Investigations. The ^1H , ^{13}C , and ^{195}Pt NMR spectra of the diacetylplatinum(II) complexes **3**–**5** give proof of their identities. At room temperature, in the ^1H and ^{13}C NMR spectra of **3b**–**d** and **5b** some signals are

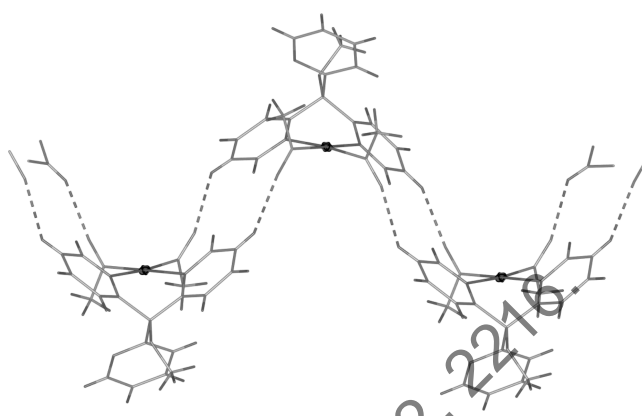


Figure 5. Wire model showing the zigzag arrangement of the molecules in crystals of **3b**.

broadened, pointing to a dynamic process. Thus, low-temperature and temperature-dependent NMR measurements in CD_3OD were also performed.

At room temperature, the ^1H NMR spectrum of $[\text{Pt}(\text{COMe})_2\{(2\text{-py})_3\text{COH}\}]$ (**3a**) displayed one signal for both acetyl ligands and two sets of signals with a 2:1 intensity in the aromatic area reflecting a mirror-symmetric structure of the complex in solution. In contrast, at room temperature, the ^1H NMR spectra of $[\text{Pt}(\text{COMe})_2\{(2\text{-py})_3\text{COR}\}]$ ($\text{R} = \text{Me}$ (**3b**), Et (**3c**), Bn (**3d**)) exhibited broad signals for the protons both of the acetyl ligands and of the coordinated pyridine rings, as shown in Figure 6 for complex **3b**. At -20°C , these signals were found to be split up, indicating a dynamic process that leads to a loss of the mirror-symmetric structure of the complexes in solution (Table 1). In contrast, the ^1H NMR spectrum of **3a** ($\text{R} = \text{H}$) recorded even at -80°C still displayed only one sharp signal for the acetyl ligands and—in addition to the signals of the pendant pyridyl group—only one set of signals for the protons of the two coordinated pyridine rings.

The similar type **4** and **5** complexes $[\text{Pt}(\text{COMe})_2\{(2\text{-py})_2\text{PhCOR}\}]$ ($\text{R} = \text{H}$ (**4a**), Me (**4b**)) and $[\text{Pt}(\text{COMe})_2\{(2\text{-py})_2(m\text{-Tol})\text{COH}\}]$ (**5a**), where the pendant pyridyl group is replaced by a phenyl or *m*-tolyl group, do not show any dynamics, whereas the complex $[\text{Pt}(\text{COMe})_2\{(2\text{-py})_2(m\text{-Tol})\text{COMe}\}]$ (**5b**) shows a dynamics (although not all proton signals are split up) analogous to that of complexes **3b**–**d** (Table 1). Thus, in compliance with complexes **3**, the dynamics depend on both the symmetry of the pendant group (unsymmetrically substituted as py, *m*-Tol versus symmetrically substituted as Ph) and the substitution pattern at the backbone C atom (OR with $\text{R} = \text{Me}$, Et, Bn versus OH).

In general, the same observations were made in the ^{13}C NMR spectra of compounds **3**–**5**. At room temperature, spectra of **3b**–**d** and **5b** exhibited broad signals (which split up at lower temperatures) or even two sets of signals for the C atoms of the acetyl ligands and of the coordinated pyridine rings. On the other hand, the ^{13}C NMR room-temperature spectra of **3a**, **4**, and **5a** reflect a mirror-symmetric structure of the complexes in solution.

The conditions for the existence of mirror-symmetric structures in solution should be both a fast rotation of the acetyl ligands and a fast rotation of the substituent R at the backbone of the $(2\text{-py})_3\text{COR}$ ligand as well as of the noncoordinated pyridine/*m*-tolyl ring. Since a hindered rotation of the acetyl ligands can be excluded due to experience with a number of other diacetylplatinum(II) complexes,^{5,7,13}

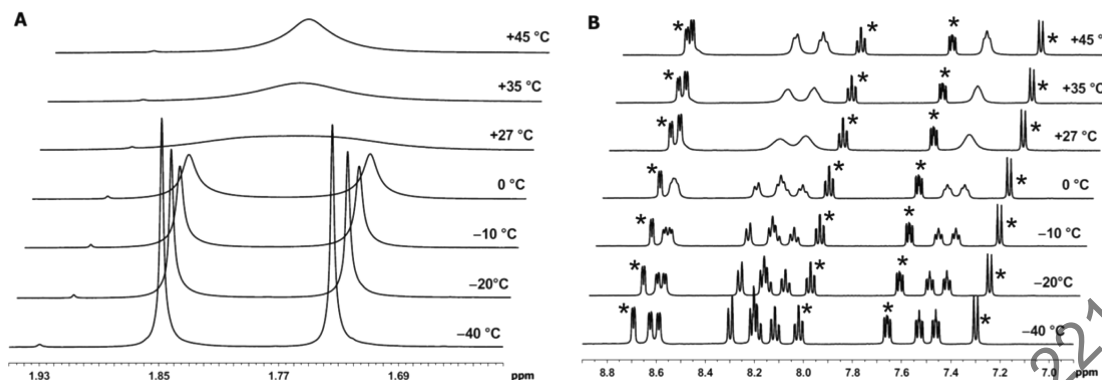


Figure 6. Variable-temperature ^1H NMR spectra of **3b** measured in CD_3OD : (A) region related to the acetyl ligands.; (B) aromatic region. Signals of the noncoordinated pyridyl group are marked with asterisks.

Table 1. Temperature-Dependent Characteristic Proton Shifts (in ppm) of the Acetyl Ligands and of the Coordinated Pyridyl Groups of $[\text{Pt}(\text{COMe})_2\{(2\text{-py})_3\text{COR}\}]$ ($\text{R} = \text{Me}$ (3b**), Et (**3c**), Bn (**3d**)) and $[\text{Pt}(\text{COMe})_2\{(2\text{-py})_2(m\text{-Tol})\text{COMe}\}]$ (**5b**)^a**

	T (°C)	δ_{acetyl}	$\delta_{\text{H}3}$	$\delta_{\text{H}4}$	$\delta_{\text{H}5}$	$\delta_{\text{H}6}$
3b ^b	+27	1.79	8.21	8.11	7.44	8.62
	-20	1.74/1.85	8.20/8.29	8.11/8.18	7.45/7.52	8.60/8.63
3c ^b	+27	1.79	8.21	8.11	7.44	8.62
	-20	1.73/1.85	8.19/8.28	8.11/8.19	7.45/7.52	8.60/8.63
3d ^b	+27	1.80	8.26	8.12	7.45	8.65
	-20	1.75/1.85	8.21/8.33	8.10/8.18	7.45/7.52	8.62/8.64
5b ^b	+27	1.76	8.20	8.10	ca. 7.4 ^c	8.65
	-20	1.72/1.80	8.22	8.13	ca. 7.4 ^c	8.61/8.67
3a ^b	+27	1.76	8.38	8.10	7.43	8.59
4a ^c	+27	1.71	8.43	7.96	7.25	8.64
4b ^d	+27	1.79	8.04	7.88	7.25	8.83
5a ^b	+27	1.74	8.40	8.10	7.43	8.63

^aFor comparison, the corresponding values of complexes **3a**, **4a,b**, and **5a** without dynamics are shown. ^bMeasured in CDOD_3 . ^cMeasured in CD_2Cl_2 . ^dMeasured in CDCl_3 . ^eOverlapped with other signals.

these results imply that in complexes **3b–d** and **5b** at least one of the other aforementioned rotations is hindered and thus is the reason for the observed phenomena in NMR spectroscopy.

To get an impression of the thermodynamic parameters of these potentially hindered rotations, the signals of the acetyl ligands were used for an analysis of this dynamics by NMR techniques. Thus, variable-temperature ^1H NMR studies were performed to estimate the coalescence temperatures. Furthermore, from line-shape analyses¹⁴ of spectra recorded in a range close to the coalescence temperatures (283–318 K), the activation parameters ΔH^\ddagger and ΔS^\ddagger have been determined by Eyring plots (Figure 7). The Gibbs free energies of activation at the coalescence temperature were calculated according to $\Delta G_C^\ddagger = \Delta H^\ddagger - T_C^\ddagger \Delta S^\ddagger$. The compilation of ΔG_C^\ddagger and related parameters in Table 2 shows that the coalescence temperatures (296–303 K) as well as the Gibbs free energies of activation at the coalescence temperature (14.6–15.8 kcal mol⁻¹) for all compounds were found in a narrow range. The enthalpies of activation (ca. 9.2 kcal mol⁻¹) and entropies of activation (ca. -18.7 cal mol⁻¹ K⁻¹) calculated for complexes **3b–d** are in a narrow range as well. In contrast, the corresponding values of complex **5b** were found to be $\Delta H^\ddagger = 12.8$ kcal mol⁻¹ and $\Delta S^\ddagger = -8.5$ cal mol⁻¹ K⁻¹, thus being higher by about 2.6 kcal mol⁻¹ and about 10.2 cal mol⁻¹ K⁻¹, respectively. For comparison, the requisite values of the well-studied dimethylformamide as the “benchmark” are given: $\Delta G_C^\ddagger = 21.5$ kcal mol⁻¹ at $T_C = 114$ °C;¹⁵ $\Delta H = 21.2$ kcal mol⁻¹, $\Delta S = -1.6$ cal mol⁻¹ K⁻¹.¹⁶

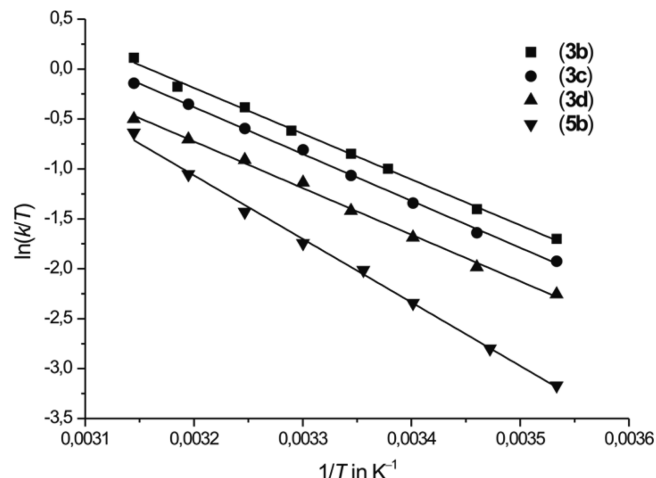


Figure 7. Eyring plots of complexes $[\text{Pt}(\text{COMe})_2\{(2\text{-py})_3\text{COR}\}]$ ($\text{R} = \text{Me}$ (**3b**), Et (**3c**), Bn (**3d**)) and $[\text{Pt}(\text{COMe})_2\{(2\text{-py})_2(m\text{-Tol})\text{COMe}\}]$ (**5b**).

2.4. DFT Calculations. For an additional qualitative and quantitative analysis of the dynamics found in complexes **3b–d** and **5b**, quantum-chemical calculations on the DFT level of theory were performed using the B3LYP functional and high-quality basis sets for all atoms and a pseudopotential for Pt considering relativistic effects (for details, see the Experimental Section). In all calculations solvent effects (MeOH) were

Organometallics

Article

Table 2. Gibbs Free Energies of Activation and Related Parameters for the Dynamics in Complexes 3b–d and 5b

	ΔH^\ddagger (kcal mol ⁻¹)	ΔS^\ddagger (cal mol ⁻¹ K ⁻¹)	ΔG_C^\ddagger (kcal mol ⁻¹)	T _C (K)
3b	9.1 ± 0.5	-18.5 ± 1.4	14.6 ± 0.8	296
3c	9.3 ± 0.3	-18.2 ± 1.0	14.8 ± 0.6	301
3d	9.2 ± 0.4	-19.1 ± 1.4	15.0 ± 0.8	303
5b	12.8 ± 0.9	-8.5 ± 3.0	15.4 ± 1.8	302

considered according to Tomasi's polarized continuum model.¹⁷ To analyze the dynamics, the complexes $[\text{Pt}(\text{COMe})_2\{(2\text{-py})_3\text{COMe}\}]$ (3b) and $[\text{Pt}(\text{COMe})_2\{(2\text{-py})_2(m\text{-Tol})\text{COMe}\}]$ (5b) were chosen. Furthermore, for comparison, the complex $[\text{Pt}(\text{COMe})_2\{(2\text{-py})_3\text{COH}\}]$ (3a) showing a mirror-symmetric structure even at -80 °C was included into the calculations.

At first the equilibrium structures of reasonable conformers (four for each complex) were calculated: see Figure 8 for 3b*²⁷ and the Supporting Information for 3a* and 5b*. The standard Gibbs energies (ΔG^\ddagger) are given in Table 3. As expected, in all structures the $\text{C}(\mu\text{-py})_2\text{Pt}$ units adopt a boat conformation with the platinum atom and the backbone carbon atom of the (2-py)₃COR or the (2-py)₂(m-Tol)COMe ligand at the apexes. In the global minimum (Table 3, entry 1), the OR groups are equatorially positioned, while the asymmetric pendant groups (py in 3a*/3b*, m-Tol in 5b*) are in an axial position and are thus curled toward the platinum center. Moreover, the substituents R and the pendant rings (py/m-Tol) are in mutually *gauche* positions. These conformations (R = H, (3a*)(py_{ax}/gauche); R = Me (3b*(py_{ax}/gauche), 5b*(Tol_{ax}/gauche))) were found in crystals of type 3 complexes except for the *transoid* position of the acetyl ligands which is—in general—favored over a *cisoid* position.⁹ The *cisoid* position found in crystals of 3 is a consequence of intermolecular hydrogen bonds (see section 2.2).

The conformers having an *anti* (fully staggered) conformation of the R—O—C—C_i dihedral angle (instead of a *gauche* conformation) are 4.2–5.7 kcal mol⁻¹ higher in their standard Gibbs free energies (Table 3, entry 2), which might be caused by steric interactions. Furthermore, two conformers, each with an inverted boat unit, have to be considered. This results in an equatorial position of the pendant pyridyl/m-tolyl groups (py_{eq}/Tol_{eq}). Moreover, the N—C_i—C—O dihedral angles (for 5b* C₂—C_i—C—O) can be *syn* or *anti*. All these conformers are, at least, 3.2 kcal mol⁻¹ higher in their standard Gibbs energies (Table 3, entries 3 and 4).

Table 3. Calculated Standard Gibbs Free Energies (in kcal mol⁻¹) of the Conformers of 3a*, 3b*, and 5b* Relative to the Most Stable Conformer

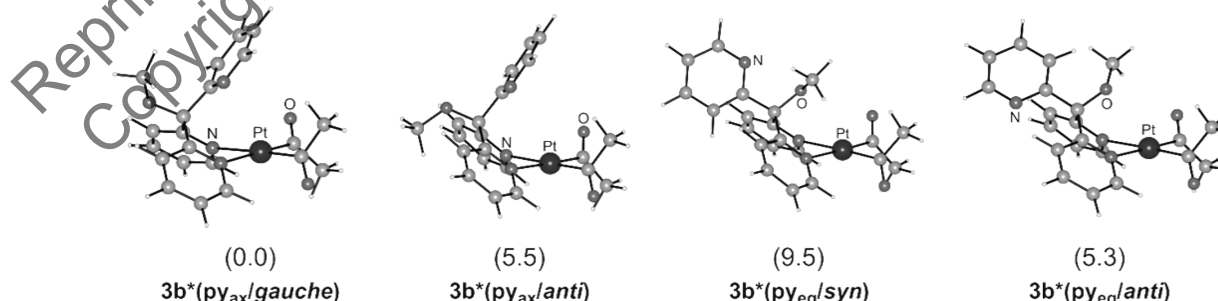
entry	conformer	3a*	3b*	5b*
1	py _{ax} /gauche ^a	0	0	0
2	py _{ax} /anti ^a	4.2	5.5	5.7
3	py _{eq} /syn ^b	7.2	9.5	6.9
4	py _{eq} /anti ^b	3.2	5.3	6.4

^aConformation characterized by the R—O—C—C_i dihedral angle (C_i = *ipso*-C atom of the pyridine and tolyl ring, respectively).

^bConformation determined by the N—C_i—C—O (for 5b* C₂—C_i—C—O) dihedral angle.

As discussed in section 2.3, the dynamics observed may be caused by a hindered rotation of the asymmetric pendant group and/or of the substituent R. In Figure 9 the Gibbs free energy diagram for the rotation of the pendant pyridyl group is shown starting from the most stable *gauche* conformers of 3a* and 3b*. Here and in the following, the dynamics of 5b* are very similar to those of 3b*; thus, the diagrams for 5b* are only given in the Supporting Information. Apart from these conformers (py_{ax}/gauche; Figure 9, a) only one further equilibrium structure each could be located. They are also py_{ax}/gauche conformers (Figure 9, c), their energies being only slightly above the global minima. In the case of 3a* (R = H), the two activation barriers (Figure 9, b/d) are significantly different; thus, a flip-flop-type motion could be operative: the activation barrier of the flip-flop-type motion where the N atom of the pendant pyridine ring is directed toward the substituent R = H (Figure 9, a → c via b) is 4.2 kcal mol⁻¹, whereas that where the 3-C—H group of the pendant pyridine ring is directed toward the substituent R = H (Figure 9, a → c via d) is 13.7 kcal mol⁻¹. In the case of 3b* (R = Me) the two activation barriers (Figure 9, b/d) are of the same order of magnitude (17.8/19.5 kcal mol⁻¹) and are significantly higher than that for 3a*. Thus, for 3b*, even at room temperature, a rotation of the pendant pyridine group is expected to be hindered.

In Figure 10 the Gibbs free energy diagram for the rotation of R for the complexes 3a* and 3b* is shown. An inspection of the Newman projections makes it clear that a rotation of the substituent R by 360° includes the following conversions: *gauche* (Figure 10, a; global minimum; R pointed toward the N atom of the pyridine ring) → *anti* (Figure 10, c) → *gauche* (Figure 10, e; lone electron pair of the O atom pointed toward the N atom) → *gauche* (Figure 10, a; global minimum). Obviously, the activation barriers (Figure 10, b/d) are mainly a

**Figure 8.** Calculated equilibrium structures of different conformers of $[\text{Pt}(\text{COMe})_2\{(2\text{-py})_3\text{COMe}\}]$ (3b*). The conformers are designated with indices showing an axial (py_{ax}) or equatorial (py_{eq}) position of the noncoordinated pyridine group and characterizing the dihedral angles R—O—C—C_i (*gauche*, *anti*) and N—C_i—C—O (*syn*, *anti*) (C_i = *ipso*-C atom of the noncoordinated pyridine ring), respectively. The standard Gibbs free energies (in kcal mol⁻¹) are given in parentheses relative to the most stable conformer.

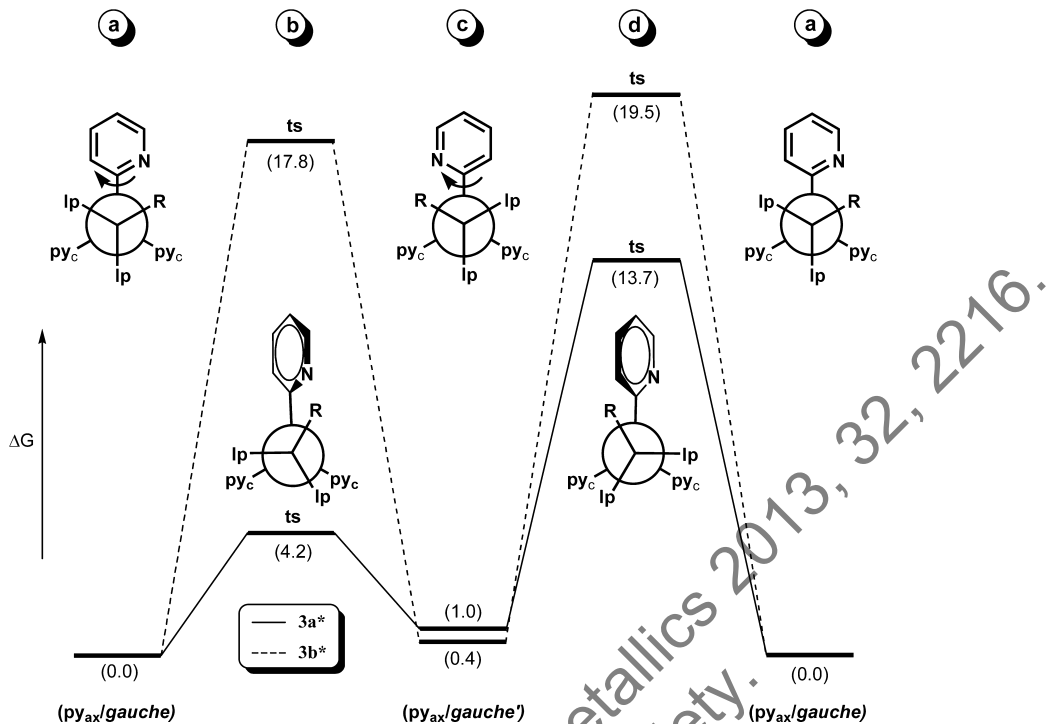


Figure 9. Gibbs free energy diagram for the rotation of the noncoordinated pyridyl group in $[\text{Pt}(\text{COMe})_2\{(2-\text{py})_3\text{COR}\}]$ ($\text{R} = \text{H}$ ($3\mathbf{a}^*$) Me ($3\mathbf{b}^*$))). The Gibbs energies (in kcal mol⁻¹) are given in parentheses relative to the most stable isomer (ts = transition state). The Newman projections (lp = lone electron pair; py_c = coordinated pyridyl) are along the O–C vector of the backbone of the $(2-\text{py})_3\text{COR}$ ($\text{R} = \text{H}, \text{Me}$) ligands.

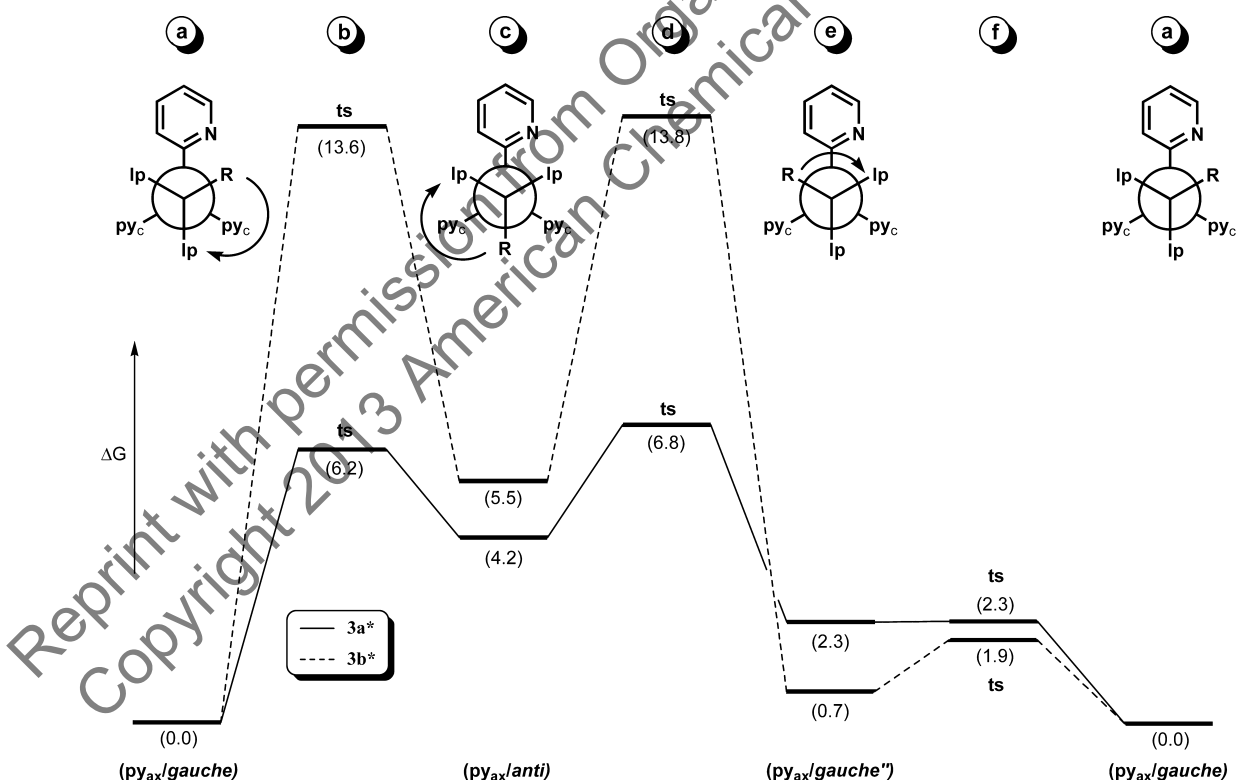


Figure 10. Gibbs free energy diagram for the rotation of the substituent R in $[\text{Pt}(\text{COMe})_2\{(2-\text{py})_3\text{COR}\}]$ ($\text{R} = \text{H}$ ($3\mathbf{a}^*$), Me ($3\mathbf{b}^*$))). The Gibbs energies (in kcal mol⁻¹) are given in parentheses relative to the most stable isomer (ts = transition state). The Newman projections (lp = lone electron pair; py_c = coordinated pyridyl) are along the O–C vector of the backbone of the $(2-\text{py})_3\text{COR}$ ($\text{R} = \text{H}, \text{Me}$) ligands.

consequence of steric repulsion between the substituent R and the 3-CH groups of the coordinated pyridine rings (py_c). Thus,

as expected, for $\text{R} = \text{H}$ ($3\mathbf{a}^*$) the barriers are remarkably lower than for $\text{R} = \text{Me}$ ($3\mathbf{b}^*$): 6.2/6.8 vs 13.6/13.8 kcal mol⁻¹.

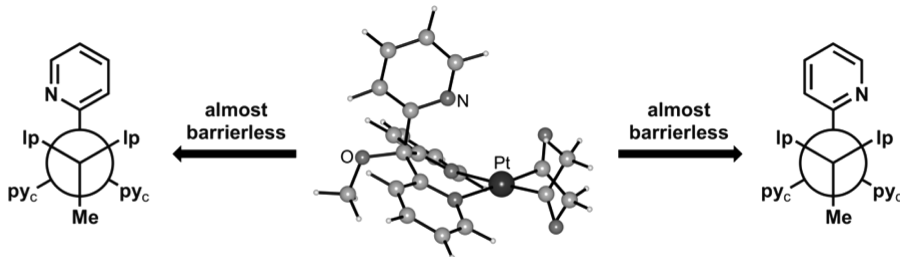


Figure 11. Calculated equilibrium structure of the *anti* conformer $3b^*$ (py_{ax} /*anti*) with the N atom of the pendant pyridine ring aligned toward the Pt atom.

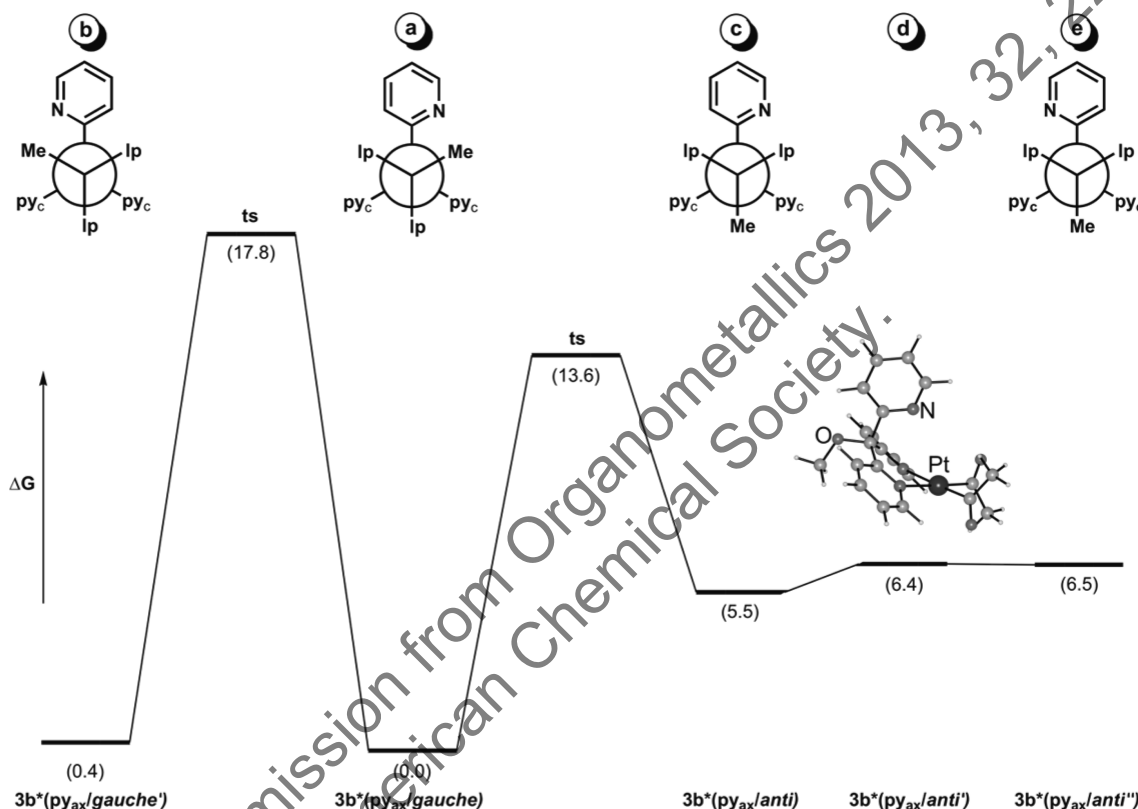


Figure 12. Gibbs free energy diagram for the dynamics in $[\text{Pt}(\text{COMe})_2\{(2-\text{py})_3\text{COMe}\}]$ ($3b^*$). The Gibbs energies (in kcal mol^{-1}) are given in parentheses relative to the most stable isomer (ts = transition state). The Newman projections (Ip = lone electron pair; py_c = coordinated pyridyl) are along the O–C vector of the backbone of the $(2-\text{py})_3\text{COMe}$ ligand.

Since for the *gauche* conformer of $3b^*$ the activation barriers for the rotation of the pendant pyridine ring (Figure 9, b/d) are significantly higher than those calculated for the *gauche*–*anti* isomerization (17.8/19.5 vs 13.6/13.8 kcal mol^{-1}), calculations concerning the rotation of the pendant groups of the *anti* conformers were performed. In addition to the equilibrium structure of the thermodynamically most stable *anti* conformer described above ($3b^*(\text{py}_{\text{ax}}/\text{anti})$ in Figure 8), another one ($3b^*(\text{py}_{\text{ax}}/\text{anti}'')$) was found lying 0.9 kcal mol^{-1} over the aforementioned one (Figure 11). In this structure the pendant pyridyl group is positioned perpendicular to the complex plane while the N atom is aligned toward the Pt atom. The rotation of 90° both clockwise and anticlockwise was found to be almost barrierless; thus, a flip-flop-type motion could be operative (Figure 11). In contrast, a similar structure having the C–H group oriented toward the Pt atom is a transition state, which lies in its Gibbs free energy 3.6 kcal mol^{-1} above the most

stable *anti* conformer (see the Gibbs free energy diagram in Figure S2 (Supporting Information)).

For the rotation of the *m*-tolyl group in the *anti* conformer of $3b^*$ only insignificant activation barriers were found, and thus, a 360° rotation could be operative in this case. Although irrelevant (because the *gauche*–*anti* isomerization is higher in Gibbs free energy than the flip-flop-type motion of the pyridyl group in the *gauche* conformer), the rotation of the pyridine ring in the *anti* conformer of $3a^*$ was calculated. In this case two activation barriers of 6.2 and 7.3 kcal mol^{-1} were found (see the Gibbs free energy diagram in Figure S1 (Supporting Information)).

All structures of the conformers with the inverted boat structure ($\text{py}_{\text{eq}}/\text{syn}$ and $\text{py}_{\text{eq}}/\text{anti}$) lie between 3.2 and 6.9 kcal mol^{-1} above the global minimum equilibrium structures ($\text{py}_{\text{ax}}/\text{gauche}$). Furthermore, for the inversion of the boat structure (which might proceed according a dissociative mechanism),¹⁸ a relatively high barrier can be assumed. Thus, although it cannot

be strictly ruled out, these conformers should not play a role in the dynamics observed.

2.5. Conclusions. Within this work, the synthesis and characterization of diacetylplatinum(II) complexes bearing κ^2 -bonded ligands of type $(2\text{-py})_3\text{COR}$ ($R = \text{H, Me, Et, Bn}$), $(2\text{-py})_2\text{PhCOR}$, and $(2\text{-py})_2(m\text{-Tol})\text{COR}$ ($R = \text{H, Me}$) have been described. Furthermore, both a qualitative and quantitative analyses of the dynamics found in complexes **3b–d** and **5b** bearing asymmetric pendant groups (py/*m*-Tol) and etherified ligands ($R \neq \text{H}$) by NMR techniques and DFT calculations have been presented. The results of the DFT calculations indicate that the dynamics observed is caused by an interplay of a hindered and unhindered rotation, respectively, of the substituent R and/or of the pendant py/*m*-Tol group.

(1) For complexes with an etherified ligand ($R \neq \text{H}$) and an asymmetric pendant pyridyl group (**3b–d**; in the following discussed with **3b*** as an example) it can be stated that, starting from the *gauche* conformer, the activation barrier for the *gauche–anti* isomerization (Figure 12, **a** → **c**) is remarkably lower than that for the rotation of the pendant pyridyl group (Figure 12, **a** → **b**). For the *anti* conformer a flip-flop-type motion of the pendant group (py) has an insignificant activation barrier and thus is favorable (Figure 12, **c** → **e** via **d**). In accordance with the NMR experiments, the mirror symmetry of complexes in solution is retained, at least at higher temperatures, due to the activation barrier of 13.6 kcal mol^{−1} (**3b***) for the *gauche–anti* isomerization.

(2) The situation of complex **5b** having an etherified ligand ($R = \text{Me}$) and an asymmetric pendant *m*-tolyl group is analogous to that described above, but—instead of a flip-flop-type motion of the pendant group in the *anti* conformer—a full 360° rotation takes place, which proved to be nearly barrierless (see Figure S5 (Supporting Information) for **5b***).

(3) For complexes with an alcohol group ($R = \text{H}$) and an asymmetric pendant pyridyl or *m*-tolyl group (**3a**, **5a**; in the following discussed with **3a*** as an example, see Figures 12 and 10) it can be stated that a flip-flop-type motion of the pendant group of the *gauche* conformer (global minimum) retains the mirror symmetry, whereas the *gauche–anti* isomerization does not play a role. In accordance with the NMR experiments, due to the activation barrier of 4.2 kcal mol^{−1}, the dynamics are operative even at lower temperatures.

(4) For complexes with a symmetric pendant phenyl group (**4a,b**), irrespective whether the ligand is etherified ($R = \text{Me}$) or not ($R = \text{H}$), mirror-symmetric structures were observed NMR spectroscopically. Obviously, the situation is analogous to the *m*-tolyl complex **5b***, but due to the symmetric pendant phenyl group a loss of the complex symmetry due to hindered rotation is irrelevant.

The present study gives a detailed insight into the nature of the dynamics in diacetylplatinum(II) complexes bearing κ^2N,N' -coordinated ligands of types $(2\text{-py})_3\text{COR}$, $(2\text{-py})_2\text{PhCOR}$, and $(2\text{-py})_2(m\text{-Tol})\text{COR}$. Moreover, a very good agreement between the values obtained from NMR experiments ($\Delta G_{298} = 14.6$ kcal mol^{−1} (**3b**), 14.7 kcal mol^{−1} (**3c**), 14.9 kcal mol^{−1} (**3d**), 15.3 kcal mol^{−1} (**5b**)) and from DFT calculations ($\Delta G_{298} = 13.6/14.5$ kcal mol^{−1} (**3b*/5b***)) was found.

Thus, overall there are three types of diacetylplatinum(II) complexes with κ^2N,N' -coordinated ligands having an additional pendant N-donor site at their disposal, namely type **III** complexes (see Scheme 1) with anionic tris(pyrazolyl)borate ligands, type **IV** complexes (see Scheme 1) with neutral

tris(pyrazolyl)methane ligands, and complexes of type **3** with neutral tris(pyridyl)methanol and tris(pyridyl)methyl ether ligands discussed here. In type **IV** complexes, molecular rearrangement (exchange of coordinated and noncoordinated pyrazolyl rings via intermediates having only κ^1N -coordinated ligands) was observed, pointing to a weak coordination of the neutral tris(pyrazolyl)methane ligands.⁶ Type **III** complexes do not show any molecular dynamics, indicating, as expected, a stronger coordination of the scorpionate ligands due to their negative charge.⁵ In the neutral type **3** complexes discussed here, which have pyridine type donor sites, the molecular dynamics observed are due to a rotation or a flip-flop-type motion of the pendant (noncoordinated) pyridine group but not due to a decoordination/recoordination mechanism as in type **IV** complexes. This is in accord with a stronger σ donor ability of pyridine in comparison with that of pyrazole.⁹ Thus, the donor ability of such ligands depends both on the overall charges of the ligands and complexes, respectively, and on the nature of the donor N atoms.

3. EXPERIMENTAL SECTION

3.1. General Comments. All reactions were performed under an argon atmosphere using standard Schlenk techniques. Solvents were dried (diethyl ether and THF over Na/benzophenone) and distilled prior to use. If not otherwise stated, NMR spectra were recorded at 27 °C with Varian VXR 400 and Unity 500 spectrometers. Chemical shifts are relative to solvent signals (CDCl_3 , $\delta_{\text{H}} 7.24$, $\delta_{\text{C}} 77.0$; CD_2Cl_2 , $\delta_{\text{H}} 5.32$, $\delta_{\text{C}} 53.8$; CD_3OD , $\delta_{\text{H}} 3.31$, $\delta_{\text{C}} 49.0$) as internal references; $\delta(^{195}\text{Pt})$ is referenced to $\text{Na}_2[\text{PtCl}_6]$. If necessary, 2D NMR techniques (H,H , ^{13}C COSY, HMBC, and NOESY) were used to assign the signals in ¹H and ¹³C NMR spectra. Temperature calibration for variable-temperature measurements was performed using CD_3OD .¹⁹ IR spectra were recorded with a Bruker Tensor 28 spectrometer with a Platinum ATR unit. Microanalyses were performed by the University of Halle microanalytical laboratory using a CHNS-932 (LECO) elemental analyzer. The high-resolution ESI mass spectra were obtained from a Bruker Apex III Fourier transform ion cyclotron resonance (FT-ICR) mass spectrometer (Bruker Daltonics) equipped with an Infinity cell, a 7.0 T superconducting magnet (Bruker), an rf-only hexapole ion guide, and an external APOLLO electrospray ion source (Agilent, off-axis spray). The sample solutions were introduced continuously via a syringe pump with a flow rate of 120 $\mu\text{L h}^{-1}$. The complexes $[\text{Pt}_2\{(\text{COMe})_2\text{H}\}_2(\mu\text{-Cl})_2]$ (**1**) and $[\text{Pt}(\text{COMe})_2(\text{NH}_2\text{Bn})_2]$ (**2**) were prepared according to literature methods.^{1,7} Syntheses and spectroscopic data of the ligands, which, in part, have not yet been described in the literature, are reported in the Supporting Information.

3.2. Syntheses of the Diacetylplatinum(II) Complexes (3–5). $[\text{Pt}(\text{COMe})_2(\text{NH}_2\text{Bn})_2]$ (**2**; 100 mg, 0.2 mmol) and an equimolar amount of the respective ligand were dissolved in THF (5 mL) and stirred for 30 min. The volume of the yellow solution was reduced in vacuo to about 2 mL, and diethyl ether (8 mL) was added. The yellow precipitate that formed was filtered off, washed with diethyl ether (3 × 2 mL), and dried in vacuo.

3.2.1. $[\text{Pt}(\text{COMe})_2((2\text{-py})_3\text{COH})]$ (3a**).** Yield: 87 mg (80%). HRMS (ESI): m/z calcd for $[\text{C}_{20}\text{H}_{19}\text{O}_3\text{N}_3\text{PtH}]^+$ 545.11487, found for $[\text{M} - \text{H}]^+$ 545.11456. ¹H NMR (400 MHz, CD_3OD): δ 1.76 (s, 6H, COCH_3), 7.10 (m, 1H, H^9 py), 7.43 (m, 2H, $H^{5/5'}$ py), 7.49 (m, 1H, H^{11} py), 7.89 (m, 1H, H^{10} py), 8.10 (m, 2H, $H^{4/4'}$ py), 8.38 (m, 2H, $H^{3/3'}$ py), 8.56 (m, 1H, H^{12} py), 8.59 (m, 2H, $H^{6/6'}$ py). ¹³C NMR (100 MHz, CD_3OD): δ 43.9 (s + d, $^3J_{\text{Pt},\text{H}} = 343.7$ Hz, COCH_3), 85.0 (s, $(2\text{-py})_3\text{COH}$), 124.6 (s, C^{11} py), 125.0 (s, $\text{C}^{3/3'}$ py), 125.5 (s, $\text{C}^{5/5'}$ + C^9 py), 138.8 (s, C^{10} py), 140.7 (s, $\text{C}^{4/4'}$ py), 150.5 (s, C^{12} py), 152.2 (s, $\text{C}^{6/6'}$ py), 162.5 (s, $\text{C}^{2/2'}$ py), 164.8 (s, C^8 py), 236.5 (s + d, $^3J_{\text{Pt},\text{H}} = 128.6$ Hz, COCH_3). Here and in the following, the two coordinated pyridine rings are numbered 1–6 and 1'–6', respectively; non-coordinated pyridine rings are numbered 7–12. ¹⁹⁵Pt NMR (107

Organometallics

MHz, CD₂Cl₂): δ -3221.8 (s). IR: ν(CO) 1624, ν(CO) 1601, ν(CO) 1576, ν(CO) 1562 cm⁻¹.

3.2.2. [Pt(COMe)₂(2-py)₃COMe]⁺ (3b). Yield: 82 mg (73%). HRMS (ESI): *m/z* calcd for [C₂₁H₂₁O₃N₃PtH]⁺ 559.13053, found for [M - H]⁺ 559.13046. ¹H NMR (500 MHz, CD₃OD, -20 °C): δ 1.74 (s, 3H, COCH₃), 1.85 (s, 3H, COCH₃), 3.29 (s, 3H, OCH₃), 7.28 (m, 1H, H⁹ py), 7.45/7.52 (m, 2H, H⁵ + H^{5'} py), 7.64 (m, 1H, H¹¹ py), 8.00 (m, 1H, H¹⁰ py), 8.11/8.18 (m, 2H, H⁴ + H^{4'} py), 8.20/8.29 (m, 2H, H³ + H^{3'} py), 8.60/8.63 (m, 2H, H⁶ + H^{6'} py), 8.69 (m, 1H, H¹² py). ¹H NMR (500 MHz, CD₃OD, +27 °C): δ 1.79 (s (br), 6H, COCH₃), 3.29 (s, 3H, OCH₃), 7.22 (m, 1H, H⁹ py), 7.44 (s (br), 2H, H^{5'/5} py), 7.59 (m, 1H, H¹¹ py), 7.96 (m, 1H, H¹⁰ py), 8.11 (s (br), 2H, H^{4/4'} py), 8.21 (s (br), 2H, H^{3/3'} py), 8.62 (m, 2H, H^{6/6'} py), 8.66 (m, 1H, H¹² py). ¹³C NMR (50 MHz, CD₂Cl₂, -80 °C): δ 43.4/43.5 (s, 2 × COCH₃), 53.6 (s, OCH₃), 88.2 (s, (2-py)₃COMe), 122.6/123.1/123.6/124.2/125.7 (s, C³ + C^{3'} + C⁵ + C^{5'} + C¹¹ py), 136.2 (s, C¹⁰ py), 138.3/138.7 (s, C⁴ + C^{4'} py), 149.2/150.4/151.3 (s, C⁶ + C^{6'} + C¹² py), 156.9/158.2/159.6 (s, C² + C^{2'} + C⁸ py), 229.0/230.3 (s, 2 × COCH₃). ¹³C NMR (100 MHz, CD₂Cl₂, +27 °C): δ 43.5 (s (br), COCH₃), 54.1 (s, OCH₃), 89.4 (s, (2-py)₃COMe), 123.5 (s (br), C^{3/3'} py), 123.8 (s, C¹¹ py), 124.1/124.6 (s (br), C⁵ + C^{5'} py), 126.5 (s, C⁹ py), 136.8 (s, C¹⁰ py), 138.8 (s (br), C^{4/4'} py), 149.8 (s, C¹² py), 151.5/152.6 (s (br), C⁶ + C^{6'} py), 158.9/161.1 (s (br), C² + C^{2'} py), 159.3 (s, C⁸ py), 226.6/227.8 (s (br), 2 × COCH₃). ¹⁹⁵Pt NMR (107 MHz, CD₂Cl₂): δ -3221.8 (s). IR: ν(CO) 1600, ν(CO) 1583, ν(CO) 1564 cm⁻¹.

3.2.3. [Pt(COMe)₂(2-py)₃COEt]⁺ (3c). Yield: 97 mg (85%). HRMS (ESI): *m/z* calcd for [C₂₂H₂₃O₃N₃PtH]⁺ 545.14619, found for [M - H]⁺ 573.14627. ¹H NMR (500 MHz, CD₃OD, -20 °C): δ 1.40 (t, 3H, OCH₂CH₃), 1.73 (s, 3H, COCH₃), 1.85 (s, 3H, COCH₃), 3.30 (m, 2H, OCH₂CH₃), 7.25 (m, 1H, H⁹ py), 7.45/7.52 (s, 2H, H⁵ + H^{5'} py), 7.63 (m, 1H, H¹¹ py), 7.99 (m, 1H, H¹⁰ py), 8.11/8.19 (s, 2H, H⁴ + H^{4'} py), 8.19/8.28 (s, 2H, H³ + H^{3'} py), 8.60/8.63 (m, 2H, H⁶ + H^{6'} py), 8.67 (m, 1H, H¹² py). ¹H NMR (500 MHz, CD₃OD, +27 °C): δ 1.33 (t, 3H, OCH₂CH₃), 1.79 (s (br), 6H, COCH₃), 3.33 (s, (br), 2H, OCH₂CH₃), 7.19 (m, 1H, H⁹ py), 7.44 (s (br), 2H, H^{5'/5} py), 7.57 (m, 1H, H¹¹ py), 7.94 (m, 1H, H¹⁰ py), 8.11 (s (br), 2H, H^{4/4'} py), 8.21 (s (br), 2H, H^{3/3'} py), 8.62 (m, 2H, H^{6/6'} py), 8.64 (m, 1H, H¹² py). ¹³C NMR (100 MHz, CD₃OD, -20 °C): δ 15.5 (s, OCH₂CH₃), 43.9/44.2 (s, 2 × COCH₃), 63.0 (s, OCH₂CH₃), 89.9 (s, (2-py)₃COEt), 125.0/125.1/125.3/125.6/126.2/127.9 (s, C³ + C^{3'} + C⁵ + C^{5'} + C¹¹ py), 138.9/140.9/141.3 (s, C⁴ + C^{4'} + C¹⁰ py), 150.5/152.0/153.1 (s, C⁶ + C^{6'} + C¹² py), 159.8/160.8/161.7 (s, C² + C^{2'} + C⁸ py), 235.4/237.7 (s, 2 × COCH₃). ¹³C NMR (100 MHz, CD₂Cl₂, +27 °C): δ 15.4 (s, OCH₂CH₃), 43.5 (s (br), COCH₃), 62.0 (s, OCH₂CH₃), 89.2 (s, (2-py)₃COEt), 123.4 (s (br), C^{3/3'} py), 123.6 (s, C¹¹ py), 124.1/124.7 (s (br), C⁵ + C^{5'} py), 126.3 (s, C⁹ py), 136.8 (s, C¹⁰ py), 138.8/139.9 (s (br), C⁴ + C^{4'} py), 149.7 (s, C¹² py), 154.4/152.5 (s (br), C⁶ + C^{6'} py), 159.2/161.3 (s (br), C² + C^{2'} py), 159.9 (s, C⁸ py), 227.2/228.4 (s (br), 2 × COCH₃). ¹⁹⁵Pt NMR (107 MHz, CD₂Cl₂): δ -3213.4 (s). IR: ν(CO) 1615, ν(CO) 1585 cm⁻¹.

3.2.4. [Pt(COMe)₂(2-py)₃COBn]⁺ (3d). Yield: 89 mg (70%). HRMS (ESI): *m/z* calcd for [C₂₇H₂₅O₃N₃PtH]⁺ 635.16188, found for [M - H]⁺ 635.16155. ¹H NMR (500 MHz, CD₃OD, -20 °C): δ 1.75 (s, 3H, COCH₃), 1.85 (s, 3H, COCH₃), 4.42 (m, 2H, OCH₂Ph), 7.30 (m, 1H, H⁹ py), 7.33 (m, 1H, p-CH Ph), 7.39 (m, 2H, m-CH Ph), 7.44 (m, 2H, o-CH Ph), 7.45/7.52 (s, 2H, H⁵ + H^{5'} py), 7.61 (m, 1H, H¹¹ py), 7.96 (m, 1H, H¹⁰ py), 8.10/8.18 (s, 2H, H⁴ + H^{4'} py), 8.21/8.33 (s, 2H, H³ + H^{3'} py), 8.62/8.64 (m, 2H, H⁶ + H^{6'} py), 8.68 (m, 1H, H¹² py). ¹H NMR (500 MHz, CD₃OD, +27 °C): δ 1.80 (s (br), 6H, COCH₃), 4.44 (s (br), 2H, OCH₂Ph), 7.23 (m, 1H, H⁹ py), 7.30 (m, 1H, p-CH Ph), 7.35–7.42 (m, 4H, o-CH + m-CH Ph), 7.45 (s (br), 2H, H^{5'/5} py), 7.56 (m, 1H, H¹¹ py), 7.90 (m, 1H, H¹⁰ py), 8.12 (s (br), 2H, H^{4/4'} py), 8.26 (s (br), 2H, H^{3/3'} py), 8.65 (m, 3H, H^{6/6'} + H¹² py). ¹³C NMR (50 MHz, CDCl₃, -80 °C): δ 43.5/43.6 (s, 2 × COCH₃), 67.0 (s, OCH₂Ph), 88.2 (s, (2-py)₃COBn), 122.7/123.1/123.4/123.7/124.3/125.3 (s, C³ + C^{3'} + C⁵ + C^{5'} + C¹¹ py), 126.4/128.1 (s, m- + o-CH Ph), 127.4 (s, p-CH Ph), 136.6 (s, C¹⁰ py), 136.7 (s, i-C Ph), 138.5/138.7 (s, C⁴ + C^{4'} py), 149.2/150.6/151.3 (s, C⁶ + C^{6'} + C¹² py), 157.2/158.5/159.1 (s, C² + C^{2'} + C⁸ py), 229.2/

230.2 (s, 2 × COCH₃). ¹³C NMR (125 MHz, CDCl₃, +27 °C): δ 43.3/43.6 (s (br), 2 × COCH₃), 67.9 (s, OCH₂Ph), 89.1 (s, (2-py)₃COBn), 122.8/123.0 (s (br), C^{3/3'} py), 123.5 (s, C¹¹ py), 123.7/124.5 (s (br), C⁵ + C^{5'} py), 126.6 (s, C⁹ py), 127.1 (s, m-CH Ph), 128.0 (s, o-CH Ph), 128.6 (s, p-CH Ph), 136.6 (s, C¹⁰ py), 137.2 (s, i-C Ph), 138.6 (s (br), C^{4/4'} py), 149.5 (s, C¹² py), 151.5/153.1 (s (br), C⁶ + C^{6'} py), 158.4/160.8 (s (br), C² + C^{2'} py), 158.8 (s, C⁸ py), 226.4/229.5 (s (br), 2 × COCH₃). ¹⁹⁵Pt NMR (107 MHz, CD₂Cl₂): δ -3213.4 (s). IR: ν(CO) 1614, ν(CO) 1583 cm⁻¹.

3.2.5. [Pt(COMe)₂(2-py)₂PhCOH]⁺ (4a). Yield: 98 mg (90%). HRMS (ESI): *m/z* calcd for [C₂₁H₂₀O₃N₂PtH]⁺ 544.11965, found for [M - H]⁺ 544.11945. ¹H NMR (500 MHz, CD₂Cl₂): δ 1.71 (s, 6H, COCH₃), 6.92 (m, 2H, o-CH Ph), 7.25 (m, 2H, H^{5'/5} py), 7.32 (m, 2H, m-CH Ph), 7.39 (m, 1H, p-CH Ph), 7.96 (m, 2H, H^{4/4'} py), 8.43 (m, 2H, H^{3/3'} py), 8.64 (m, 2H, H^{6/6'} py). ¹³C NMR (125 MHz, +27 °C, CD₂Cl₂): δ 43.2 (s + d, ²J_{Pt,C} = 355.2 Hz, COCH₃), 82.9 (s, (2-py)₂PhCOH), 123.7 (s, C^{3/3'} py), 124.0 (s, C^{5'/5} py), 128.3 (s, p-CH Ph), 128.4 (s, o-CH Ph), 128.8 (s, m-CH Ph), 138.7 (s, C^{4/4'} py), 145.8 (s, i-C Ph), 151.4 (s, C^{6/6'} py), 161.2 (s, C^{2/2'} py), 230.5 (s + d, ¹J_{Pt,C} = 1304.7 Hz, COCH₃). ¹⁹⁵Pt-NMR (107 MHz, CD₂Cl₂): δ -3249.4 (s). IR: ν(CO) 1599, ν(CO) 1576 cm⁻¹.

3.2.6. [Pt(COMe)₂(2-py)₂PhCOMe]⁺ (4b). Yield: 87 mg (78%). HRMS (ESI): *m/z* calcd for [C₂₂H₂₂O₃N₂PtH]⁺ 558.13531, found for [M - H]⁺ 558.13487. ¹H NMR (400 MHz, CDCl₃): δ 1.79 (s, 6H, COCH₃), 3.18 (s, 3H, OCH₃), 6.95 (m, 2H, o-CH Ph), 7.25 (m, 2H, H^{5'/5} py), 7.39–7.44 (m, 3H, m-CH + p-CH Ph), 7.88 (m, 2H, H^{4/4'} py), 8.04 (m, 2H, H^{3/3'} py), 8.83 (m, 2H, H^{6/6'} py). ¹³C NMR (125 MHz, +27 °C, CDCl₃): δ 43.5 (s + d, ²J_{Pt,C} = 377.6 Hz, COCH₃), 88.4 (s, (2-py)₂PhCOMe), 122.8 (s, C^{3/3'} py), 123.9 (s, C^{5'/5} py), 128.6 (s, m-CH Ph), 128.8 (s, p-CH Ph), 130.4 (s, m-CH Ph), 138.3 (s, C^{4/4'} py), 139.2 (s, i-C Ph), 152.5 (s, C^{6/6'} py), 160.0 (s, C^{2/2'} py), 230.5 (s + d, ¹J_{Pt,C} = 1304.7 Hz, COCH₃). ¹⁹⁵Pt NMR (107 MHz, CDCl₃): δ -3206.3 (s). IR: ν(CO) 1599, ν(CO) 1576 cm⁻¹.

3.2.7. [Pt(COMe)₂(2-py)₂(m-Tol)COH]⁺ (5a). Yield: 80 mg (72%). HRMS (ESI): *m/z* calcd for [C₂₂H₂₂O₃N₂PtH]⁺ 558.13531, found for [M - H]⁺ 558.13508. ¹H NMR (400 MHz, CD₃OD): δ 1.74 (s, 6H, COCH₃), 2.30 (s, 3H, 3-CH₃Ph), 6.72 (m, 1H, H⁶ m-Tol), 6.76 (s, 1H, H² m-Tol), 7.27–7.34 (m, 2H, H⁴ + H⁵ m-Tol), 7.43 (m, 2H, H^{5'/5} py), 8.10 (s, 2H, H^{4/4'} py), 8.40 (m, 2H, H^{3/3'} py), 8.63 (s, 2H, H^{6/6'} py). ¹³C NMR (100 MHz, CD₃OD): δ 21.6 (s, 3-CH₃Ph), 43.9 (s, COMe), 53.5 (s, OCH₃), 82.3 (s, (2-py)₂(m-Tol)COH), 124.9 (s, C^{3/3'} py), 125.4 (s, C^{5'/5} py), 126.9 (s, C⁶ m-Tol), 130.0 (s, C⁴ + C⁵ m-Tol), 130.6 (s, C² m-Tol), 139.6 (s, C³ m-Tol), 140.5 (s, C^{4/4'} py), 147.1 (s, C¹ m-Tol), 152.4 (s, C^{6/6'} py), 163.2 (s, C^{2/2'} py), 236.9 (s, COCH₃). ¹⁹⁵Pt NMR (107 MHz, CD₂Cl₂): δ -3244.8 (s). IR: ν(CO) 1618, ν(CO) 1600, ν(CO) 1574 cm⁻¹.

3.2.8. [Pt(COMe)₂(2-py)₂(m-Tol)COMe]⁺ (5b). Yield: 78 mg (68%). HRMS (ESI): *m/z* calcd for [C₂₃H₂₄O₃N₂PtH]⁺ 545.15097, found for [M - H]⁺ 572.15109. ¹H NMR (500 MHz, CD₃OD, -20 °C): δ 1.72 (s, 3H, COCH₃), 1.80 (s, 3H, COCH₃), 2.34 (s, 3H, 3-CH₃Ph), 3.24 (s, 3H, OCH₃), 6.77 (m, 1H, H⁶ m-Tol), 6.84 (s, 1H, H² m-Tol), 7.32–7.49 (m, 4H, H⁴ + H⁵ m-Tol + H^{5'/5} py), 8.13 (s, 2H, H^{4/4'} py), 8.22 (m, 2H, H^{3/3'} py), 8.61/8.67 (m, 2H, H⁶ / H^{6'} py). ¹H NMR (500 MHz, CD₃OD, +27 °C): δ 1.76 (s (br), 6H, COCH₃), 2.33 (s, 3H, 3-CH₃Ph), 3.25 (s, 3H, OCH₃), 6.76 (m, 1H, H⁶ m-Tol), 6.81 (s, 1H, H² m-Tol), 7.31–7.45 (m, 4H, H⁴ + H⁵ m-Tol + H^{5'/5} py), 8.10 (s, 2H, H^{4/4'} py), 8.20 (m, 2H, H^{3/3'} py), 8.65 (s (br), 2H, H^{6/6'} py). ¹³C NMR (125 MHz, -20 °C, CD₃OD): δ 21.7 (s, 3-CH₃Ph), 43.4/44.1 (s, 2 × COMe), 54.2 (s, OCH₃), 89.6 (s, (2-py)₂(m-Tol)COH), 125.0/125.2 (s, C³ + C^{3'} py), 125.7/125.8 (s, C⁵ + C^{5'} py), 128.7 (s, C⁶ m-Tol), 130.0 (s, C⁵ m-Tol), 130.8 (s, C⁴ m-Tol), 132.5 (s, C² m-Tol), 139.6 (s, C³ m-Tol), 140.9/141.0 (s, C⁴ + C^{4'} py), 139.1 (s, C¹ m-Tol), 152.6/152.9 (s, C⁶ + C^{6'} py), 160.9/161.5 (s, C² + C^{2'} py), 236.4/237.3 (s, 2 × COCH₃). ¹³C NMR (125 MHz, +27 °C, CDCl₃): δ 21.5 (s, 3-CH₃Ph), 43.4 (s (br), COMe), 53.5 (s, OCH₃), 88.4 (s, (2-py)₂(m-Tol)COH), 122.8 (s (br), C^{3/3'} py), 123.8 (s (br), C^{5'/5} py), 127.4 (s, C⁶ m-Tol), 128.5 (s, C⁵ m-Tol), 129.5 (s, C⁴ m-Tol), 131.1 (s, C² m-Tol), 138.2 (s, C³ m-Tol), 138.3 (s (br), C^{4/4'} py), 139.1 (s, C¹ m-Tol), 152.4 (s (br), C^{6/6'} py), 159.9/160.2 (s (br), C² + C^{2'} py),

Table 4. Crystal Data and Structure Refinement for 3a–d

	3a·CH ₂ Cl ₂	3b	3c	3d
empirical formula	C ₂₁ H ₂₁ Cl ₂ N ₃ O ₃ Pt	C ₂₁ H ₂₁ N ₃ O ₃ Pt	C ₂₂ H ₂₃ N ₃ O ₃ Pt	C ₂₇ H ₂₅ N ₃ O ₃ Pt
formula wt	629.4	558.5	572.5	634.6
cryst syst	monoclinic	orthorhombic	orthorhombic	monoclinic
space group	P2 ₁ /c	P2 ₁ 2 ₁ 2 ₁	P2 ₁ 2 ₁ 2 ₁	P2 ₁ /c
<i>a</i> (Å)	8.3991(9)	8.1635(3)	8.2151(7)	14.315(3)
<i>b</i> (Å)	15.800(1)	13.7797(6)	13.932(1)	10.722(1)
<i>c</i> (Å)	17.095(2)	17.8650(7)	18.546(2)	16.602(2)
β (deg)	100.74(1)			108.82(2)
<i>V</i> (Å ³)	2228.4(4)	2009.6(1)	2122.5(3)	2412.1(6)
<i>Z</i>	4	4	4	4
<i>D</i> _{calcd} (g cm ⁻³)	1.876	1.846	1.792	1.747
μ (Mo K α) (mm ⁻¹)	6.563	7.008	6.638	5.851
<i>F</i> (000)	1216	1080	1112	1240
θ range (deg)	2.43–26.01	2.28–28.00	2.64–25.93	2.30–25.84
no. of rflns collected	15455	11935	12293	16605
nol of obsd rflns (<i>I</i> > 2 σ (<i>I</i>))	3603	4395	3848	3736
no. of indep rflns	4306 ($R_{\text{int}} = 0.0741$)	4757 ($R_{\text{int}} = 0.0424$)	4080 ($R_{\text{int}} = 0.0333$)	4640 ($R_{\text{int}} = 0.0569$)
no. of data/restraints/params	4306/0/274	4757/0/256	4080/0/264	4640/0/309
goodness of fit on <i>F</i> ²	0.978	1.037	1.047	1.010
final <i>R</i> indices (<i>I</i> > 2 σ (<i>I</i>))	R1 = 0.0312 wR2 = 0.0551	R1 = 0.0293 wR2 = 0.0546	R1 = 0.0250 wR2 = 0.0562	R1 = 0.0317 wR2 = 0.0729
<i>R</i> indices (all data)	R1 = 0.0393 wR2 = 0.0572	R1 = 0.0349 wR2 = 0.0558	R1 = 0.0280 wR2 = 0.0570	R1 = 0.0439 wR2 = 0.0768
largest difference peak, hole (e Å ⁻³)	0.893, -0.782	0.776, -0.917	1.064, -0.430	1.418, -1.260

227.8/227.9 (s (br), 2 × COCH₃). ¹⁹⁵Pt NMR (107 MHz, CD₂Cl₂): δ –3205.2 (s). IR: ν (CO) 1618, ν (CO) 1600, ν (CO) 1573 cm⁻¹.

3.3. X-ray Crystallography. Data for X-ray diffraction analyses of single crystals were collected on a Stoe-IPDS (3a,b,d) or a Stoe-IPDS 2T diffractometer (3b) at 200 K using Mo K α radiation ($\lambda = 0.71073$ Å, graphite monochromator). A summary of the crystallographic data, the data collection parameters, and the refinement parameters is given in Table 4. Absorption corrections were applied empirically with the PLATON program package (T_{\min}/T_{\max} : 0.04/0.15, 3a·CH₂Cl₂; 0.23/0.47, 3b; 0.10/0.17, 3c; 0.45/0.71, 3d).²⁰ The structures were solved with direct methods using SHELXS-97²¹ and refined using full-matrix least-squares routines against *F*² with SHELXL-97.²² All non-hydrogen atoms were refined with anisotropic displacement parameters and hydrogen atoms with isotropic parameters. H atoms were placed in calculated positions according to the riding model.

3.4. Computational Details. DFT calculations were performed with the Gaussian09 program package²³ using the functional B3LYP.²⁴ The 6-311++G(d,p) basis sets as implemented in Gaussian09 were employed for main-group atoms, while the relativistic pseudopotential of the Ahlrichs group and related basis functions of TZVPP quality were employed for the Pt atom.²⁵ The appropriateness of the functional in combination with the basis sets and effective core potential used for reliable interpretation of structural and energetic aspects of related platinum complexes has been demonstrated.²⁶ All systems were fully optimized without any symmetry restrictions. The resulting geometries were characterized as equilibrium structures and transition states, respectively, by the analysis of the force constants of normal vibrations. Solvent effects (methanol) were considered according to Tomasi's polarized continuum model.¹⁷ The method was used as implemented in Gaussian 09,²³ which is much more sophisticated than in previous Gaussian versions, especially because solvent effects are considered in each optimization step.

ASSOCIATED CONTENT

Supporting Information

Text, tables, figures, and CIF files giving synthesis details and spectroscopic data of the ligands, energies and Cartesian coordinates of all calculated molecules, Gibbs free energy

diagrams for 5b* and 3a*/3b* (*anti* conformer), and crystallographic data for 3a·CH₂Cl₂ and 3b–d. This material is available free of charge via the Internet at <http://pubs.acs.org>. Supplementary crystallographic data (3a·CH₂Cl₂, CCDC 922887; 3b, CCDC 922888; 3c, CCDC 922889; 3d, CCDC 922890) can also be obtained free of charge via <http://www.ccdc.cam.ac.uk/deposit>.

AUTHOR INFORMATION

Notes

The authors declare no competing financial interest.

REFERENCES

- Steinborn, D.; Gerisch, M.; Merzweiler, K.; Schenzel, K.; Pelz, K.; Bögel, H.; Magull, J. *Organometallics* **1996**, *15*, 2454.
- Steinborn, D. *Dalton Trans.* **2005**, 2664.
- (a) Gerisch, M.; Bruhn, C.; Vyater, A.; Davies, J. A.; Steinborn, D. *Organometallics* **1998**, *17*, 3101. (b) Vyater, A.; Wagner, C.; Merzweiler, K.; Steinborn, D. *Organometallics* **2002**, *21*, 4369.
- (a) Trofimenko, S. *Scorpionates: The Coordination Chemistry of Polypyrazolylborate Ligands*; Imperial College Press: London, 1999. (b) Pettinari, C. *Scorpionates II: Chelating Borate Ligands*; Imperial College Press: London, 2008.
- Bette, M.; Rüffer, T.; Bruhn, C.; Schmidt, J.; Steinborn, D. *Organometallics* **2012**, *31*, 3700.
- Bette, M.; Schmidt, J.; Steinborn, D. *Eur. J. Inorg. Chem.* **2013**, DOI: 10.1002/ejic.201201468.
- Kluge, T.; Bette, M.; Vetter, C.; Schmidt, J.; Steinborn, D. *J. Organomet. Chem.* **2012**, *71S*, 93.
- Pettinari, C.; Pettinari, R. *Coord. Chem. Rev.* **2005**, *249*, 525.
- Szczepura, L. F.; Witham, L. M.; Takeuchi, K. *J. Coord. Chem. Rev.* **1998**, *174*, 5.
- Jameson, D. L.; Blaho, J. K.; Kruger, K. T.; Goldsby, K. A. *Inorg. Chem.* **1989**, *28*, 4312.
- Jeffrey, G. A. *An Introduction to Hydrogen Bonding*; Oxford University Press: Oxford, U.K., 1997.
- Steiner, T. *Cryst. Rev.* **1996**, *6*, 1.

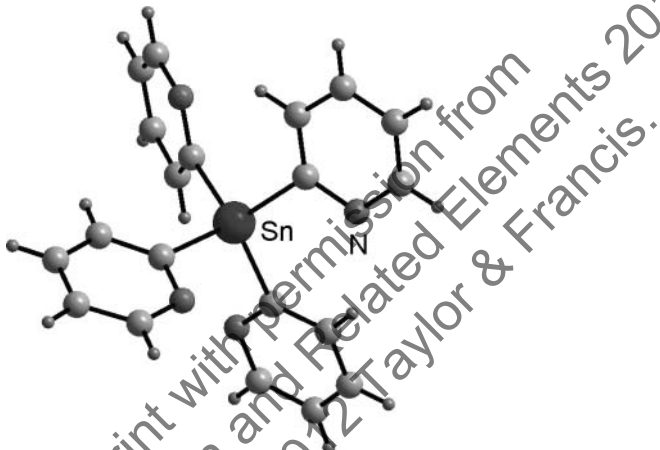
- (13) Werner, M.; Bruhn, C.; Steinborn, D. *J. Organomet. Chem.* **2008**, 693, 2369.
- (14) Budzelaar, P. H. M.; *gNMR, NMR Simulation Program, Version 5.0.6.0*; ivorysoft, Centennial, CO, 2006.
- (15) Kessler, K. *Angew. Chem., Int. Ed. Engl.* **1970**, 9, 219.
- (16) Sandström, J. *Dynamic NMR Spectroscopy*; Academic Press: London, 1982.
- (17) (a) Cancès, E.; Mennucci, B.; Tomasi, J. *J. Chem. Phys.* **1997**, 107, 3032. (b) Cossi, M.; Barone, V.; Mennucci, B.; Tomasi, J. *Chem. Phys. Lett.* **1998**, 286, 253. (c) Mennucci, B.; Tomasi, J. *J. Chem. Phys.* **1997**, 106, 5151.
- (18) Jalón, F. A.; Manzano, B. R.; Otero, A.; Rodríguez-Pérez, M. C. *J. Organomet. Chem.* **1995**, 494, 179.
- (19) Findeisen, M.; Brand, T.; Berger, S. *Magn. Reson. Chem.* **2007**, 45, 175.
- (20) (a) *MULscanABS, PLATON for Windows Taskbar v1.15*; University of Glasgow, Glasgow, Scotland, 2008. (b) Spek, A. L. *J. Appl. Crystallogr.* **2003**, 36, 7.
- (21) Sheldrick, G. M., *SHELXS-97, Program for Crystal Structure Solution*; University of Göttingen, Göttingen, Germany, 1998.
- (22) Sheldrick, G. M. *SHELXS-97, Program for the Refinement of Crystal Structures*; University of Göttingen, Göttingen, Germany, 1997.
- (23) Frisch, M. J.; Trucks, G. W.; Schlegel, H. B.; Scuseria, G. E.; Robb, M. A.; Cheeseman, J. R.; Scalmani, G.; Barone, V.; Mennucci, B.; Petersson, G. A.; Nakatsuji, H.; Caricato, M.; Li, X.; Hratchian, H. P.; Izmaylov, A. F.; Bloino, J.; Zheng, G.; Sonnenberg, J. L.; Hada, M.; Ehara, M.; Toyota, K.; Fukuda, R.; Hasegawa, J.; Ishida, M.; Nakajima, T.; Honda, Y.; Kitao, O.; Nakai, H.; Vreven, T.; Montgomery, J. A., Jr.; Peralta, J. E.; Ogliaro, F.; Bearpark, M.; Heyd, J. J.; Brothers, E.; Kudin, K. N.; Staroverov, V. N.; Kobayashi, R.; Normand, J.; Raghavachari, K.; Rendell, A.; Burant, J. C.; Iyengar, S. S.; Tomasi, J.; Cossi, M.; Rega, N.; Millam, J. M.; Klene, M.; Knox, J. E.; Cross, J. B.; Bakken, V.; Adamo, C.; Jaramillo, J.; Gomperts, R.; Stratmann, R. E.; Yazyev, O.; Austin, A. J.; Cammi, R.; Pomelli, C.; Ochterski, J. W.; Martin, R. L.; Morokuma, K.; Zakrzewski, V. G.; Voth, G. A.; Salvador, P.; Dannenberg, J. J.; Dapprich, S.; Daniels, A. D.; Farkas, Ö.; Foresman, J. B.; Ortiz, J. V.; Cioslowski, J.; Fox, D. J. *Gaussian 09, Revision B.01*; Gaussian, Inc., Wallingford, CT, 2009.
- (24) Becke, A. D. *J. Chem. Phys.* **1993**, 98, 5648.
- (25) (a) Weigend, F.; Häser, M.; Patzelt, H.; Ahlrichs, R. *Chem. Phys. Lett.* **1998**, 294, 143. (b) Leininger, T.; Nicklaß, A.; Küchle, W.; Stoll, H.; Dolg, M.; Bergner, A. *Chem. Phys. Lett.* **1996**, 255, 274. (c) Andrae, D.; Häussermann, U.; Dolg, M.; Stoll, H.; Preuss, H. *Theor. Chim. Acta* **1990**, 77, 123.
- (26) (a) Steinborn, D.; Schwieger, S. *Chem. Eur. J.* **2007**, 13, 9668. (b) Werner, M.; Lis, T.; Bruhn, C.; Lindner, R.; Steinborn, D. *Organometallics* **2006**, 25, 5946. (c) Vetter, C.; Kaluderović, G. N.; Paschke, R.; Gómez-Ruiz, S.; Steinborn, D. *Polyhedron* **2009**, 28, 3699. (d) Schwieger, S.; Heinemann, F. W.; Wagner, C.; Kluge, R.; Damm, C.; Israel, G.; Steinborn, D. *Organometallics* **2009**, 28, 2485.
- (27) Throughout the paper calculated complexes are marked with an asterisk. The index in parentheses is explained in the caption of Figure 8.

SYNTHESIS, CHARACTERIZATION, AND STRUCTURES OF TETRAKIS(2-PYRIDYL)TIN COMPOUNDS

Martin Bette and Dirk Steinborn

Institute of Chemistry—Inorganic Chemistry, Martin Luther University of Halle-Wittenberg, Halle, Germany

GRAPHICAL ABSTRACT



Abstract. Reactions of 2-bromopyridine and 2-bromo-6-methylpyridine with *n*-BuLi and tin tetrachloride afforded $\text{Sn}(2\text{-py})_4$ (**1a**) and $\text{Sn}(6\text{-Me-2-py})_4$ (**1b**), respectively. The identities of the two compounds were unambiguously proved by microanalyses, NMR (^1H , ^{13}C , ^{119}Sn) spectroscopy, and single-crystal X-ray diffraction studies.

Keywords: Tetrakis(2-pyridyl)tin compounds; scorpionate ligands; X-ray crystal structure studies

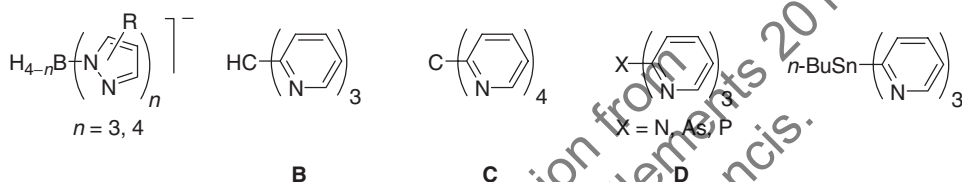
INTRODUCTION

Anionic tris- and tetrakis(pyrazolyl)borates (Scheme 1, **A**), so-called scorpionates, have been established in recent decades as versatile flexidentate nitrogen donor ligands which are usually capable of facially tripodal coordination in octahedral complexes.¹ In contrast, neutral tris(2-pyridyl)methane (**B**) and, especially, tetrakis(2-pyridyl)methane ligands (**C**) have received far less attention, although pyridine is considered to be both a

Received 15 March 2012; accepted 23 May 2012.

Address correspondence to D. Steinborn, Institut für Chemie, Martin-Luther-Universität Halle-Wittenberg, Kurt-Mothes-Straße 2, Halle 06120, Germany. E-mail: dirk.steinborn@chemie.uni-halle.de

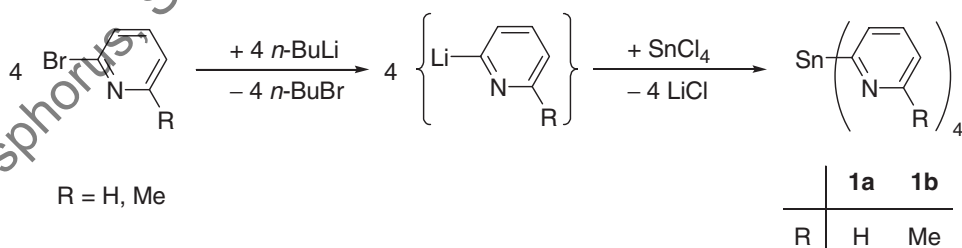
better σ -donor and a better π -acceptor ligand than pyrazole.² This may be due to the challenging multistep laborious synthesis forming these ligands only in moderate yields in many cases.^{3,4} The exchange of the bridgehead carbon atom by phosphorus, arsenic, or nitrogen (**D**) opens the way to other types of tris(2-pyridyl) tripodal ligands which proved to be more easily accessible than type **B** compounds.^{2,5} With tin as bridgehead atom, tris(pyridyl) compounds are also accessible. Thus, the synthesis of $^n\text{BuSn}(2\text{-py})_3$ (Scheme 1, **E**) and its ability to act as facially coordinating tripodal ligand in molybdenum and tungsten complexes⁶ as well as in copper and lithium compounds is reported.⁷ Furthermore, lithium tris(2-pyridyl)stannate compounds have been synthesized.⁸ Tetrakis(2-quinolyl)tin, only described in a patent,⁹ is the only one tin homologue of a type **C** compound. Here we present the synthesis, characterization, and structures of tetrakis(2-pyridyl)tin (**1a**) and tetrakis(6-methyl-2-pyridyl)tin (**1b**).



Scheme 1 Tris- and tetrakis(pyrazolyl)borates (A) and analogous compounds (B – E) derived from it.

RESULTS AND DISCUSSION

Tin tetrachloride was found to react according to Scheme 2 with 2-lithiopyridine or 2-lithio-6-methylpyridine in a 1:4 molar ratio under formation of $\text{Sn}(2\text{-py})_4$ (**1a**) and $\text{Sn}(6\text{-Me-2-py})_4$ (**1b**), respectively. 2-Lithiopyridines were synthesized *in situ* by the reaction of the respective 2-bromopyridines with *n*-butyllithium at -78°C in diethyl ether. Due to their thermolability, decomposition was observed above -30°C ,¹⁰ also the reactions with tin tetrachloride were performed at -78°C . Usual work-up procedures of the reaction mixtures resulted in isolation of **1a** and **1b** as white to pale yellow solids in moderate yields of 34 % and 32 %, respectively. Their identities were unambiguously proved by microanalyses, NMR (^1H , ^{13}C , ^{119}Sn) spectroscopy, and single-crystal X-ray diffraction studies.



Scheme 2 Synthesis of **1a,b**.

Characteristic NMR spectroscopic parameters of **1a,b** along with the data of $\text{Me}_3\text{Sn}(2\text{-py})^{11}$ for comparison are given in Tables 1 and 2. In the ^1H and ^{13}C NMR spectra all signals were found in the expected shift range with correct intensities in the

STRUCTURES OF TETRAKIS(2-PYRIDYL)TIN COMPOUNDS

1273

Table 1 Selected ^1H and ^{119}Sn NMR spectroscopic parameters of **1a,b** (δ in ppm)

	$\delta_{\text{H}3}$	$\delta_{\text{H}4}$	$\delta_{\text{H}5}$	$\delta_{\text{H}6}$	δ_{Sn}
$\text{Sn}(2\text{-py})_4$ (1a)	7.87	7.56	7.18	8.78	-301.5
$\text{Sn}(6\text{-Me-2-py})_4$ (1b)	7.76	7.42	7.01	-	-313.4
$\text{Me}_3\text{Sn}(2\text{-py})^{\text{a)}$	7.27	7.14	6.78	8.77	-52.2

^aGiven for comparison. Values taken from Ref.^{11a}

proton NMR spectra. The assignment of all resonances was verified by two-dimensional NMR (H,H and C,H COSY) experiments.

The δ_{H} values of the aromatic protons in **1b** were found to be slightly high-field shifted in comparison to **1a** ($\Delta\delta_{\text{H}}$ 0.11–0.17 ppm). This may be due to the electron-donating effect of the methyl group at position 6. In contrast, this additional methyl group does not influence the δ_{C} values and corresponding coupling constants of the aromatic carbon atoms. In compliance with the values reported for $\text{Me}_3\text{Sn}(2\text{-py})$ the coupling constants follow the sequence $^1J_{\text{Sn},\text{C}2} > ^2J_{\text{Sn},\text{C}3} > ^3J_{\text{Sn},\text{C}6} > ^3J_{\text{Sn},\text{C}4} > ^4J_{\text{Sn},\text{C}5}$. The ^{119}Sn NMR spectra display single resonances at -301.5 (**1a**) and -313.4 ppm (**1b**). Compared to SnPh_4 (-128 ppm),¹² the δ_{Sn} values of **1a,b** are shifted to much higher fields, as also found in Me_3SnPh ($\delta_{\text{Sn}} = -28.7$)¹² and $\text{Me}_3\text{Sn}(2\text{-py})$ ($\delta_{\text{Sn}} = -52.9$).^{11a}

Single crystals of **1a** and **1b** suitable for X-ray structural analyses were obtained from methylene chloride solutions with a layer of *n*-pentane at 4°C. In the crystals of the two compounds isolated molecules are present without unusual intermolecular interactions (shortest distance between nonhydrogen atoms: 3.473(4) Å, C5…C19', **1a**; 3.403(3) Å, C9…N1', **1b**). The molecular structures are shown in Figures 1 and 2; selected structural parameters are given in the Figure captions. The tin atoms are tetrahedrally coordinated by four pyridyl ligands. The angles around the tin atoms are all close to 109° (107.0(1) – 111.6(1)° for **1a** and 105.3(1) – 112.2(1)° for **1b**). Within the 3σ criterion, the Sn–C bonds in **1a** (2.147(2) – 2.155(2) Å) and in **1b** (2.148(3) – 2.162(3) Å) are of the same length and, furthermore, of equal length such as the Sn–C bonds in the structurally similar SnPh_4 (2.143(5) Å).¹³

In conclusion, the one-pot synthesis of $\text{Sn}(2\text{-py})_4$ (**1a**) and $\text{Sn}(6\text{-Me-2-py})_4$ (**1b**) described in this work gives easy access to tin homologues of tetrakis(2-pyridyl)methane. Thus, compounds **1a,b** are potentially flexidentate *N* ligands and their action as facially κ^3N,N',N'' -binding tripodal ligands in octahedral complexes or as κ^2N,N' coordinating bidentate ligands in square-planar complexes can be envisioned.

Table 2 Selected ^{13}C NMR spectroscopic parameters of **1a,b** (δ in ppm, J in Hz)

	$\delta_{\text{C}2}$ ($^1J_{\text{Sn},\text{C}}$)	$\delta_{\text{C}3}$ ($^2J_{\text{Sn},\text{C}}$)	$\delta_{\text{C}4}$ ($^3J_{\text{Sn},\text{C}}$)	$\delta_{\text{C}5}$ ($^4J_{\text{Sn},\text{C}}$)	$\delta_{\text{C}6}$ ($^3J_{\text{Sn},\text{C}}$)
$\text{Sn}(2\text{-py})_4$ (1a)	170.2 (687.1)	134.1 (93.4)	134.3 (40.8)	123.2 (14.0)	151.0 (79.7)
$\text{Sn}(6\text{-Me-2-py})_4$ (1b)	170.4 (682.2)	131.1 (91.3)	134.0 (41.9)	122.4 (13.8)	158.9 (79.2)
$\text{Me}_3\text{Sn}(2\text{-py})^{\text{a)}$	173.4 (605.5)	131.6 (93.2)	133.4 (37.2)	122.4 (12.0)	150.6 (68.7)

^aGiven for comparison. Values taken from Ref.^{11b}

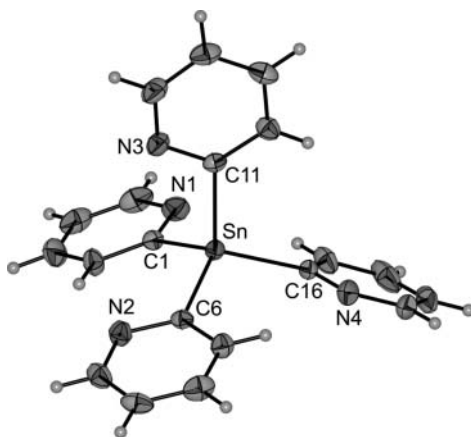


Figure 1 Molecular structure of $\text{Sn}(2\text{-py})_4$ (**1a**). The ellipsoids are shown with a probability of 30%. Selected structural parameters (distances in Å, angles in deg): $\text{Sn}-\text{C}1$ 2.147(2), $\text{Sn}-\text{C}6$ 2.149(2), $\text{Sn}-\text{C}11$ 2.155(2), $\text{Sn}-\text{C}16$ 2.150(2), $\text{C}1-\text{Sn}-\text{C}6$ 111.6(1), $\text{C}1-\text{Sn}-\text{C}11$ 107.2(1), $\text{C}1-\text{Sn}-\text{C}16$ 140.9(4), $\text{C}6-\text{Sn}-\text{C}11$ 107.0(1), $\text{C}6-\text{Sn}-\text{C}16$ 111.2(1), $\text{C}11-\text{Sn}-\text{C}16$ 108.8(1).

EXPERIMENTAL

General Comments

All reactions were performed in argon atmosphere using standard Schlenk techniques. The work-up procedures were done under aerobic conditions. Diethyl ether was dried over Na/benzophenone and freshly distilled prior to use. The pyridines were distilled and stored

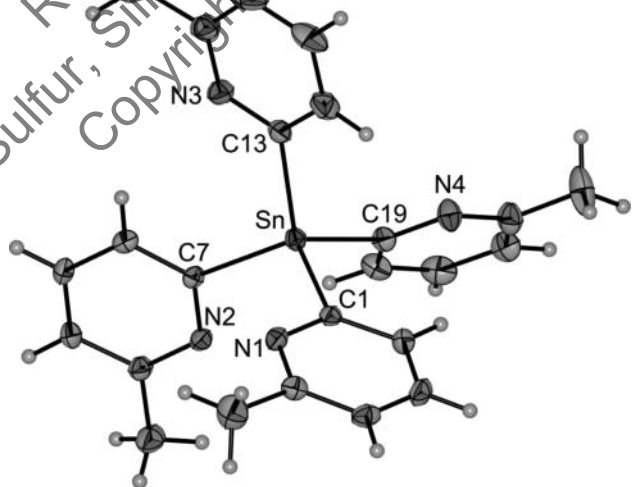


Figure 2 Molecular structure of $\text{Sn}(6\text{-Me-2-py})_4$ (**1b**). The ellipsoids are shown with a probability of 30%. Selected structural parameters (distances in Å, angles in deg): $\text{Sn}-\text{C}1$ 2.155(3), $\text{Sn}-\text{C}7$ 2.148(3), $\text{Sn}-\text{C}13$ 2.156(3), $\text{Sn}-\text{C}19$ 2.162(3), $\text{C}1-\text{Sn}-\text{C}7$ 109.8(1), $\text{C}1-\text{Sn}-\text{C}13$ 108.6(1), $\text{C}1-\text{Sn}-\text{C}19$ 105.3(1), $\text{C}7-\text{Sn}-\text{C}13$ 110.4(1), $\text{C}7-\text{Sn}-\text{C}19$ 110.4(1), $\text{C}13-\text{Sn}-\text{C}19$ 112.2(1).

STRUCTURES OF TETRAKIS(2-PYRIDYL)TIN COMPOUNDS

1275

over 4 Å molecular sieves at 4°C. NMR spectra were recorded at 27°C with a Varian Unity 500 spectrometer. Chemical shifts are relative to solvent signals (CDCl_3 , $\delta_{\text{H}} = 7.24$, $\delta_{\text{C}} = 77.0$) as internal references; $\delta(^{119}\text{Sn})$ is referenced to SnMe_4 . Microanalyses were carried out by the University of Halle microanalytical laboratory using CHNS-932 (LECO) elemental analyzer.

Data for X-ray diffraction analyses of single crystals were collected on a Stoe-IPDS 2T diffractometer (**1a**) and on a Stoe-IPDS diffractometer (**1b**) at 200 K using Mo $\text{K}\alpha$ radiation ($\lambda = 0.71073 \text{ \AA}$, graphite monochromator). A summary of the crystallographic data, the data collection parameters, and the refinement parameters is given in Table 3. Absorption corrections were applied empirically with the PLATON program package¹⁴ ($T_{\min}/T_{\max} = 0.61/0.73$, **1a**; $T_{\min}/T_{\max} = 0.57/0.93$, **1b**). The structures were solved with direct methods using SHELXS-97¹⁵ and refined using full-matrix least-squares routines against F^2 with SHELXL-97.¹⁶ All nonhydrogen atoms were refined with anisotropic displacement parameters and hydrogen atoms with isotropic ones. H atoms were placed in calculated positions according to the riding model. CCDC 871145 (**1a**), 871146 (**1b**) contain the supplementary crystallographic data for this paper. These data can be obtained free of charge from the Cambridge Crystallographic Data Centre via www.ccdc.cam.ac.uk/data_request/cif.

Synthesis of SnR_4 ($\text{R} = 2\text{-py}$, **1a**; 6-Me-2-py, **1b**)

To a stirred solution of 2-bromopyridine (6.81 g, 43.9 mmol) or 2-bromo-6-methylpyridine (7.38 g, 43.9 mmol) in diethyl ether (200 mL) at -78°C a solution of *n*-BuLi in *n*-hexane (48.0 mmol, 1.5 M) was added dropwise within 30 min yielding a dark

Table 3 Crystal data and structure refinement of **1a** and **1b**

	1a	1b
Empirical formula	$\text{C}_{20}\text{H}_{16}\text{N}_4\text{Sn}_1$	$\text{C}_{24}\text{H}_{24}\text{N}_4\text{Sn}_1$
Formula weight	431.06	487.16
Crystal system	Orthorhombic	Monoclinic
Space group	<i>Pbca</i>	<i>P2₁/c</i>
<i>a</i> (Å)	13.7997(8)	11.4532(8)
<i>b</i> (Å)	15.6737(6)	11.4657(8)
<i>c</i> (Å)	16.6711(7)	19.395(2)
β (°)	—	118.026(8)
<i>V</i> (Å ³)	3605.8(3)	2248.3(3)
<i>Z</i>	8	4
D_{calc} (g cm ⁻³)	1.588	1.439
$\mu(\text{Mo K}\alpha)$ (mm ⁻¹)	1.426	1.153
<i>F</i> (000)	1712	984
θ range (°)	2.60–28.00	2.01–25.00
Reflections collected	46200	15855
Reflections observed [$I > 2\sigma(I)$]	3375	3081
Independent reflections	4358 [$R_{\text{int}} = 0.0352$]	3889 [$R_{\text{int}} = 0.0726$]
Data/Restraints/Parameter	4358/0/226	3889/0/266
Goodness-of-fit on F^2	0.918	0.946
Final <i>R</i> indices [$I > 2\sigma(I)$]	$R_1 = 0.0212$ $wR_2 = 0.0483$	$R_1 = 0.0256$ $wR_2 = 0.0541$
<i>R</i> indices (all data)	$R_1 = 0.0366$ $wR_2 = 0.0517$	$R_1 = 0.0386$ $wR_2 = 0.0572$
Largest difference peak and hole (e·Å ⁻³)	0.400 and -0.644	0.513 and -0.325

red reaction mixture. After stirring at -78°C for 3 h, tin tetrachloride (2.77 g, 10.3 mmol) was added dropwise resulting in a yellow suspension which was further stirred for 2 h. After warming to room temperature, the mixture was hydrolyzed with acetone/isopropanol (1/1; 100 mL) and finally with water (50 mL). The solution was concentrated in vacuo up to approximately 150 mL. Then, the reaction mixture was extracted with methylene chloride (3×50 mL), the combined organic layers were dried (Na_2SO_4) and the solvent was reduced in vacuo to about 5 mL. After addition of *n*-pentane (15 mL), white to pale yellow solids were obtained, which were filtered off, washed with *n*-pentane (2×10 mL), and dried in vacuo.

Sn(2-py)₄ (1a). Yield: 1.5 g (34 %). Anal. Calcd. for $\text{C}_{20}\text{H}_{16}\text{N}_4\text{Sn}_1$ (431.06 g/mol): C, 55.73; H, 3.74; N, 12.99. Found: C, 55.50; H, 3.48; N, 12.95 %. ¹H NMR (500 MHz, CDCl_3): $\delta = 7.18$ (m, 4H, H^5 py), 7.56 (m, 4H, H^4 py), 7.87 (m, 4H, H^3 py), 8.78 (m, 4H, H^6 py). ¹³C NMR (125 MHz, CDCl_3): $\delta = 123.2$ (s+d, $^4J_{\text{Sn},\text{C}} = 14.0$ Hz, C^3 py), 134.1 (s+d, $^2J_{\text{Sn},\text{C}} = 93.4$ Hz, C^3 py), 134.3 (s+d, $^3J_{\text{Sn},\text{C}} = 40.8$ Hz, C^4 py), 151.0 (s+d, $^3J_{\text{Sn},\text{C}} = 79.7$ Hz, C^6 py), 170.2 (s+d, $^1J_{\text{Sn},\text{C}} = 687.1$ Hz, C^2 py). ¹¹⁹Sn NMR (186 MHz, CDCl_3): $\delta = -301.5$.

Sn(6-Me-2-py)₄ (1b). Yield: 1.6 g (32 %). Anal. Calcd. for $\text{C}_{24}\text{H}_{24}\text{N}_4\text{Sn}_1$ (487.19 g/mol): C, 59.17; H, 4.97; N, 11.50. Found: C, 58.77; H, 4.75; N, 11.32 %. ¹H NMR (500 MHz, CDCl_3): $\delta = 2.55$ (s, 12H, CH_3), 7.01 (m, 4H, H^5 py), 7.42 (m, 4H, H^4 py), 7.76 (m, 4H, H^3 py). ¹³C NMR (125 MHz, CDCl_3): $\delta = 24.8$ (s, CH_3), 122.4 (s+d, $^4J_{\text{Sn},\text{C}} = 13.8$ Hz, C^5 py), 131.1 (s+d, $^2J_{\text{Sn},\text{C}} = 91.3$ Hz, C^3 py), 134.0 (s+d, $^3J_{\text{Sn},\text{C}} = 41.9$ Hz, C^4 py), 158.9 (s+d, $^3J_{\text{Sn},\text{C}} = 79.2$ Hz, C^6 py), 170.4 (s+d, $^1J_{\text{Sn},\text{C}} = 682.2$ Hz, C^2 py). ¹¹⁹Sn NMR (186 MHz, CDCl_3): $\delta = -313.4$.

REFERENCES

1. Pettinari, C. *Scorpines II: Chelating Borate Ligands*; Imperial College Press: London, 2008.
2. Szczepura, L. F.; Witham, L. M.; Takeuchi, K. J. *Coord. Chem. Rev.* **1998**, 174, 5–32.
3. (a) White, D. L.; Faller, J. W. *Inorg. Chem.* **1982**, 21, 3119–3122 (b) Faller, J. W.; Ma, Y. *J. Am. Chem. Soc.* **1991**, 113, 1579–1586.
4. Matsumoto, K.; Kannami, M.; Oda, M. *Tetrahedron Lett.* **2003**, 44, 2861–2864.
5. (a) Mann, F. G.; Watson, J. J. *Org. Chem.* **1948**, 13, 502–531 (b) Keene, F. R.; Snow, M. R.; Stephenson, P. J.; Tiekkink, E. R. T. *Inorg. Chem.* **1988**, 27, 2040–2045 (c) Yang, W.; Schmidler, H.; Wu, Q.; Zhang, Y.; Wang, S. *Inorg. Chem.* **2000**, 39, 2397–2404.
6. Morales, D.; Pérez, J.; Riera, L.; Riera, V.; Miguel, D. *Organometallics* **2001**, 20, 4517–4523.
7. Beswick, M. A.; Belle, C. J.; Davies, M. K.; Halcrow, M. A.; Raithby, P. R.; Steiner, A.; Wright, D. S. *Chem. Commun.* **1996**, 2619–2620.
8. (a) Reichart, F.; Kischel, M.; Zeckert, K. *Chem. Eur. J.* **2009**, 15, 10018–10020 (b) Zeckert, K.; Zahn, S.; Kirchner, B. *Chem. Commun.* **2010**, 46, 2638–2640.
9. Ramsden, H. E. GB 825039 (A) of 12-09-1959.
10. Wibaut, J. P.; de Jonge, A. P.; Van der Voort, H. G. P.; Otto, P. P. H. L. *Recl. Trav. Chim. Pays-Bas* **1951**, 70, 1054–1066.
11. (a) Riedmiller, F.; Jockisch, A.; Schmidbaur, H. *Z. Naturforsch., B: Chem. Sci.* **1999**, 54, 13–17 (b) Wrackmeyer, B.; Maisel, H. E.; Milius, W. *Z. Naturforsch., B: Chem. Sci.* **1995**, 50, 809–815.
12. Cox, P. J.; Garden, S. J.; Howie, R. A.; Melvin, O. A.; Wardell, J. L. *J. Organomet. Chem.* **1996**, 516, 213–224.
13. Engelhardt, L. M.; Leung, W. P.; Raston, C. L.; White, A. H. *Aust. J. Chem.* **1982**, 35, 2383–2384.

STRUCTURES OF TETRAKIS(2-PYRIDYL)TIN COMPOUNDS

1277

14. (a) MULscanABS, PLATON for Windows Taskbar v1.15, University of Glasgow, **2008** (b) Spek, A. L. *J. Appl. Cryst.* **2003**, *36*, 7–13.
15. Sheldrick, G. M. *SHEL XS-97, Program for Crystal Structure Solution*; University of Göttingen: Göttingen, **1998**.
16. Sheldrick, G. M. *SHEL XS-97, Program for the Refinement of Crystal Structures*; University of Göttingen: Göttingen, **1997**.

Phosphorus, Sulfur, Silicon and Related Elements 2012, 187, 1271.
Reprint with permission from
Copyright 2012 Taylor & Francis.

Danksagung

Meinem sehr verehrten Lehrer, Herrn Prof. Dr. D. Steinborn, möchte ich an dieser Stelle für die Überlassung des interessanten Themas und für die gewährte Freiheit bei dessen Bearbeitungen danken. Weiterhin bin ich für seinen Beitrag zu den quantenchemischen Rechnungen und für seine stete Diskussionsbereitschaft (auch außerhalb der normalen Dienstzeiten) sowie seine Hinweise und Anregungen beim Anfertigen der Arbeit zu großem Dank verpflichtet.

Mein besonderer Dank gilt meinem geschätzten Kollegen Herrn Diplom.-Chem. T. Kluge, da die von Ihm durchgeführten quantenchemischen Rechnungen und NMR-Messungen sowie unsere produktiven Diskussionen und die sehr gute Zusammenarbeit im Arbeits- bzw. Laboralltag wesentlich zum Gelingen dieser Arbeit beigetragen haben.

Bei den Herren Prof. Dr. K. Merzweiler, Prof. Dr. S. Ebbinghaus, Dr. T. Rüffer und Dr. C. Wagner bedanke ich mich für die gewährte Hilfe bei der praktischen und theoretischen Einarbeitung in die Röntgeneinkristallstrukturanalyse.

Dem NMR-Team um Herrn Dr. D. Ströhle danke ich für die Aufnahme der zahlreichen Spektren und die Erfüllung von diversen Sonderwünschen.

Herrn Dr. J. Schmidt danke ich für die Aufnahme der hochauflösenden ESI-Massenspektren und Herrn Dr. T. Müller für die Anfertigung der thermoanalytischen Messungen.

Für das sehr angenehme Arbeitsklima und die ausgesprochen große Hilfsbereitschaft möchte ich mich bei allen ehemaligen und aktiven Mitgliedern der Arbeitsgruppe um Prof. Steinborn bedanken. Außerdem danke ich allen Mitgliedern des Institutes, die zum Gelingen der Arbeit beigetragen haben.

Weiterhin möchte ich mich besonders bei meiner Verlobten Eileen für Ihren Rückhalt und Ihr Verständnis, besonders nach nicht so optimal verlaufenden Arbeitstagen, bedanken. Ohne sie wäre die Anfertigung dieser Arbeit nicht möglich gewesen. Auch meinen Eltern, meiner Familie und meinen Freunden möchte ich für die stets gewährte Unterstützung an dieser Stelle danken.

Lebenslauf

Name	Martin Bette
Geburtsdatum	03.06.1982
Geburtsort	Meißen
Familienstand	ledig
Staatsangehörigkeit	deutsch
Wohnanschrift	Jacobstraße 18, 06110 Halle (Saale)
10/2008 – 10/2012	Wissenschaftlicher Mitarbeiter an der Martin-Luther-Universität Halle-Wittenberg im Arbeitskreis von Prof. Dr. D. Steinborn
10/2003 – 07/2008	Studium der Chemie an der Martin-Luther-Universität Halle-Wittenberg, Abschluss: Diplom-Chemiker
07/2002 – 03/2003	Wehrdienst
08/1993 – 06/2002	Gymnasium Jessen, Abschluss Abitur

Halle (Saale), 02.04.2013

Eidesstattliche Erklärung

Hiermit erkläre ich an Eides statt, dass ich die vorliegende Arbeit selbstständig und nur unter Verwendung der angegebenen Quellen und Hilfsmittel angefertigt habe.

Diese Arbeit wurde bisher an keiner anderen Universität oder Hochschule vorgelegt.

Halle (Saale), 02.04.2013